# Piezo - Resistivity Electric Cone Penetration Technology Investigation of the M-Basin at the Savannah River Site, Aiken, SC (U)

by

B. Bowers (Contact)

Westinghouse Savannah River Company
Savannah River Site
Aiken, South Carolina 29808

J. Rossabi

J. D. Shinn

W. Bratton



DOE Contract No. DE-AC09-89SR18035

## DISCLAIMER

# PIEZO-RESISTIVITY ELECTRIC CONE PENETRATION TECHNOLOGY INVESTIGATION OF THE M-BASIN AT THE SAVANNAH RIVER SITE, AIKEN, SOUTH CAROLINA

Work performed for

**Westinghouse Savannah River Company**
under
Argonne National Laboratories
Contract No. 21042401

Performance Period
1 May 1992 to 31 October 1992.

Work performed by

James D. Shinn, II
Wesley L. Bratton

Applied Research Associates, Inc.
New England Division
RD1, Box 120A Waterman Rd.
South Royalton, Vermont 05068

## TABLE OF CONTENTS


| Section | | Page |
|---|---|---|
| 1 | PROJECT BACKGROUND | 1 |
| | INTRODUCTION | 1 |
| | M-BASIN SITE DESCRIPTION | 2 |
| | PROJECT SCOPE | 2 |
| | REPORT ORGANIZATION | 3 |
| 2 | TESTING EQUIPMENT AND PROCEDURES | 8 |
| | INTRODUCTION | 8 |
| | PIEZO-ELECTRIC CONE PENETROMETER TEST | 8 |
| | Saturation of the Piezo-Cone | 10 |
| | Field Calibrations | 11 |
| | Penetration Data Format | 12 |
| | DATA EDITING | 13 |
| | Pore Pressure Correction of Tip Stress | 13 |
| | Numerical Editing of the Penetration Data | 14 |
| | RESISTIVITY CONE PENETROMETER TEST | 15 |
| | WATER SAMPLING | 16 |
| | GAS SAMPLING | 16 |
| | STEAM CLEANING | 16 |
| | GROUTING UPON RETRIEVAL | 17 |
| | Self-Grouting Module | 17 |
| | Tremie Grouting Method | 18 |
| 3 | DATA ANALYSIS TECHNIQUES | 24 |
| | SOIL CLASSIFICATION | 24 |
| | HYDRAULIC CONDUCTIVITY | 26 |
| | RELATIVE DENSITY | 27 |
| 4 | DATA DISCUSSION AND ANALYSIS | 33 |
| | FIELD EFFORTS | 33 |
| | DESCRIPTION OF TYPICAL P/R-CPT DATA | 35 |
| | CPT CONSISTENCY | 38 |
| | Deep Penetration Test and the Green Clay Layer | 40 |
| | Typical Cross Section | 41 |
| | Green Clay Contour Maps | 41 |
| | Soil Gas Sampling | 42 |
| 5 | STUDY OF THE INFLUENCE OF DNAPLs ON SURFACE AND DOWNHOLE ELECTRICAL RESISTIVITY | 56 |
| | OVERVIEW | 56 |
| | DC RESISTIVITY MODEL | 57 |

## TABLE OF CONTENTS (CONTINUED)

**Section** **Page**


TYPICAL RESISTIVITY PROPERTIES AND PROFILES AT THE SRS SITE . . . . . 60
WELL LOG RESISTIVITY DATA . . . . . 60
PARAMETRIC DOWNHOLE RESISTIVITY CALCULATIONS . . . . . 61
PARAMETRIC SURFACE RESISTIVITY CALCULATIONS . . . . . 64
SUMMARY OF CALCULATION RESULTS . . . . . 66

6 LABORATORY TEST PROGRAM . . . . . 77
OBJECTIVE OF PROGRAM . . . . . 77
SOIL DESCRIPTIONS . . . . . 77
RESISTIVITY TEST CELL . . . . . 78
EVALUATION OF ARCHIE'S LAW . . . . . 79
RESISTIVITY PREDICTIONS BASED ON DEGREE OF SATURATION . . . . 81
INFLUENCE OF DNAPL ON RESISTIVITY . . . . . 83
FRAMEWORK TO EVALUATE DNAPL CONCENTRATION . . . . . 86
COMPARISON OF PREDICTED AND MEASURED RESISTIVITY DATA . . . 86

7 SUMMARY, CONCLUSIONS AND RECOMMENDATIONS . . . . . 113
SUMMARY . . . . . 113
CONCLUSIONS . . . . . 114
Site Characterization using the P/R-CPT . . . . . 114
Resistivity Data . . . . . 114
Grouting on Retraction and Tremie Grouting of the CPT Sounding . . . . 115
Soil Gas and Groundwater Sampling . . . . . 115
Field Analysis of Soil Gas Samples Using a Multi-Gas Monitor . . . . . 115
Evaluation of a CPT-Based Soil Classification System . . . . . 116
Predictions Using Resistivity Data . . . . . 116
RECOMMENDATIONS . . . . . 116

LIST OF REFERENCES . . . . . 119


**Appendices**


APPENDIX A CPT DATA AND PROPERTIES DERIVED FROM THE DATA

APPENDIX B CPT PREDICTED RESISTIVITY BELOW THE WATER TABLE AND DEGREE OF SATURATION

## LIST OF TABLES


| Table | | Page |
|---|---|---|
| 2.1 | Grout mixture ratios. | 18 |
| 4.1 | Summary of piezocone tests | 34 |
| 5.1 | Resistivities of sediments | 57 |
| 5.2 | SRS Parametric surface resistivity calculations for "clean" and contaminated soil zones | 62 |
| 6.1 | Summary of soils data | 77 |
| 6.2 | Laboratory resistivity cell test results for 40' clay | 89 |
| 6.3 | Laboratory resistivity cell test results for vadose sand | 90 |
| 6.4 | Laboratory resistivity cell test results for saturated sand | 91 |
| 6.5 | Laboratory resistivity cell test results for clayey sand | 92 |
| 6.6 | Laboratory resistivity cell test results for green clay | 93 |
| 6.7 | Fit constants for laboratory resistivity tests on SRS soils | 83 |

## LIST OF FIGURES


| Figure | | Page |
|---|---|---|
| 1.1 | Map showing the location of the Savannah River Site | 5 |
| 1.2 | Proposed cone penetrometer locations | 6 |
| 1.3 | Schematic diagram showing relationship between clay layers and hydrologic features | 7 |
| 2.1 | Schematic of ARA's standard cone penetrometer probe | 19 |
| 2.2 | A typical penetration profile from the SRS site | 20 |
| 2.3 | ARA's water sampler for use with 1.4 inch O.D. cone rods | 21 |
| 2.4 | Soil gas sampling module for use with cone penetration testing | 22 |
| 2.5 | Schematic of ARA's self grouting cone penetrometer | 23 |
| 3.1 | Soil classification system based on ECPT data developed by ARA | 29 |
| 3.2 | Typical analysis profiles developed from ECPT data from the SRS site | 30 |
| 3.3 | Empirical correlation between hydraulic conductivity and soil relative density for a friction ratio $\simeq$ 1 at the Texas site (Chiang, 1992) | 31 |
| 3.4 | Influence of compressibility on N.C. uncemented, unaged, predominantly quartz sands (after Jamiolkowski et. al., 1985) | 32 |
| 4.1 | CPT location map | 43 |
| 4.2 | Plot of typical CPT data from the M-Basin study area | 44 |
| 4.3 | Plot of analysis results from P-ECPT data obtained from the M-Basin study | 45 |
| 4.4 | Overlay of the CPT measurements made at locations 18A (solid line) and 18B (dashed line) | 46 |
| 4.5 | Overlay of the CPT determined parameters made at location 18A (solid line) and 18B (dashed line) | 47 |
| 4.6 | Plot of deep CPT penetration through the green clay layer showing the tip, sleeve, pore pressure and friction ratio | 48 |
| 4.7 | Plot of deep CPT penetration through the green clay layer showing soil resistivity, relative density, hydraulic conductivity and soil classification | 49 |
| 4.8 | Cross-sections of the tip stress profiles at location CPT-09, CPT-07, CPT-05, and CPT-02 in the M-Basin study area | 50 |
| 4.9 | Cross-section of the tip stress profiles at locations CPT-11, CPT-10, CPT-09, CPT-21 and CPT-17 in the M-Basin study area | 51 |
| 4.10 | Contour map of the top of the green clay layer. Map is based solely on CPT data | 52 |
| 4.11 | Contour map of the bottom of the green clay layer. Map is based solely on CPT data | 53 |
| 4.12 | Contour map of the green clay layer. Thickness map is based solely on CPT data | 54 |
| 4.13 | Measured chemical concentrations using soil gas sampling with the ECPT in the M-Basin study area | 55 |
| 5.1 | Resistivity ranges for various terrain materials | 67 |
| 5.2 | 1,2 - dichloroethane vs. electrical conductivity (water analysis, industrial site) | 67 |
| 5.3 | Electrical conductivity of water as a function of DNAPL concentration | 68 |

## LIST OF FIGURES (Continued)


| Figure | | Page |
|---|---|---|
| 5.4 | Typical borehole well log showing both 16" and 64" logs. Near surface logs show bandedge of data. CPT resistivity logs show higher values in the near surface area | 69 |
| 5.5 | Overlay of 64" resistivity data, with average profile overlayed | 70 |
| 5.6 | Comparison of clean site with 5% DNAPL contamination. DNAPL assumed in the clay rich layers | 71 |
| 5.7 | Comparison of clean site with 50% DNAPL contamination. DNAPL assumed in the clay rich layers | 72 |
| 5.8 | Comparison of clean site to a sequence of 5%, 100%, 5% DNAPL contamination. 100% DNAPL layer is two ft thick and lies on top of the green clay layer | 73 |
| 5.9 | Comparison of 4 and 5 layer inversions to original profile. All profiles assume no DNAPL contamination | 74 |
| 5.10 | Comparison of clean baseline resistivity profile to 50% DNAPL forward calculation and inversions using both 4 and 5 layer cases | 75 |
| 5.11 | Comparison of clean baseline profile to profiles with 100% DNAPL just above the green layer | 76 |
| 6.1 | Grain size distribution curves for soil from the SRS integrated demonstration | 94 |
| 6.2 | Schematic of two-ring resistivity cell used to determine soil resistivity as a function of porosity and water content | 95 |
| 6.3 | Comparison of measured soil resistivities versus calculated for the 156 ft clayey sand. Four test series are plotted where the initial moisture content was varied | 96 |
| 6.4 | Comparison of ratio of calculated to measured resistivity as a function of degree of saturation. Data shown for the 156 ft deep clayey sand | 97 |
| 6.5 | Plot of 156 ft depth clayey sand resistivity data as a function of saturation. Fit to the data is superimposed | 98 |
| 6.6 | Plot of vadose zone resistivity test data versus saturation. Fit to the data is superimposed | 99 |
| 6.7 | Plot of saturated sand resistivity test data as a function of saturation. Fit is shown superimposed on the data | 100 |
| 6.8 | Plot of 40 ft clay resistivity test data versus saturation. Fit to the data is superimposed | 101 |
| 6.9 | Plot of green clay resistivity test versus saturation. Fit to the data is superimposed | 102 |
| 6.10 | Comparison of fits to resistivity test data. Average fit is for the 40 ft clay, saturated sand and green clay layers only | 103 |
| 6.11 | Plot of 5% DNAPL test with saturation calculated based on water and DNAPL volume | 104 |

## LIST OF FIGURES (Continued)


| Figure | | Page |
|---|---|---|
| 6.12 | Plot of 5% DNAPL test with saturation calculated based on water volume. Conductive pore space reduced by DNAPL volume | 105 |
| 6.13 | Calculation results showing the influence of DNAPL concentration on soil resistivity for SRS clayey soils | 106 |
| 6.14 | Calculation results showing the influence of DNAPL concentration on soil resistivity for the SRS vadose sand | 107 |
| 6.15 | Framework for evaluating DNAPL concentration from CPT technique | 108 |
| 6.16 | Comparison of predicted and measured resistivities below the groundwater table and of predicted degrees of saturation for sounding CPT-017 | 109 |
| 6.17 | Comparison of predicted and measured resistivities below the groundwater table and of predicted degrees of saturation for sounding CPT-004 | 110 |
| 6.18 | Comparison of predicted and measured resistivities below the groundwater table and of predicted degrees of saturation for sounding CPT-015A | 111 |
| 6.19 | Comparison of predicted and measured resistivities below the groundwater table end of predicted degrees of saturation for sounding CPT-003 | 112 |
| 7.1a | Diffusion coefficients for Hanford soils under the Landfill site showing strong dependence on water content and weak dependence on soil type | 118 |
| 7.1b | Hydraulic conductivity results for the same soils showing dependence on both soil type and water content | 118 |

# SECTION 1
# PROJECT BACKGROUND

## INTRODUCTION

This report documents the results of a combined field and laboratory investigation program to: 1) delineate the geologic layering and 2) determine the location of a dense non-aqueous liquid-phase (DNAPL) contaminated plume beneath the M Area Hazardous Waste Management Facility at the Savannah River Plant. During April of 1991, DNAPLs were detected in monitoring well (MSB-3D), located adjacent to the capped M-Area Settling Basin. Solvents in the well consisted mainly of tetrachloroethylene (PCE) and trichloroethylene (TCE), which are also the main solvents found in groundwater in the M Area. In permeable soils, DNAPLs move downward rapidly due to their high density and low viscosity as compared to water. Within the vadose zone, DNAPLs tend to be held by the less permeable clay and silts by capillary force. In the saturated zone, the downward movement is slowed by clays and silts and the DNAPL tends to pool on this layer, then spread laterally. The lateral movement continues until a permeable layer is encountered, which can be a sand lens, fault, fracture or other high conductivity seam. The DNAPL then moves downward, until another low permeability layer is encountered (Westinghouse Savannah River Company, 1992). Prediction of the lateral and vertical spread of an M Area DNAPL plume requires detailed mapping of both the lateral and vertical soil stratigraphy and hydraulic conductivity.

Applied Research Associates was contracted by the Westinghouse Savannah River Company (WSRC) through the Department of Energy Argonne National Laboratory to conduct a program to: 1) field demonstrate the utility of Cone Penetration Technology (CPT) to investigate DOE contaminant sites and, 2) conduct a laboratory and field program to evaluate the use of electric resistivity surveys to locate DNAPL contaminated soils. The field program was conducted in the M-Basin and laboratory tests were conducted on samples from the major stratigraphy units as identified in Eddy et. al, 1991. Cone Penetration Technology was selected to investigate the M-Basin as it: 1) is minimally invasive, 2) generates minimal waste, 3) is faster and less costly than drilling, 4) provides continuous,

detailed in situ characterization data, 5) permits real-time data processing, and 6) can obtain soil, soil gas and water samples without the need for a boring.

## M-BASIN SITE DESCRIPTION

The Department of Energy Savannah River Plant is located near Aiken, South Carolina, with the M-Basin located south of the SRS administrative area as shown in Figure 1.1. Locations of borings and proposed CPT soundings are plotted in Figure 1.2. Soils at the Savannah River Plant are approximately 1,000 ft thick and are dominated by the Atlantic Coastal Plain. The site is stratified with the soil type and thickness highly variable in both the lateral and vertical direction. Soils at the site were deposited in shallow marine environments during the Middle to Upper Eocene (Eddy et. al, 1991), and vary from clean sands, clayey sands to sandy clays.

Previous studies of the site (Eddy et. al., 1991) have identified four clay layers with the top of these clay layers at nominal elevations of 325 ft, 300 ft, 270 ft, and 200 ft. These clays are generally referred to as the 325 ft clay, 300 ft clay, tan clay zone at elevation 270 ft, and green clay at elevation 200 ft. The upper two clays are discontinuous and the lower clays are regionally continuous. The tan clay zone is observed in all of the well data, not as a continuous zone, but as a sequence of interbedded sandy clays and clayey sands. The green clay is the confining unit that separates the semi-confined aquifer from the confined aquifer in the M-Basin study area (Eddy et. al., 1991). The water table is located at a nominal elevation of 230 ft, approximately 140 ft below the ground surface. A generalized schematic of the site geology is given in Figure 1.3.

## PROJECT SCOPE

A principal objective of this project was to demonstrate the Synergistic Site Characterization Method developed by ARA for the Argonne National Laboratory, as well as gathering data for use in defining the site geology. The project is divided into three phases: 1) field testing consisting of CPT and surface resistivity surveys and field data analysis; 2)

laboratory investigation of the soils from the study area to evaluate the influence of DNAPLs on the electrical properties of soils and an analysis of the data to evaluate the utility of surface resistivity for locating DNAPLs, and 3) analysis of the CPT data and laboratory data to develop 2- and 3-D maps of the site stratigraphy. Specific objectives which were achieved and presented in this report are:

- Soil characterization using the piezo-CPT
- Resistivity measurements using the CPT
- Grouting on retraction and tremie grouting of the CPT sounding
- Soil gas and groundwater sampling
- Field analysis of soil gas samples using a multi-gas monitor
- Evaluation of a CPT-based soil classification system
- Preliminary predictions of hydraulic conductivities and soil resistivity below the water table and vadose zone degree of saturation

Data from the field and laboratory investigation programs were entered into TechBase®, a geologic database system that was used to analyze the data and to prepare two and three dimensional representations of the site stratigraphy.

## REPORT ORGANIZATION

Section 2 of this report contains a description of the CPT testing method which documents the field techniques, calibration methods, grouting methods and data acquisition system. Section 3 documents the methods used to derive properties and stratigraphy from the CPT data. Discussion of the efforts during the field testing program, along with a discussion of the data are presented in Section 4. Also presented in Section 4 is an evaluation of the CPT-based soil classification system, cross-sections showing stratigraphy, contour plots of the green clay layer and a discussion of the hydraulic conductivities calculated based on CPT data. Volume rendering of the calculated low and high hydraulic conductivity zones are also presented.

Section 5 contains a discussion of the analysis to evaluate the utility of surface resistivity surveying to locate DNAPL plumes. The laboratory test program and analysis of the resistivity soil model are discussed in Section 6, as well as an analysis of the CPT resistivity data. Section 7 contains the Summary, Conclusions and Recommendations. Appendix A contains profiles of both the CPT data and properties derived from this data. Appendix B contains the properties derived from the electric resistivity data.

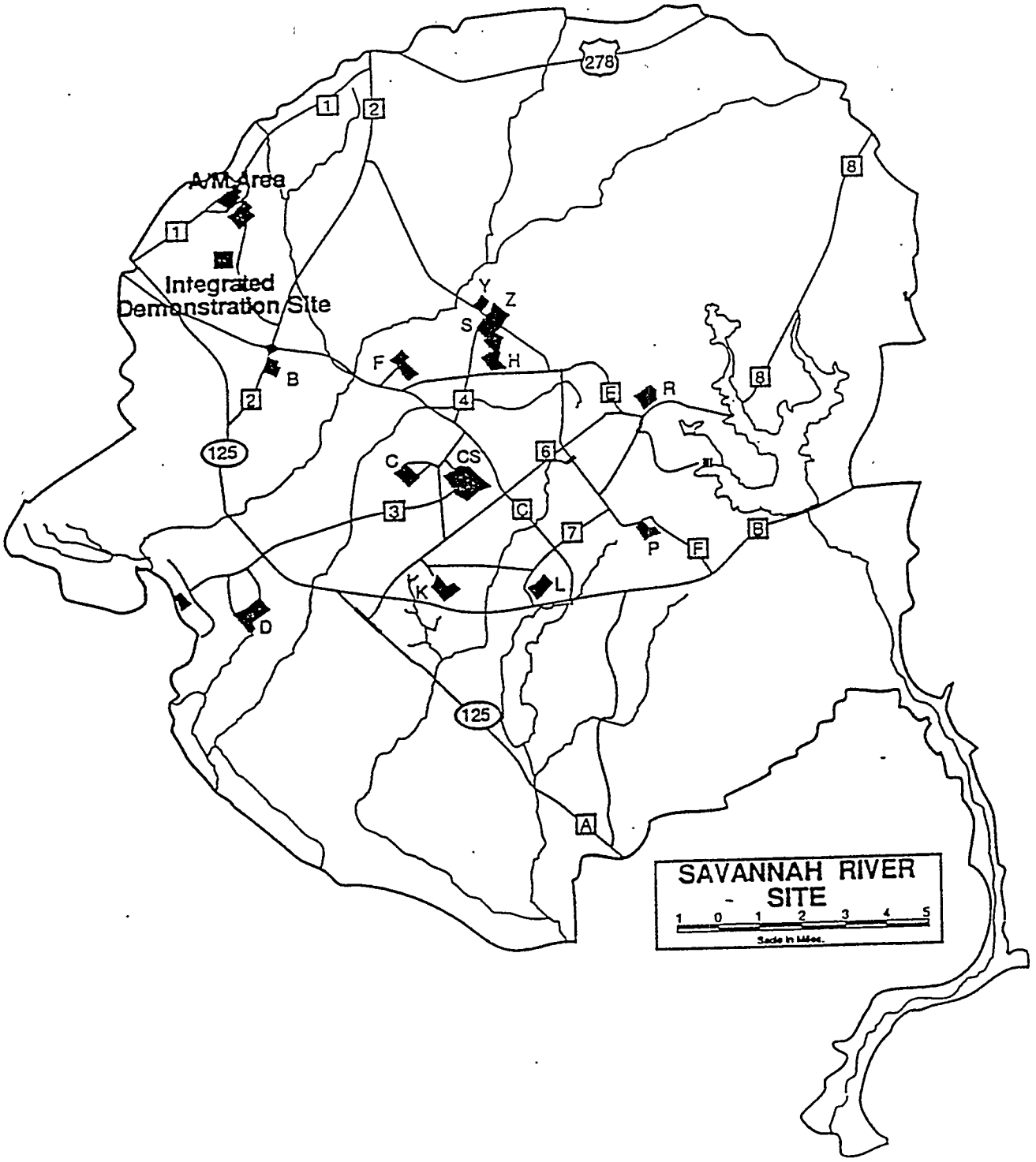


Figure 1.1. Map showing the location of the Savannah River Site.(Eddy, et. al., 1991).

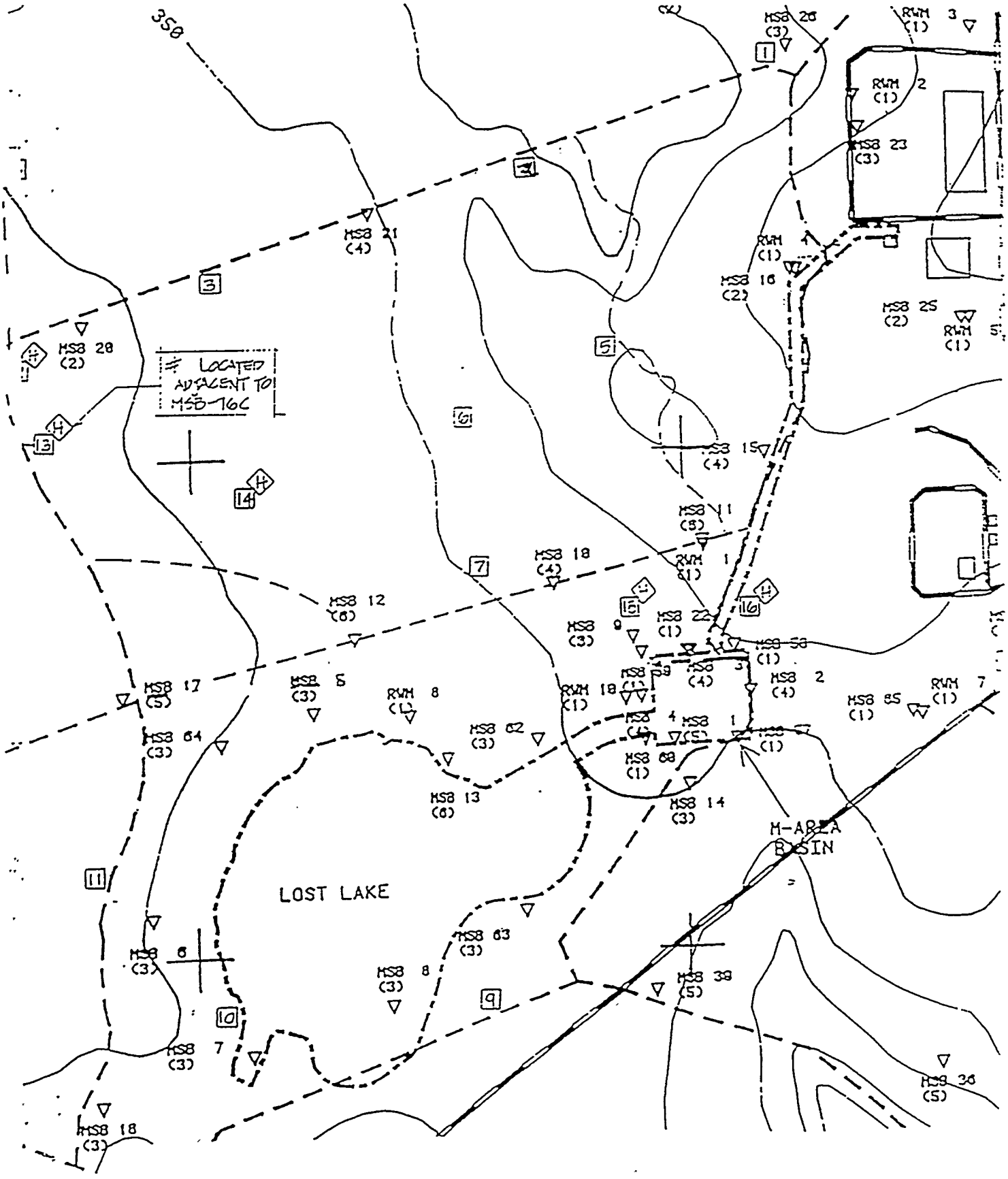


Figure 1.2. Proposed cone penetration locations (WSRC, 1992).

- BORING LOCATION/ STRATIGRAPHY

- HYDROPUNCH/ GROUNDWATER SAMPLING

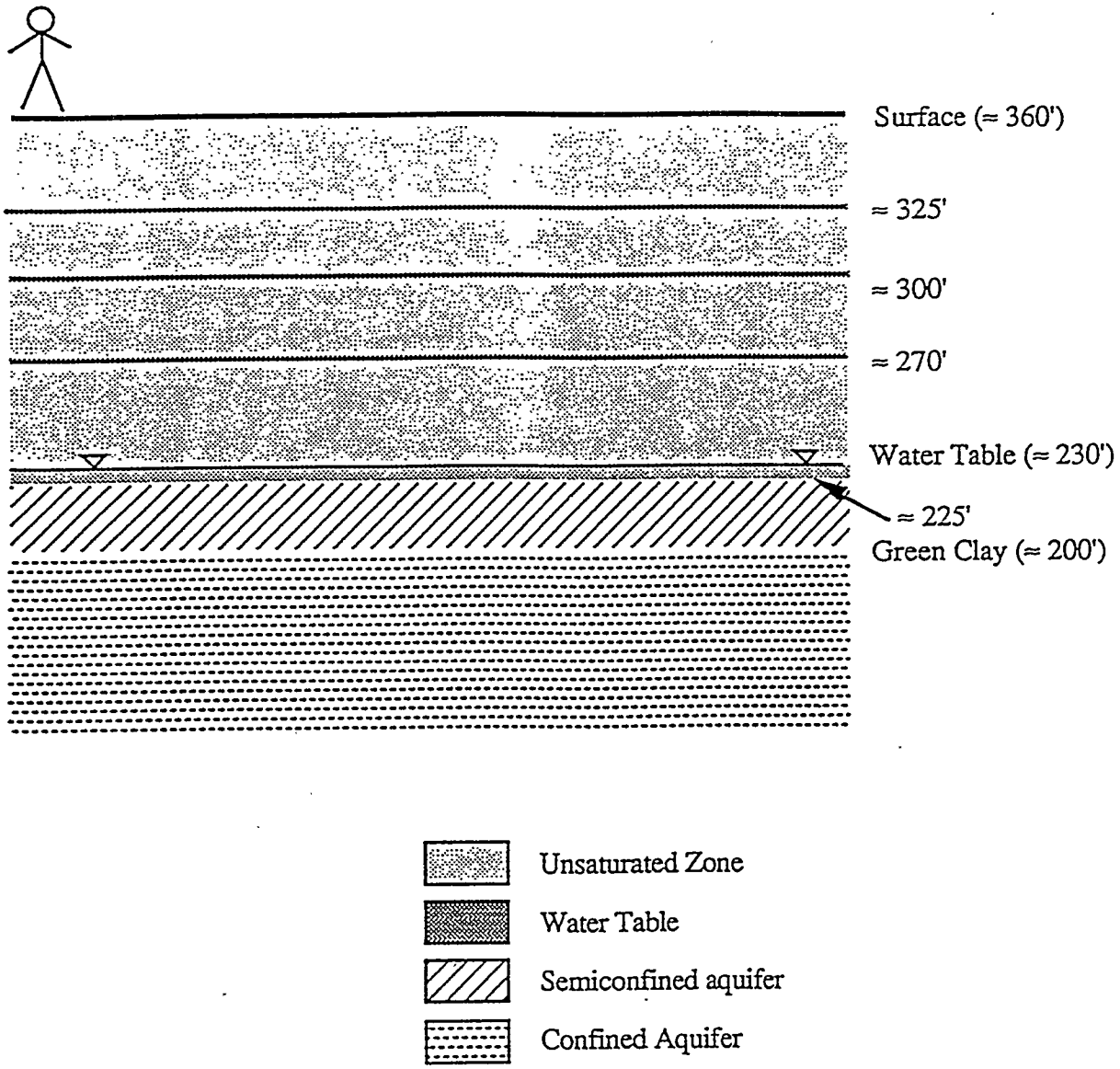


Figure 1.3. Schematic diagram showing relationship between clay layers and hydrologic features (Eddy et. al., 1991).

# SECTION 2
# TESTING EQUIPMENT AND PROCEDURES

## INTRODUCTION

The electronic cone penetrometer test (ECPT) was originally developed for use in consolidated clay soils. Over the years, cone and push system designs have evolved to the point where they can now be used in strong cemented soils and even soft rock. ARA's penetrometer consists of an instrumented probe which is forced into the ground using a hydraulic load frame mounted on a heavy truck with the weight of the truck providing the necessary reaction mass. The probe has a conical tip and a friction sleeve which independently measures vertical resistance beneath the tip as well as frictional resistance on the side of the probe as functions of depth. A schematic view of ARA's penetrometer probe is shown in Figure 2.1. A pressure transducer in the cone is used to measure the pore water pressure as the probe is pushed into the ground (Piezo-ECPT). The probe may also include three seismic transducers, which are used to perform downhole seismic surveys. In addition, a resistivity module may be attached to the cone assembly to measure variances in soil conductance, which assists in locating contamination plumes.

## PIEZO-ELECTRIC CONE PENETROMETER TEST

The cone penetrometer tests are conducted using the ARA penetrometer truck. The penetrometer equipment is mounted inside a 18 ft van body attached to a ten-wheel truck chassis with a turbo-charged diesel engine. Ballast in the form of metal weights and a steel water tank, which can hold 5,000 lbs of water, are added to the truck to achieve an overall push capability of 45,000 lbs. This push capacity is limited in strong soils by the structural bending capacity of the 1.405 in OD push rods, and not the weight of the truck. There is the possibility of the push rods buckling, which is the reason for the current 45,000 lb limitation. Penetration force is supplied by a pair of large hydraulic cylinders bolted to the truck frame.

The penetrometer probe is of standard dimensions having a 1.405 in diameter, 60° conical tip, and a 1.405 in diameter by 5.27 in long friction sleeve. The shoulder between the base of the tip and the porous filter is 0.08 in long. A 1.5 in expander, located 5.25 in behind the top of the friction sleeve, pushes the penetration hole open and reduces the frictional drag on the push tubes behind the probe. The penetrometer is normally advanced vertically into the soil at a constant rate of 48 in/min, although this rate must sometimes be reduced as hard layers are encountered. The electronic cone penetrometer test is conducted in accordance with ASTM D3441.

Inside the probe (see Figure 2.1), two load cells independently measure the vertical resistance against the conical tip and the side friction along the sleeve. Each load cell is a cylinder of uniform cross section inside the probe which is instrumented with four strain gages in a full-bridge circuit. Forces are sensed by the load cells and the data are transmitted from the probe assembly via a cable running through the push tubes. The analog data are digitized, recorded, and plotted by computer in the penetrometer truck. A set of data is normally recorded each second, for a minimum resolution of about one data point every 0.8 in of cone advance. The depth of penetration is measured using a string potentiometer mounted on the push frame.

As shown in Figure 2.1, the piezo-cone probe senses the pore pressure immediately behind the tip. Currently, there is no accepted standard for the location of the sensing element. ARA chose to locate the sensing element behind the tip as the filter is protected from the direct thrust of the penetrometer and the measured pore pressure can be used to correct the tip resistance data (discussed below) as recommended by Robertson and Campanella (1988). The magnitude of the penetration pore pressure is a function of the soil compressibility and, most importantly, permeability. In freely draining soil layers, the measured pore pressures will be very close to the hydrostatic pressure computed from the elevation of the water table. When low permeability soil layers are encountered, excess pore pressures generated by the penetration process can not dissipate rapidly and this results in measured pore pressures which are significantly higher than the hydrostatic pressures. Whenever the penetrometer is stopped to add another section of push tube, or when a pore

pressure dissipation test is run, the excess pore pressure may begin to dissipate. When the penetration is resumed, the pore pressure quickly rises to the level measured before the penetrometer was stopped. This process causes some of the spikes that may appear in the penetration pore pressure data.

Electronic data acquisition equipment for the cone penetrometer consists of an IBM compatible 486 computer with a graphics monitor and a rack of eight customized signal conditioners. Analog signals are transmitted from the probe to the signal conditioners where the ECPT data are amplified and filtered at 1 Hz. Seismic signals are amplified as required and filtered at 1000 Hz. Once amplified, the analog signals are transmitted to a MetraByte Hi Res 16 bit high speed analog-to-digital converter board, where the signals are digitized; usually at the rate of one sample per second for the penetration data and 5,000 samples per second for the seismic data. The digital data are then read into memory, plotted on a graphics monitor, and written to the internal hard disk for future processing. Data displayed on screen can be used to determine site layering as it is encountered. This allows important decisions to be made in real-time directly in the field. Upon completion of the test, the penetration, dissipation, and resistivity data are plotted. Plots can typically be available within 30 minutes of completing the test. Floppy disks containing the data are brought to ARA's New England Division in South Royalton, Vermont, for preparation of final report plots and analysis.

### Saturation of the Piezo-Cone

As shown in Figure 2.1, penetration pore pressures are measured with a pressure transducer located behind the tip in the lower end of the probe. Water pressures in the soil are sensed through a 250 $\mu$in porous polyethylene filter which is 0.25 in high and 0.202 in thick. The pressure transducer is connected to the porous filter through a pressure port as shown in Figure 2.1. The pressure port and the filter are filled with a high viscosity silicone oil.

In order for the pressure transducer to respond rapidly and correctly to changing pore pressures upon penetration, the filter and pressure port must be saturated with oil upon assembly of the probe. A vacuum pump is used to de-air the silicone oil before use and also to saturate the porous filters with oil. The probe is assembled with the pressure transducer up and the cavity above the pressure transducer filled with de-aired oil. A previously saturated filter is then placed on a tip and oil is poured over the threads. When the cone tip is then screwed into place, excess oil is ejected through the pressure port and filter thereby forcing out any trapped air.

Saturation of the piezo cone is verified with field calibrations performed before the probe is inserted into the ground. The high viscosity of the silicone oil coupled with the small pore space in the filter prevents the loss of saturation as the cone is pushed through dry soils. Saturation of the cone can be verified with a calibration check at the completion of the penetration. Extensive field experience has proven the reliability of this technique with no known case where saturation of the piezo-cone was lost.

## Field Calibrations

Many factors can effectively change the calibration factors used to convert the raw instrument readouts, measured in volts, to units of force or pressure. As a quality control measure, as well as a check for instrument damage, the load cells, the pressure transducer, and the resistivity sensor are routinely calibrated in the field. Calibrations are completed with the probe ready to insert into the ground so that any factor affecting any component of the instrumentation system will be included and detected during the calibration.

The tip and sleeve load cells are calibrated with the conical tip and friction sleeve in place on the probe. For each calibration, the probe is placed in the push frame and loaded onto a precision reference load cell. The reference load cell is periodically calibrated in ARA's laboratory against NIST traceable standards. To calibrate the pore pressure transducer, the saturated probe is inserted into a pressure chamber with air pressure supplied by the compressor on the truck. The reference transducer in the pressure chamber is also

periodically calibrated against an NIST traceable instrument in ARA's laboratory. Additionally, the string potentiometer, used to measure the depth of penetration, is periodically checked against a tape measure.

Each instrument is calibrated using a specially-written computer code that displays the output from the reference device and the probe instrument in graphical form. During the calibration procedure, the operator checks for linearity and repeatability in the instrument output. At the completion of each calibration, this code computes the needed calibration factors using a linear regression algorithm. At a minimum, each probe instrument is calibrated at the beginning of each day of field testing. Furthermore, the pressure transducer is recalibrated each time the porous filter is changed and the cone is resaturated. Calibrations are also performed to verify the operation of any instrument if damage is suspected.

### Penetration Data Format

A penetration profile, from the SRS site, is shown in Figure 2.2. Plotted as a function of elevation are the measured tip resistance, sleeve friction, friction ratio, and pore pressure. When the surface elevation of the test location is unknown, the penetration data is plotted against depth.

Tip resistance, $q_c$ (lb/in$^2$), is obtained by dividing the vertical force on the conical tip by the effective tip area (1.550 in$^2$). The tip resistance is then corrected for pore pressures acting behind the conical tip as discussed in the next section. The corrected tip resistance, $q_T$ (lb/in$^2$), is plotted in the penetration profile. Sleeve friction, $f_s$ (lb/in$^2$), is obtained by dividing the total frictional force on the sleeve by the sleeve's surface area (23.26 in$^2$). The offset between the depth at the tip and the depth at the friction sleeve is corrected by shifting the sleeve friction profile downward so that it corresponds to the depth at the centroid of the tip. In addition to the tip resistance and sleeve friction, a friction ratio profile is plotted for each location. This ratio is simply the sleeve friction expressed as a percentage of the tip resistance at a given depth. In uncemented soils, the friction ratio can be correlated to soil

type. The final profile shown in Figure 2.2 is the pore pressure that is measured as the probe is advanced. This measurement is useful for identifying clay layers as the pore pressure rises significantly above the hydrostatic level.

## DATA EDITING

### Pore Pressure Correction of Tip Stress

Cone penetrometers, by necessity, must have a joint between the tip and sleeve. Pore pressure acting behind the tip decreases the total tip resistance that would be measured if the penetrometer was without joints. The influence of pore pressure in these joints is compensated for by using the net area concept (Robertson and Campanella, 1988). The corrected tip resistance is given by:

$$q_T = q_c + u\left[1 - \frac{A_n}{A_T}\right] \tag{2.1}$$

where:

$q_T$ = corrected tip resistance

$q_c$ = measured tip resistance

u = penetration pore pressure measured behind the tip

$A_n$ = net area behind the tip not subjected to the pore pressure (1.257 $in^2$)

$A_T$ = projected area of the tip (1.550 $in^2$).

Hence, for the ARA cone design, the tip resistance is corrected as:

$$q_T = q_c + u(.1890) \tag{2.2}$$

Laboratory calibrations have verified Equation 2.2 for ARA's piezo-cone design.

A joint also exists behind the top of the sleeve (see Figure 2.1). However, since the sleeve is designed to have the same cross sectional area on both ends, the pore pressures

acting on the sleeve cancel out. Laboratory tests have verified that the sleeve is subjected to equal end area effects. Thus, no correction for pore pressure is needed for the sleeve friction data.

The net effect of applying the pore pressure correction is to increase the tip resistance and to decrease the friction ratio. Generally, this correction is only significant when the pore pressures are high while measured tip resistance is very low.

### Numerical Editing of the Penetration Data

Any time that the cone penetrometer is stopped or pulled back during a test, misleading data can result. For instance, when the probe is stopped to add the next push tube section, or when a pore pressure dissipation test is run, the excess pore pressures will dissipate toward the hydrostatic pore pressure. When the penetration is resumed, the pore pressure generally rises very quickly to the pressures experienced prior to the pause in the test. In addition, the probe is sometimes pulled back and cycled up and down at intervals in deep holes to reduce soil friction on the push tubes. This results in erroneous tip stress data when the cone is advanced in the previously penetrated hole.

To eliminate this misleading data from the penetration profile, the data is numerically edited before it is plotted or used in further analysis. Each time the penetrometer stops or backs up, as apparent from the depth data, the penetration data is not plotted. Plotting of successive data is resumed only after the tip is fully re-engaged in the soil by one tip length (1.22 in) of new penetration. This algorithm also eliminates any data acquired at the ground surface before the tip has been completely inserted into the ground. The sleeve data is similarly treated and this results in the first data point not occurring at the ground surface, as can be seen in some tip and sleeve profiles. These procedures ensure that all of the penetration data that is plotted and used for analysis was acquired with the probe advancing fully into undisturbed soil. Gaps in the data will exist when repeated cycling and only very short gains in depth are achieved. To avoid this situation, heavy weight push vehicles should be used. These vehicles have sufficient push capacity to avoid excessive cycling.

## RESISTIVITY CONE PENETROMETER TEST

Resistivity, one of the oldest geophysical exploration techniques, was originally developed to locate mineral and oil deposits and ground water supplies. The measurement principal exploited by resistivity surveying is that an electrical contrast exists between different geological materials and that this electrical contrast can be used to identify and locate geologic materials. Resistivity surveys are being increasingly used in contaminated site investigation programs to delineate the extent and degree of contamination at a site. These surveys rely on the electric contrasts that typically exist between contaminated soils and uncontaminated soils. For example, leachate from a landfill will contain a higher concentration of dissolved solids, which will decrease the resistivity of the groundwater (Shinn, 1990). Soils contaminated with hydrocarbons (fuel oils, cleaning solvents, etc.) will typically have higher resistivity than uncontaminated soils as the hydrocarbon can act as an insulator.

The Resistivity-ECPT (R-ECPT) is an adaptation of conventional borehole tools. The R-ECPT probe is in direct contact with the soil and pore fluid which eliminates two problems associated with borehole resistivity surveys; 1) intrusion of drilling fluids into borehole walls which changes the resistivity of the media and 2) the requirement that any casing material be non-conducting.

Figure 2.1 is a schematic of ARA's R-ECPT probe. The probe consists of 4 electrodes separated by high strength (Kevlar-nylon) plastic reinforced insulators. The outer two electrodes induce an electric current into the soil and the inner two electrodes measure the potential drop, which is proportional to the resistivity of the soil. To avoid polarization effects the four electrode array is operated at a frequency of 40 HZ. Electronics in the CPT vehicle are used to modulate and demodulate the current and potential measurement signals to and from the probe. The probe is calibrated in a large water solution in which the conductivity is varied. The data from the calibration tests is used to determine the probe calibration factor, which is dependent on the probe geometry.

## WATER SAMPLING

Using cone penetrometer technology, groundwater samples can be efficiently obtained from specific depths. The water samples are obtained by pushing a hollow rod with a sampling tip down to the desired depth. The rods are then retracted 6 to 12 inches, exposing a stainless steel filter, as shown in Figure 2.3. The filter allows groundwater to enter the rods. The water samples are then bailed using a bottom filling Teflon® bailer. Samples are then labeled and properly stored to ensure sample quality.

## GAS SAMPLING

If samples are to be obtained from above the water table, a stainless steel or plastic filter, as shown in Figure 2.4, can be used to obtain gas samples as the cone is both inserted and retrieved. This is accomplished by connecting one end of a flexible teflon tube to the sampling module and the other end to a vacuum pump. Using a vacuum pump located in the penetrometer truck, gas samples can be obtained at any desired depth, or continuously during the penetration with the gas stream being directed to a measurement device.

The measurement device used at SRS was a gas monitor developed by Bruel and Kjaer. This device operates on photoacoustic technology and has detection limits down to 0.2 ppm and 0.03 ppm for trichloroethylene (TCE) and tetrachloroethylene (PCE), respectively. The advantages of this device were that it would accept a continuous gas stream and make periodic measurements with a measurement time of typically under one minute, allowing a chemical concentration profile of the contaminants to be determined.

## STEAM CLEANING

To prevent the possibility of cross-contamination between boreholes and also to ensure worker safety, the rods are steam cleaned after removal from the ground and prior to entering the truck. This operation takes place by drawing all the rods up through the steam cleaning module located on the bottom of the guide tube. High pressure hot water is applied

to the rods in a swirling motion only as the rods are being drawn up. This operating process minimizes the amount of water used. The waste water generated can either be collected or allowed to return down the hole as directed by the client.

## GROUTING UPON RETRIEVAL

Cone penetration testing, by nature of the test, leaves holes which represent potential contamination pathways for surface and subsurface contaminants to enter the groundwater and also for contaminated soil vapors to enter the atmosphere. To prevent these types of contamination, the test holes must be grouted to seal the hole and eliminate the contaminant pathway. Grouting of the CPT hole upon retraction increases worker safety and reduces risks to the environment. Due to the importance of retraction grouting, ARA operates two different grouting methods. The first method involves use of our self-grouting module. This module also allows grouting to be performed on retrieval of the cone equipment, saving time. The other method is a tremie grouting method and requires a second push to place the grout rods in the hole.

### Self-Grouting Module

The self-grouting method involves a grouting module located behind the instrumented portion of the cone. This module allows the full complement of CPT instrumentation to be used (i.e., resistivity, seismic and pore pressure), however, the diameter of the module is larger than the push rod's, and therefore requires higher push forces. The schematic for this module is shown in Figure 2.5. The module is connected to a flexible tube which runs through the center of the push rods. Upon retrieval of the cone the protective sleeve slides off of the probe, exposing the grouting holes and a grout mixture is pumped under pressure down the tube to the grouting modules. As the cone is retracted, the cavity is filled with grout. This process is continued until the cone is fully removed from the penetration hole. Records are kept in the field log book of the amount of grout pumped into the hole. The volume of grout pumped is compared to the volume of the hole to determine the effectiveness of the grouting. This method is the more efficient but requires the use of larger diameter

push tubes thereby increasing the total penetration force needed to attain the desired test depth. When cycling, the slide ring in Figure 2.5 can move, exposing the grout ports to soil and increasing the likelihood of jamming the grout ports. Therefore, cycling should be minimized with this method.

### Tremie Grouting Method

The tremie grouting method requires that the instrumented cone be fully retracted from the hole and then empty push tubes (not containing a cable or cone tip) are pushed down the same hole. Once the empty push tubes are advanced to the same depth as the ECPT, a flexible tube is inserted into the top of the tubes and grout is pumped down the core. As the grout is pumped, the rods are retracted and removed from the stack. Grout is continuously pumped into the hole until the hole is full. The volume of grout used is recorded in the field log book.

The same grout mixture is used for all grouting methods. The grout mixture ratios are shown in Table 2.1. The grout mixture used consists of a standard ratio of water to cement to create a neat cement mixture. This material is easily obtained and commonly accepted on many environmental sites.

**Table 2.1. Grout mixture ratios.**

| | |
|---|---|
| Cement | One 94 lb bag |
| Water | 6 gallons |

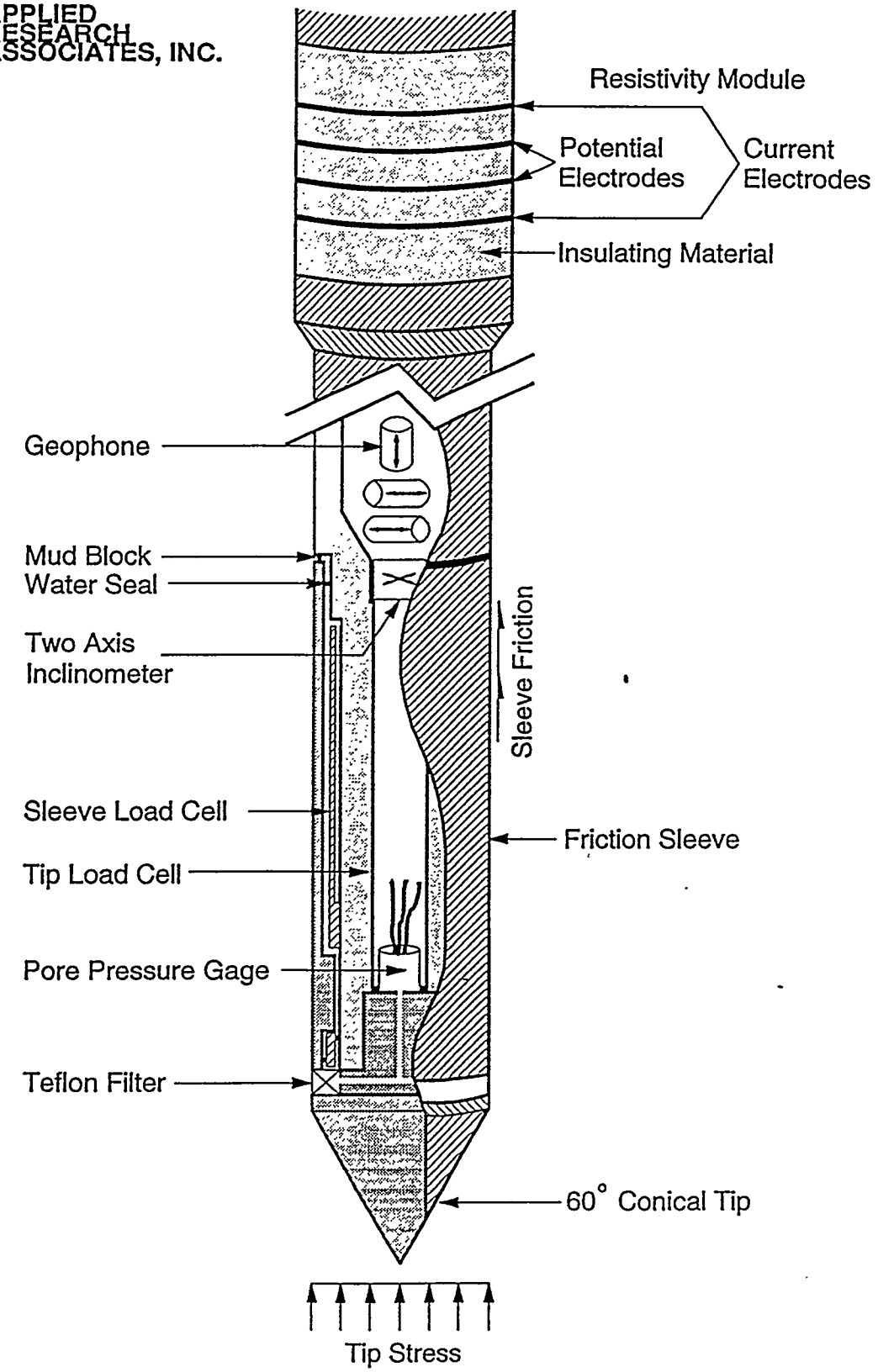


Figure 2.1. Schematic of ARA's cone penetrometer probe.

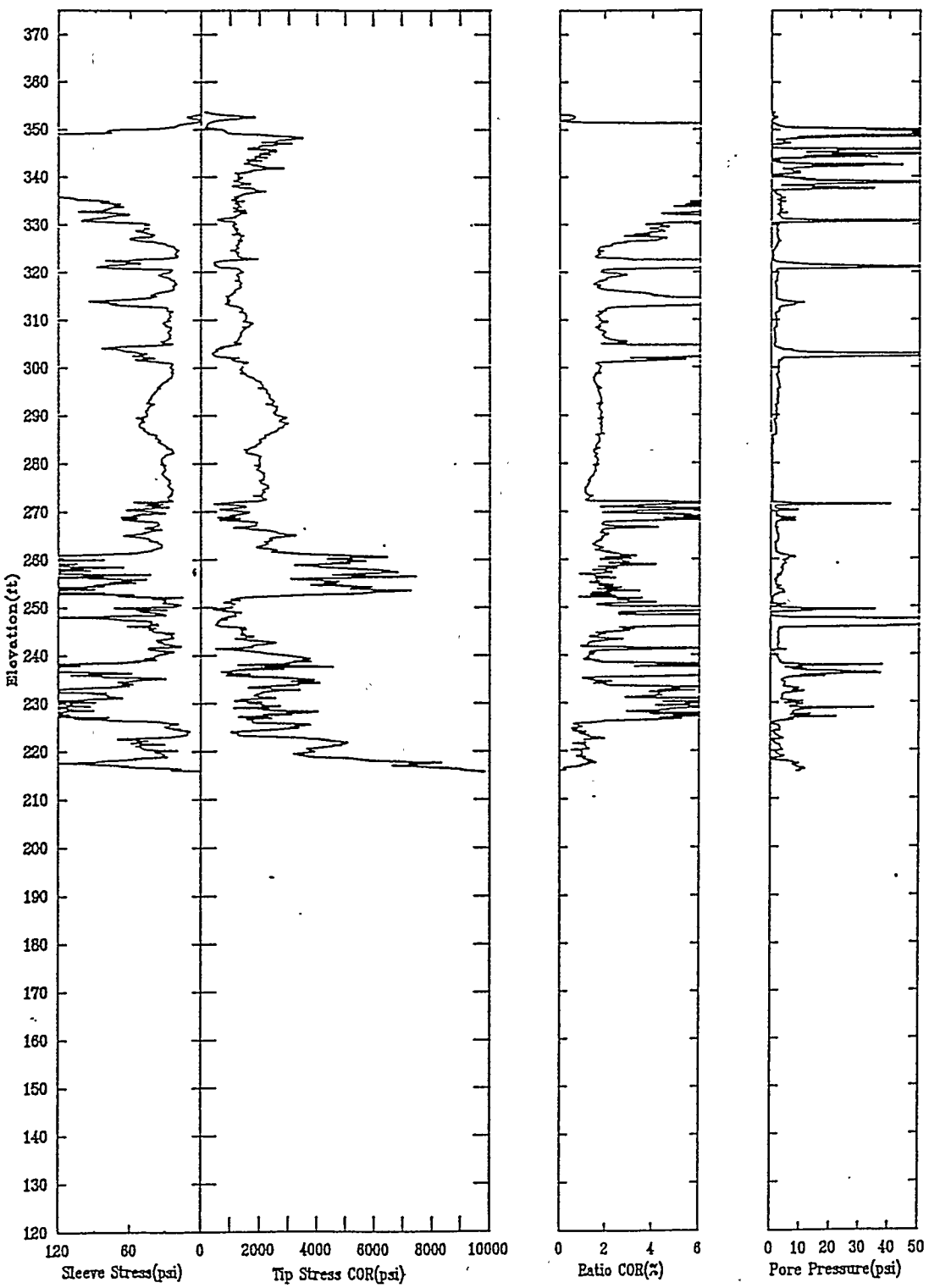


Figure 2.2. A typical penetration profile from the SRS site.

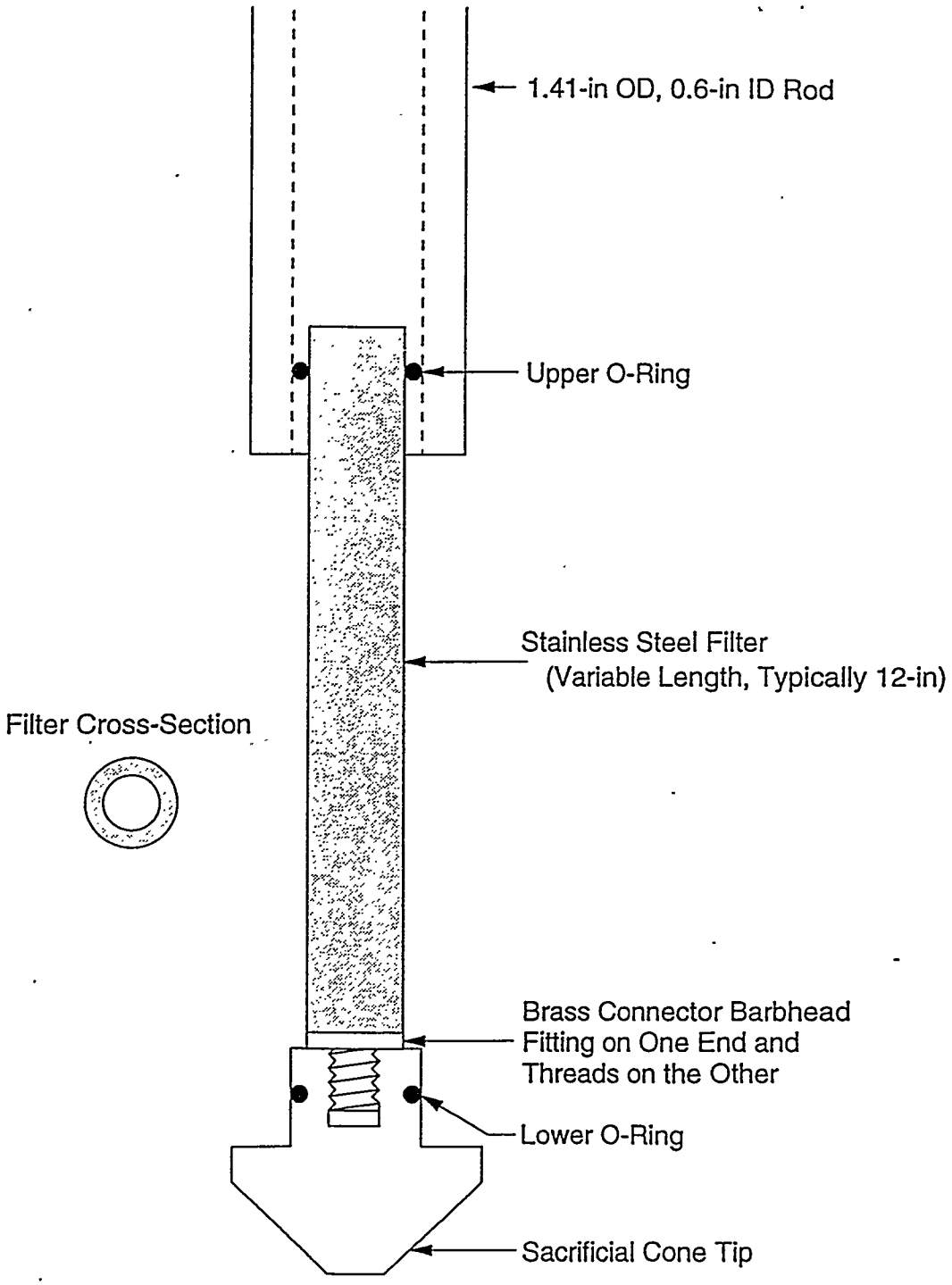


Figure 2.3. ARA's water sampler for use with 1.4 inch O.D. cone rods.

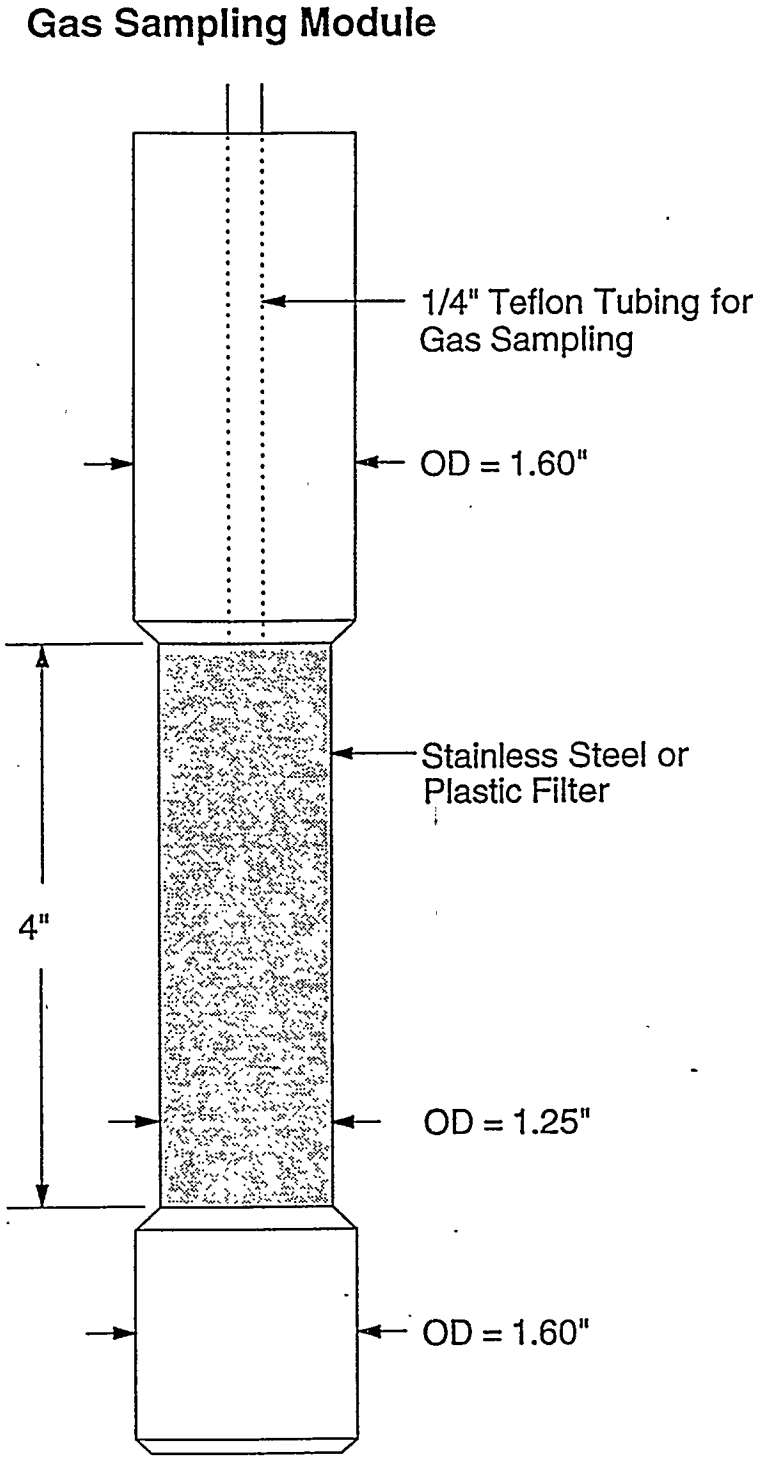


Figure 2.4. Soil gas sampling module for use with cone penetration testing.

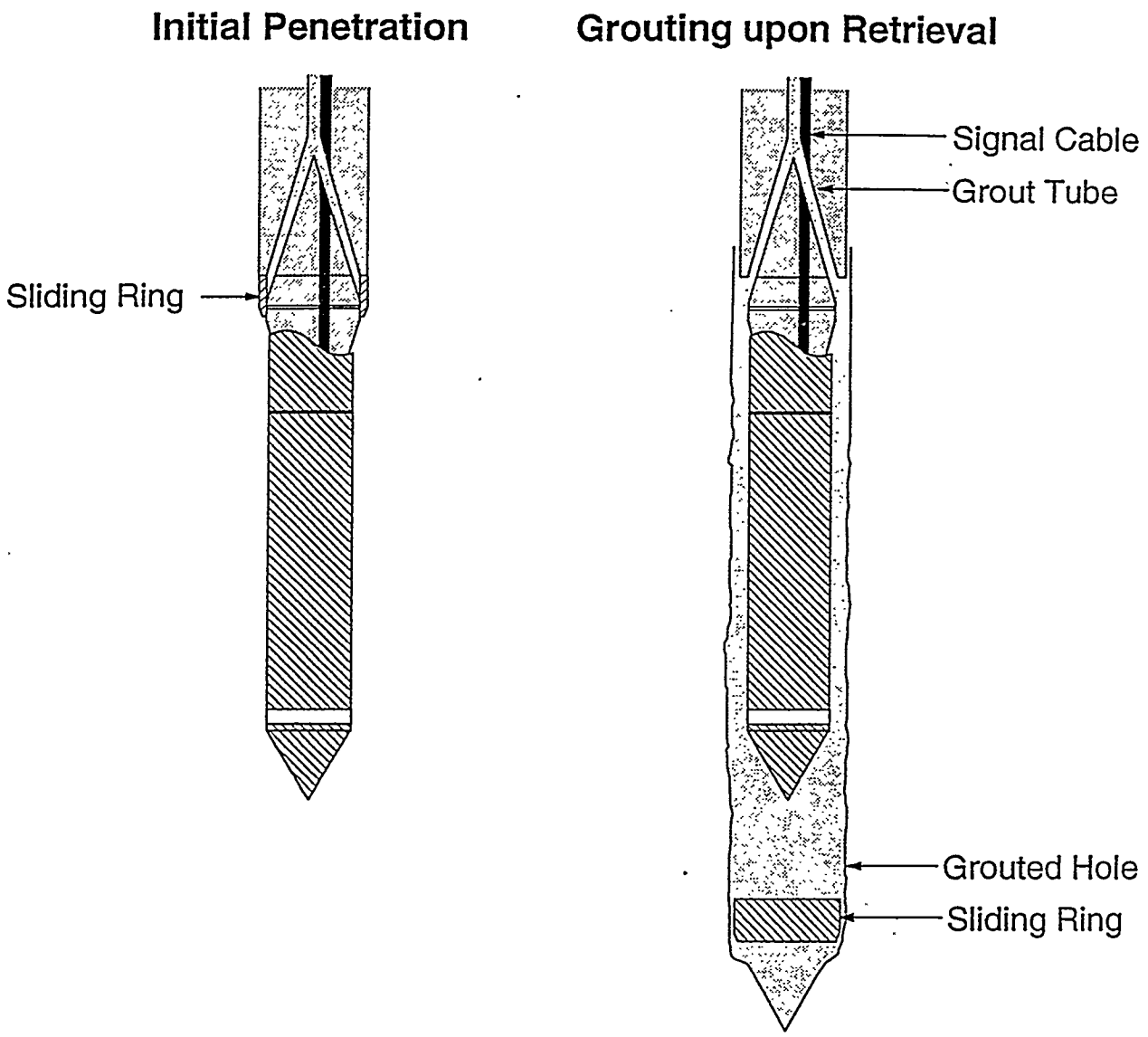


APPLIED RESEARCH ASSOCIATES, INC.

Figure 2.5. Schematic of ARA's self grouting cone penetrometer.

# SECTION 3
# DATA ANALYSIS TECHNIQUES

This section describes the various techniques and models used to interpret ECPT data and to estimate in situ soil properties. Application of these techniques to the 25 sites indicated in Table 4.1 are described in Section 4.

## SOIL CLASSIFICATION

The tip resistance, friction ratio, and pore pressure values from ECPT profiles can be used to determine soil classification versus depth. The methodology used in this report to classify the soils is based on specific empirical correlations that were described in Timian, 1992, and are summarized in the two charts shown in Figure 3.1. In general, clean, coarse grained soils have high strengths with relatively low sleeve friction, while finer grained soils have low strengths and high side friction (cohesion). Similarly, as shown in the second chart of Figure 3.1, a correlation exists between soil type and the ratio of tip stress to pore pressure response. Clean, coarse grained soils tend to have high strengths, but are permeable and develop little or no excess pore pressure during penetration. Fine grained soils are weak and impermeable and tend to develop high excess pore pressures during penetration.

Soil classification can be determined from the charts by comparing the normalized tip resistance to the pore pressure ratio or to the normalized friction ratio. The tip resistance is normalized according to:

$$q_n = \frac{q_T - \sigma_{vo}}{\sigma_{vo}'} \tag{3.1}$$

where:

$q_n$ = normalized tip stress

$q_T$ = corrected tip resistance from Equation 2.2

$\sigma_{vo}$ = total overburden stress

$\sigma_{vo}'$ = effective overburden stress

The pore pressure ratio, $B_q$, is defined as:

$$B_q = \frac{u_{meas} - u_o}{q_T - \sigma_{vo}} \tag{3.2}$$

where: $u_{meas}$ = measured penetration pore pressure

$u_o$ = static pore pressure, determined from the water table elevation

and the normalized friction ratio, $f_{SN}$ is defined as:

$$f_{SN} = \frac{f_s}{q_T - \sigma_{vo}} \; x \; 100\% \tag{3.3}$$

The plot of any point of the $q_n$ versus $B_q$ or $f_{SN}$ value normally falls in a classification zone of Figure 3.1. The classification zone number corresponds to a soil type as shown in the figure. This classification zone number is then obtained for each elevation of a penetration test. At some depths, the ECPT data will fall outside of the range of the classification chart. When this occurs, no data is obtained and a break occurs in the classification profile.

Between adjacent soil types shown as single value regions in Figure 3.1, the classification zone boundaries defined by the standard deviations of the raw data either overlapped or were separated. In either case, this area is defined as a transition zone of mixed soils which is a more realistic representation of the in situ conditions.

The next step in developing the soil classification profile is reconciliation of the similarities and differences between the two soil classification methods shown in Figure 3.1 into a single unified estimate, as shown in the classification profile indicated in Figure 3.2. This profile represents a point by point weighted average of the two methods, with weighting factors based on confidence levels established for each measurement used in the classifications. These confidence levels are based on measurement amplitudes, consistency, and engineering experience with ECPT data.

The classification profiles are very detailed, frequently indicating significant variability in soil types over small changes in elevation. In order to provide a simplified soil stratigraphy for comparison to standard boring logs, a layering and generalized classification system was implemented (i.e., soil unit descriptions located to the right of the classification profile). A minimum layer thickness of 3.0 feet was selected. Layer thicknesses are determined based on the variability of the soil classification profile. The layer sequence is started at the ground surface and layer thicknesses are determined based on deviation from the running mean of the soil classification number. Whenever an additional 9 inch increment deviates from the running mean by more than 0.50, a new layer is started, otherwise, this material is added to the layer above and the next 9 inch section is evaluated.

The soil type for the layer is determined by the mean value for the complete layer. The ten types are classified as:

| Classification Range | Soil Type |
|---|---|
| 1.00 - 2.25 | Sensitive Clay |
| 2.25 - 2.75 | Soft Clay |
| 2.75 - 3.25 | Clay |
| 3.25 - 3.75 | Silty Clay |
| 3.75 - 4.25 | Clayey Silt |
| 4.25 - 4.75 | Sandy Fine Grained |
| 4.75 - 5.75 | Sand Mixture |
| 5.75 - 6.75 | Sand |
| 6.75 - 7.50 | Gravelly Sand |
| 7.50 - 9.00 | Over Consolidated (OC) |

Again, a more detailed classification can be determined from the classification profile plotted just to the left of the soil type (unit) layers. The layering provides a summary of the engineering classification of soil stratigraphy.

## HYDRAULIC CONDUCTIVITY

To further assist in the determination of the thin clay layers that are present at SRS, calculations of the hydraulic conductivity were performed. Hydraulic conductivity simplifies the identification of clay layers, since it varies over several orders of magnitude, with clays having low permeabilities and the sands and sand mixtures having significantly higher values.

Calculation of the hydraulic conductivity was based on Equation 3.4 shown below (Chiang, 1992).

$$log\ k = 0.508 - 0.6\ Rd \tag{3.4}$$

where k = hydraulic conductivity in cm/sec

and Rd = relative density.

The above equation was an empirical fit to data obtained from a Texas site (see Figure 3.3). Although the correlation coefficient was determined to be 0.9, this equation should only be used to estimate the order of magnitude of the hydraulic conductivity. The soils at the Texas site generally had friction ratios of approximately one, indicating sandy soils. For this reason, the equation was only used on soils from the SRS site with friction ratios which ranged from 0.25 to 1.75. Soils outside this range were assumed to have a hydraulic conductivity of $1x10^{-5}$ cm/sec for plotting purposes, but are recognized as having hydraulic conductivities of this value or less. This value was selected based on previous measurements at the SRS and engineering judgement.

## RELATIVE DENSITY

Relative density determinations were made using an empirical relationship developed by Robertson and Campanella, 1988. This relationship is shown below and also in Figure 3.4 which presents the data set used to determine the empirical relationship.

$$Rd = -98 + 66\ log_{10} \frac{q_c}{(\sigma_{vo}')^{0.5}} \tag{3.5}$$

where: Rd = relative density

$q_c$ = uncorrected tip resistance

$\sigma_{vo}'$ = effective overburden stress

Since density is required to determine the effective overburden stress, this equation is used in an iterative manner to determine the relative density. Density estimates are determined using a minimum and maximum density of 80 and 125 pcf respectively. The

density estimates are used in the overburden stress calculation in the soil classification routine and the relative density is used in the hydraulic conductivity estimates.

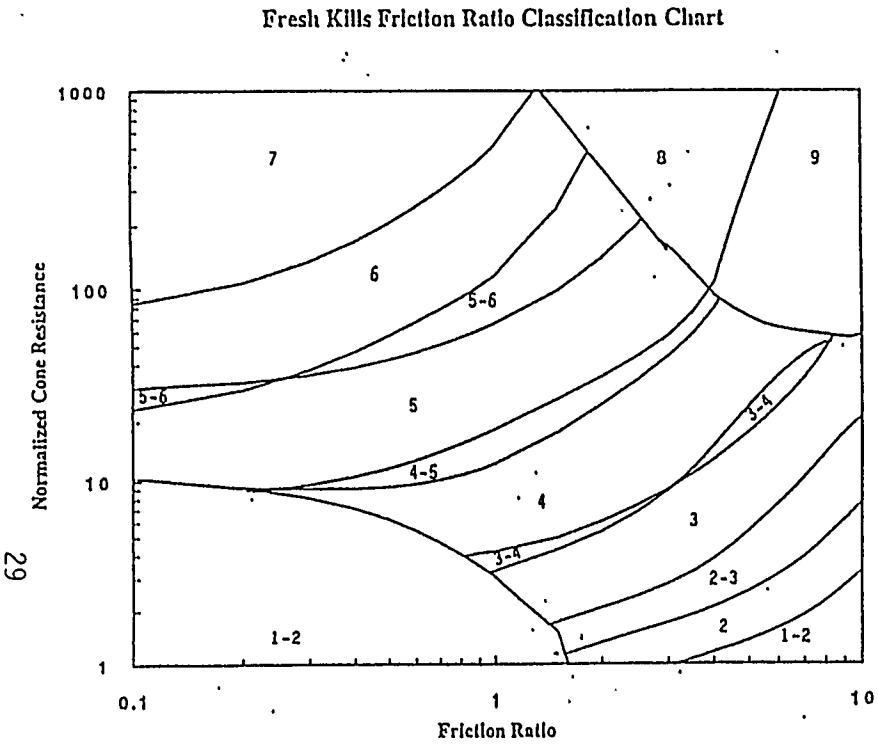


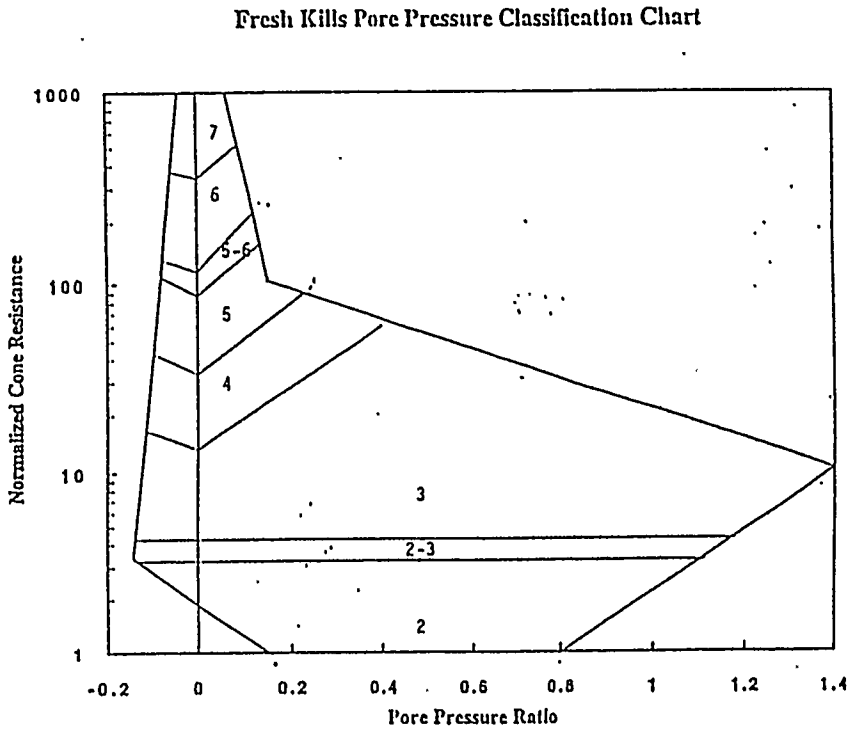


FRICTION RATIO $\frac{f_s}{q_t - \sigma_{vo}} \times 100\%$

1. Sensitive, Fine Grained
2. Organic Soils-Peat
3. Clays - Clay to Silty Clay
4. Silty Mixtures - Clayey Silt to Sandy Silt
5. Sand Mixtures - Silty Sand to Sandy Silt

PORE PRESSURE RATIO $B_q = \frac{u - u_o}{q_t - \sigma_{vo}}$

6. Sands - Clean Sand to Silty Sand
7. Gravelly Sand to Sand
8. Very Stiff Sand to Clayey* Sand
9. Very Stiff, Fine Grained*

(*) Heavily Overconsolidated or Cemented

Figure 3.1. Soil classification system based on ECPT data developed by ARA.

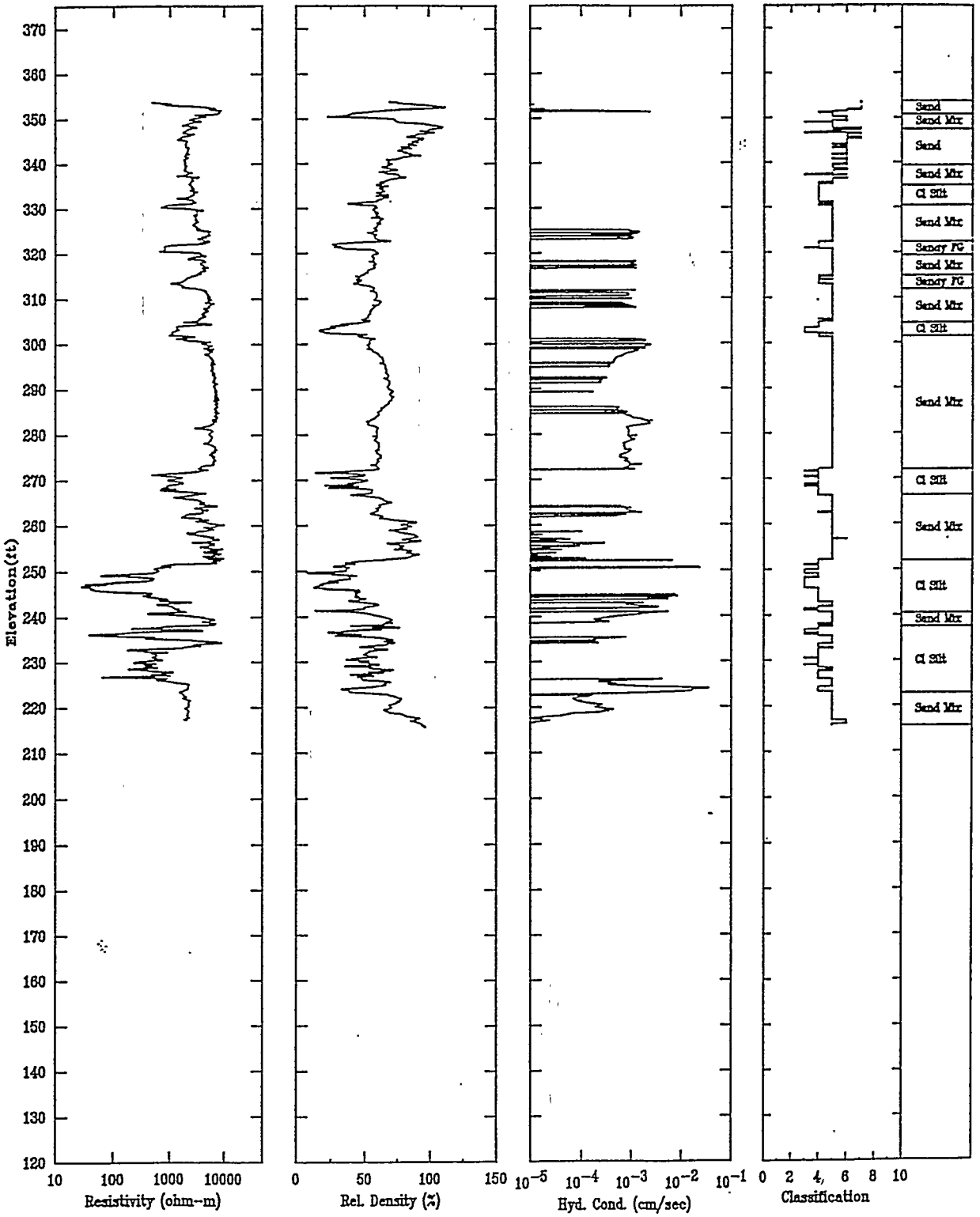


Figure 3.2. Typical analysis profiles devleoped from ECPT data from the SRS site.

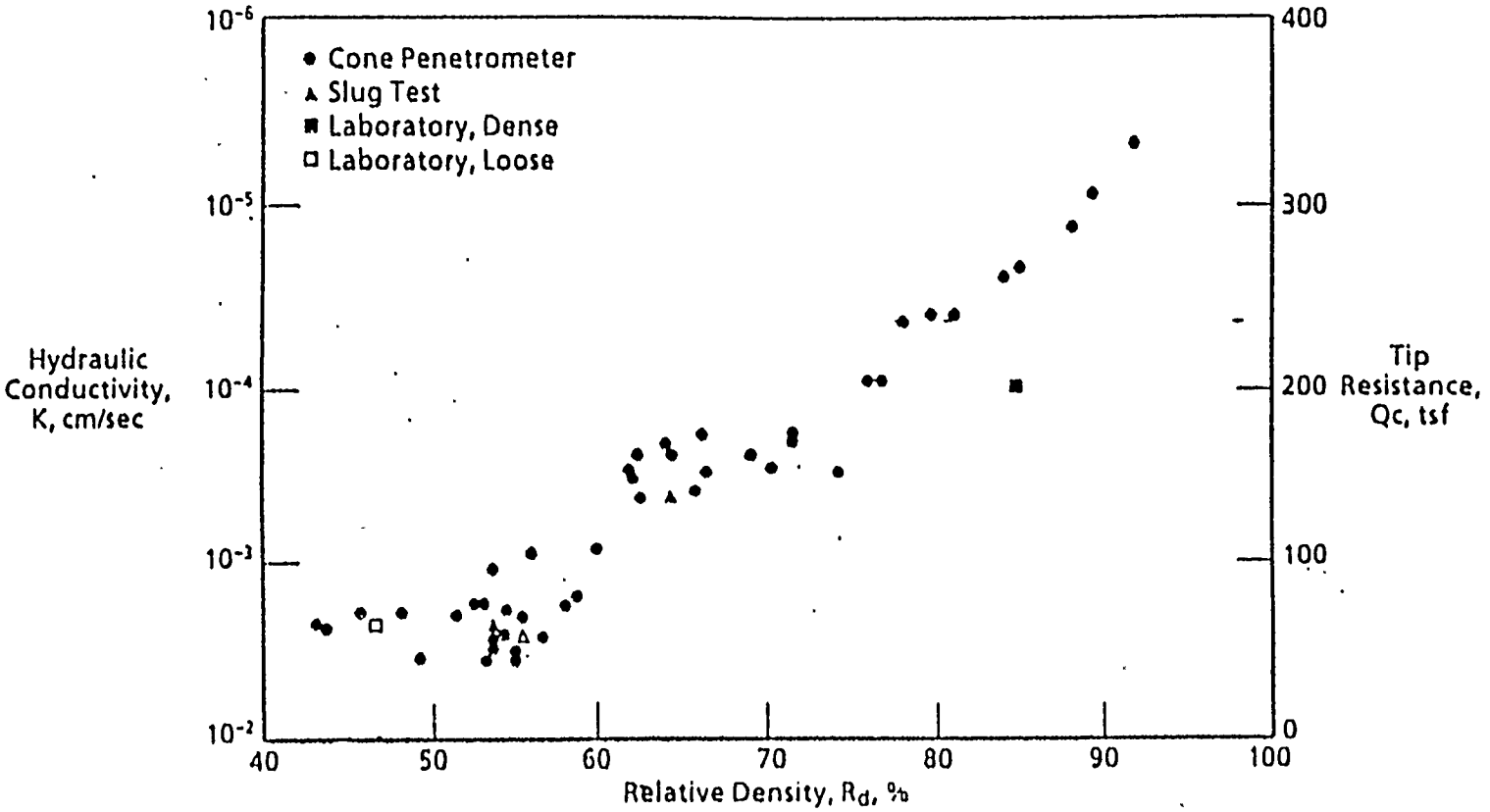


Figure 3.3. Empirical correlation between hydraulic conductivity and soil relative density for a friction ratio ≅ 1 at the Texas site (Chiang, 1992).

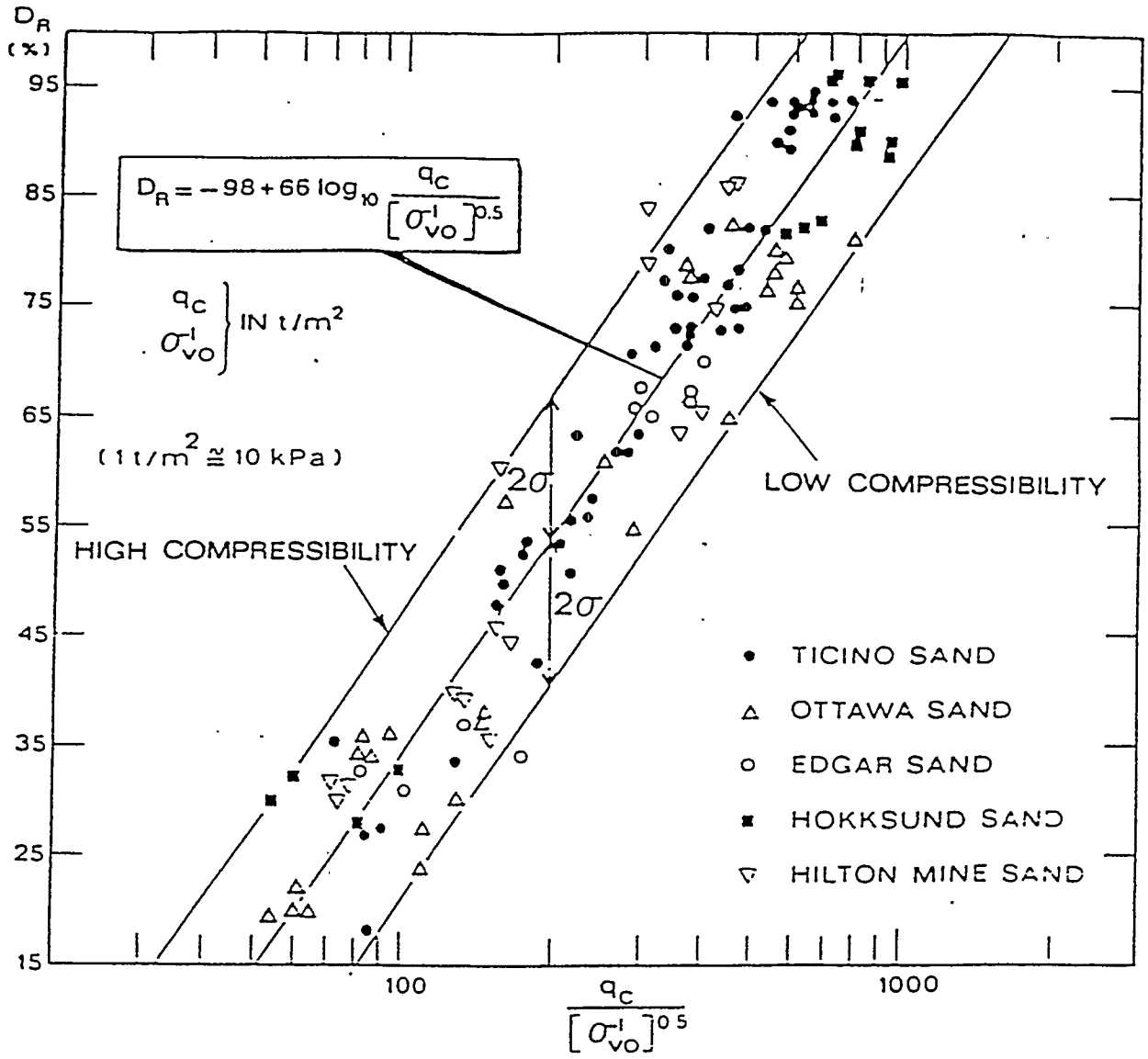


Figure 3.4 Influence of Compressibility on N.C. Uncemented, Unaged, Predominantly Quartz Sands
(After Jamiolkowski et al, 1985)

# SECTION 4
# DATA DISCUSSION AND ANALYSIS

## FIELD EFFORTS

The CPT truck and field crew were mobilized to the M-Area of SRS and began field operations on June 1, 1992, with field operations concluding on July 30, 1992. During the field program, 4,077 lineal feet of penetration testing was completed at 27 locations; P/R-ECPT tests were conducted at 25 locations and soil gas and water sampling were obtained at the remaining two locations. The average sounding depth was 151 ft, with the deepest sounding being 186 ft deep. The target depth of 160 ft was achieved in 12 of the 25 P/R-ECPT tests. The first sounding (CPT-013) was terminated at a depth of 140 ft to evaluate the self grouting module. At the remaining 12 test locations a very strong layer was encountered and the push forces required to penetrate the layer exceeded the capacity of the 1.405 in ID push rods (45,000 lbs). Figure 4.1 shows the CPT locations, and Table 4.1 lists the tests, locations, depths of penetration, and quantity of grout placed.

The soils at the M-Area vary from weak clays to strong, cemented sands and gravel soils at depth, with CPT test vehicles typically having difficulty penetrating to depths of 150 ft or greater at this site. ARA initially began the field efforts using a self-grouting probe, which requires the use of 1.75 in OD by 1 in ID high strength push tubes. The ability to self grout with this system was demonstrated at the first sounding location; however, the larger rod size limited the depth of penetration as the larger rod size required an increased push capacity. Attempts were made at alternate locations using the self-grouting probe, with all of the tests meeting refusal at less than the target depth of 160 ft. A field decision was made to use the standard 1.405 in diameter rods, and tremie grout the sounding with a separate push. In addition, ARA mobilized our heaviest CPT truck which has a push capacity of 27 tons (since this work, ARA has demonstrated a 33 ton push capacity rig at both the Hanford and SRS sites). With this vehicle, the target depth was exceeded at a number of locations.

Table 4.1. Summary of piezocone tests.

| TEST ID | DATE | NORTHING | EASTING | ELEVATION | DEPTH (ft) | TYPE OF TEST | GROUT (gal) |
|---|---|---|---|---|---|---|---|
| CPT1 | 7/14/92 | 104527.29 | 48761.45 | 353.70 | 138.27 | P/R | 35 |
| CPT2 | 7/16/92 | 104243.57 | 47884.75 | 349.70 | 169.31 | P/R | 38 |
| CPT3 | 7/20/92 | 103251.70 | 45819.40 | 351.00 | 170.50 | P/R | 43 |
| CPT4 | 7/18/92 | 104120.5 | 45512.11 | 357.70 | 165.60 | P/R | 42 |
| CPT5 | 7/11/92 | 103874.72 | 47863.29 | 360.20 | 186.64 | P/R | 47 |
| CPT6 | 7/13/92 | 103064.78 | 48469.71 | 370.50 | 164.64 | P/R | 38 |
| CPT7 | 7/24/92 | 102444.36 | 47586.21 | 349.80 | 185.72 | P/R | 57 |
| CPT9 | 6/24/92 | 100993.00 | 47696.68 | 344.90 | 165.60 | P/R | |
| CPT10 | 7/22/92 | 100505.84 | 46714.64 | 343.10 | 148.87 | P/R | 43 |
| CPT11 | 7/22/92 | 101349.24 | 46114.51 | 353.80 | 169.83 | P/R | 42 |
| CPT12 | 7/17/92 | 103267.58 | 45036.43 | 360.10 | 170.07 | P/R | 40 |
| CPT13A | 6/19/92 | 103066.76 | 45297.14 | 350.40 | 139.74 | P/R | 47 |
| CPT13B | 7/25/92 | 103083.19 | 45312.23 | 350.20 | 170.50 | P/R | |
| CPT14 | 7/01/92 | 102736.28 | 46433.01 | 349.10 | 158.40 | P/R | 25 |
| CPT15A | 7/06/92 | 102963.77 | 48778.89 | 367.30 | 159.60 | P/R | 30 |
| CPT15B | 7/30/92 | 102957.82 | 48785.38 | 367.30 | 153.12 | W/SAMP | 40 |
| CPT17 | 7/21/92 | 101955.15 | 50104.06 | 344.30 | 154.05 | P/R | 67 |
| CPT18A | 6/22/92 | 102198.82 | 48487.15 | 358.10 | 110.70 | P/R | 40 |
| CPT18B | 7/23/92 | 102232.17 | 48511.10 | 358.40 | 119.01 | P/R | 20 |
| CPT19A | 6/23/92 | 102264.49 | 48257.85 | 356.20 | 157.03 | P/R | 40 |
| CPT19B | 7/29/92 | 102268.82 | 48250.51 | 356.00 | 122.50 | W/SAMP | |
| CPT20A | 7/07/92 | 102448.19 | 47921.33 | 354.90 | 123.96 | P/R | |
| CPT20B | 7/11/92 | 102500.20 | 47906.81 | 356.20 | 116.42 | P/R | 25 |
| CPT21 | 6/30/92 | 101383.04 | 48590.50 | 340.00 | 148.80 | P/R | |
| CPT22 | 7/24/92 | 102495.85 | 48316.81 | 354.90 | 118.68 | P/R | 28 |
| CPT23A | 7/27/92 | 103862.03 | 46704.50 | 349.30 | 120.01 | P/R | 30 |
| CPT23B | 7/28/92 | 103812.47 | 46596.17 | 350.00 | 166.44 | P/R | 48 |

The P/R ECPT testing did require the use of cycling and friction reducers to reduce rod friction. As the soil collapses around the push rods, friction forces on the rods begins to build and can quickly exceed the push capacity of the CPT truck. Two techniques were used to reduce rod friction: the first was friction reducers, which consist of hardened steel sections welded to the push tubes that push the soil away from the rods, reducing the total friction force; the second was cycling, which consists of raising and lowering the push rod string. At some locations, up to two hours of cycling were required to break through hard layers. Once through the hard layers, the CPT probe could typically reach the required depth of penetration. The layers in which the CPT probe encountered difficulty were up to 10 ft thick. No other major problems were encountered during the field testing program. A significant finding of this program indicate that heavy CPT trucks (with push forces greater than 27 tons) will be required at the SRS site.

## DESCRIPTION OF TYPICAL P/R-CPT DATA

The CPT is considered one of the premier in-situ techniques for determining soil stratigraphy and type. As the technique is relatively new to the United States geotechnical and environmental communities, a basic description of the process used to analyze CPT data is provided, followed by comparison of adjacent profiles to show the consistency of the CPT data.

Comparison of tip stress, friction ratio and penetration pore pressure profiles are the most important parameters to analyze when estimating soil type and stratigraphy from CPT data. The magnitude of the tip resistance is a function of the strength of the soil, with stronger materials having higher tip resistances. In general, tip resistance increases as the coarse grained soil content increases and decreases as the fine grained content increases. This trend can be affected by the degree of consolidation of the soils, with the degree of consolidation increasing both the tip and sleeve stresses. Over consolidation can be caused by previous loading of the soil or desiccation. For a given soil the tip stress increases with depth due to the increase in geostatic stresses.

The friction ratio is a good indicator of the cohesiveness of the soil, which in turn reflects the fine grained soil content. Soils which are predominately fine grained have friction ratios generally greater than 2, and sandy soils have ratios of 2 or less. The penetration pore pressure response is a function of the soil's shear stiffness, hydraulic conductivity and density. For normally consolidated soils, the penetration pore pressure will be greater than the static pore pressure for clays and silts and equal to the static pore pressure for clean sands. In overconsolidated, dense soils the pore pressure response can be less than the static pore pressure, especially in those soils which tend to dilate, such as silty sands. The combination of the friction ratio and pore pressure response provides a good visual identification of the soil stratigraphy. With this basic understanding of the P-ECPT data, an analyst can interpret the stratigraphy and soil types visually as described below.

Plotted in Figure 4.2 is the CPT data from penetration CPT-018A, showing the friction sleeve, tip, friction ratio and pore pressure data plotted as a function of elevation. Low tip resistance is observed from the surface to elevation 355 ft. This soil is interpreted to be topsoil. The tip resistance then increases gradually from elevation 355 ft to elevation 350 ft where a jump is seen in both the tip and pore pressure response. The friction ratio is 6 or greater to elevation 340 indicating a high fine grained soil content. The fact that the soils are fine grained is confirmed by the high penetration pore pressures from elevation 353 ft to 343 ft (note that the water table is located at elevation 220 ft, which is below this elevation). The high penetration pore pressure from elevation 355 ft to elevation 340 ft is occurring in a partially saturated clayey soil. As the CPT is pushed into the soil, large volumetric strains are created, compressing the soil adjacent to the cone. For soils with a high degree of saturation, this compression crushes the air voids, resulting in saturation near the cone tip. This is the mechanism creating the high pore pressures from elevation 355 to 340 ft in the fine grained soils.

Below elevation 340 ft the friction ratio decreases, indicating a decrease in the fine grained soil content to elevation 335 where the ratio increases over a two ft depth. This increase is accompanied by a decrease in the tip stress, and both parameters together indicate a clay layer. In general, the friction ratio is roughly 1 or less for the bulk of the profile,

indicating a sandy soil with spikes in the friction ratio at several depths. These spikes correspond to decreases in the tip resistance, indicating clayey layers, as highlighted in Figure 4.2. The tip resistance varies between 2000 psi and 4000 psi for the bulk of the profile, indicating a competent soil. At elevation 251 ft the tip resistances begin to increase to a maximum of 10,000 psi at elevation 249 ft. Refusal occurred at elevation 247.5 ft. The soils in this interval are interpreted to be very dense, sandy, possibly gravelly soils due to the very high tip resistances.

The penetration pore pressure in Figure 4.2 shows no pore pressure for the bulk of the profile, as would be expected since the water table is deeper than the test depth. In the clayey layers, a positive pore pressure is observed, due to the mechanism discussed above. Further discussions of penetration pore pressures can be found in Mayne and Holtz, 1988, Mayne and Kay, 1990 and Robertson and Campanella, 1988.

Plotted in Figure 4.3 is the resistivity profile, calculated relative density, hydraulic conductivity, and soil classification. The resistivity profile will be discussed later, but generally varies between 1000 ohm-m and 10,000 ohm-m, indicating a very resistive soil. Resistivity this high is generally found only in dry, sandy soils. The low resistivity at elevations 357, 259, and 255 to 250 ft are an indication of a clay-rich zone, with a higher degree of saturation. The high degree of saturation is confirmed by the positive penetration pore pressure measurements in Figure 4.2.

Also plotted in Figure 4.3 is the estimated relative density, which is used to estimate a hydraulic conductivity of the sandy soils. High relative densities reflect materials with high densities, whereas a low relative density can be expected for low density materials. As discussed in Section 3, the relative density is used to estimate the hydraulic conductivity of the sandy soils. As the relative density for a given soil unit increases, the void space decreases, leading to a decrease in the hydraulic conductivity. The empirical equations discussed in Section 3 were used as a first order estimate for those soils having a friction ratio of $1 \pm .75$. Soils within this band are normally classified as sandy soils. As shown in Figure 4.3, the estimated hydraulic conductivity of the sandy soils at SRS is high, indicating

a soil which readily transmits fluid flow. The estimated hydraulic conductivity in Figure 4.3 agrees with the site-wide values as determined from slug tests (Eddy et. al., 1991). The maximum, minimum and average values from Eddy et. al. (1991) are shown as bands on Figure 4.3. At this time, the values shown in Figure 4.3 should be used only to delineate between the low and high permeability layers. These values will be used later in this report to prepare iso-surfaces of materials with similar conductivities as an aid in interpreting the stratigraphy. For low permeability layers, it has been assumed the conductivity is $10^{-5}$ cm/sec or less. The empirical equations need further refinements to include more specific soil types and site specific data.

Soil classifications and stratigraphic units are also plotted in Figure 4.3, using the soil classification charts and algorithms discussed in Section 3. The classification chart is in general agreement with the borehole data available from well MSB-3B. These soil classifications should also be treated as preliminary until additional well log data is compared to the CPT-derived system. The CPT-derived soil classification system shows that the site consists of sands with varying percentages of fine grained material. The zones calculated to have low hydraulic conductivities correspond quite well with those layers classified as clays or sands with fine grained material.

## CPT CONSISTENCY

An important aspect of any field investigation method is to have an accurate, repeatable measurement system. A major advantage of the CPT is that the measuring system can be field calibrated so that these precise, repeatable measurements are made. At CPT location 18, penetration tests CPT18A and CPT 18B were conducted 41 ft apart and one month apart in time using two different ARA CPT trucks. Comparison of these two tests presents an evaluation of the accuracy and repeatability of the CPT test.

Overlays of the CPT tip sleeve and penetration pore pressure responses are given in Figure 4.4. The overall character of the two penetrations is quite similar. Both profiles show the tip and sleeve stresses increasing from the surface to elevation 350 ft, where the

sleeve stresses in both soundings are greater than 120 psi, indicating a cemented soil. Below elevation 350 ft, the sleeve stress and tip stresses decrease and the sleeve stresses in both profiles are generally less than 20 psi. Sounding CPT-018A indicates a number of thin clayey seams, as can be seen at elevations 335 ft, 320 ft, 314 ft, 309 ft, 294 ft and 289 ft. These seams are identified by the decrease in tip resistance and increase in sleeve stress. In profile CPT18B only the clay seams at elevation 294 ft and 290 ft are clearly evident. The seam at elevations 310 to 305 shows up as a rapid fluctuation in the sleeve stress, indicating a thinly layered soil. The difference in the location and thickness of the clay seams observed in these two profiles is real and demonstrates the spacial variability of this site. The penetration pore pressure profiles of both soundings do not show pore pressure for the bulk of the profile as expected. However, high positive pore pressures are observed near the surface and at elevations 295 ft, 257 ft and 252 ft. These positive pore pressures occur in clay seams, as can be readily identified from the tip and sleeve data. As discussed above, positive penetration pore pressures can be expected in nearly saturated soils because the ECPT probe compresses the air void space from the soil as it passes through the media.

Figure 4.5 is an overlay of CPT 18A and 18B resistivity and interpreted relative density, hydraulic conductivity, and soil classification. The resistivity profiles essentially overlay, indicating good repeatability of the CPT resistivity data. Sharp reductions in the resistivity are observed in both profiles at elevation 295 ft, 290 ft, 260 ft and 254 ft in both profiles. These sharp reductions occur in the clay-rich seams. At elevation 337 ft a sharp reduction in the resistivity is observed in profile CPT18B, which is due to an increased clay content. This reduction is not observed in CPT18A, indicating that there is less clay in the soil at this location. This trend is also observed in the tip and sleeve data.

The relative density and hydraulic conductivity profiles show essentially the same trend. The permeability of the soil is quite low from the surface to elevation 335 ft, where the permeability increases. From elevation 335 ft to roughly elevation 267 ft the conductivity increases from the lower bound to the average SRS site-wide values. Below elevation 267 ft the general trend is for the number of clay layers to increase, resulting in a general decrease in the overall hydraulic conductivity. This decrease in hydraulic

conductivity occurs in the zone that is locally known as the tan clay zone (described in Eddy et. al. (1991)) as a sequence of interbedded clays and sands with variable thicknesses.

Comparison of the soil classification profiles shows good correlations as should be expected, given the correlation between the tip, sleeve and pore pressure data. Both profiles show clayey soils near surface to elevation 336 ft. From elevation 336 ft to elevation 315 ft the profiles show a relatively clean sand overlying a sand mixture to elevation 270 ft. Below elevation 270 ft the layering becomes more variable in the tan clay zone.

### Deep Penetration Test and the Green Clay Layer

A deep penetration test (CPT009) which penetrated the water table and the green clay layer into the confined aquifer is plotted in Figure 4.6, with the resistivity and interpreted properties plotted in Figure 4.7. The overall profile is very similar to that of CPT-18A and B, with a high tip and sleeve resistance, low permeability layer extending from the surface to elevation 317, overlying a sandy, more permeable sandy soil to elevation 250 ft. The major difference in this profile and the CPT-18 location is that this location becomes much more clayey at elevation 250 ft, as is observed in both CPT data and interpreted material properties. From elevation 205 ft to 200 ft a clay layer is penetrated, which is the green clay layer. This layer has very low tip and sleeve resistances, a relatively high friction ratio and high penetration pore pressures, and low resistivity (less than 100 ohm-m). Detailed examination of the data shows that there is some sand in the clay between elevations 205 ft to 202 ft, with the clay being much less sandy between elevation 200 ft and 202 ft. This conclusion is based on the tip resistance, which is quite low over this depth interval. The general characteristic of the CPT data over the depth interval of 208 ft to 200 ft was used to locate the green clay layer in the CPT soundings and to develop cross sections and contour plots of the top, bottom and thickness of the layer discussed in the following sections.

## Typical Cross Section

Figures 4.8 and 4.9 are plots of the CPT tip resistance for cross sections A-A′ and B-B′ shown in Figure 4.1, and are generally in the E-W and N-S directions respectively. Major stratigraphic units and the green clay layer are shown on the figures. Both sections have been divided into 7 major units: the upper low permeability clayey sand from surface to a depth of roughly 20 ft; a sand layer with some fine grained content from 15 to 30 ft thick; a sandy clayey zone varying in thickness from 3 to 10 ft; overlying another sand zone varying from 10 to 35 ft thick; the tan clay zone varying in thickness from 30 to 65 ft over the green clay layer which is from 2 to 5 ft thick; overlying the confined layer which consists of sequences of clayey and sandy interbedded soils.

The green clay layer in the E-W direction in Figure 4.8 is found at elevation 200 ft, except toward the western end of the section where the green clay begins to dip downward. In the N-S section in Figure 4.9, the green clay is at elevation 200 ft on the southern end of the section, but begins to dip downward toward the north side of the site. At CPT-005 the top green clay is at elevation 190 ft, indicating a 10 ft elevation decrease, then begins to rise at CPT-002 to elevation 192 ft. Contour plots of the green clay were made to examine the surface of the green clay.

## Green Clay Contour Maps

Plotted in Figures 4.10, 4.11, and 4.12 are very preliminary contour plots of the top, bottom and thickness of the green clay as determined from the CPT data. Contour maps are sensitive to the number and distribution of data points. As these maps are made from only the CPT data, the plots are being treated as preliminary, and are used to show only general trends. Additional data needs to be obtained to reduce the uncertainty in these plots. This data can be obtained either from additional CPT soundings or boring logs.

The contour plot of the top of the green clay layer in Figure 4.10 indicates that the green clay tends to dip toward the north, with the clay at its highest elevation in the

southeast. A ridge like structure extends along a NW-SE line, with the green clay deeper on the NE side of this line. The circular contour lines in the NW corner of the contour map are due to one CPT sounding where the green clay was observed at a depth of 188 ft. The shape of the contour plot at this location is highly biased by this one point and does not reflect the actual shape of the green clay surface. Figure 4.11 shows a contour map of the bottom of the green clay layer and shows the same general trends as the map of the top of the clay. The contour map of the thickness of the green clay layer in Figure 4.12 shows that it is thickest to the SE and NW, and thinnest in the center of the area investigated.

### Soil Gas Sampling

Soil gas samples were obtained at one location using the B-K multi-gas sampler. Plotted in Figure 4.13 are the results of soil gas sampling on the sounds, along with companion CPT soundings. The concentration of TCE and PCE as measured by the BK monitor are plotted in parts per million (ppm). The plot shows low concentrations of TCE and PCE, except at two elevations. At elevation 274 ft the PCE concentration increases to about 150 ppm in the gas phase, then decreases to background at elevation 263 ft. The PCE gas concentration increases again just above a clay layer. At an elevation of 244 ft both the PCE and TCE gas concentrations begin to increase rapidly with the PCE exceeding 1,500 ppm in the gas phase, and the TCE reaching a concentration of roughly 500 ppm. At the shallower depth the increased gas concentration of both the TCE and PCE is associated with a clay layer. The conceptual TCE and PCE contaminant transport model (Eddy et. al., 1991) is supported by the gas samples obtained with the CPT; that is, the contaminant will tend to concentrate in clay layers in the unsaturated zone.

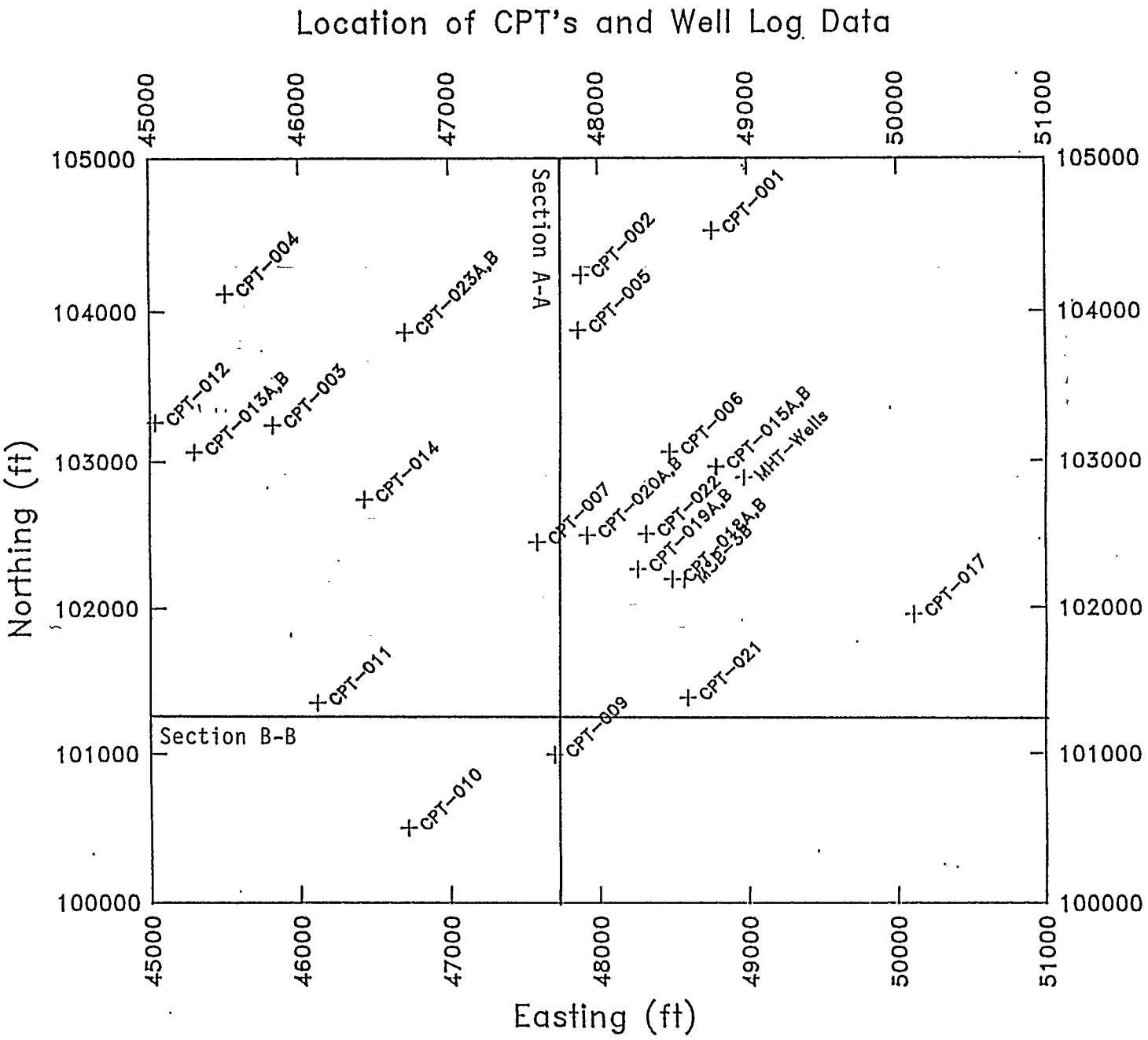


Figure 4.1. CPT location map.

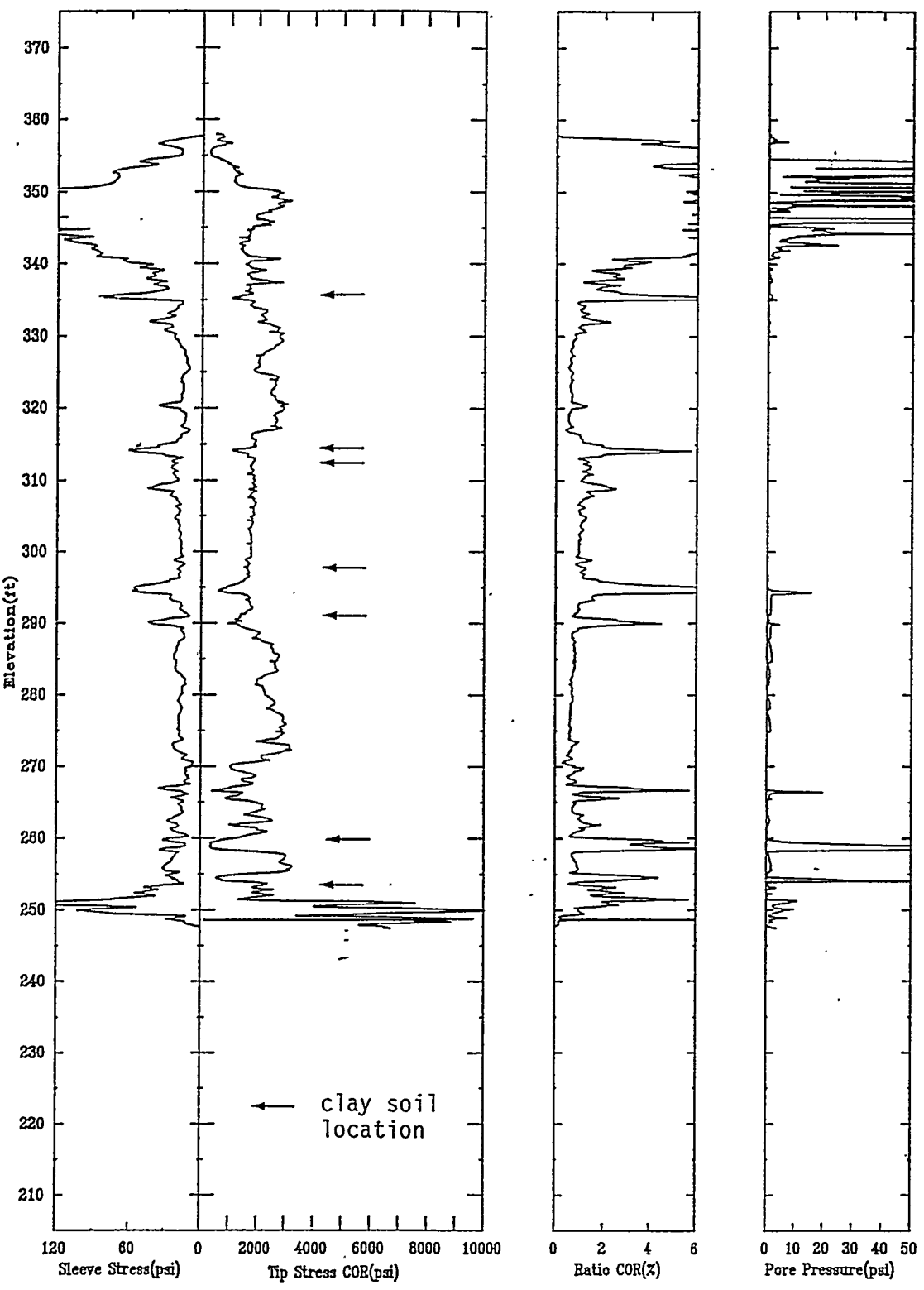


Figure 4.2. Plot of typical CPT data from the M-basin study area.

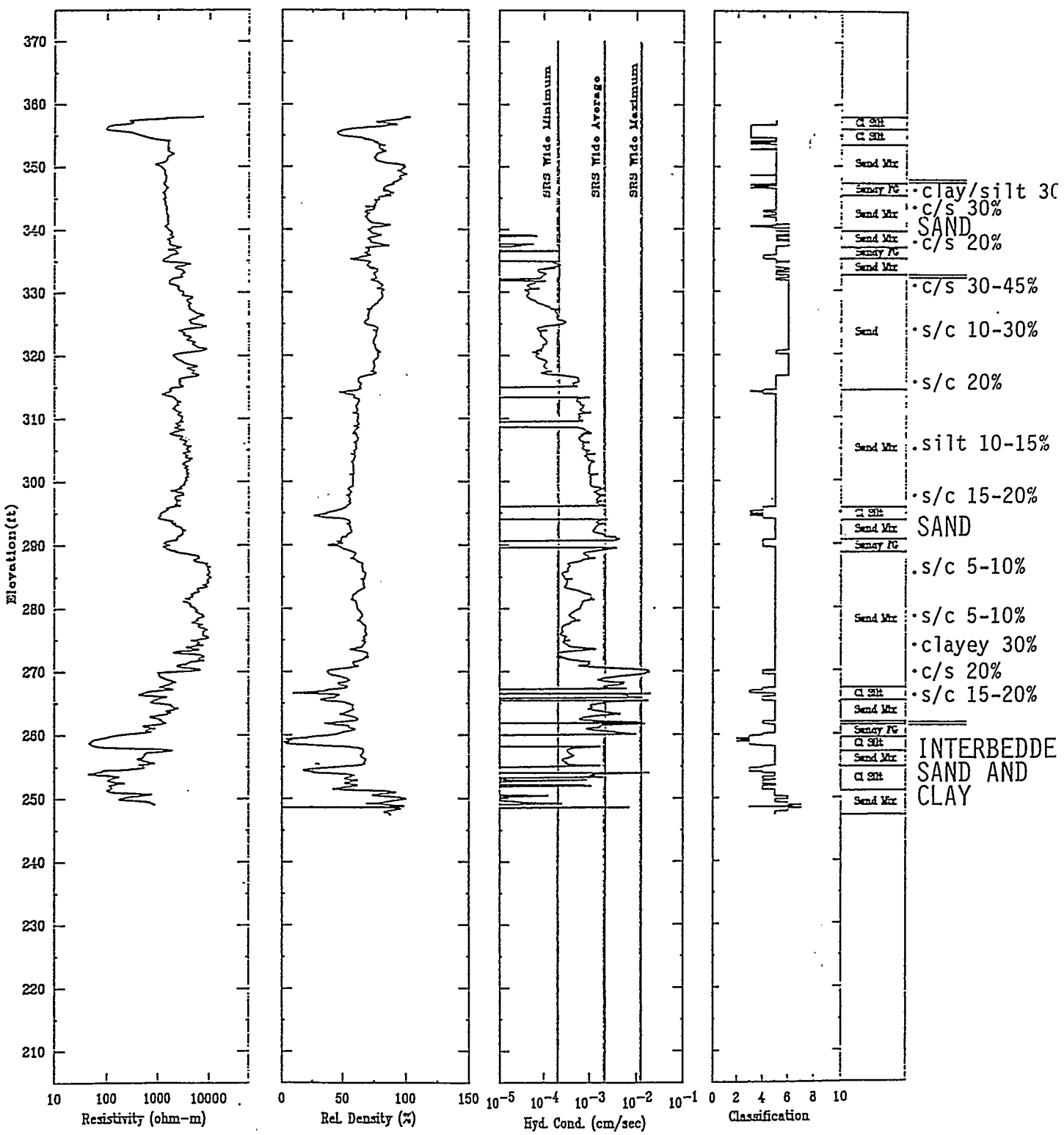


Figure 4.3. Plot of analysis results from R-ECPT data obtained from the M-basin study area.

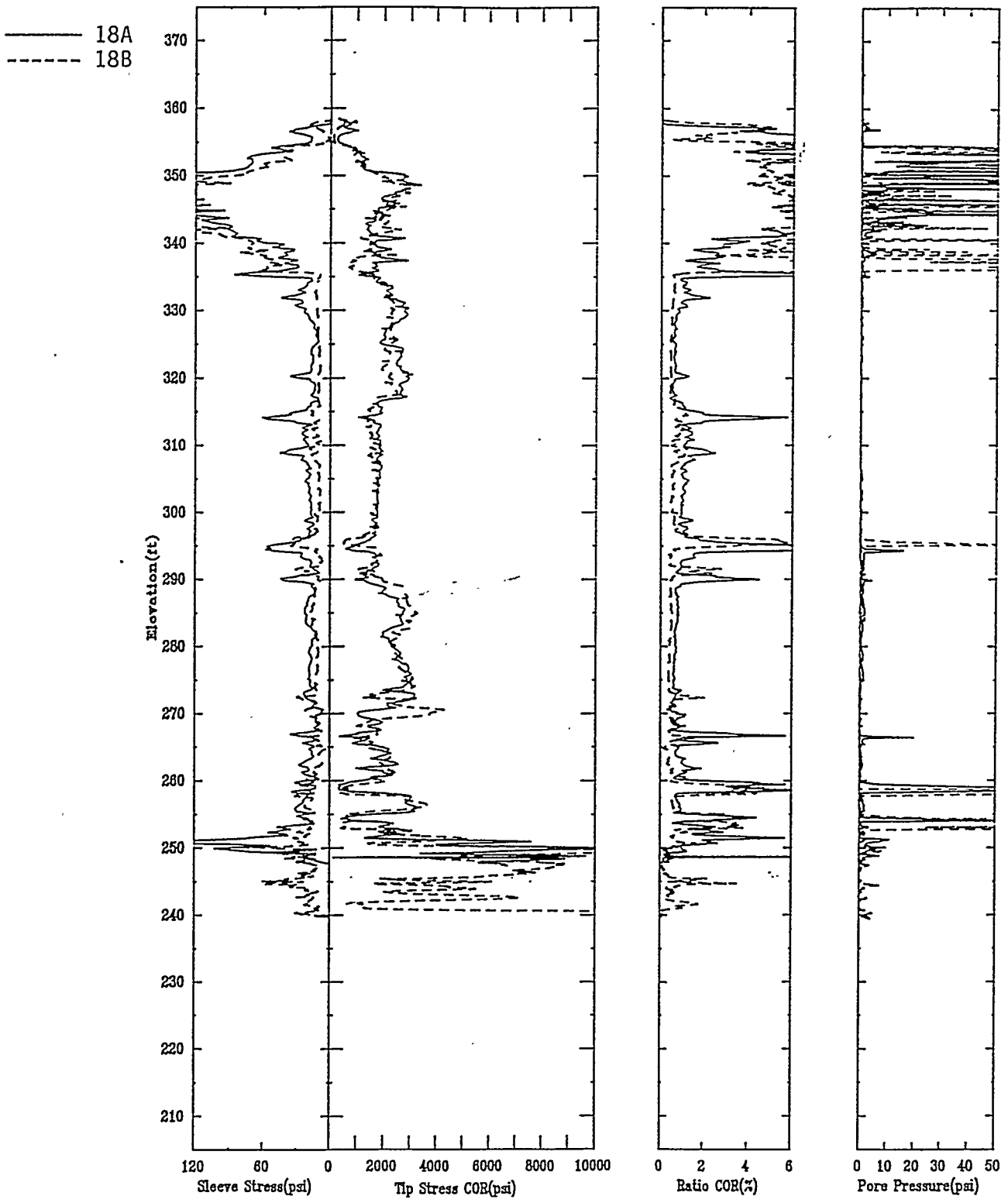


Figure 4.4. Overlay of the CPT measurements made at locations 18A (solid line) and 18B (dashed line).

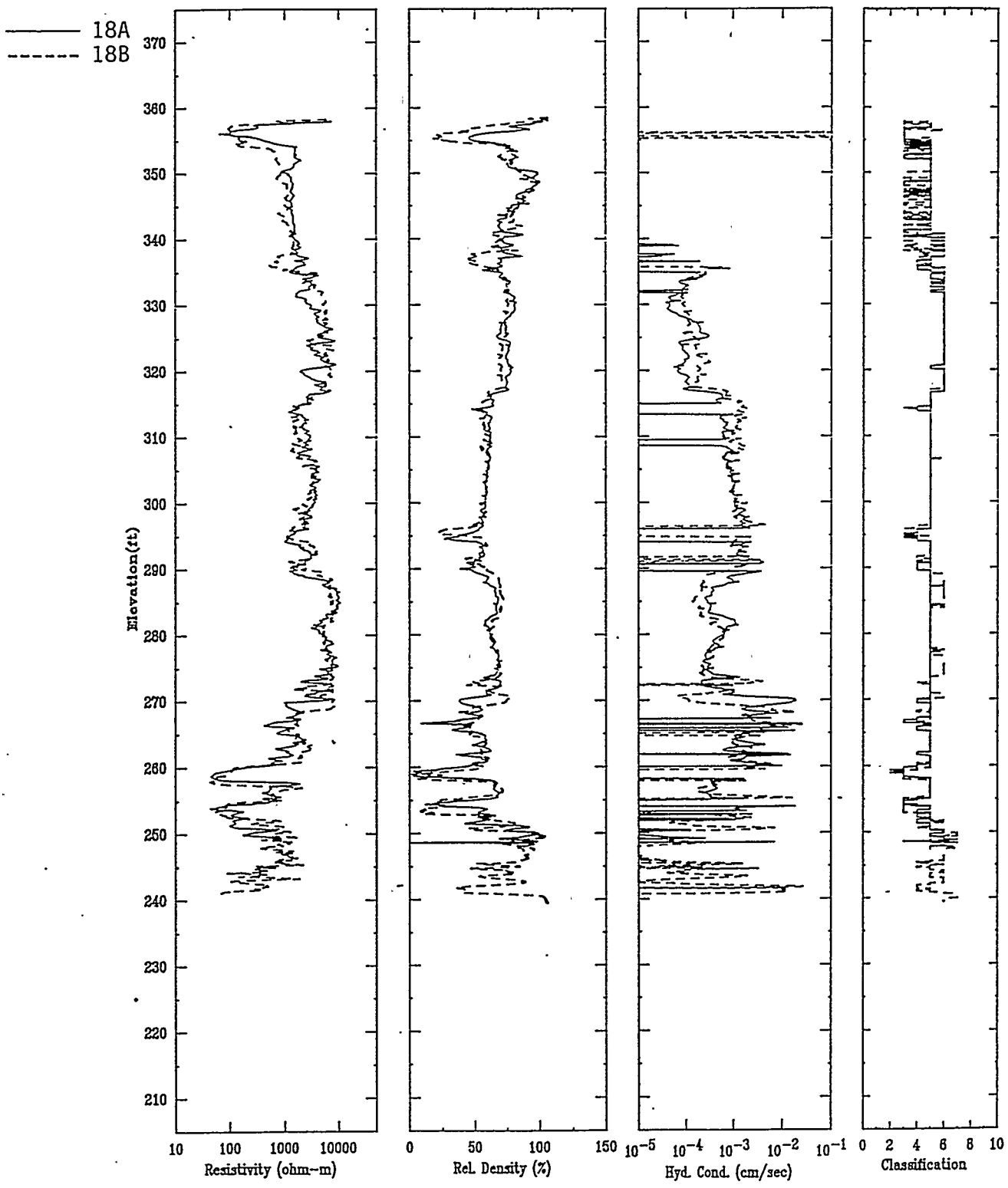


Figure 4.5. Overlay of the CPT determined parameters made at location 18A (solid line) and 18B (dashed line).

CPT-009 APPLIED RESEARCH ASSOCIATES, INC. 06/24/92
Integrated Demo Site

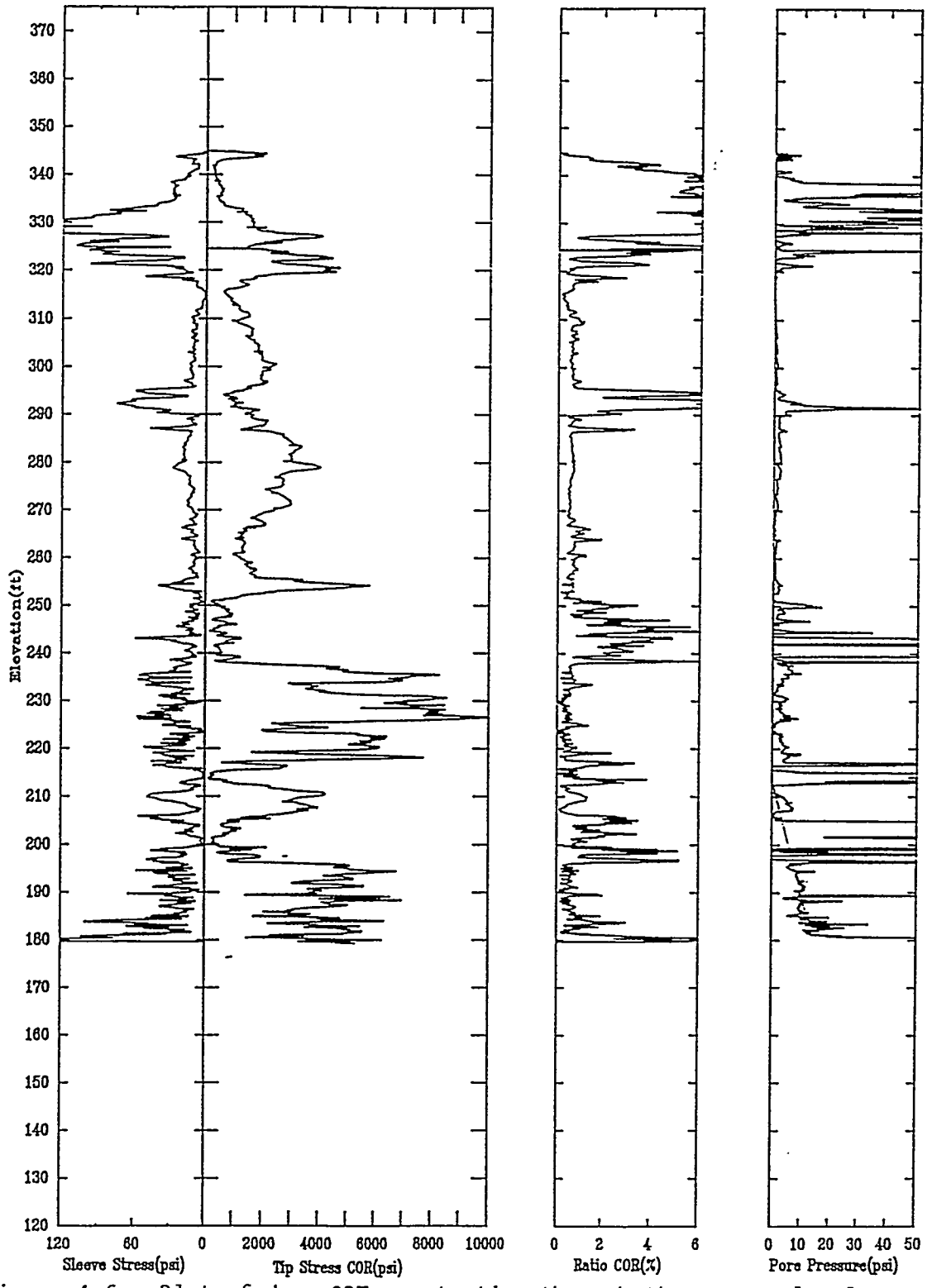


Figure 4.6. Plot of deep CPT penetration through the green clay layer showing the tip, sleeve, pore pressure and friction ratio.

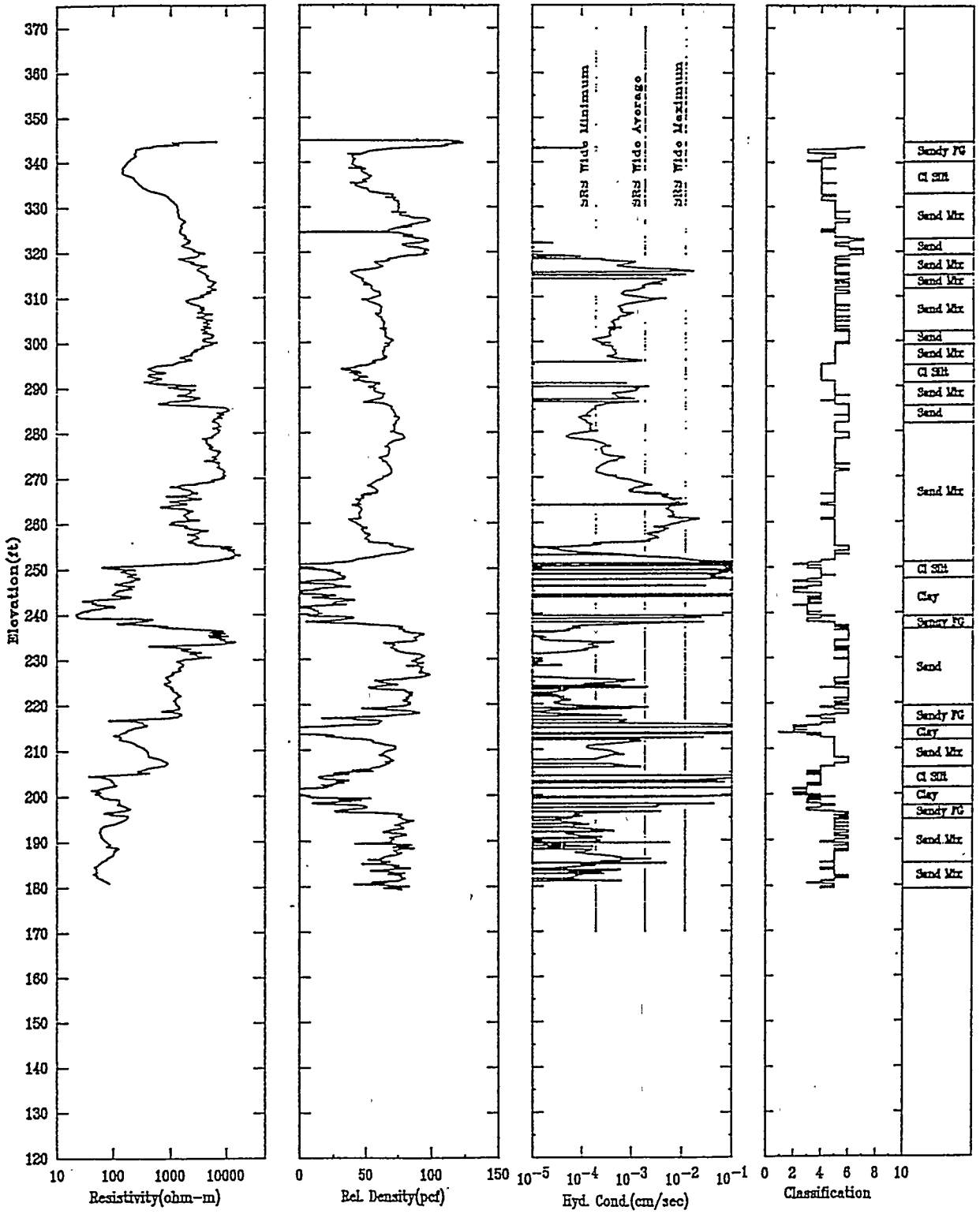


Figure 4.7. Plot of deep CPT penetration through the green clay layer showing soil resistivity, relative density, hydraulic conductivity and soil classification.

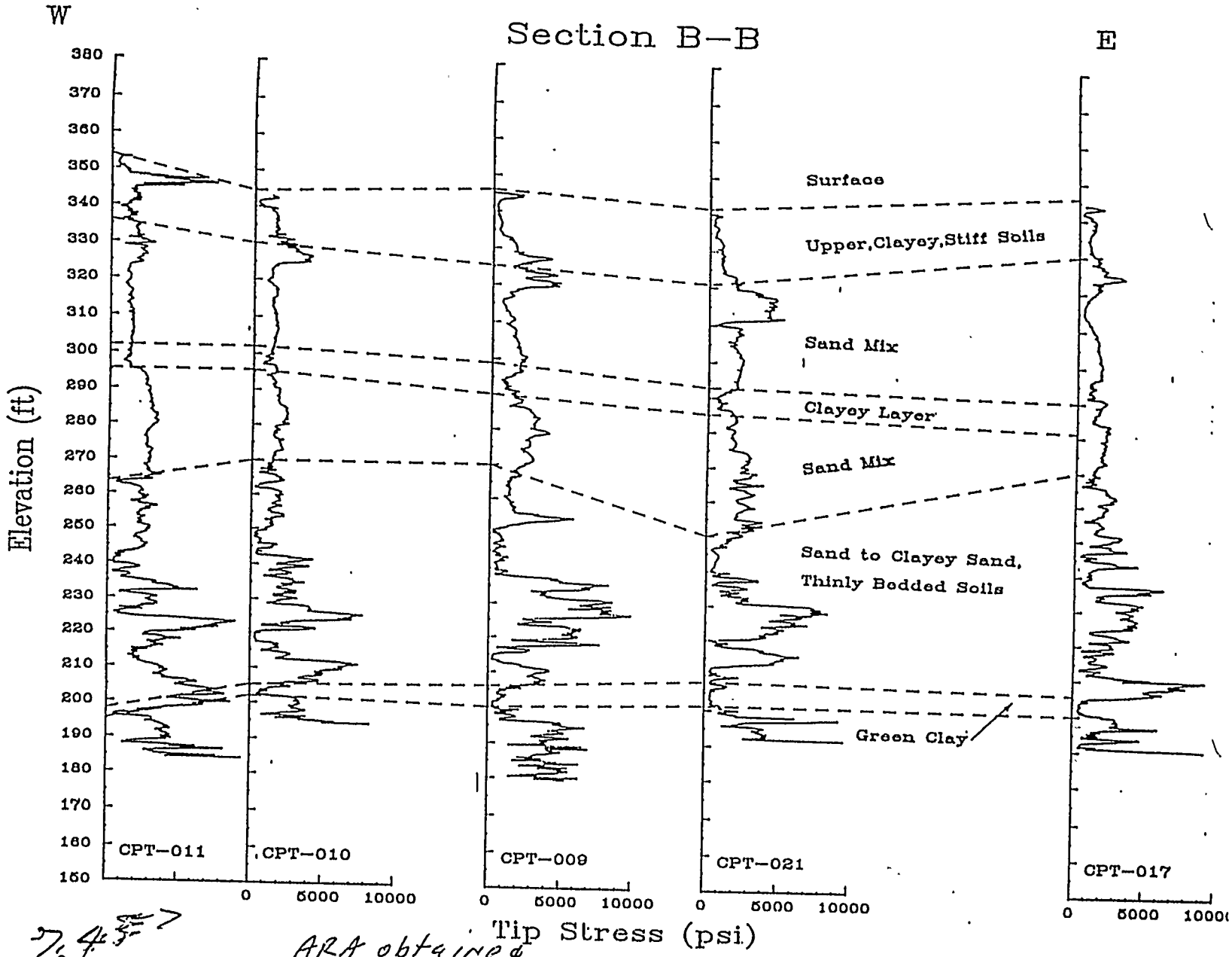


Figure 4.8. Cross-section of the tip stress profiles at location CPT-11, CPT-10, CPT-9, CPT-21 and CPT-17 in the M-basin study area; section shows major stratigraphic SRS soil units

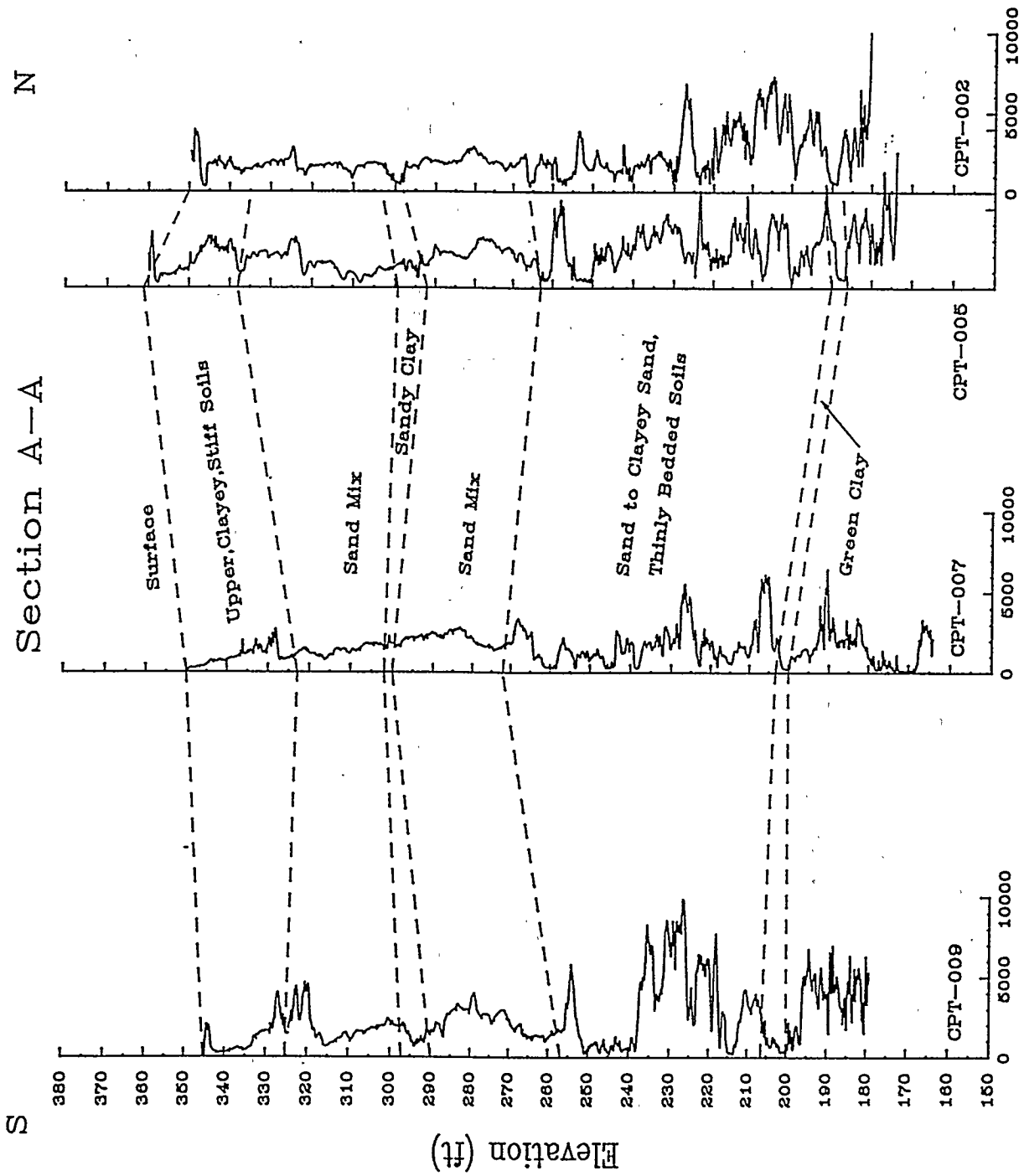


Figure 4.9. Cross-sections of the tip stress profiles at location CPT-09, CPT-07, CPT-05, and CPT-02 in the M-basin study area.

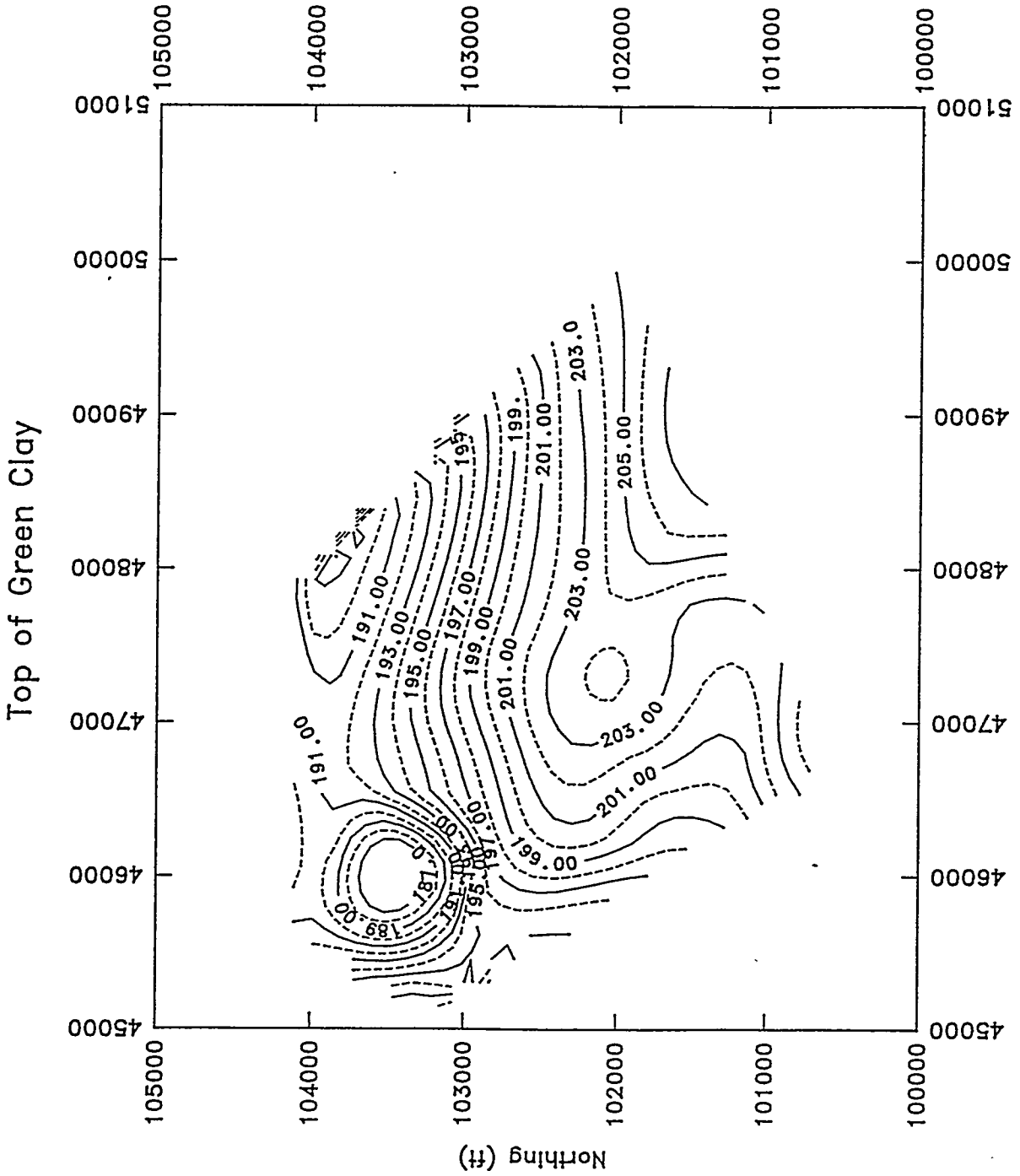


Figure 4.10. Contour map of the top of the green clay layer. Map is based solely on CPT data.

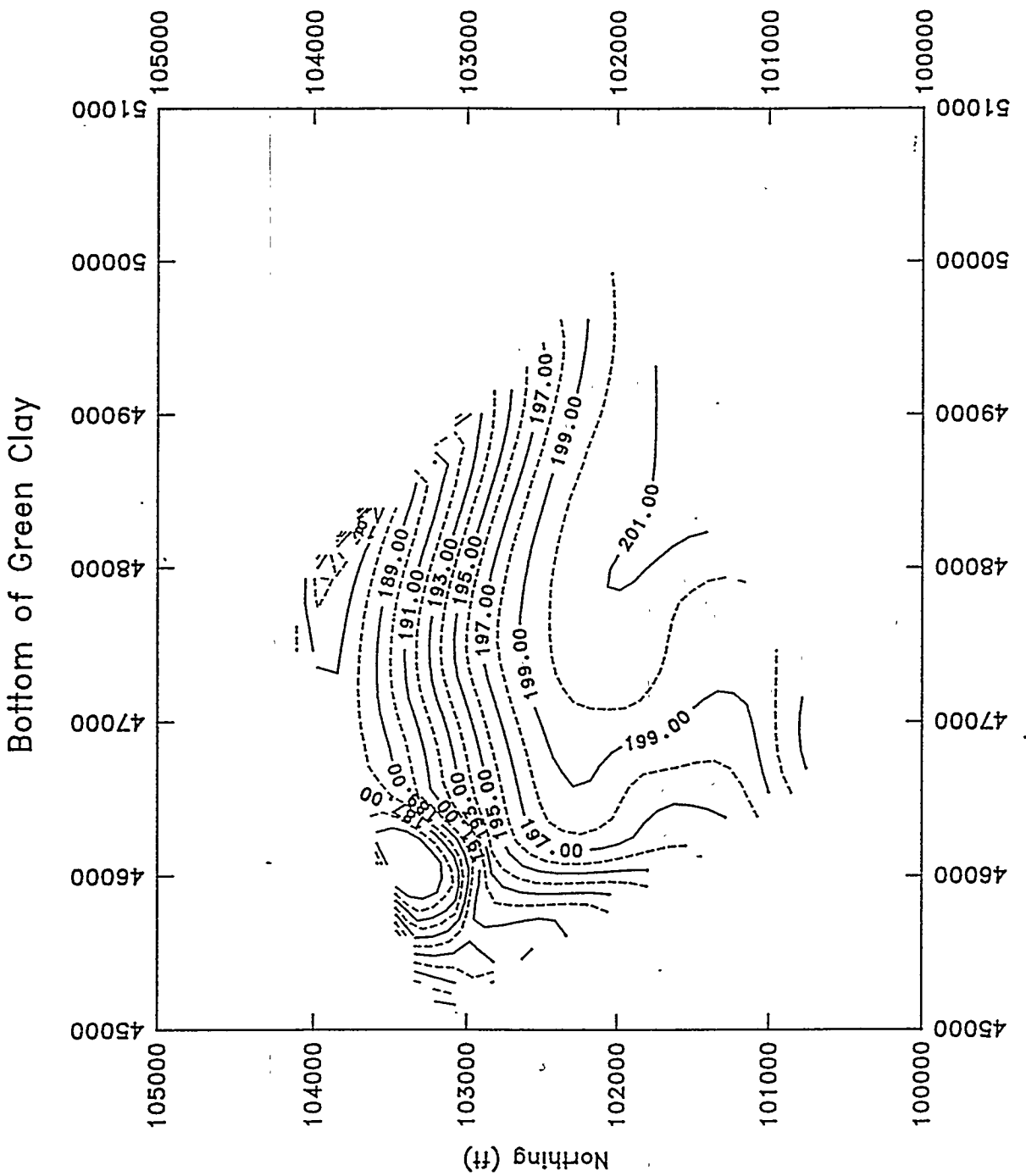


Figure 4.11. Contour map of the bottom of the green clay layer. Map is based solely on CPT data.

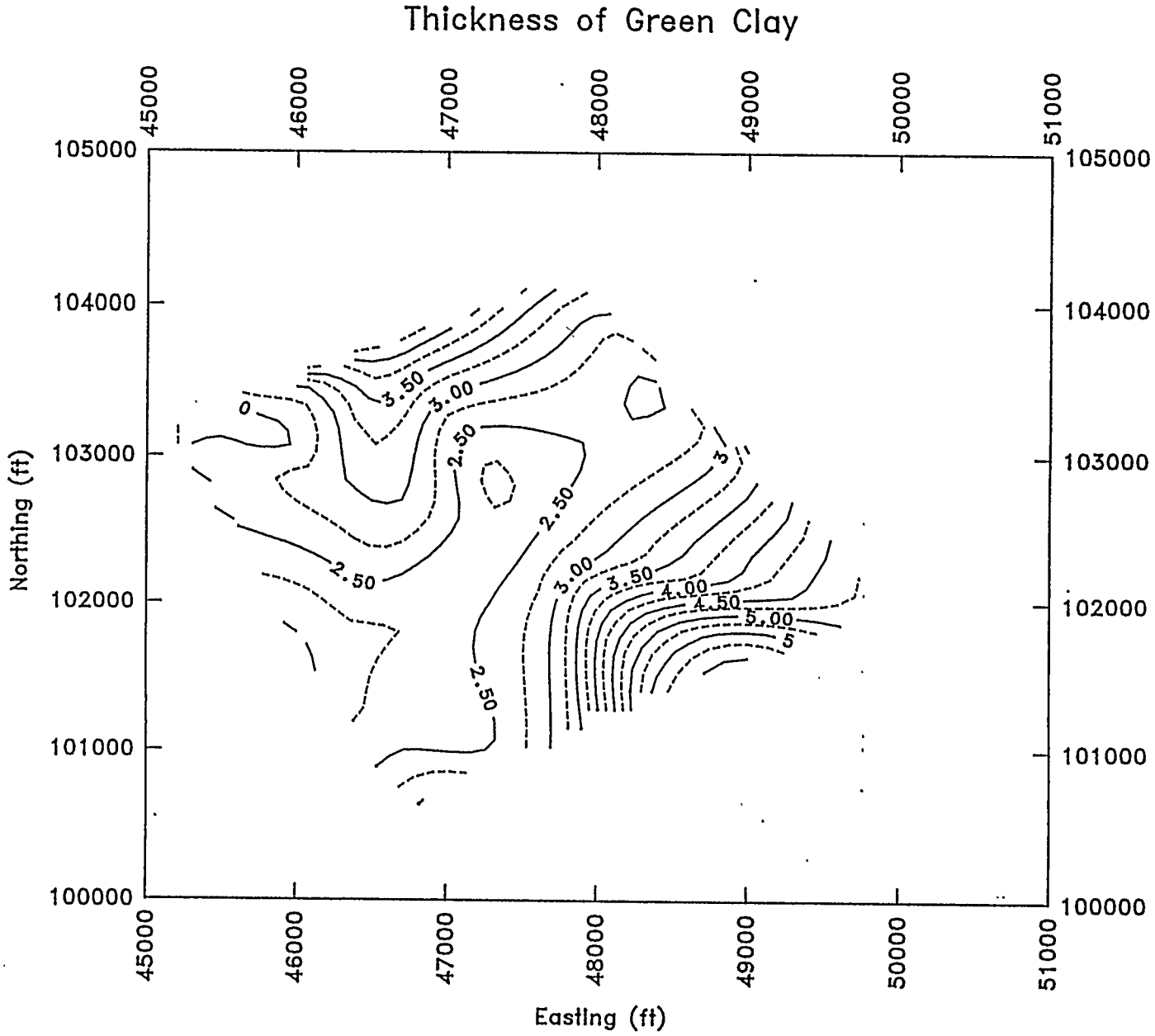


Figure 4.12. Contour map of the green clay layer. Thickness map is based solely on CPT data.

CPT-019A APPLIED RESEARCH ASSOCIATES, INC. 06/23/92
North 102265.49 East 48785.38 Elevation 356.2

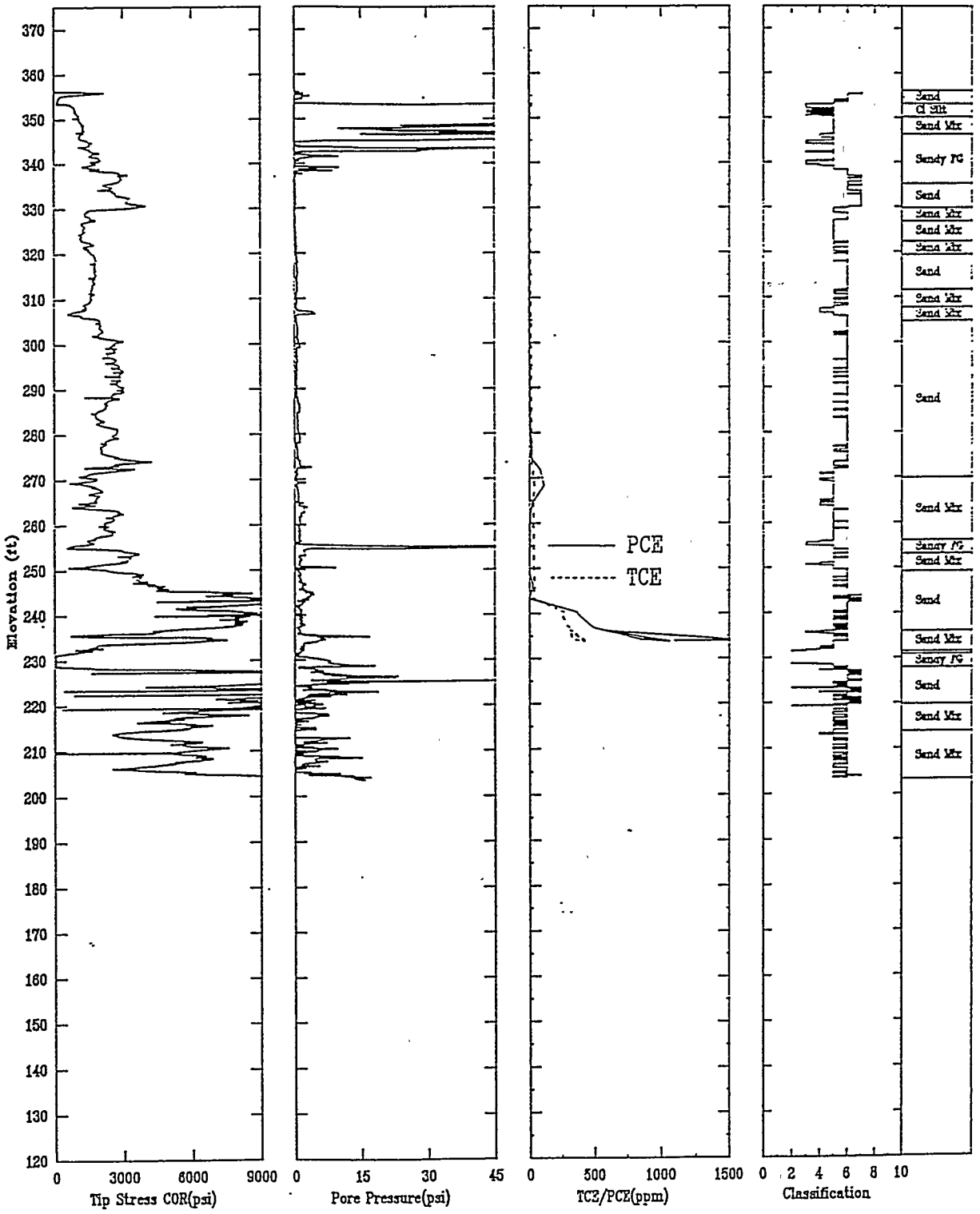


Figure 4.13. Measured chemical concentrations using soil gas sampling with the ECPT in the M-Basin study area.

# SECTION 5

# STUDY OF THE INFLUENCE OF DNAPLs ON SURFACE AND DOWNHOLE ELECTRICAL RESISTIVITY

## OVERVIEW

A primary objective of the project was to assess the sensitivity of surface and downhole electrical resistivity to DNAPL contamination. As discussed in Eddy, 1991, and Westinghouse Savannah River Company, 1992, DNAPLs are hypothesized to travel rapidly downward in the saturated zone until a clay is encountered, and then pool on the clay layer and spread laterally in disconnected and loosely connected ganglia, until a higher hydraulic conductivity layer is encountered. The DNAPL then flows downward until another clay is encountered. In the vadose zone, DNAPLs move downward until clay zones are reached. The DNAPL then sorbs to the clay until a sorbent capacity is reached. The separate phase then continues down through the subsurface. It has been hypothesized that the resistivity contrast existing between water and DNAPL saturated soils can be used to locate DNAPLs if continuous ganglia are present. The P/R-ECPT sounding is expected to provide high vertical resolution data, with the surface survey expected to give greater lateral coverage, at the expense of resolution.

Calculations, based on empirical and analytical models of surface and downhole CPT resistivity soundings, were conducted to evaluate the sensitivity of resistivity to DNAPL concentration and to guide the field and laboratory programs. The results of these calculations are summarized in this section. The calculations indicate that the P/R-ECPT can be used to locate DNAPLs pooled on top of clay lenses within the saturated zone. Surface resistivity, when used in conjunction with the P/R-ECPT can locate DNAPLs pooled on top of the green clay layer if a widespread, thick separate phase exists. The parametric calculations were conducted using average resistivity profiles and properties. The profiles and properties were determined from well log data from the Integrated demonstration site. Well log properties were used as the CPT data was not available at the time of these studies.

## DC RESISTIVITY MODEL

Geophysical resistivity surveys measure the electric resistivity contrast of earth materials and has been used for many years to locate mineral and oil deposits. The resistivity of natural deposits is a function of the soil type, degree of consolidation, water content, pore fluid, and conductivity. Of these parameters, soil type and pore fluid conductivity have the largest influence. Location of separate phase DNAPLs exploits the resistivity contrast that will exist between a DNAPL saturated soil and a water saturated soil. DNAPLs and other hydrocarbons act as insulators, whereas soil moisture acts as a conductor. Studies by Seusy (1992), Annan (1991), and Shinn (1990) indicated that both surface and downhole resistivity surveys can be used to located DNAPLS.

Electrical properties of natural deposits of soils can span six orders of magnitude, with the dominant variables being the soil porosity, conductivity of the pore fluid and clay content. Table 5.1 and Figure 5.1 present typical conductivities of soils and pore water. These values are useful in preliminary modeling calculations to determine where significant contrasts can be achieved.

**Table 5.1. Resistivities of sediments (after W.M. Telford et al.)**

| Rock Type | Resistivity Range (Ωm) |
|---|---|
| Consolidated shales | 20 to 2 x $10^3$ |
| Argillites | 8 to 10 x $10^2$ |
| Conglomerates | 2 x $10^3$ to $10^4$ |
| Sandstones | 1 to 6.4 x $10^8$ |
| Limestones | 50 to $10^7$ |
| Dolomite | 3.5 x $10^2$ to 5 x $10^3$ |
| Unconsolidated wet clay | 20 |
| Marls | 3 to 70 |
| Clays | 1 to 100 |
| Alluvium and sands | 10 to 800 |
| Oil sands | 4 to 800 |

Electrical models of the response of saturated and partially saturated soils and rocks have been developed, with the most widely used model being Archie's law or variants of Archie's Law. Archie's Law (Suksa, 1987) is an empirically derived model which relates the total conductivity (the reciprocal of resistivity) of a soil, pore water and contaminant mixture as:

$$\sigma_T = \frac{\sigma_w \, s^b \, n_t^m}{a} \tag{5.1}$$

where $\sigma_T$ = total observed electrical conductivity, smho/m

$\sigma_w$ = conductivity of fluid constituent, smho/m

$n_t$ = total porosity

s = degree of saturation

a, b, m = empirical factors: a $\simeq$ 1, b $\simeq$ 2, m = 1.3 to 2 for unconsolidated sediments.

Equation 5.1 assumes that the soil matrix does not constitute a flow path for the electrical current. This is valid when the soil grain conductivity is much less than that of the pore fluid. A more general solution is to replace $\sigma_w$ with the bulk conductivity of the soil defined as:

$$\sigma_b = \sigma_w + \sigma_m + \sigma_s \tag{5.2}$$

where $\sigma_b$ = bulk conductivity, smho/m

$\sigma_w$ = conductivity of fluid constituent, smho/m

$\sigma_m$ = conductivity of the soil grains, smho/m

$\sigma_s$ = the conductivity of the grain surface double layer.

The grain surface conductivity can increase the bulk conductivity by 15% to 30% (Pfannkuch 1969). In very saline solutions, the influence of $\sigma_s$ is probably not large. Saksa, et al. (1987) suggest that bulk resistivity can be modeled using:

$$\sigma_m = 0.0001$$

$$\sigma_s = 0.1 \; abs(log \; \sigma_w) \; \sigma_w \tag{5.3}$$

which yields $\sigma_s = 0\%$ of $\sigma_w$ when $\sigma_w = 1.0$ smho/m

$\sigma_s = 30\%$ of $\sigma_w$ when $\sigma_w = 0.0001$ smho/m

Major uncertainties associated with these predictions are the water resistivity as a function of degree of contamination (which is determined from laboratory testing), clay content (which greatly affects the soil grain conductivity), and degree of saturation and soil porosity. Of these, the clay content, degree of saturation and soil porosity have the greatest influence on the accuracy of the resistivity calculations.

The major variable left out of Archie's model for the SRS site is the effect of DNAPLs on conductivity. There are two effects: the influence of the contaminant on the aqueous phase, and a separate phase on conductivity. Figure 5.2 plots the effect of chlorinated compounds on the conductivity of water (Saksa, 1987). A four order of magnitude change in chlorinated hydrocarbon concentration resulted in only an order of magnitude change in fluid conductivity, indicating only a minor effect. Figure 5.3 is a plot of TCE and PCE concentration in water vs. conductivity for the SRS site (data from Eddy, et. al, 1991). This data also shows only a very weak relationship between TCE and PCE concentration and pore fluid conductivity. Based on these two figures, the influence of aqueous phase chlorinated hydrocarbon concentration on fluid conductivity is minimal and will not be modelled.

The effect the separate phase DNAPL concentration has on the resistivity occurs by the DNAPL displacing the more conductive water phase, especially at high concentrations. This effect is modelled (Eslinger and Pevear, 1988) assuming that the non-conducting DNAPLs reduce the water filled pore space, effectively reducing the soil porosity. The effect of separate phase DNAPL was modelled by modifying Equation 5.1 to reduce the soil porosity by the DNAPL volume.

## TYPICAL RESISTIVITY PROPERTIES AND PROFILES AT THE SRS SITE

A baseline resistivity profile was developed, based on well borehole logs which had been previously obtained by SRS (Eddy et al, 1991). Properties of the baseline resistivity profiles were then modelled using equations and properties chosen to replicate the average SRS downhole resistivities for each soil unit. Conductivity of the pore water was determined from water samples obtained from wells and porosities were selected which were consistent with Eddy et al., 1991. Soil and resistivity profiles were selected which were generally consistent with the profile in Figure 1.1 and the available well-log resistivity data.

## WELL LOG RESISTIVITY DATA

Resistivity borehole data (Eddy et al., 1991) was obtained using normal logs with electrode arrangements of 16" and 64". The longer 64" spacing is designed to measure the resistivity away from the mud invasion zone and provides an estimate of the average resistivity beyond the invaded zone for a radius of about twice the electrode spacing. The 16" spacing provides good vertical resolution; however, it is more affected by the mud invasion zone. This type of logging tool gives poor results in highly resistive soils and rocks (Keys and MacCary, 1971). Plotted in Figure 5.4 is the borehole resistivity log from location MHT-6C. This log was selected as it was closest to sounding location CPT-15 where resistivity, soil gas and water samples were obtained with the CPT.

The 16" and 64" borehole logs show similar overall shapes through most of the log, with the 16" log having better detail of the site layering in the near surface region. Both logs show band-edging of the measured resistivity at about 3400 ohm-m in the near surface region. A number of the 16" logs show this limitation, indicating that higher resistance materials are present, but standard methods can not be used to measure these peak resistances. As will be shown in Section 6, the CPT derived resistivities were generally higher than the well logs. Both the 16" and 64" logs show sharp reductions in the resistivity profile at a number of depths. These reductions correspond to clay layers in which the moisture content is increased. The combination of increased moisture content (as evident

from the CPT pore pressure response) and clay content increases the conductance of the soil. At elevation 320 ft the general trend is for a decreasing resistivity with depth to elevation 245. At elevation 230 ft the resistivity significantly increases. This layer is interpreted to be more sandy. Below elevation 230 ft the resistivity begins to decrease to the bottom of the borehole. The water table is at a nominal elevation of 220 ft. The soils at this site are generally clayey, and one would expect the resistivity to be lower than the values that were measured. The borehole log shows that the site has a high resistivity, indicating a very dry soil, as supported by measured moisture contents of 5 to 15% (Rossabi, May 1993).

The 16" survey indicated higher resistivity than the 64" survey, which is the opposite of the expected results. In general the 16" survey is expected to be influenced by the drilling mud which is quite conductive and results in lower resistivities than the 64" survey. For this report, the 64" survey was selected to evaluate average site properties as this length survey is believed to give a better indication of the average resistivity of the media.

Figure 5.5 is an overlay of ten 64" resistivity surveys in the MHT well series. The 10 logs which are overlayed were obtained in an area 300 by 500 ft. As can be seen, a great deal of variability exist in the well-log data. In the vadose zone, the resistivity varies from less than 500 ohm-m in the clays to over 3000 ohm-m in the sandy zones. The resistivity in the tan clay zone is reduced as compare to the more sandy layers above elevation 270 ft. Below the water table, the resistivity is much more uniform. The data in Figure 5.5 was analyzed to derive average resistivity values for each of the major zones. These average values are shown in Figure 5.5 as a heavy solid line. The soil type assumed for each layer, resistivity and layer depth are listed in Table 5.2.

## PARAMETRIC DOWNHOLE RESISTIVITY CALCULATIONS

Calculations using Equation 5.1, 5.2, and 5.3, at DNAPL concentrations of 5%, 50%, and 100% (by percent of pore space) were conducted. The DNAPL was assumed to be concentrated either in or just above the clay layers. The calculation matrix is presented in Table 5.2; the layers assumed to be contaminated are highlighted. Comparison of the clean

Table 5.2. SRS Parametric Surface Resistivity Calculations for "clean" and Contaminated Soil Zones.

| Soil Type | El. Top (ft) | El. Bottom (ft) | Depth Top (ft) | Depth Bottom (ft) | Clean Resist. (ohm-m)* | 5% Cont. Resist. (ohm-m)* | 50% Cont. Resist. (ohm-m)* | 5% Cont. Resist. in Vadose Zone 100% Cont. Resist. in Sat. Zone (ohm-m)* |
|---|---|---|---|---|---|---|---|---|
| SC dry | 365 | 345 | 0 | 20 | 3150 | 3150 | 3150 | 3150 |
| SC moist | 345 | 324 | 20 | 42 | 1400 | 1400 | 1400 | 1400 |
| CH | 324 | 317 | 42 | 48 | 850 | 1470 | 2700 | 850 |
| SC | 317 | 300 | 48 | 65 | 1400 | 1400 | 1400 | 1400 |
| CH | 300 | 296 | 65 | 69 | 850 | 1470 | 2700 | 850 |
| Sand | 296 | 281 | 65 | 84 | 2400 | 2400 | 2400 | 2400 |
| SC | 281 | 271 | 84 | 94 | 1400 | 1400 | 1400 | 1400 |
| CH | 271 | 229 | 94 | 136 | 850 | 1470 | 2700 | 850 |
| SC | 229 | 203 | 136 | 162 | 500 | 530 | 970 | 530 * |
| SC | 203 | 201 | 162 | 164 | 500 | 530 | 970 | 4340 ** |
| GR CH | 201 | 196 | 164 | 169 | 300 | 320 | 550 | 550 * |
| SC | 196 | 500 | 169 | -135 | 500 | 500 | 500 | 500 |

NOTES: 100% saturation assumed at elevation 229 ft
* 5% DNAPL saturated
** 100% DNAPL saturated

baseline and calculated contaminated profiles are plotted in Figures 5.6 through 5.8 and discussed below.

Comparison of the clean profile and 5% profile in Figure 5.6 shows good contrast between the contaminated and clean layers for each contaminated layer. However, the contrast between the contaminated layer and the clean layers (sandy) above and below it are very small. This lack of contrast makes detection difficult without either 1) resistivity data from the location prior to contamination, or 2) if a very accurate resistivity model based on soil type was available. The CPT data would be used to determine soil classification. In general, the 5% DNAPL calculation shows less than a factor of 2 contrast between adjacent clean and contaminated layers, which is less than the scatter observed in the borehole data. Based on these calculations, detection of a 5% DNAPL concentration would be very difficult.

Figure 5.7 shows that at a 50% DNAPL content, the layer from elevation 270 ft to 230 ft has over a factor of 2 contrast between adjacent clean and contaminated layers. This contrast could be identified easily by the CPT resistivity. Using an accurate resistivity model, the thin contaminated layer at elevation 320 ft could be identified by the CPT. However, the layer at elevation 300 ft has less than a factor of 2 contrast with the layer below elevation 296 ft and would be difficult to detect.

Figure 5.8 shows the 100% DNAPL calculation which assumed that pure DNAPL was located in a layer 2 ft thick just above the green clay. A 5% DNAPL concentration was assumed in the sands just above and below this layer. The pure DNAPL is clearly evident in the profile and should be easily detected. The 5% DNAPL layer just above the 100% layer shows only a slight contrast and will be difficult to detect with the CPT.

The calculations above indicate that the P/R-CPT will be able to detect highly contiguous DNAPL concentrations. When the CPT resistivity data is coupled with a highly accurate resistivity model and used with the CPT's ability to identify soil types, the DNAPL detection limit can be reduced to lower concentrations, but not as low as 5%. The degree of

detection is dependant upon the uniformity of the geology and model accuracy. Detection of limits and model assumption will be further discussed in Section 6.

## PARAMETRIC SURFACE RESISTIVITY CALCULATIONS

Detection of DNAPLs using surface resistivity is based on analytic modelling of the resistivity profile. The data from a surface survey is analyzed to back calculate the profile based on the measured data. A layer with high DNAPL concentration will show up in the backcalculated profile as having higher resistivity than expected. The sensitivity of this method depends on the complexity of the site, degree of contamination, and thickness. Parametric calculations were conducted to evaluate the influence of these parameters on the backcalculated properties for a Wenner array. The Wenner array is a special case of four electrode dipole-dipole configurations. The apparent resistivity from a Wenner array is:

$$\rho A = 2\pi A \frac{\Delta v}{I} \tag{5.4}$$

where: A = equal spacing between electrodes
$\Delta$v = voltage between the inner electrodes
I = current through the outer electrode

The apparent resistivity is in ohm-meters if A is in meters, $\Delta$v in volts and $I$ in amperes. The parametric calculations of Wenner array soundings were conducted using the resistivity profiles and properties in Table 5.2 and the RESIX-PLUS computer program developed by Interpex Limited, of Golden, Colorado. Calculations were performed by first conducting a forward calculation using the profiles in Table 5.1 to develop a synthetic data set, then conducting inversion calculations, assuming either 4 or 5 layered sites. The ability to resolve the original layering is discussed in the following paragraphs for a clean site and the 50% to 100% DNAPL contaminated profiles. Based on the calculations in the previous section, it was decided that a surface survey could not detect a 5% DNAPL contaminated layer. Figures 5.9, 5.10 and 5.11 show the results of the calculations.

Figure 5.9 is a comparison of the baseline clean profile to 4 and 5 layer inversions based on the synthetic data generated from the forward calculation. These calculations were conducted to evaluate how well inversion routines predict site sensitivity profiles. Both the 4 and 5 layer cases tended to average out the details of the site profile above the water table. The high resistivity near surface layer and water table depth were predicted quite well by both calculations; however, the high resistivity layer from elevation 296 ft to 282 ft was missed by both calculations. These calculations indicated that any subtle details in a resistivity profile can not be backcalculated from a surface survey. Therefore, low degrees of DNAPL contamination, which cause only subtle changes in the resistivity, can not be detected by a surface survey.

Figure 5.10 shows comparisons of the clean baseline resistivity profile to a profile with 50% DNAPL case. Inversion calculations for the 4 and 5 layer cases are compared to the clean baseline and 50% DNAPL baseline profile. These calculations show that a significant contrast exists between the clean baseline calculations and forward calculation as was discussed previously and the inversion calculations. The inversion calculations for both the 4 and 5 layer case show over a factor of two increase in the resistivity at elevation 260 ft to 212 ft, which can be detected with a surface survey. The contaminated layers above elevation 296 ft show up as a slight increase in the overall resistivity, which could not be delineated from the scatter in the data set. These calculations tend to indicate that a thick DNAPL layer with a high degree of contamination can be located by surface resistivity surveying. However thin layers with less than 100% DNAPL contamination will be difficult to locate. While the calculations indicate that surface surveys can locate these thick layers, this condition has not been observed at the SRS site in any of the monitoring wells drilled at the site. Therefore surface surveys to locate the DNAPLs in the vadose zone appear to have little utility.

The final calculation profile assumes that a thin layer of 100% DNAPL is located just above the green clay layer. This condition potentially exist at some locations as DNAPL product was found in one well. The 100% DNAPL is clearly visible in the contaminated profile as the spike in resistivity at elevations 203 ft to 201 ft. Examination of the 4 layer

profile shows that it did not predict the resistivity of the DNAPL layer. The effect of the DNAPL layer was to predict a slightly higher resistivity below the water table depth, but at the actual DNAPL layer depth the 4 layer case predicts essentially the resistivity of the saturated layer.

The 5 layer case did predict the DNAPL layer location as a thicker lower resistivity layer, centered around the actual layer depth. The predicted resistivity is well above the resistivity of the saturated layer and could be used to locate potential DNAPL concentrations, although volume estimates of contaminated soil may contain significant errors.

## SUMMARY OF CALCULATION RESULTS

The downhole resistivity calculations indicate that the P/R-CPT has the ability to resolve fine detail and contiguous ganglia DNAPL concentrations in clay zones potentially as low as 5% of available pore space. By comparing measured resistivity to resistivity model predictions based on the CPT derived soil type and degree of saturation, one can evaluate if the soil is contaminated. This approach requires that the model used to predict the resistivity profile be accurate to less than the resistivity data scatter, which is roughly a factor of 2 (see Figure 5.5). The laboratory program presented in the next section was conducted to evaluate the accuracy of Archie's law for the SRS site. As will be discussed, Archie's law does not appear to fit the SRS data well due to the low degree of saturation in the vadose zone. An alternate model was developed to fill this need.

The surface resistivity calculations indicate that surface resistivity can locate either: 1) DNAPL concentrations as low as 50% in the vadose zone if the layer is thick, or 2) thin layers of DNAPL at high concentrations if the DNAPL is located below the water table. As these conditions have not been observed at the SRS site it was deemed prudent to conduct P/R-CPT surveys to determine if such conditions may exist before conducting any field surface surveys.

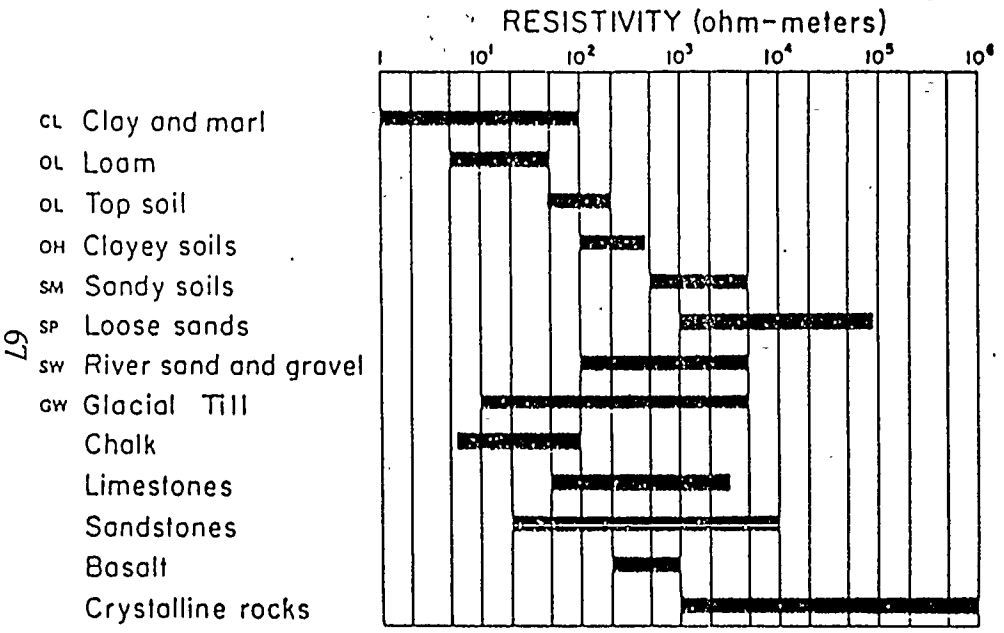


Figure 5.1. Resistivity ranges for various terrain materials (after Culley et al.)

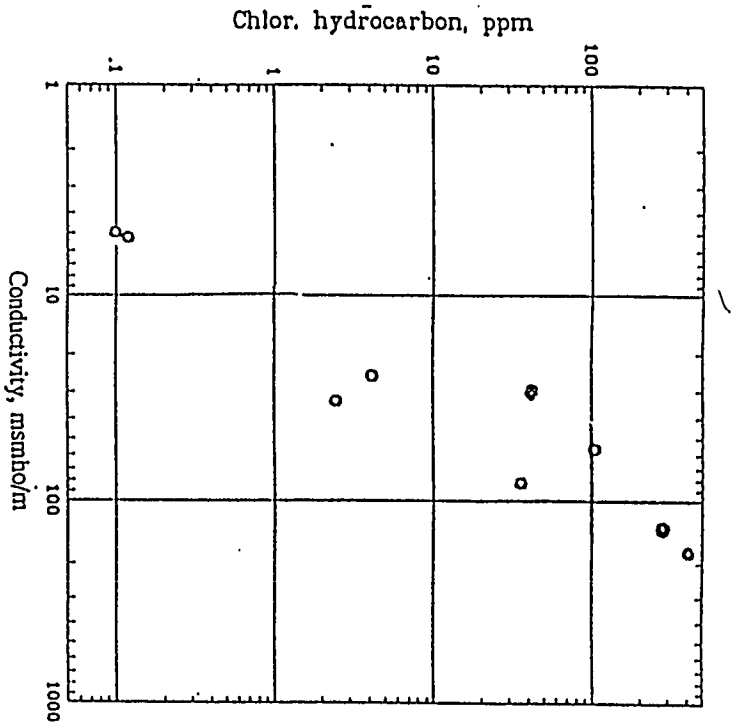


Figure 5.2. 1, 2 - dichloroethane vs. electrical conductivity (water analysis, industrial site) (Ref. Saksa and Korkealaakso).

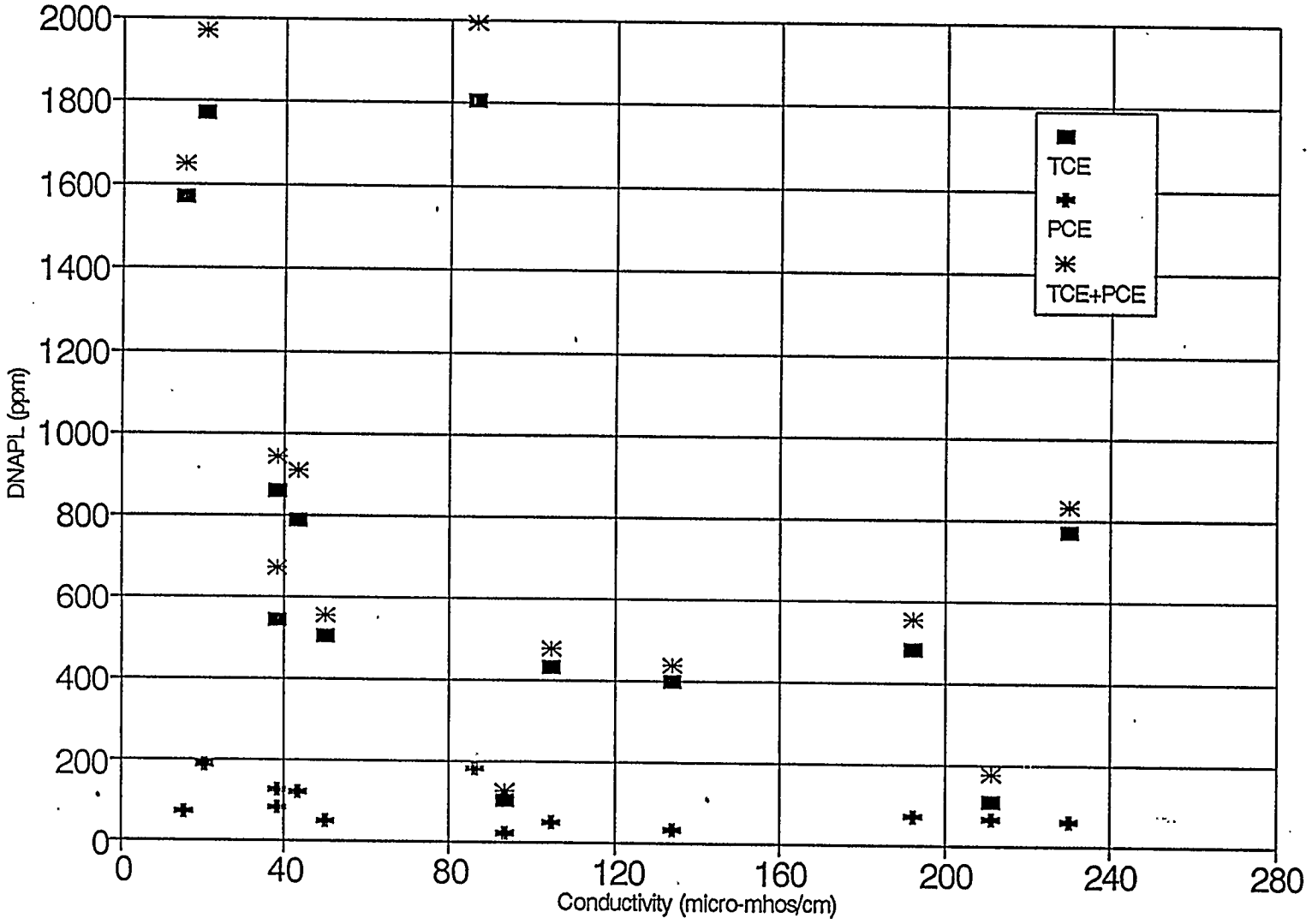


Figure 5.3. Electrical conductivity of water as a function DNAPL concentration.

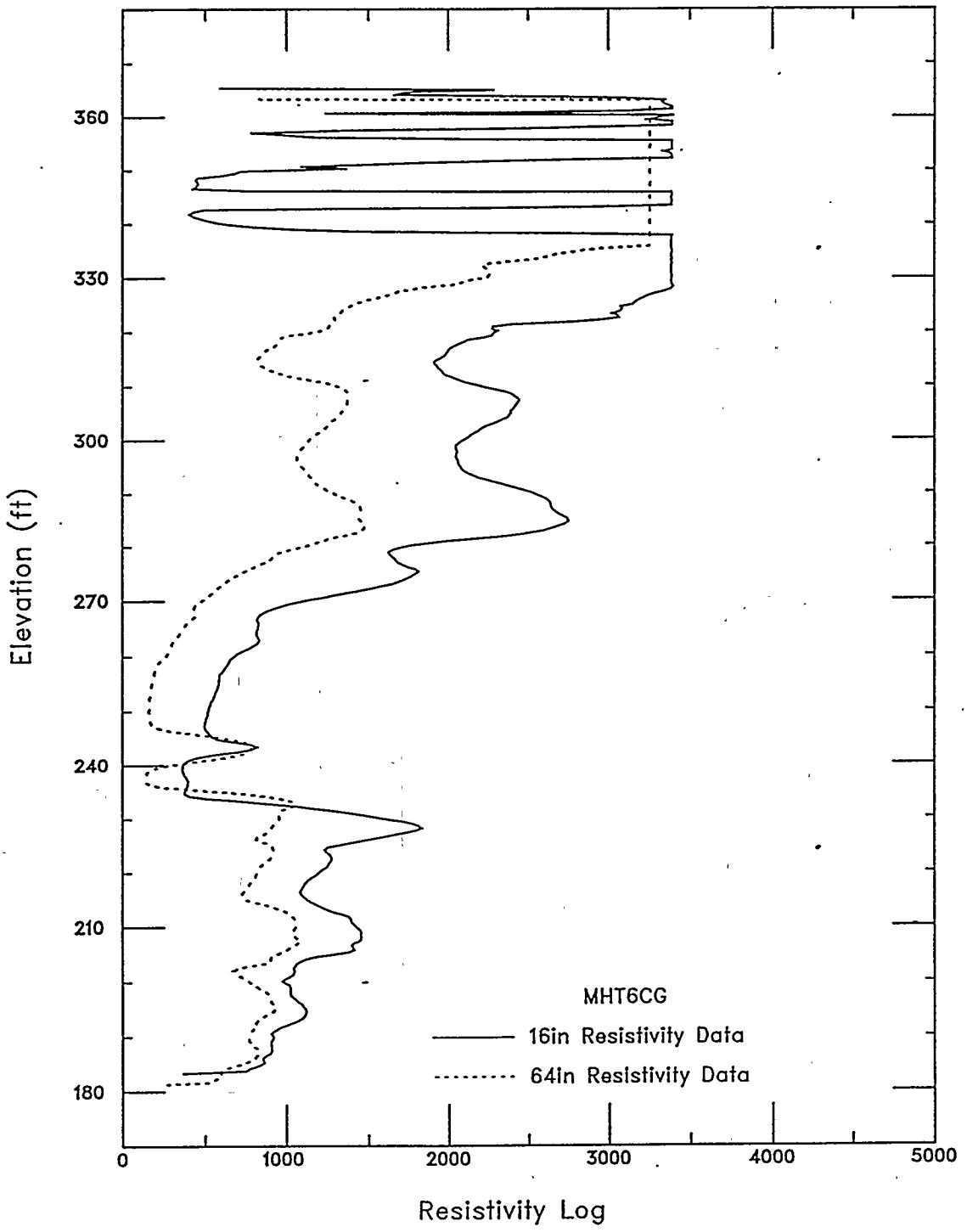


Figure 5.4. Typical borehole well log showing both 16" and 64" logs. Near surface logs show bandedge of data. CPT resistivity logs show higher values in the near surface area.

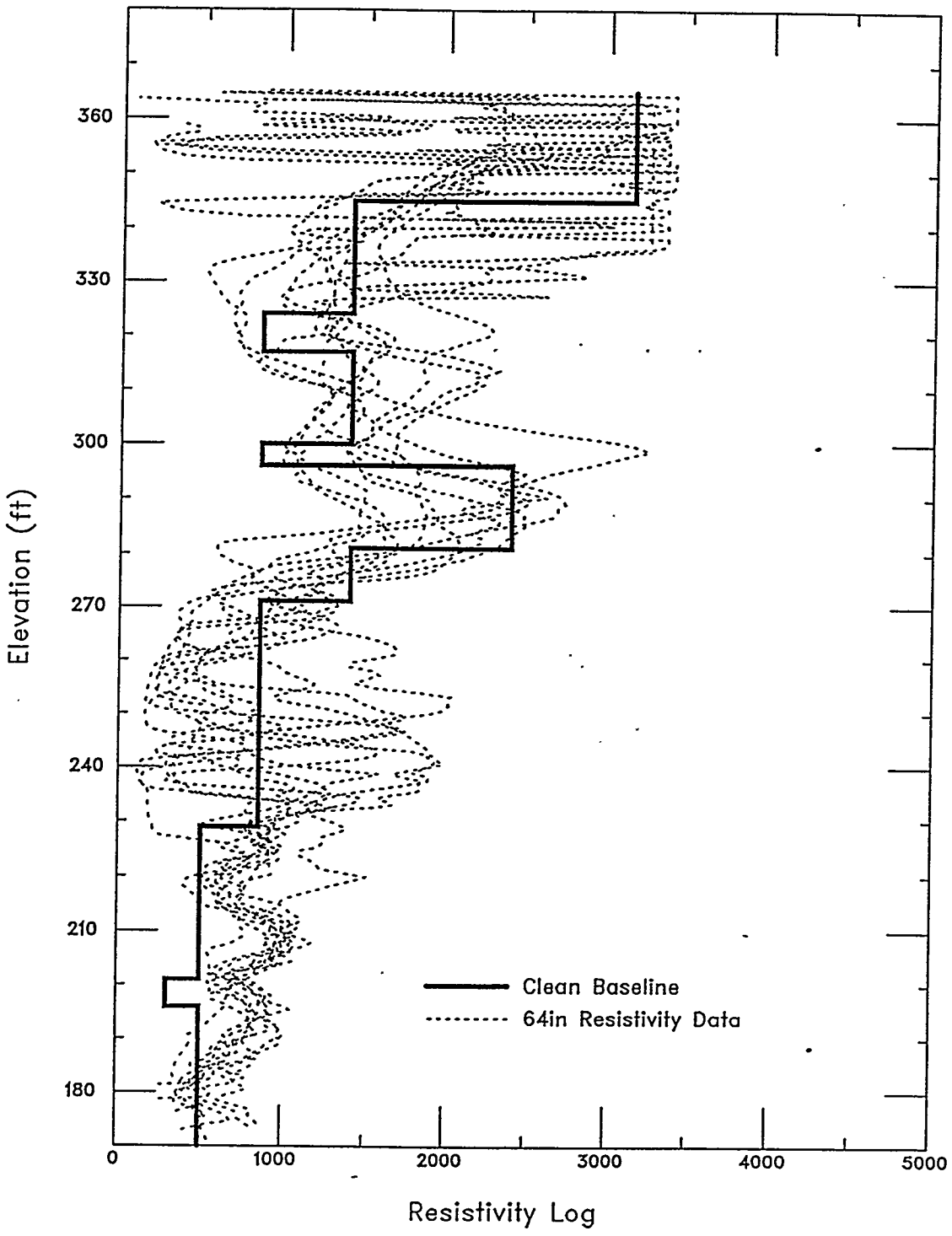


Figure 5.5. Overlay of 64" resistivity data, with average profile overlayed.

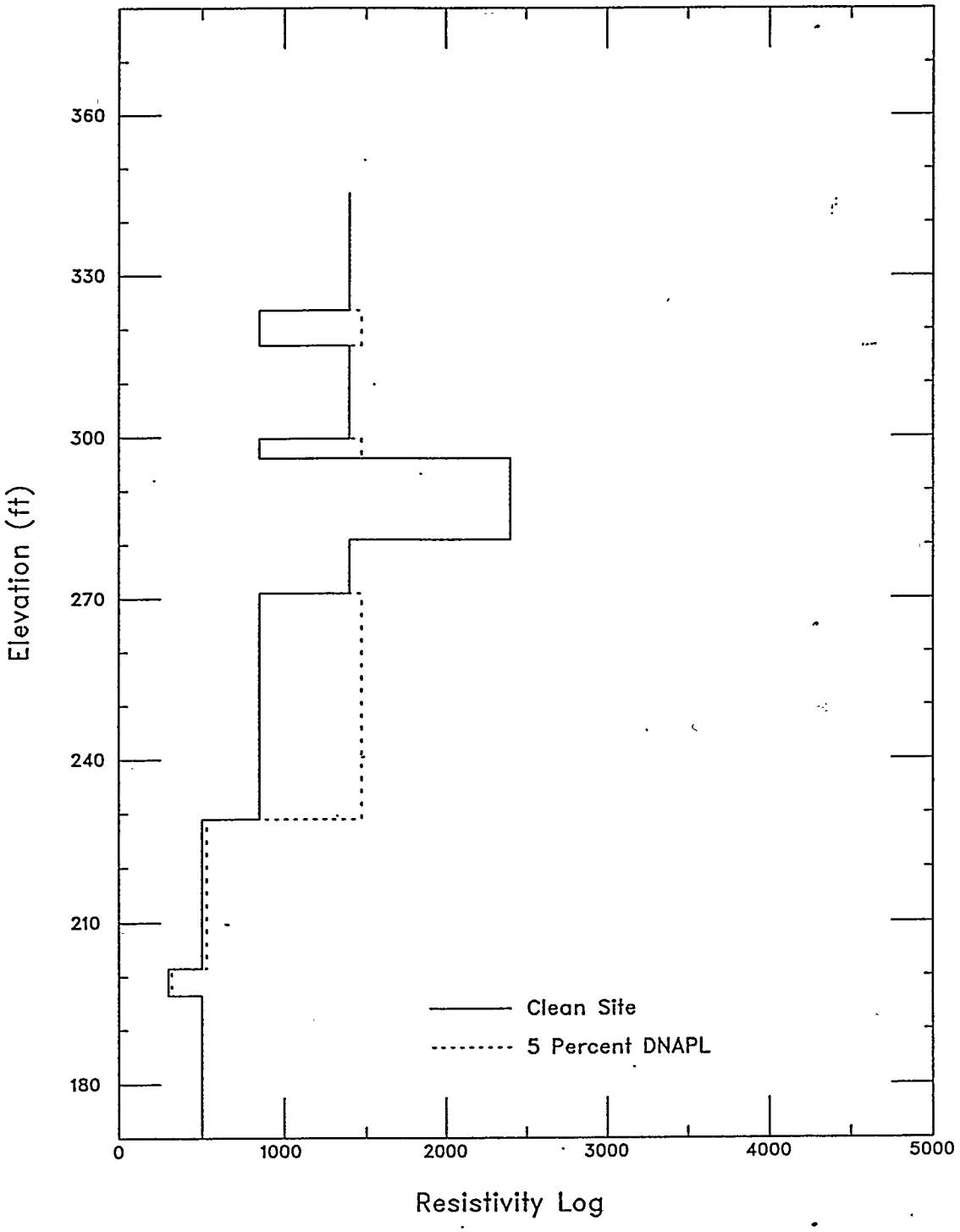


Figure 5.6. Comparison of clean site with 5% DNAPL contamination. DNAPL assumed in the clay rich layers.

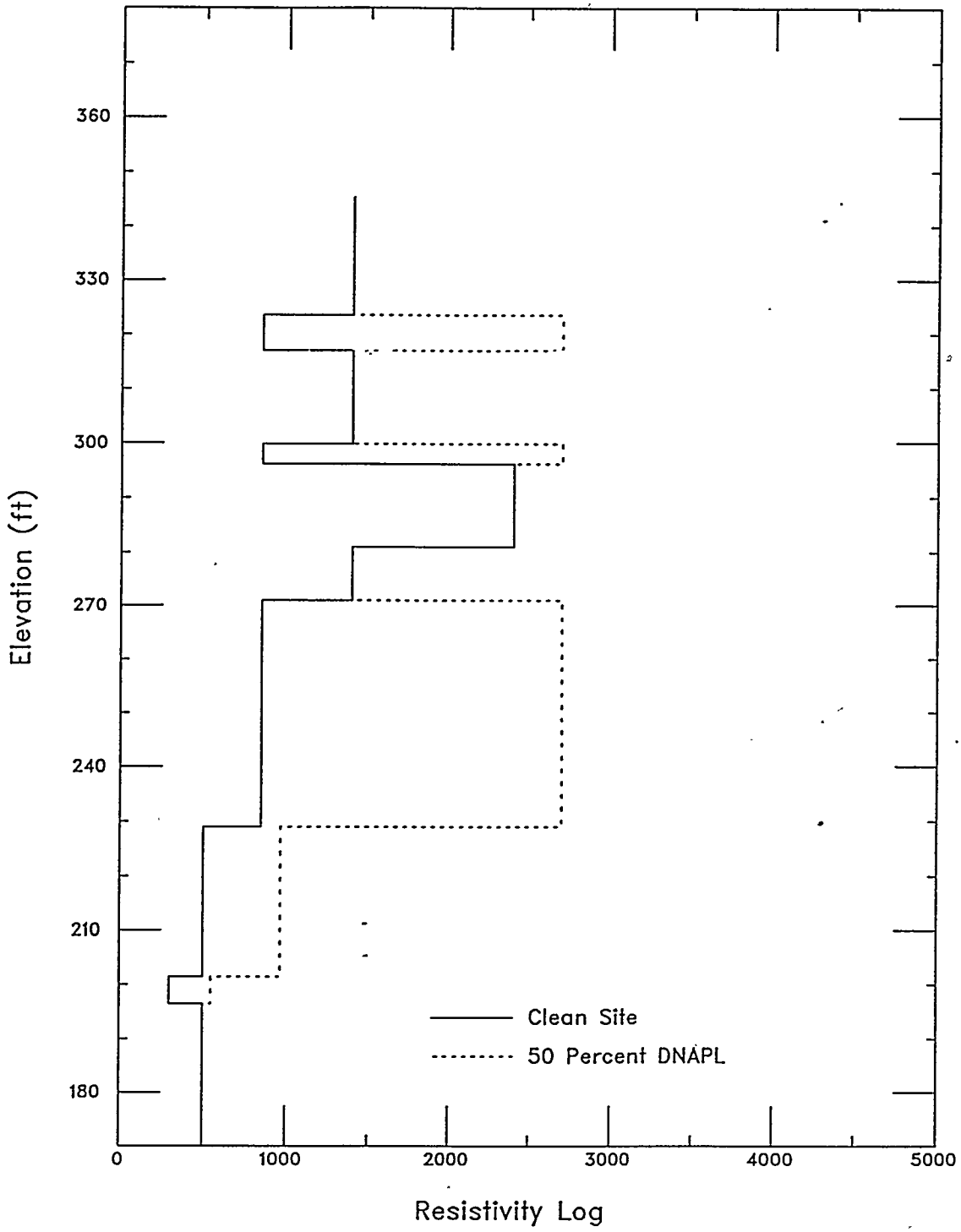


Figure 5.7. Comparison of clean site with 50% DNAPL contamination. DNAPL assumed in the clay rich layers.

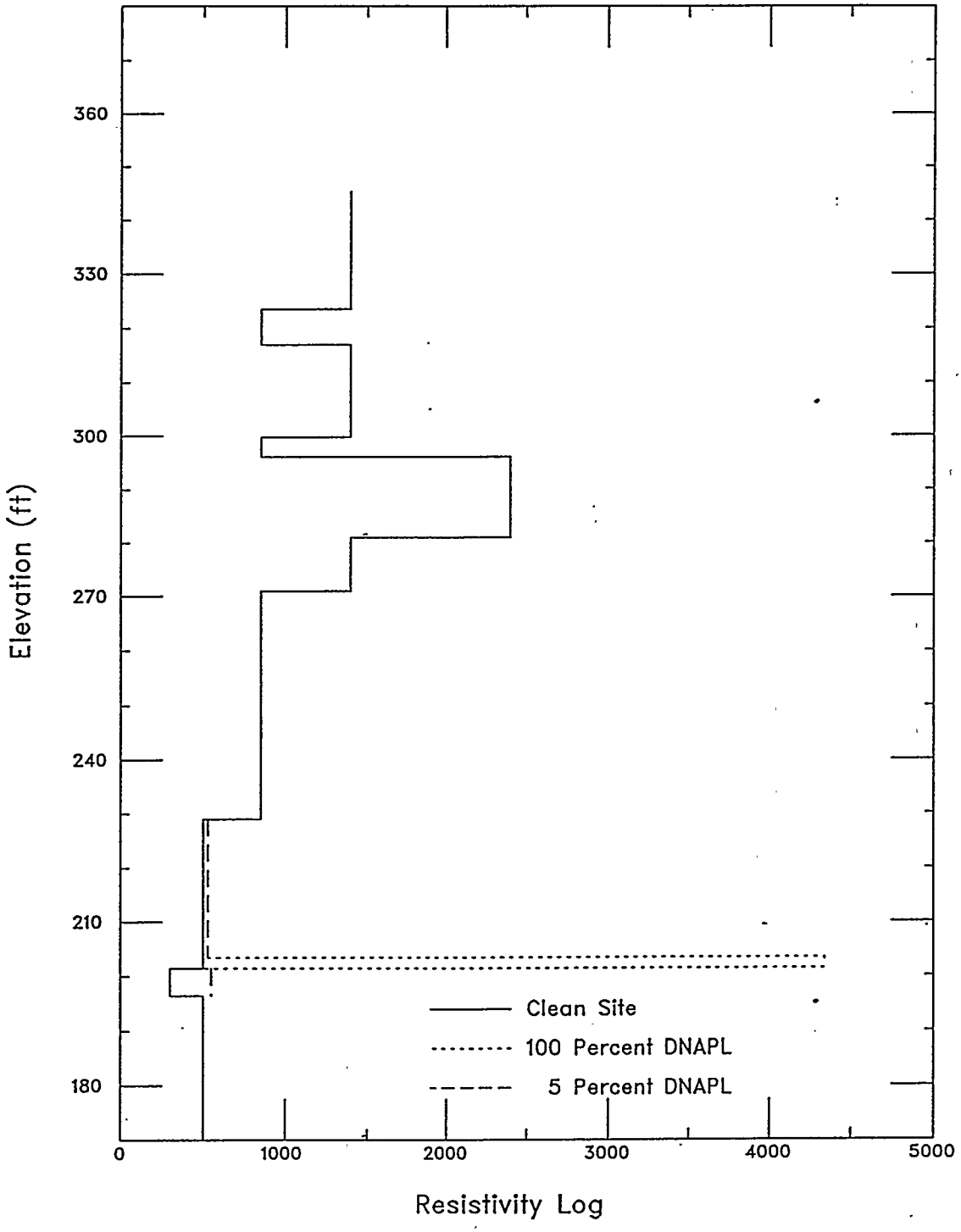


Figure 5.8. Comparison of clean site to a sequence of 5%, 100%, 5% DNAPL contamination. 100% DNAPL layer is two ft. thick and lies on top of the green clay layer.

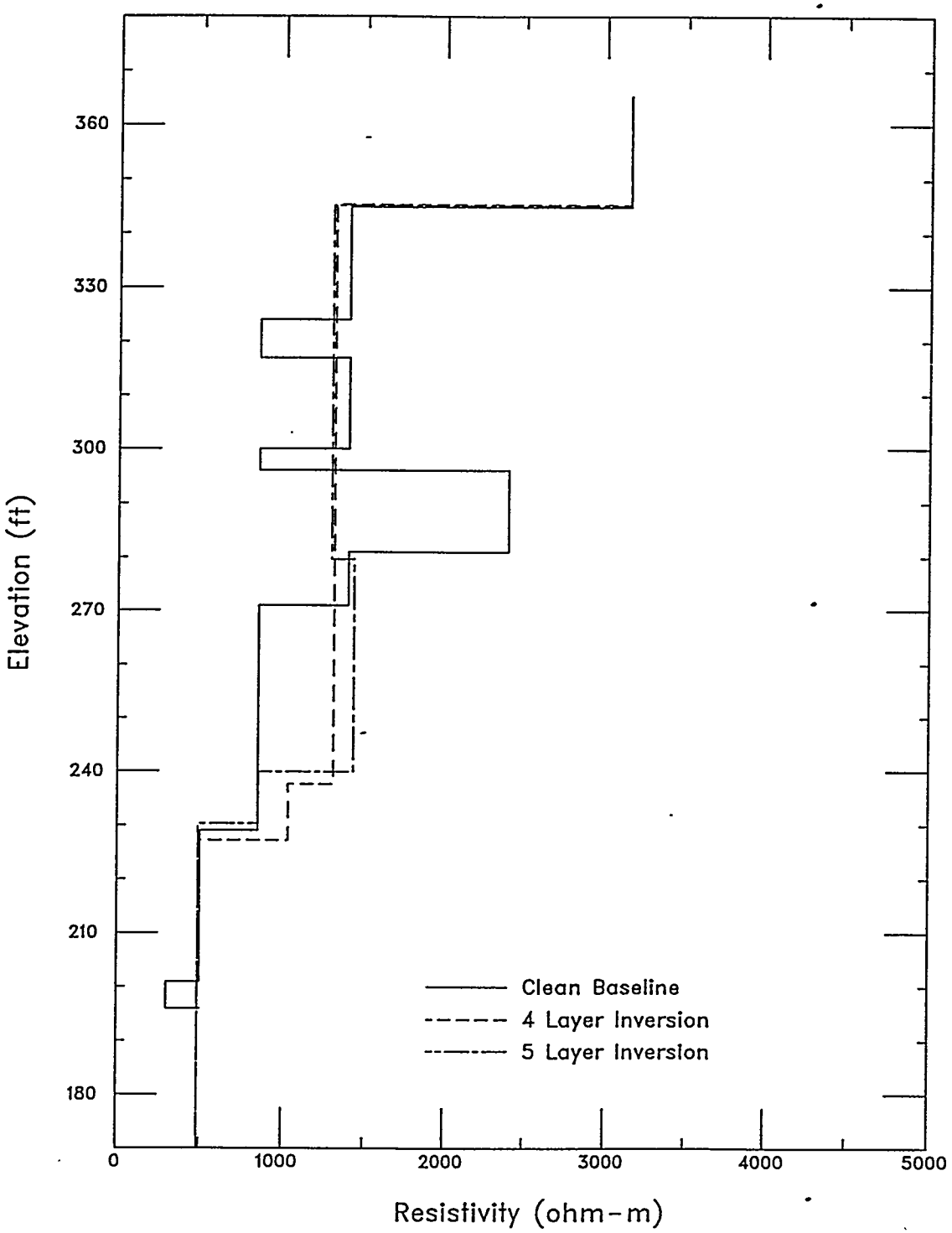


Figure 5.9. Comparison of 4 and 5 layer inversions to original profile. All profiles assume no DNAPL contamination.

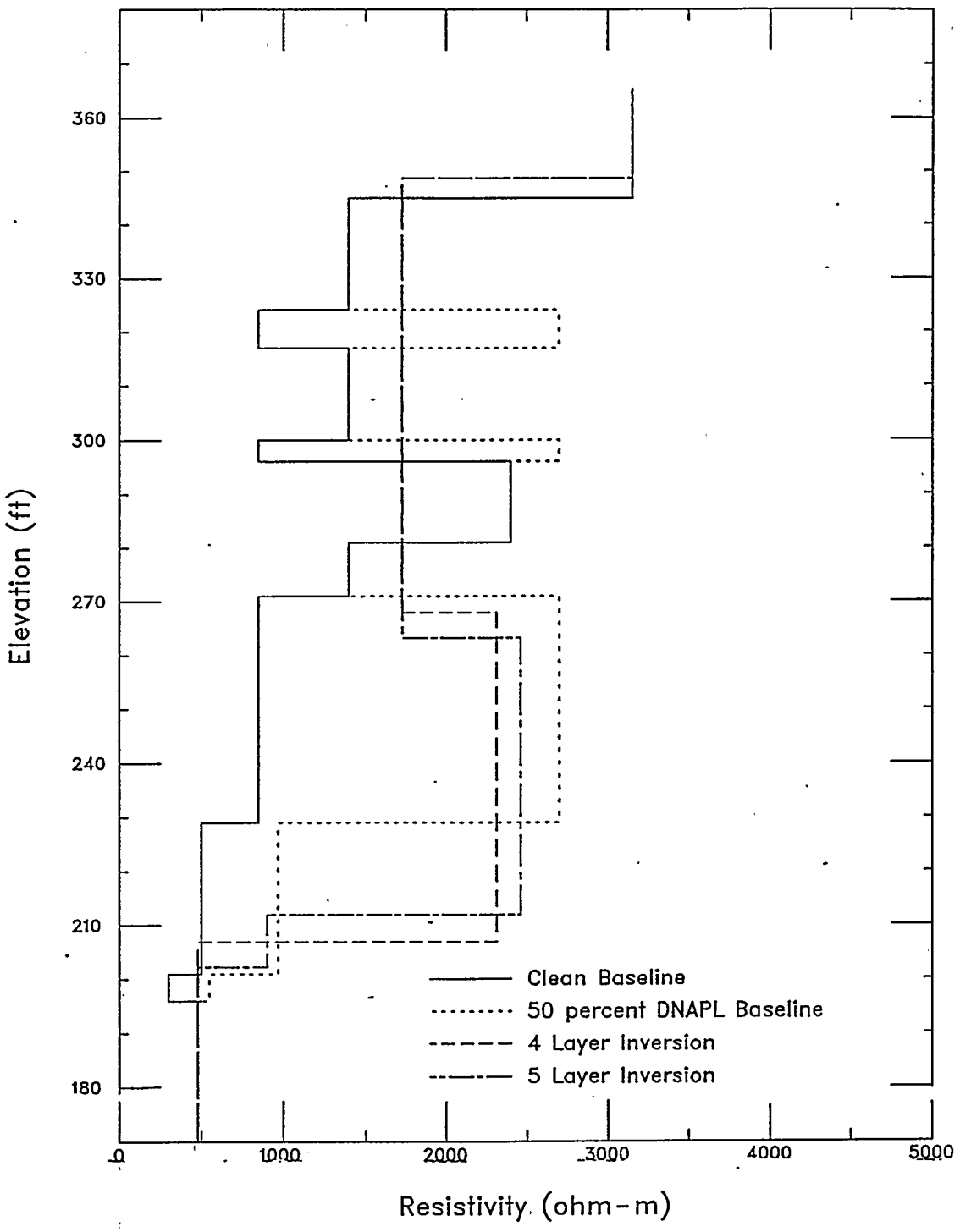


Figure 5.10. Comparison of clean baseline resistivity profile to 50% DNAPL forward calculation and inversions using both 4 and 5 layer cases.

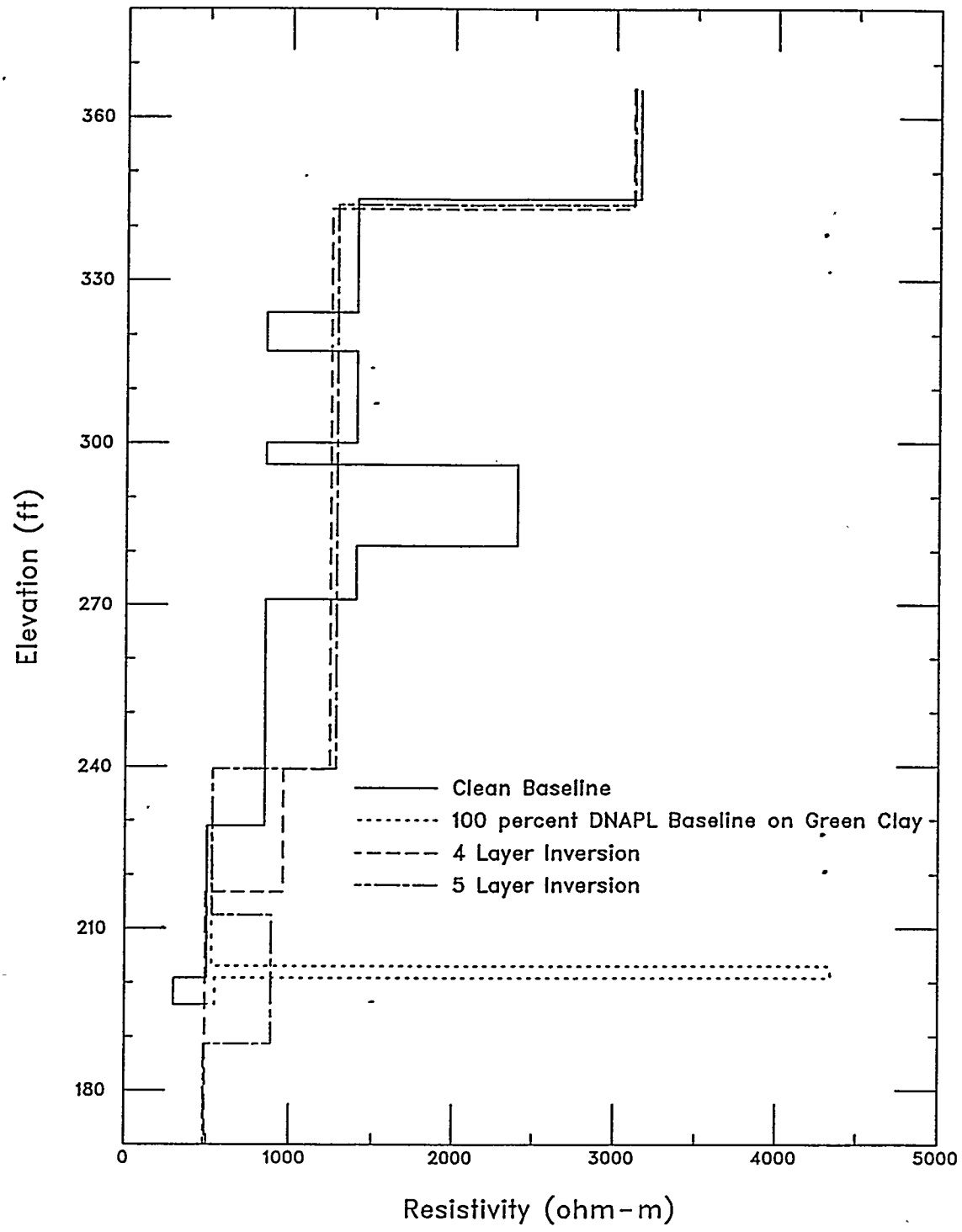


Figure 5.11. Comparison of clean baseline profile to profiles with 100% DNAPL just above the green layer.

# SECTION 6
# LABORATORY TEST PROGRAM

## OBJECTIVE OF PROGRAM

Laboratory testing was conducted on soil samples from the Integrated Demonstration Site to evaluate empirical models used to calculate the influence of DNAPLs on soil resistivity. The laboratory test program consisted of index testing to determine the grain size distribution, followed by tests in a resistivity cell to evaluate the influence of soil type, density, water content, and DNAPL concentration on the resistivity of the soil sample. Soils which were tested are listed in Table 6.1. Presented in this section are the results of the grain size test, a discussion of the laboratory resistivity test cell procedures, the test results and evaluation and development of resistivity models.

Table 6.1. Summary of soils data.

| Soil Name | Depth (ft) | Dry Weight of Sample (gm) | W (%) | -200 Material % | $D_{10}$ | $D_{50}$ |
|---|---|---|---|---|---|---|
| Saturated Sand | 136-137 | 493.1 | 15.1 | 10 | .075 | .30 |
| Vadose Sand | 76-77 | 196.79 | 10.25 | 1.5 | .15 | .37 |
| Green Clay | 158.5-159.5 | 559.42 | 21.8 | 16.4 | .06 | .21 |
| Clayey Sand | 156.5-157.5 | 321.26 | 21.63 | 8.6 | .075 | .15 |
| 40' Clay | 36-37 | 206.4 | 31.1 | 23 | .045 | .21 |

## SOIL DESCRIPTIONS

Soil samples of representative strata were obtained from Boring MHT-19C at nominal depths of 36 ft, 76 ft, 136 ft, 156 ft, and 158 ft. These soils were selected to be representative of the 40 ft clay, vadose zone sand, saturated sand, and green clay. Both samples from below 155 ft were identified as the green clay. The sample at a depth of 156.5 ft to 157.5 ft contained more fine grained material than the sample from 158.5 to 159.5,

which was labeled as the green clay. The grain size distribution was determined using ASTM method D422. The results of the grain size distribution tests are plotted in Figure 6.1. Table 6.1 contains the soil classification and percentage of fine grained material, defined as soils with a grain size smaller than a No. 200 sieve (size opening of .074 mm), along with the $D_{10}$ and $D_{50}$ grain sizes ($D_{xx}$ designates the diameter at which a given percent passes). All of the soils contain greater than 50% sand content, with none of the soils containing any gravel size fragments. The soils locally classified as "green clay" and the "tan clay" zone both contain 16% and 23% fine grain material respectively. The saturated sand, green clay and 40 ft clay all have similar grain size distributions. As suspected from the visual examination, the clayey sand at a depth of 156.5 ft to 157.5 ft has a higher percentage of fine material as is evident by a $D_{50}$ of .15 mm (clays and silts are typically assumed to have a particle size of .074 mm or less). These four soils contain sufficient clays, silts and fine sand to significantly reduce the hydraulic conductivity. The vadose sand is much coarser, contains almost no fine grained material and will have a very high hydraulic conductivity as compared to the other four soils.

## RESISTIVITY TEST CELL

The resistivity of the SRS soils was determined using a test cell in which the soil type, degrees of saturation, density, water conductivity and, for two tests, the degree of contamination were varied. Due to the small soil quantity available for testing, a small volume test cell was built in which samples could be prepared at known dry densities and water contents. The porosity and degree of saturation were varied in the cell by use of a hydraulic press to compress the samples. The cell was fabricated from KYNAR®, which is a chemically resistant, high strength plastic. Chemical resistant plastic was used in the cell to minimize cross contamination between the test series. Initial testing was conducted with a 4 ring electrode set up, much like that of the resistivity CPT and like that presented by Wheatcraft (1989). Due to the large strains applied to the test sample (as much as 20%), excessive movement of the inner rings was observed, leading to a non-linear cell calibration factor. Therefore, the measurement system was changed to a two-ring system, which is shown schematically in Figure 6.2.

The test cell was calibrated using distilled water in which Sodium Chloride (NaCL) was mixed to decrease the resistivity. The cell calibration factor was then obtained by fitting the ratio of the measured current and potential drop to the measured resistivity of the fluid in the cell as determined by a calibrated conductivity meter.

Samples were prepared to specified initial densities and water content. The samples were then placed in the hydraulic press, and the measuring electrodes were attached to the cell. For each test series, the initial density, moisture content, sample dry weight and length were measured and used to calculate the change in degree of saturation and porosity as the sample was compressed. For those samples which became saturated during the tests, the drain port was opened so that excess pore fluid could be drained as the sample was compressed. Tables 6.2 through 6.6 (located at the end of Section 6) contain the raw and reduced data for each test series.

While not used for this test series, the resistivity cell was designed so that various fluids could be passed through the test sample via the inlet and outlet ports.

## EVALUATION OF ARCHIE'S LAW

Archie's law was evaluated by comparing the laboratory derived data to model calculations. As discussed in Section 5, variables which influence soil resistivity that were tested in the laboratory include soil type, porosity, pore fluid conductivity, and degree of saturation. Resistivity of the pore fluid was best measured using pore fluid extracted from the test cell. The initial tests were conducted with deionized water, with a resistivity of 1000 ohm-m. Measurements of the pore fluid after the tests showed a significant colloidal content which greatly reduced the pore fluid resistivity. The colloidal content of the samples was due to clay in the tests and the addition of even 1% water greatly reduced the sample's resistivity, most likely due to a combination of the double layer conductivity and conduction through the clay suspended in the water phase.

Given that the soil porosity, degree of saturation and fluid conductivity were determined from the test data, the only unknown parameters in Archie's law are a, b, and m. Estimates of these parameters were made using an optimization routine contained in the Quattro® spreadsheet program. This routine derives the parameters which best fit the data. Limits are set on each of the parameters so that reasonable values are derived. These limits were chosen to be consistent with published values.

For reasonable bounds no one set of empirical constants adequately predicted the laboratory data. Typical results for the clayey sand at a depth of 156 ft are plotted in Figure 6.3. Assumed values of the empirical constants are: $\alpha = 0.1$, $m = 1.75$, $b = 2.0$ and $a = 1.0$. As is evident, calculated resistivity using Archie's Law and the laboratory data are in poor agreement with the calculation overestimating the measured resistivity. If the correlation were perfect the data would fall on a 45 degree line. Figure 6.4 is a plot of the ratio of the calculated to measured resistivity as a function of degree of saturation. This figure shows that the error in the calculated values decreases as the degree of saturation increases. At low saturation the error is as great as a factor of 50, while the error reduces to approximately a factor of 2 for saturation greater than 55%.

The principal reason for the poor agreement is that Archie's law was developed for saturated media. For high degrees of saturation, Archie's law can provide reasonable answers at the SRS site. The factor of two difference in Figure 6.4 for saturation greater than 55% could be reduced to an acceptable level. However, at the Integrated Demonstration Site, up to 150 ft of the soil profile has a low degree of saturation as is evident by the high resistivity values of the R-ECPT and borehole log data. Prediction of the DNAPL concentration relies upon an accurate resistivity model; Archie's law for low saturation levels does not meet this criteria. The primary reason for the poor agreement is associated with the conductivity of the clay double layer and colloidal conductivity, both of which are strongly dependent upon the degree of saturation and only weakly dependent upon the porosity. As discussed below, a model based on degree of saturation is more appropriate for the Integrated Demonstration Site.

## RESISTIVITY PREDICTIONS BASED ON DEGREE OF SATURATION

The measured resistivity for the clayey sands versus degree of saturation is plotted in Figure 6.5. This data shows a strong dependance on degree of saturation. As the soil degree of saturation increases, the resistivity rapidly decreases with the greatest change occurring between 0 and about 20% saturation. Over this range the resistivity changes two orders of magnitude. From 20% to 100% saturation the resistivity changes less than an order of magnitude, with the change beyond 60 % saturation being only 20 ohm-m. This figure suggests that a saturation based model can provide accurate prediction of the clayey sand resistivity. The data were fit with an exponential equation as:

$$p = 10^{(a + b \log s + c \log s^2)} \qquad (6.1)$$

where p = resistivity

a, b & c = fit parameters, and

s = degree of saturation (%)

The exponential fit shown provides a good fit to the data.

Data from tests on the vadose zone sand are plotted in Figure 6.6. This data set contains more scatter than the data set shown in Figure 6.5. A fit has been forced through all of the data. This fit indicates higher resistivities at high degrees of saturation as compared to the clayey sand data. This is expected as the vadose-sand has little fine grained material, while the clayey sand has 50% of the soils passing a .15 mm sieve size. Increased fine grained soil content, especially clay-sized materials, will decrease the resistivity of a soil.

Figure 6.7 contains the test data for the saturated sand sample, along with a fit to the data. The data and fit are in good agreement, with the maximum difference being less than a factor of 25%. Figure 6.8 contains the 40 ft clay data and fit. The data generally agrees with the model, except for the one data point at 79% saturation. This point may be affected by a sample seating problem, as this data point was obtained before the sample had been

compressed. The soil and electrode may not be in good contact leading to high contact resistance.

A plot of the green clay data and fit to the data is given in Figure 6.9. The data and fit are in good agreement except for the second data set which was obtained for a water content of 2.5%. The second data set does not fit with the bulk of the data, and it is believed that the measured water content may be in error due to a mixing problem. Other than the second data set, the green clay data agrees with the model with the greatest deviation being less than 20% at 45% saturation.

Figure 6.10 is an overlay of the fits to the resistivity data. The various models were compared to more clearly show the trends in the data. Fits to the saturated sand, 40 ft clay and green clay are in good agreement, except that the 40 ft clay tends to have higher resistivity for saturation levels of 5% or less. The clayey sand just above the green clay lies well below the bulk of the data for saturations less than 90%. The reason for this data set falling lower than the bulk of the data is the higher percentage of fine grained material as determined by the grain size analysis. Likewise the vadose zone sand falls above the bulk of the data, due to a lower fine grained material content than the other samples.

An average fit to the 40' clay, green clay and saturated sand is shown in Figure 6.10. These data sets were chosen because the data sets were of high quality and consistent with each other. This average fit will predict the laboratory test data within a factor of two or less and will be used in the modeling section discussed later. Table 6.7 contains the fit parameters for each soil type and the average fit to the 40 ft clay, saturated sand and green clay.

**Table 6.7. Fit constants for laboratory resistivity tests on SRS soils.**

| Soil Type | Empirical Constants | | |
|---|---|---|---|
| | a | b | c |
| Sat. Sand | 4.458 | -1.2557 | 0.0291 |
| Vadose Sand | 4.7297 | -1.886 | 0.4523 |
| Green Clay | 4.2848 | -0.8616 | -0.1817 |
| Clayey Sand | 4.4086 | -2.1914 | 0.4502 |
| 40' Sand | 4.32 | -0.432 | -0.433 |
| Average* | 4.368744453 | -0.870107 | -0.1852805 |

*Sat. Sand, Gr. Clay and 40' Clay only

## INFLUENCE OF DNAPL ON RESISTIVITY

The last test series consisted of mixing 5% DNAPL with the clayey soil at an oven dried and 5.0% moisture content. The objective of these experiments was to determine the influence of DNAPL on the soil bulk resistivity. Within the oil exploration industry, (Eslinger et al., 1988) the effect of oil on the bulk resistivity response is modelled as if the oil is an insulator and effectively reduces the pore space available for high conductivity fluids. Figure 6.11 is a plot of the clean soil data, along with the tests conducted with 5% DNAPL. The data is plotted using the measured porosity and calculation of the degree of saturation based on the sum of the water and DNAPL fluid content. The plot shows that the DNAPL samples do not plot with the other data, but have higher resistivity for a given degree of saturation.

Figure 6.12 is the same data, but assumes that the DNAPL acts as an insulator. For these tests the degree of saturation is calculated as:

$$S_t(\%) = V_w/(V_D + V_S) \qquad (6.2)$$

where $V_w$ = Water Volume

$V_D$ = DNAPL Volume

$V_S$ = Solids Volume

The DNAPL contaminated data set now agrees with the clean soil fit, demonstrating that the influence on DNAPLs on soil resistivity can be modelled using the same assumptions as used by the oil industry. This conclusion is preliminary as only a limited number of tests were conducted with contaminated soils due to the small quantities of soil available and the tests were conducted on fresh soil/DNAPL mixtures which have not been aged. Any long term influence of DNAPLs on the clay resistivity would not be modeled by these tests.

Equation 6.1 was used as the basis to model the effect of DNAPL concentration on resistivity and parametric calculations conducted in which the DNAPL and degree of water saturation were varied. Results of these calculations are plotted in Figures 6.13 and 6.14 using the fits to the clayey soils and vadose zone soils. The calculated resistivity is plotted as a function of the total saturation which is defined as the sum of the DNAPL and water saturation. The percentage of DNAPL was varied from 5% to 90%.

For clayey sands (the average fit to the 40 ft, saturated sand and green clay data was used in these calculations) the calculations indicated that 5% DNAPL contamination results in a significant change in the resistivity at low degrees of saturation but only a minor change in the soil resistivity at high degrees of saturation. Detection of 5% DNAPL with resistivity will be difficult as the contrast between the clean and contaminated soil is typically less than a factor of two, which is less than the scatter observed in the borelog data. At higher DNAPL contents, the contrast increases rapidly, such that at 20% DNAPL concentration there is a large contrast. With an accurate measure of the soil degree of saturation and soil type, the DNAPL concentration could be estimated for degrees of saturation less than about 50%; however, above 50% the contrast is less than a factor of 2 and resistivity would not provide a reliable estimate.

For very high DNAPL concentrations, the resistivity contrast near total saturation increases, since the DNAPLs displace a large volume of the ground water. For DNAPL

concentration greater than 50%, saturation resistivity can provide a reliable estimate if the soil type and degree of saturation are known.

For the vadose zone sands (see Figure 6.14) the influence of DNAPL concentration on resistivity is less dramatic, especially at high degrees of saturation. This should be expected as both the DNAPL and sand are poor conductors, as opposed to the more conductive clayey sands. For sands, displacement of the pore fluid by DNAPLs has the same effect as increasing the sand density. If the degree of water saturation and soil type are known, the DNAPL concentration could be estimated for those sands which have resistivity greater than 1000 ohm-m. If the resistivity is 1000 ohm-m or less this model predicts that the degree of saturation and DNAPL concentration have only a small influence on resistivity until the DNAPL concentration approaches 90% or greater where nearly all of the conductive pore fluids have been displaced by DNAPLs.

The calculations presented in Figures 6.13 and 6.14 indicate that there is a strong influence of DNAPLs on resistivity in the vadose zone, especially when the DNAPL concentration is high. However detecting DNAPLs with resistivity in the vadose zone requires accurate knowledge of the soil degree of water saturation and soil type. Even knowing these variables, resistivity can not resolve DNAPL concentrations of 5%, which are quite high. The Bruel & Kjaer multi-gas monitor demonstrated on this project resolves and delineates gas types to the ppm range and to the ppb range for some gases, making this the logical measurement system in the vadose zone. If additional attempts are made using R-ECPT, a good site specific soil classification system is required in addition to a new device for measuring moisture content. One such new sensor would use infrared technology.

Below the ground water table, where the multi-gas monitor will not work, the degree of saturation can be assumed to be 100%, and resistivity techniques can be used to estimate the occurrence of DNAPLs as presented below.

## FRAMEWORK TO EVALUATE DNAPL CONCENTRATION

The modeling work presented above indicates that the soil resistivity data is primarily sensitive to soil type and degree of saturation and only sensitive to DNAPL concentration by it's effect of displacing the more conductive water. Prediction of the degree of contamination from CPT data must relate soil type and degree of saturation, as shown schematically in Figure 6.15. Soil type is determined using the ECPT soil classification chart described in Section 3 and resistivity of clean soil is calculated using fits to laboratory data for a given soil type. If the measured resistivity is greater than the calculated resistivity, then DNAPLs contamination is suspected. Using this method requires knowledge of the in situ degree of saturation. For soils below the water table (nominal elevation of 220 ft at the Integrated Demonstration Site) the degree of saturation can be assumed to be 100% and sufficient information is available to predict the occurrence of DNAPLs. Above the water table, the degree of saturation is unknown and DC resistivity by it's self can not be used to predict the presence of DNAPLs. An independent method to estimate the degree of saturation is required. Methods to determine the degree of saturation from the ECPT data do not currently exist, however with minor modifications the ECPT DC resistivity probe could be used to estimate soil moisture from a measure of the soil dielectric constant. In addition, new sensors using infrared techniques could be used.

Presented below are preliminary evaluation of DNAPL locations below the water table and a method to estimate the degree of water saturation in the vadose zone.

## COMPARISON OF PREDICTED AND MEASURED RESISTIVITY DATA

Using the method outline in Figure 6.15 predictions of the clean soil resistivity for soundings CPT-017, 004, 003, 015A are presented. For soils classified as sands containing few fines (CPT soil classification number $\geq$ 4.5) the vadose zone fit was used to predict clean sand resistivity of 600 ohm-m for S= 100%. For soils classified as containing significant fine grained material (CPT soil classification number $\leq$ 4.5) the average fit to the clayey soils was used to predict a clean soil resistivity of 80 ohm-m for S=100%.

Comparison of the predicted resistivity and measured resistivity are plotted in Figures 6.16 through 6.19.

Soundings CPT-017 and CPT-004 (see Figures 6.16 and 6.17) show resistivity data that are in general agreement with the predicted resistivity. The low resistivity zones correspond to clayey soils and the high resistivity zones correspond to very sandy zones. Because of the strong agreement between the calculations and measured data below the water table, a high DNAPL concentration (20% or greater) is not suspected at these two locations.

Also shown in these figures is a prediction of the degree of saturation both above and below the water table. Above the water table the degree of saturation in the sand zones is predicted to be as low as 3%. In the more clayey zones the degree of saturation is predicted to increase to as high as 100 % near surface with the clays in the vadose zone predicted to be 20% saturated.

Below the water table the model predicts that most of the soils are saturated, however there are zones which are predicted to not be fully water saturated. This occurs because the measured resistivity is greater than the calculated and the model would indicate that a portion of the pore volume is filled with a non-conducting media. At this time the predicted degrees of saturation can be used only as a rough estimate due to uncertainty in the laboratory data and CPT soil classification system.

Calculations for soundings CPT-015A and CPT-003 (see Figures 6.18 and 6.19) are typical of soundings where the predicted resistivity was much less than the measured resistivity. In Figure 6.18 the shape of the predicted and measured resistivity below the water table are quite similar, however the measured resistivity is over a factor of two greater than the calculated. According to the framework in Figure 6.15 this location would be predicted to have a less than fully DNAPL saturated thick layer. Sounding CPT-015A is near the MHT well cluster where extensive water sampling has not shown a thick DNAPL layer to exist. The discrepancy between the predicted and measured resistivity data is due to

uncertainties in predicting soil resistivity. As discussed above only 5 small samples from one well were characterized in the laboratory test program. Considerable uncertainty exist regarding the spatial variation in soil resistivity at the site. While no firm conclusion can be made about lower levels of DNAPL concentration, the comparisons in Figures 6.18 and 6.19 do suggest that if DNAPLs occur at this location, the degree of DNAPL saturation is not high. Resistivity for a highly saturated DNAPL below the water table would be expected to be much greater than the measured data.

Above the water table the calculated degree of saturation for soundings CPT -015A and CPT-003 are similar to the previous data. In the vadose zone very low saturation is predicted for the sand zones, with the degree of saturation increasing in the clay rich zones.

## Table 6.2. Laboratory Resistivity Cell Test Results for 40' Clay

14-Dec-92 Soil 5, 40' Clay

Test Parameters

| | | |
|---|---|---|
| Length | 7.5 | in |
| Diameter | 1 | in |
| Spec. Grav | 2.650 | |

| Moist. Content (%) | Sample Length (in) | Wet Density (lb/ft^3) | Dry Density (lb/ft^3) | Porosity (%) | Void Ratio | Satuation (%) | Measured Resist (ohm-m) |
|---|---|---|---|---|---|---|---|
| 0.5 | 7.5 | 86.14 | 85.71 | 48.2% | 0.929 | 1.426 | 12012.99 |
| 0.5 | 7.25 | 89.11 | 88.67 | 46.4% | 0.865 | 1.532 | 12302.88 |
| 0.5 | 7 | 92.29 | 91.83 | 44.5% | 0.801 | 1.655 | 12613.23 |
| 0.5 | 6.75 | 95.71 | 95.24 | 42.4% | 0.736 | 1.799 | 12832.76 |
| 0.5 | 6.5 | 99.39 | 98.90 | 40.2% | 0.672 | 1.972 | 13302.10 |
| 0.5 | 6.25 | 103.37 | 102.85 | 37.8% | 0.608 | 2.180 | 13822.99 |
| 2.5 | 7.5 | 72.58 | 70.81 | 57.2% | 1.335 | 4.961 | 10323.27 |
| 2.5 | 7.25 | 75.08 | 73.25 | 55.7% | 1.258 | 5.268 | 10485.95 |
| 2.5 | 7 | 77.76 | 75.86 | 54.1% | 1.180 | 5.616 | 10585.55 |
| 2.5 | 6.75 | 80.64 | 78.67 | 52.4% | 1.102 | 6.013 | 10215.21 |
| 2.5 | 6.5 | 83.74 | 81.70 | 50.6% | 1.024 | 6.470 | 7735.44 |
| 2.5 | 6.25 | 87.09 | 84.97 | 48.6% | 0.946 | 7.002 | 6036.72 |
| 2.5 | 6 | 90.72 | 88.51 | 46.5% | 0.868 | 7.630 | 4673.91 |
| 5 | 7.5 | 92.79 | 88.37 | 46.6% | 0.871 | 15.208 | 1274.40 |
| 5 | 7.25 | 95.99 | 91.42 | 44.7% | 0.809 | 16.381 | 1007.34 |
| 5 | 7 | 99.42 | 94.68 | 42.7% | 0.746 | 17.750 | 784.74 |
| 5 | 6.75 | 103.10 | 98.19 | 40.6% | 0.684 | 19.368 | 679.31 |
| 5 | 6.5 | 107.06 | 101.96 | 38.3% | 0.622 | 21.311 | 586.60 |
| 5 | 6.25 | 111.35 | 106.04 | 35.9% | 0.559 | 23.688 | 518.71 |
| 5 | 6 | 115.98 | 110.46 | 33.2% | 0.497 | 26.661 | 460.70 |
| 10 | 7.25 | 100.85 | 91.68 | 44.6% | 0.804 | 32.975 | 411.97 |
| 10 | 7 | 104.45 | 94.96 | 42.6% | 0.741 | 35.741 | 329.99 |
| 10 | 6.75 | 108.32 | 98.47 | 40.4% | 0.679 | 39.013 | 294.47 |
| 10 | 6.5 | 112.49 | 102.26 | 38.2% | 0.617 | 42.946 | 247.16 |
| 10 | 6.25 | 116.99 | 106.35 | 35.7% | 0.555 | 47.759 | 221.45 |
| 10 | 6 | 121.86 | 110.78 | 33.0% | 0.493 | 53.788 | 188.05 |
| 30 | 7.5 | 107.37 | 82.59 | 50.1% | 1.002 | 79.328 | 209.92 |
| 30 | 7.25 | 111.07 | 85.44 | 48.3% | 0.935 | 84.988 | 79.34 |
| 30 | 7 | 115.04 | 88.49 | 46.5% | 0.869 | 91.517 | 64.94 |
| 30 | 6.75 | 119.30 | 91.77 | 44.5% | 0.802 | 99.133 | 60.70 |
| 30 | 6.5 | 123.89 | 95.30 | 42.4% | 0.735 | 100.000 | 55.01 |

## Table 6.3. Laboratory Resistivity Cell Test Results for Vadose Sand

14-Dec-92 Soil 2, Vadose Sand

Test Parameters

| | | |
|---|---|---|
| Length | 7.5 | in |
| Diameter | 1 | in |
| Spec. Grav | 2.650 | |

| Moist. Content (%) | Sample Length (in) | Wet Density (lb/ft^3) | Dry Density (lb/ft^3) | Porosity (%) | Void Ratio | Satuation (%) | Measured Resist (ohm-m) |
|---|---|---|---|---|---|---|---|
| 0.35 | 7.25 | 106.21 | 105.84 | 36.0% | 0.562 | 1.649 | 13436.99 |
| 0.35 | 7 | 110.01 | 109.62 | 33.7% | 0.508 | 1.824 | 13919.68 |
| 0.35 | 6.75 | 114.08 | 113.68 | 31.3% | 0.455 | 2.040 | 14297.94 |
| 0.35 | 6.5 | 118.47 | 118.06 | 28.6% | 0.401 | 2.315 | 14847.86 |
| 0.35 | 6.25 | 123.21 | 122.78 | 25.8% | 0.347 | 2.674 | 15438.68 |
| 0.35 | 6 | 128.34 | 127.89 | 22.7% | 0.293 | 3.166 | 15924.12 |
| 5 | 7.5 | 93.79 | 89.32 | 46.0% | 0.851 | 15.564 | 1275.95 |
| 5 | 7.25 | 97.02 | 92.40 | 44.1% | 0.790 | 16.780 | 1158.28 |
| 5 | 7 | 100.48 | 95.70 | 42.1% | 0.728 | 18.203 | 1040.53 |
| 5 | 6.75 | 104.21 | 99.24 | 40.0% | 0.666 | 19.889 | 916.36 |
| 5 | 6.5 | 108.21 | 103.06 | 37.7% | 0.604 | 21.919 | 829.44 |
| 5 | 6.25 | 112.54 | 107.18 | 35.2% | 0.543 | 24.411 | 779.92 |
| 5 | 6 | 117.23 | 111.65 | 32.5% | 0.481 | 27.543 | 698.22 |
| 10 | 7.5 | 96.83 | 88.03 | 46.8% | 0.879 | 30.165 | 7219.68 |
| 10 | 7.25 | 100.17 | 91.06 | 44.9% | 0.816 | 32.480 | 6959.26 |
| 10 | 7 | 103.75 | 94.32 | 43.0% | 0.753 | 35.180 | 995.89 |
| 10 | 6.75 | 107.59 | 97.81 | 40.9% | 0.691 | 38.370 | 908.19 |
| 10 | 6.5 | 111.73 | 101.57 | 38.6% | 0.628 | 42.195 | 831.80 |
| 10 | 6.25 | 116.20 | 105.63 | 36.1% | 0.565 | 46.868 | 767.79 |
| 10 | 6 | 121.04 | 110.03 | 33.5% | 0.503 | 52.705 | 698.44 |

## Table 6.4. Laboratory Resistivity Cell Test Results for Saturated Sand

14-Dec-92 Soil 1, Saturated Sand

Test Parameters
Length 7.5
Diameter 1
Spec. Grav 2.650

| Moist. Content (%) | Sample Length (in) | Wet Density (lb/ft^3) | Dry Density (lb/ft^3) | Porosity (%) | Void Ratio | Satuation (%) | Measured Resist (ohm-m) |
|---|---|---|---|---|---|---|---|
| 0.3 | 7.5 | 102.67 | 102.37 | 38.1% | 0.615 | 1.292 | 13101.89 |
| 0.3 | 7.25 | 106.21 | 105.90 | 36.0% | 0.562 | 1.416 | 13418.11 |
| 0.3 | 7 | 110.01 | 109.68 | 33.7% | 0.508 | 1.566 | 13905.71 |
| 0.3 | 6.75 | 114.08 | 113.74 | 31.2% | 0.454 | 1.752 | 14277.86 |
| 0.3 | 6.5 | 118.47 | 118.12 | 28.6% | 0.400 | 1.988 | 14966.35 |
| 0.3 | 6.25 | 123.21 | 122.84 | 25.7% | 0.346 | 2.297 | 15265.68 |
| 0.3 | 6 | 128.34 | 127.96 | 22.6% | 0.292 | 2.720 | 15750.30 |
| 2.5 | 7.5 | 78.94 | 77.02 | 53.4% | 1.147 | 5.776 | 3884.13 |
| 2.5 | 7.25 | 81.66 | 79.67 | 51.8% | 1.076 | 6.160 | 3368.37 |
| 2.5 | 7 | 84.58 | 82.52 | 50.1% | 1.004 | 6.599 | 2894.83 |
| 2.5 | 6.75 | 87.71 | 85.57 | 48.3% | 0.932 | 7.106 | 2479.00 |
| 2.5 | 6.5 | 91.09 | 88.86 | 46.3% | 0.861 | 7.696 | 2096.94 |
| 2.5 | 6.25 | 94.73 | 92.42 | 44.1% | 0.789 | 8.394 | 1835.57 |
| 2.5 | 6 | 98.68 | 96.27 | 41.8% | 0.718 | 9.231 | 1550.71 |
| 5 | 7.5 | 94.16 | 89.67 | 45.8% | 0.844 | 15.698 | 1201.30 |
| 5 | 7.25 | 97.40 | 92.76 | 43.9% | 0.783 | 16.931 | 1086.49 |
| 5 | 7 | 100.88 | 96.08 | 41.9% | 0.721 | 18.374 | 909.81 |
| 5 | 6.75 | 104.62 | 99.63 | 39.7% | 0.660 | 20.086 | 819.34 |
| 5 | 6.5 | 108.64 | 103.47 | 37.4% | 0.598 | 22.150 | 715.05 |
| 5 | 6.25 | 112.99 | 107.61 | 34.9% | 0.537 | 24.687 | 651.90 |
| 5 | 6 | 117.69 | 112.09 | 32.2% | 0.475 | 27.880 | 575.99 |
| 10 | 7.5 | 96.81 | 88.01 | 46.8% | 0.879 | 30.149 | 441.80 |
| 10 | 7.25 | 100.15 | 91.04 | 44.9% | 0.816 | 32.463 | 365.95 |
| 10 | 7 | 103.72 | 94.29 | 43.0% | 0.754 | 35.160 | 297.00 |
| 10 | 6.75 | 107.56 | 97.78 | 40.9% | 0.691 | 38.347 | 252.47 |
| 10 | 6.5 | 111.70 | 101.55 | 38.6% | 0.628 | 42.169 | 207.86 |
| 10 | 6.25 | 116.17 | 105.61 | 36.1% | 0.566 | 46.837 | 194.87 |
| 10 | 6 | 121.01 | 110.01 | 33.5% | 0.503 | 52.667 | 172.60 |
| 20 | 7.5 | 123.50 | 102.92 | 37.8% | 0.607 | 87.357 | 139.75 |
| 20 | 7.25 | 127.76 | 106.47 | 35.6% | 0.553 | 95.815 | 134.96 |
| 20 | 7 | 132.32 | 110.27 | 33.3% | 0.500 | 100.000 | 131.95 |

## Table 6.5. Laboratory Resistivity Cell Test Results for Clayey Sand

| | | |
|---|---|---|
| 14-Dec-92 | Soil 4, Clayey Sand | |
| Test Parameters | | |
| Length | 7.5 | in |
| Diameter | 1 | in |
| Soil Spec. Grav | 2.650 | |
| DNAPL Spec. Grav | 1.5 | |

| Molsture Content (%) | Sample Length (In) | Wet Density (lb/ft^3) | Dry Density (lb/ft^3) | Porosity (%) | Void Ratio | Satuation (%) | Measured Resist (ohm-m) |
|---|---|---|---|---|---|---|---|
| 0.35 | 7.5 | 88.02 | 87.72 | 47.0% | 0.885 | 1.048 | 12744.41 |
| 0.35 | 7.25 | 91.06 | 90.74 | 45.1% | 0.822 | 1.128 | 13055.70 |
| 0.35 | 7 | 94.31 | 93.98 | 43.2% | 0.759 | 1.221 | 13391.72 |
| 0.35 | 6.75 | 97.80 | 97.46 | 41.1% | 0.697 | 1.331 | 13884.92 |
| 0.35 | 6.5 | 101.57 | 101.21 | 38.8% | 0.634 | 1.463 | 14418.95 |
| 0.35 | 6.25 | 105.63 | 105.26 | 36.3% | 0.571 | 1.624 | 14995.71 |
| 0.35 | 6 | 110.03 | 109.65 | 33.7% | 0.508 | 1.825 | 15620.53 |
| 2.5 | 7 | 71.40 | 69.66 | 57.9% | 1.374 | 4.823 | 1489.28 |
| 2.5 | 6.75 | 74.05 | 72.24 | 56.3% | 1.289 | 5.140 | 1290.36 |
| 2.5 | 6.5 | 76.90 | 75.02 | 54.6% | 1.204 | 5.502 | 1111.51 |
| 2.5 | 6.25 | 79.97 | 78.02 | 52.2% | 1.093 | 5.918 | 818.26 |
| 2.5 | 6 | 83.31 | 81.27 | 50.2% | 1.009 | 6.403 | 632.42 |
| 5 | 7.25 | 99.81 | 95.05 | 42.0% | 0.724 | 17.913 | 183.44 |
| 5 | 7 | 103.37 | 98.45 | 39.9% | 0.665 | 19.494 | 169.15 |
| 5 | 6.75 | 107.20 | 102.09 | 37.7% | 0.605 | 21.382 | 153.41 |
| 5 | 6.5 | 111.32 | 106.02 | 35.3% | 0.546 | 23.673 | 143.29 |
| 5 | 6.25 | 115.77 | 110.26 | 32.7% | 0.487 | 26.515 | 136.86 |
| 10 | 7.5 | 104.76 | 95.23 | 39.8% | 0.661 | 35.988 | 117.06 |
| 10 | 7.25 | 108.37 | 98.52 | 37.7% | 0.606 | 39.058 | 105.12 |
| 10 | 7 | 112.24 | 102.04 | 35.5% | 0.550 | 42.700 | 96.92 |
| 10 | 6.75 | 116.40 | 105.82 | 33.1% | 0.495 | 47.092 | 89.93 |
| 10 | 6.5 | 120.87 | 109.88 | 30.5% | 0.440 | 52.491 | 84.34 |
| 10 | 6.25 | 125.71 | 114.28 | 22.1% | 0.283 | 59.288 | 80.16 |
| 20 | 7.5 | 102.67 | 85.56 | 40.9% | 0.692 | 56.828 | 90.79 |
| 20 | 7.25 | 106.21 | 88.51 | 38.9% | 0.636 | 61.044 | 81.30 |
| 20 | 7 | 110.01 | 91.67 | 36.7% | 0.579 | 65.937 | 74.75 |
| 20 | 6.75 | 114.08 | 95.07 | 34.3% | 0.523 | 71.682 | 70.58 |
| 20 | 6.5 | 118.47 | 98.73 | 22.7% | 0.293 | 78.524 | 65.44 |
| 20 | 6.25 | 123.21 | 102.67 | 19.6% | 0.244 | 86.809 | 63.75 |
| 20 | 6 | 128.34 | 106.95 | 16.2% | 0.194 | 97.050 | 61.76 |

## Table 6.6. Laboratory Resistivity Cell Test Results for Green Clay

14-Dec-92 Soil 3, Green Clay

Test Parameters
Length 7.5 in
Diameter 1 in
Spec. Grav 2.650

| Moist. Content (%) | Sample Length (in) | Wet Density (lb/ft^3) | Dry Density (lb/ft^3) | Porosity (%) | Void Ratio | Satuation (%) | Measured Resist (ohm-m) |
|---|---|---|---|---|---|---|---|
| 0.35 | 7.5 | 88.03 | 87.72 | 47.0% | 0.885 | 1.048 | 13130.86 |
| 0.35 | 7.25 | 91.07 | 90.75 | 45.1% | 0.822 | 1.128 | 13447.78 |
| 0.35 | 7 | 94.32 | 93.99 | 43.2% | 0.759 | 1.221 | 13790.07 |
| 0.35 | 6.75 | 97.81 | 97.47 | 41.1% | 0.697 | 1.332 | 14300.81 |
| 0.35 | 6.5 | 101.57 | 101.22 | 38.8% | 0.634 | 1.464 | 14705.09 |
| 0.35 | 6.25 | 105.64 | 105.27 | 36.3% | 0.571 | 1.625 | 15144.61 |
| 0.35 | 6 | 110.04 | 109.65 | 33.7% | 0.508 | 1.826 | 15775.63 |
| 2.5 | 7.5 | 107.05 | 104.44 | 36.8% | 0.583 | 11.358 | 7091.00 |
| 2.5 | 7.25 | 110.74 | 108.04 | 34.7% | 0.531 | 12.488 | 5489.99 |
| 2.5 | 7 | 114.70 | 111.90 | 32.3% | 0.478 | 13.867 | 4448.80 |
| 2.5 | 6.75 | 118.95 | 116.04 | 29.8% | 0.425 | 15.589 | 2873.06 |
| 2.5 | 6.5 | 123.52 | 120.51 | 27.1% | 0.372 | 17.800 | 2077.83 |
| 2.5 | 6.25 | 128.46 | 125.33 | 24.2% | 0.319 | 20.741 | 1652.80 |
| 2.5 | 6 | 133.81 | 130.55 | 21.1% | 0.267 | 24.846 | 1325.16 |
| 5 | 7.5 | 101.02 | 96.21 | 41.8% | 0.719 | 18.435 | 788.60 |
| 5 | 7.25 | 104.50 | 99.53 | 39.8% | 0.661 | 20.031 | 660.92 |
| 5 | 7 | 108.24 | 103.08 | 37.7% | 0.604 | 21.931 | 563.55 |
| 5 | 6.75 | 112.24 | 106.90 | 35.4% | 0.547 | 24.228 | 487.19 |
| 5 | 6.5 | 116.56 | 111.01 | 32.9% | 0.490 | 27.063 | 430.35 |
| 5 | 6.25 | 121.22 | 115.45 | 30.2% | 0.432 | 30.650 | 377.63 |
| 5 | 6 | 126.27 | 120.26 | 27.3% | 0.375 | 35.333 | 331.07 |
| 10 | 7.5 | 113.92 | 103.56 | 37.4% | 0.597 | 44.412 | 191.55 |
| 10 | 7.25 | 117.85 | 107.14 | 35.2% | 0.543 | 48.762 | 171.90 |
| 10 | 7 | 122.06 | 110.96 | 32.9% | 0.490 | 54.056 | 154.19 |
| 10 | 6.75 | 126.58 | 115.07 | 30.4% | 0.437 | 60.639 | 135.58 |
| 10 | 6.5 | 131.45 | 119.50 | 27.7% | 0.384 | 69.048 | 122.38 |
| 10 | 6.25 | 136.71 | 124.28 | 24.8% | 0.331 | 80.165 | 110.75 |
| 10 | 6 | 142.40 | 129.46 | 21.7% | 0.277 | 95.549 | 101.30 |
| 20 | 7.25 | 116.38 | 96.98 | 41.3% | 0.705 | 75.175 | 97.75 |
| 20 | 7 | 120.54 | 100.45 | 39.3% | 0.646 | 82.014 | 90.20 |
| 20 | 6.75 | 125.00 | 104.17 | 37.0% | 0.587 | 90.223 | 82.96 |
| 20 | 6.5 | 129.81 | 108.17 | 34.6% | 0.529 | 100.000 | 75.82 |

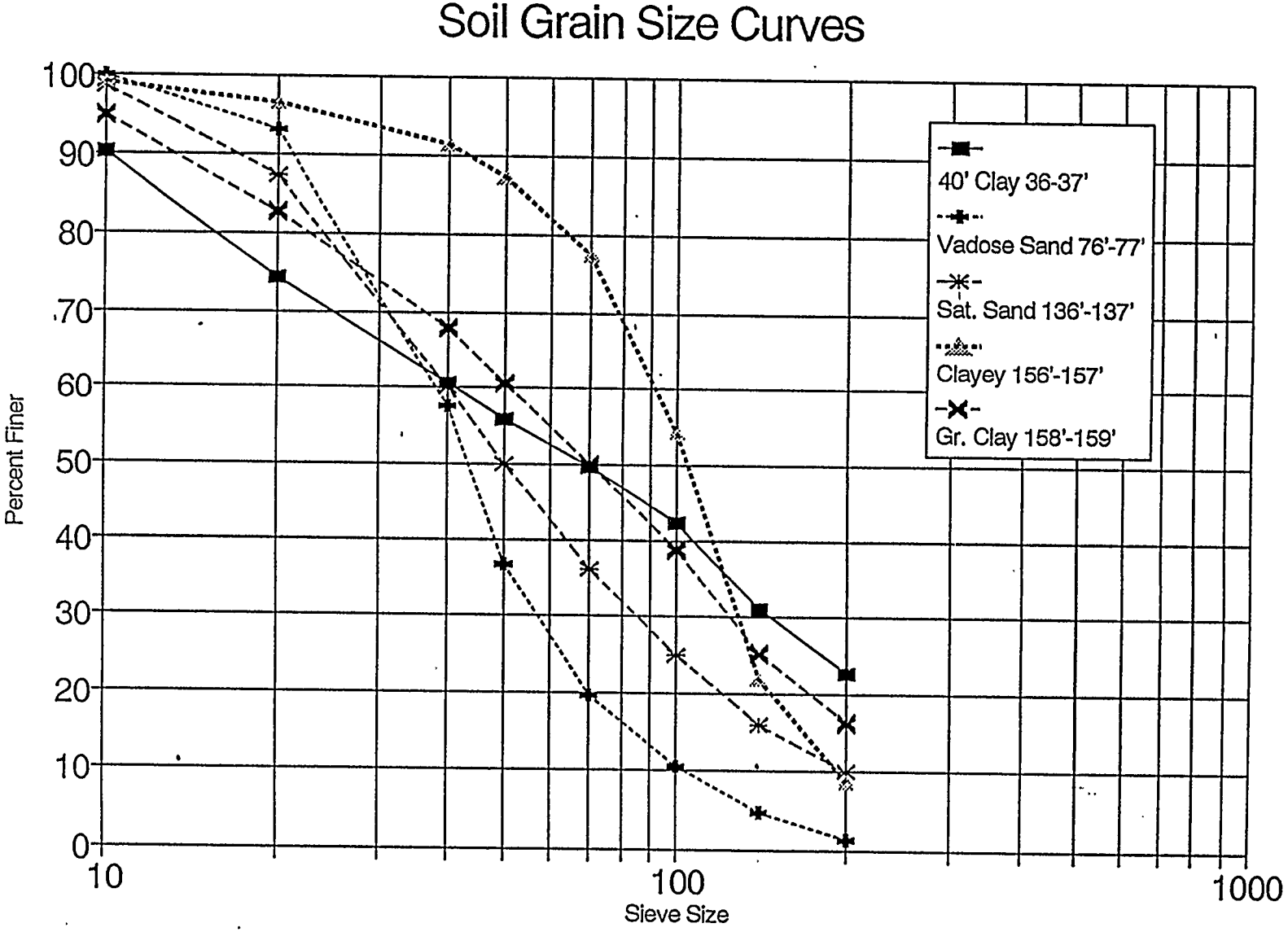


Figure 6.1. Grain size distribution curves for soil from the SRS integrated demonstration

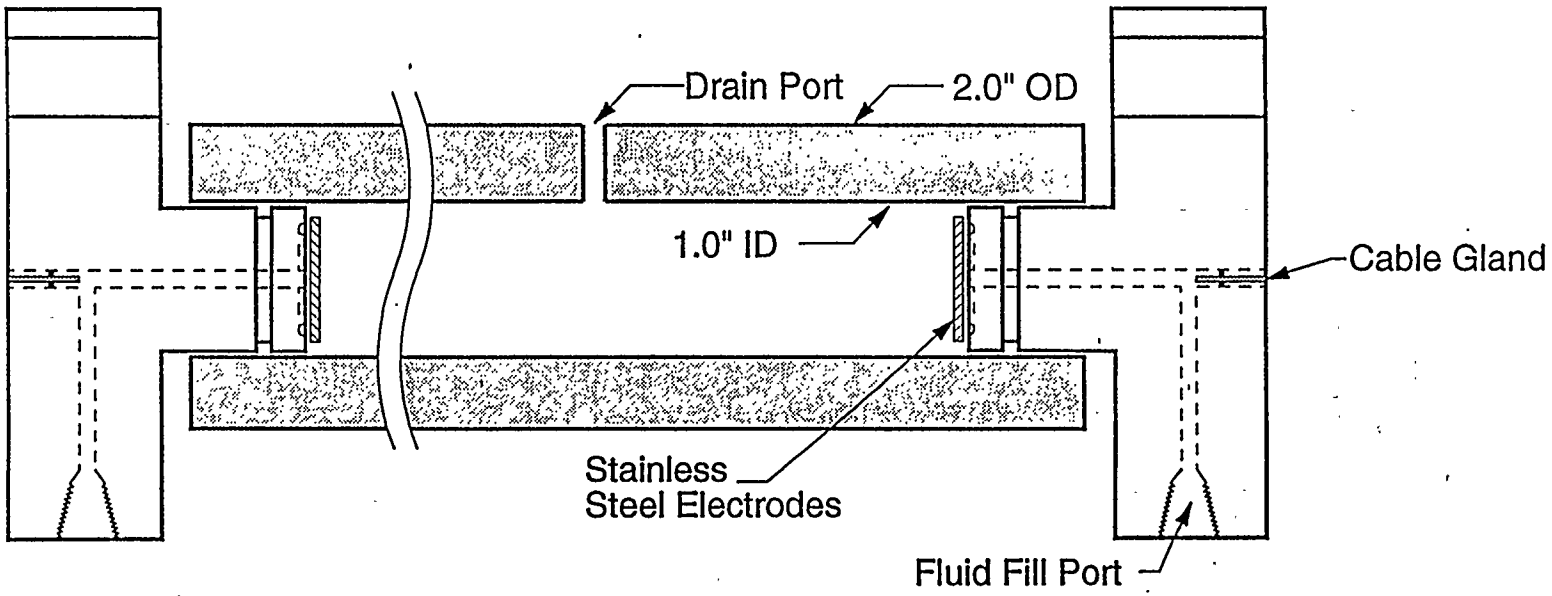


Figure 6.2. Schematic of two Ring Resistivity cell used to determine soil resistivity as a function of porosity and water content.

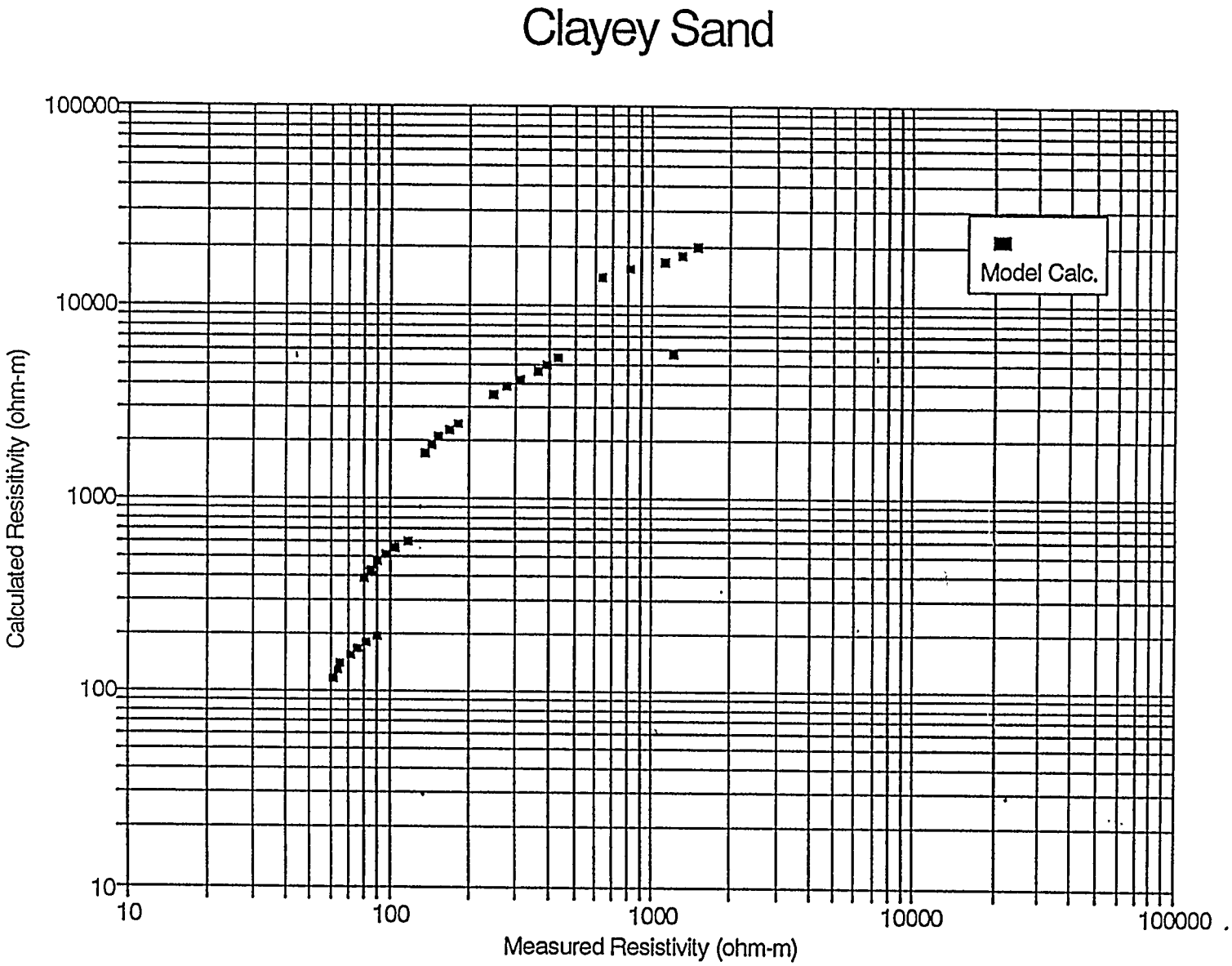


Figure 6.3. Comparison of measured soil resistivities versus calculated for the 156 ft. clayey sand. Four test series are plotted where the initial moisture content was varied.

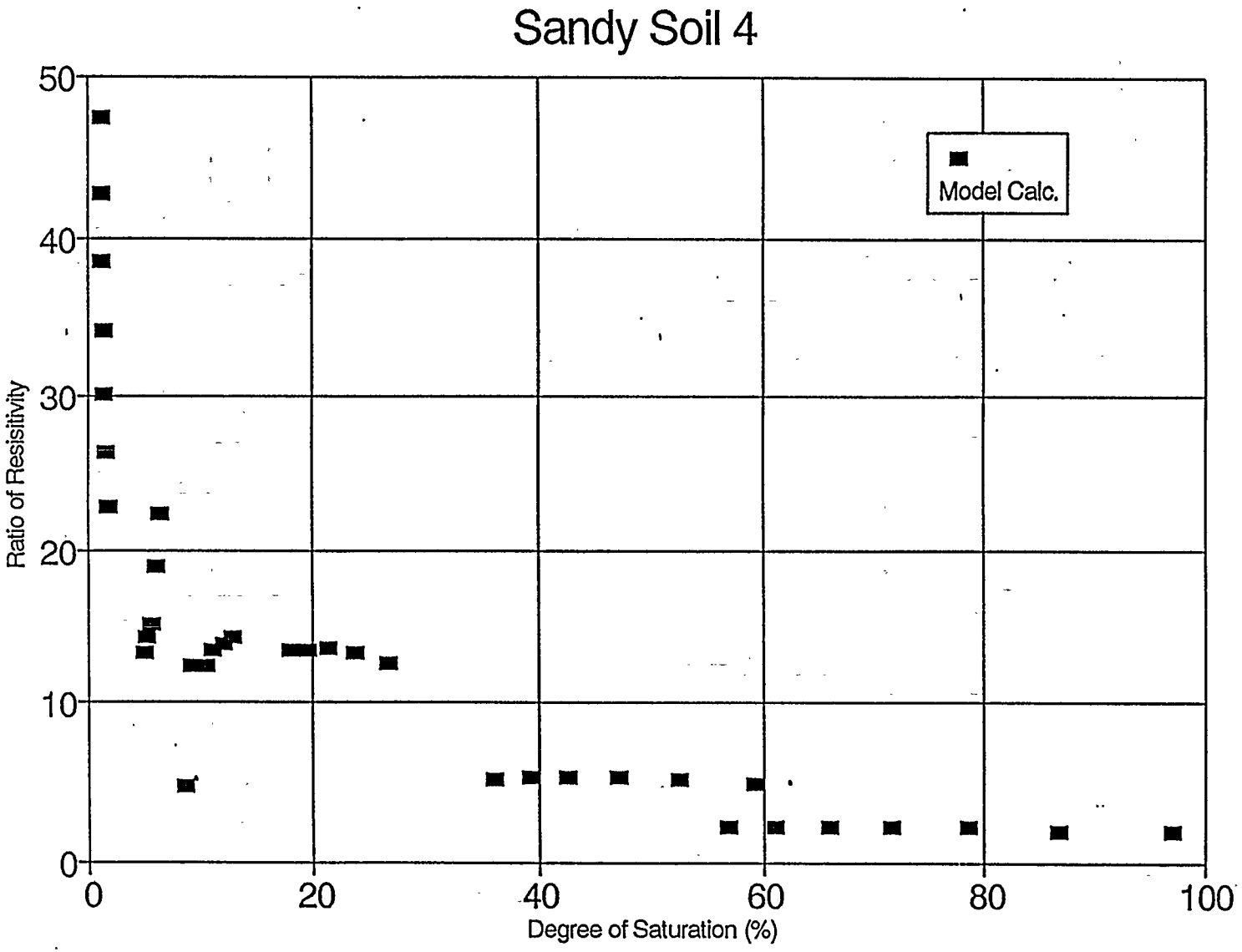


Figure 6.4. Comparison of ratio of calculated to measured resistivity as a function of degree of saturation. Data shown for the 156 ft. deep clayey sand.

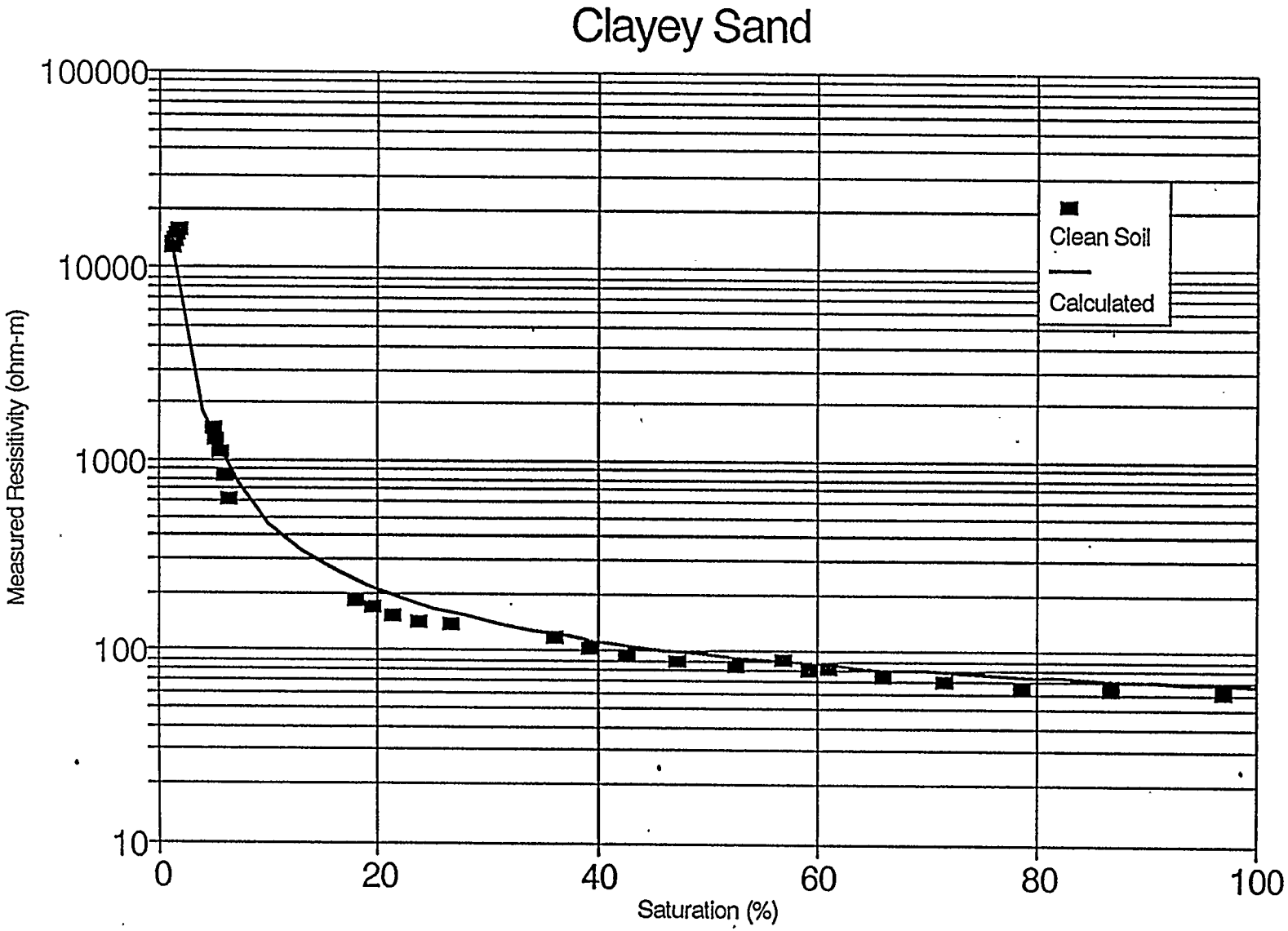


Figure 6.5. Plot of 156 ft. depth clayey sand resistivity data as a function of saturation. Fit to the data is superimposed.

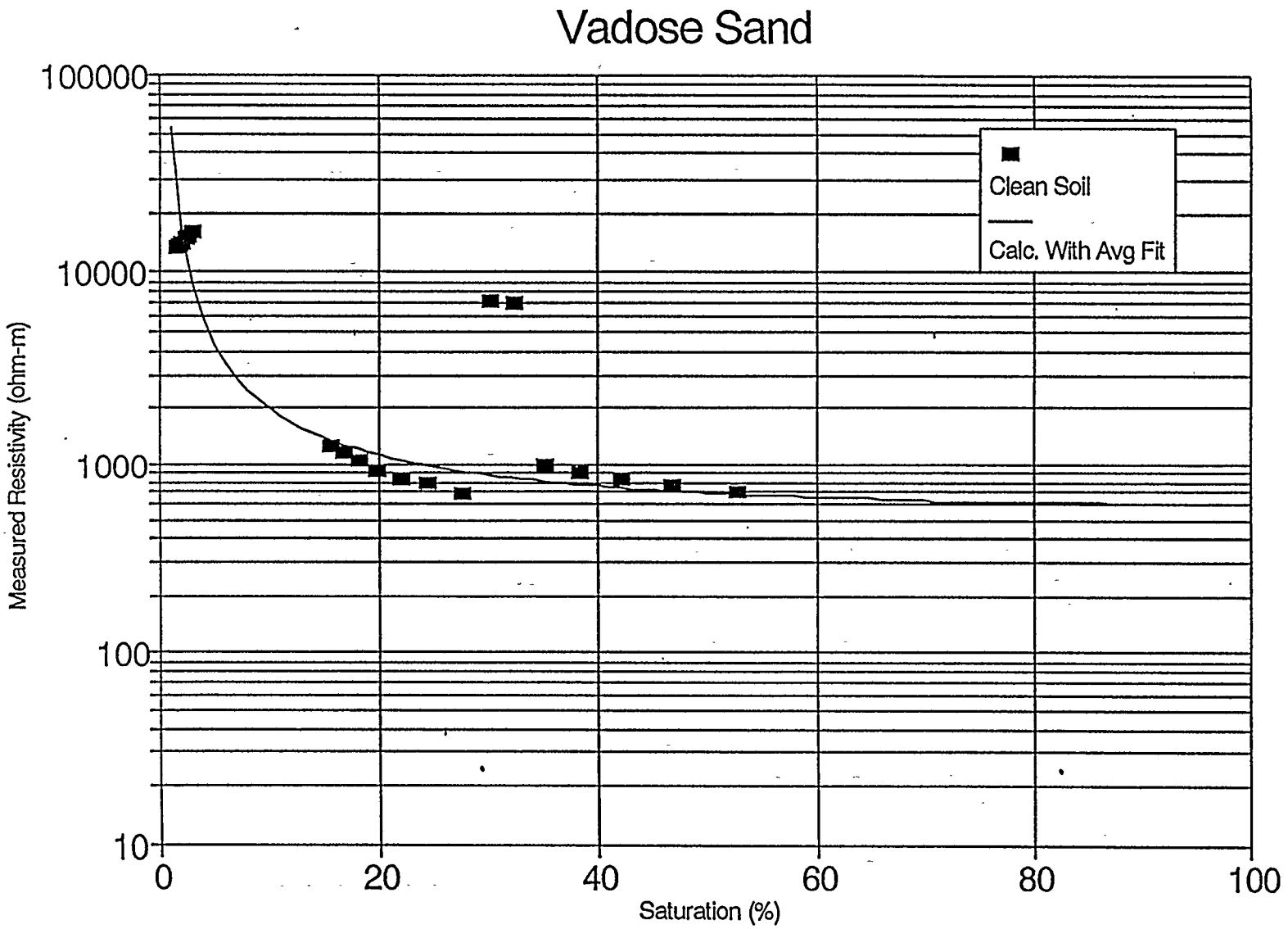


Figure 6.6. Plot of vadose zone resistivity test data versus saturation. Fit to the data is superimposed.

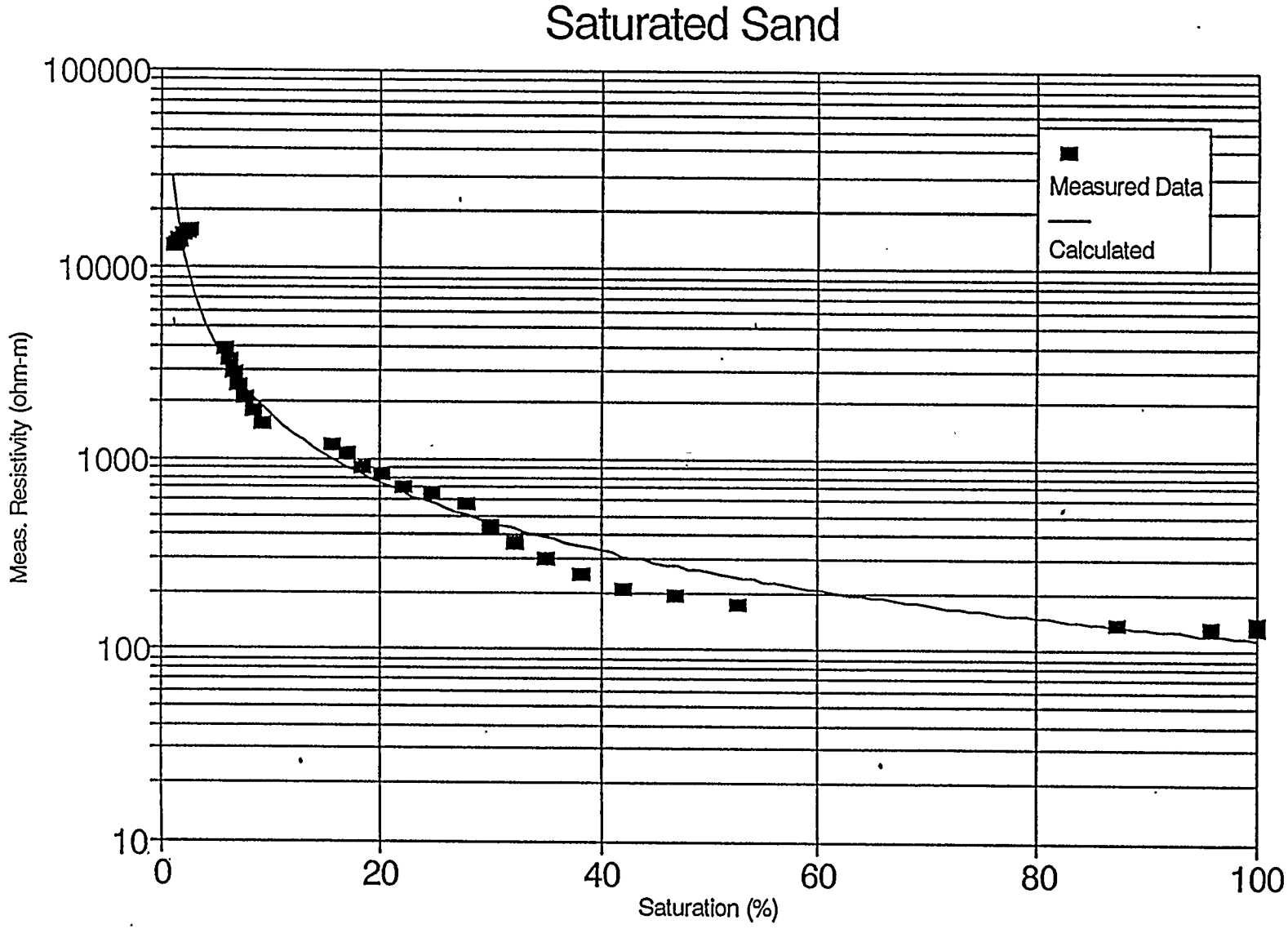


Figure 6.7. Plot of saturated sand resistivity test data as a function of saturation. Fit is shown superimposed on the data.

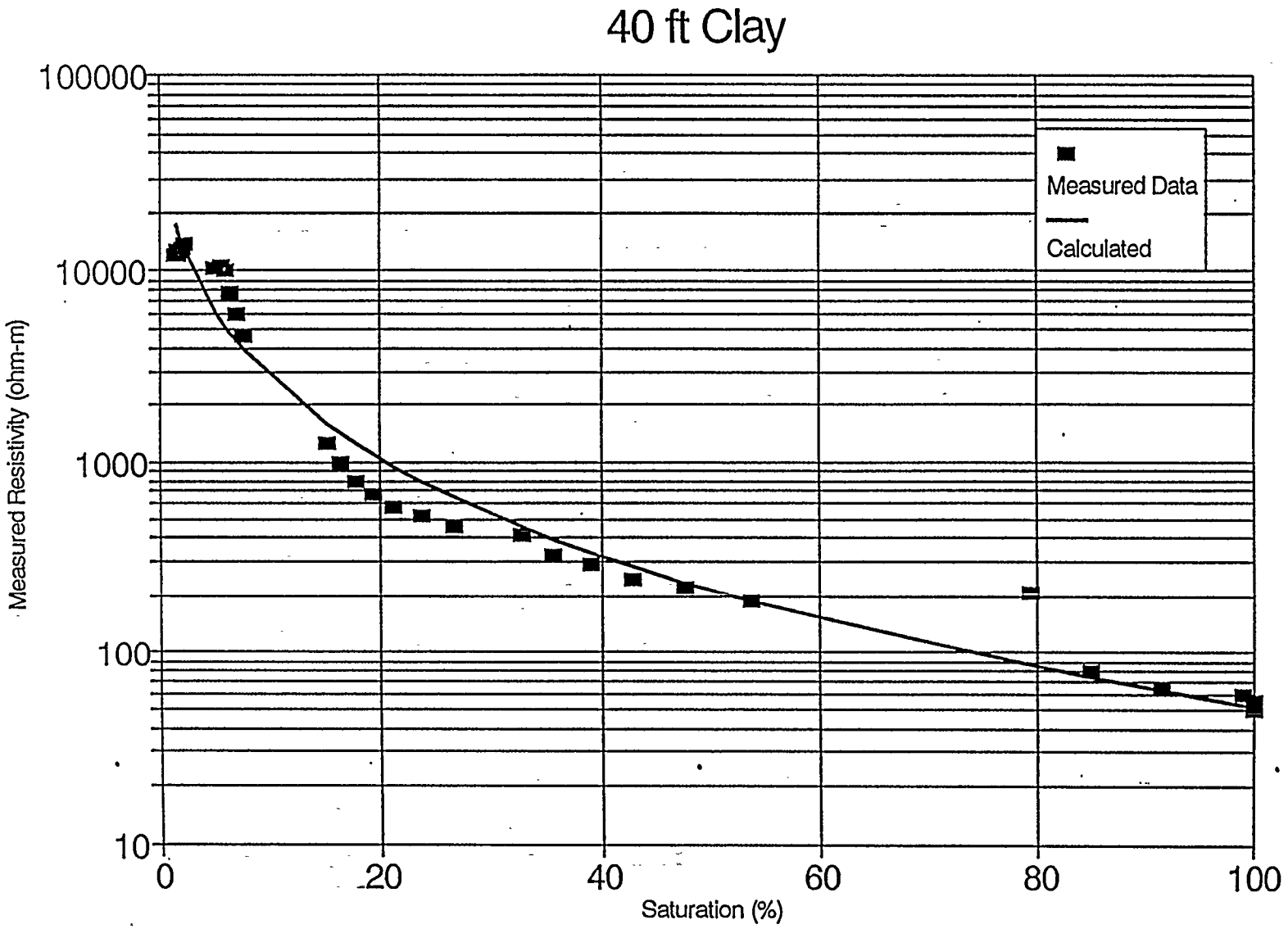


Figure 6.8. Plot of 40 ft. clay resistivity test data versus saturation. Fit to the data is superimposed.

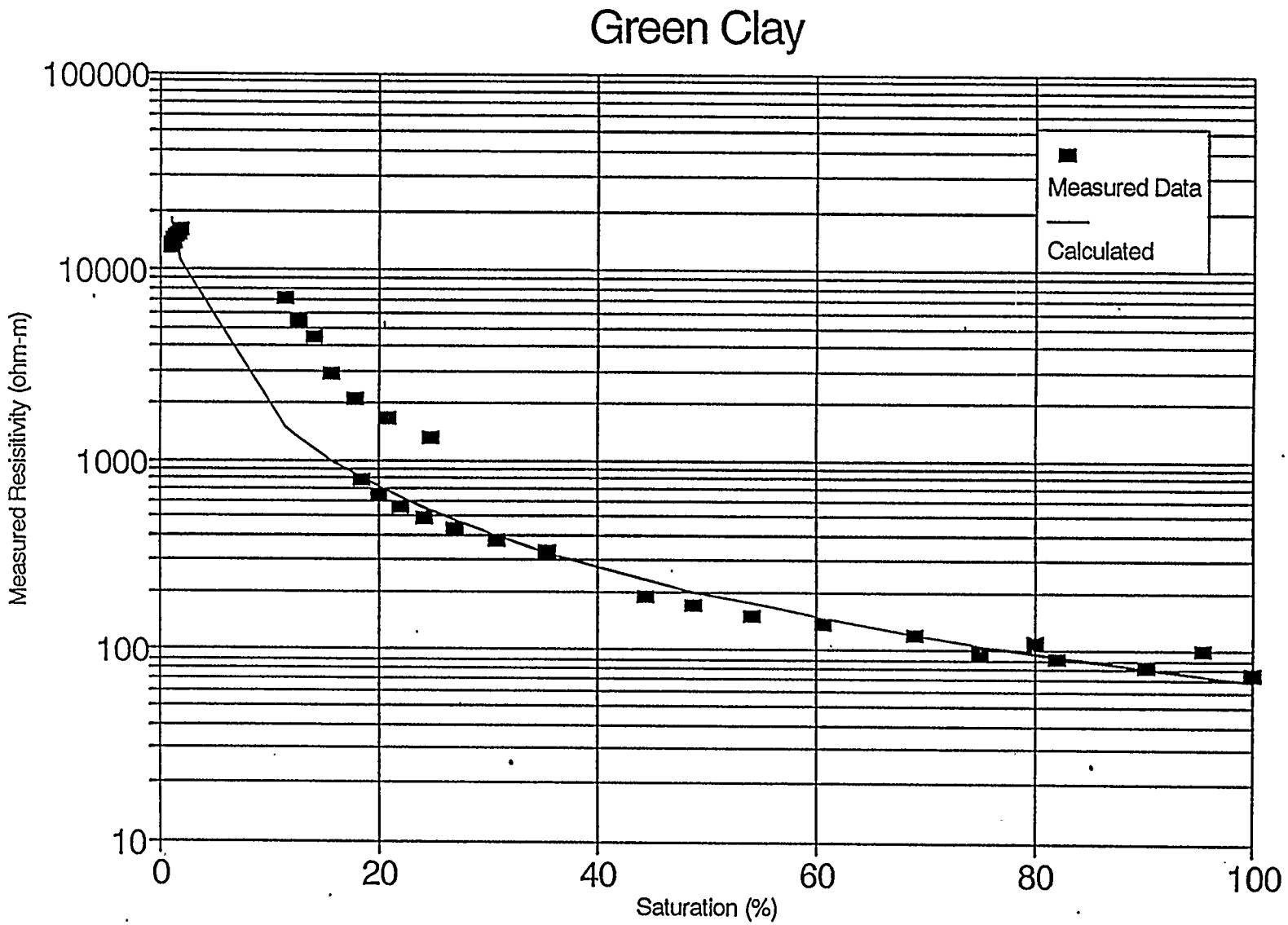


Figure 6.9. Plot of green clay resistivity test data versus saturation. Fit to the data is superimposed.

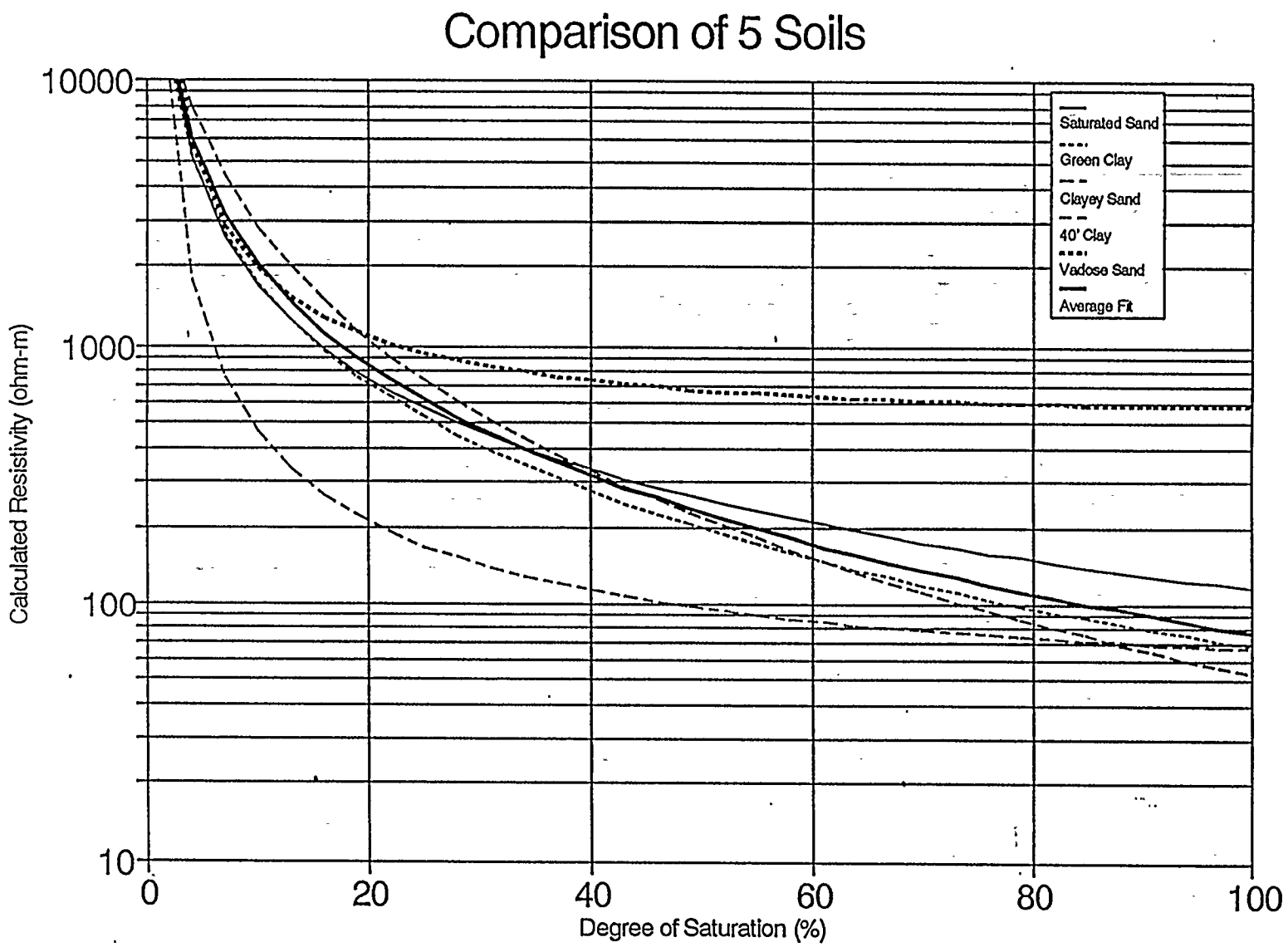


Figure 6.10. Comparison of fits to resistivity test data. Average fit is for the 40 ft. clay, saturated sand and green clay layers only.

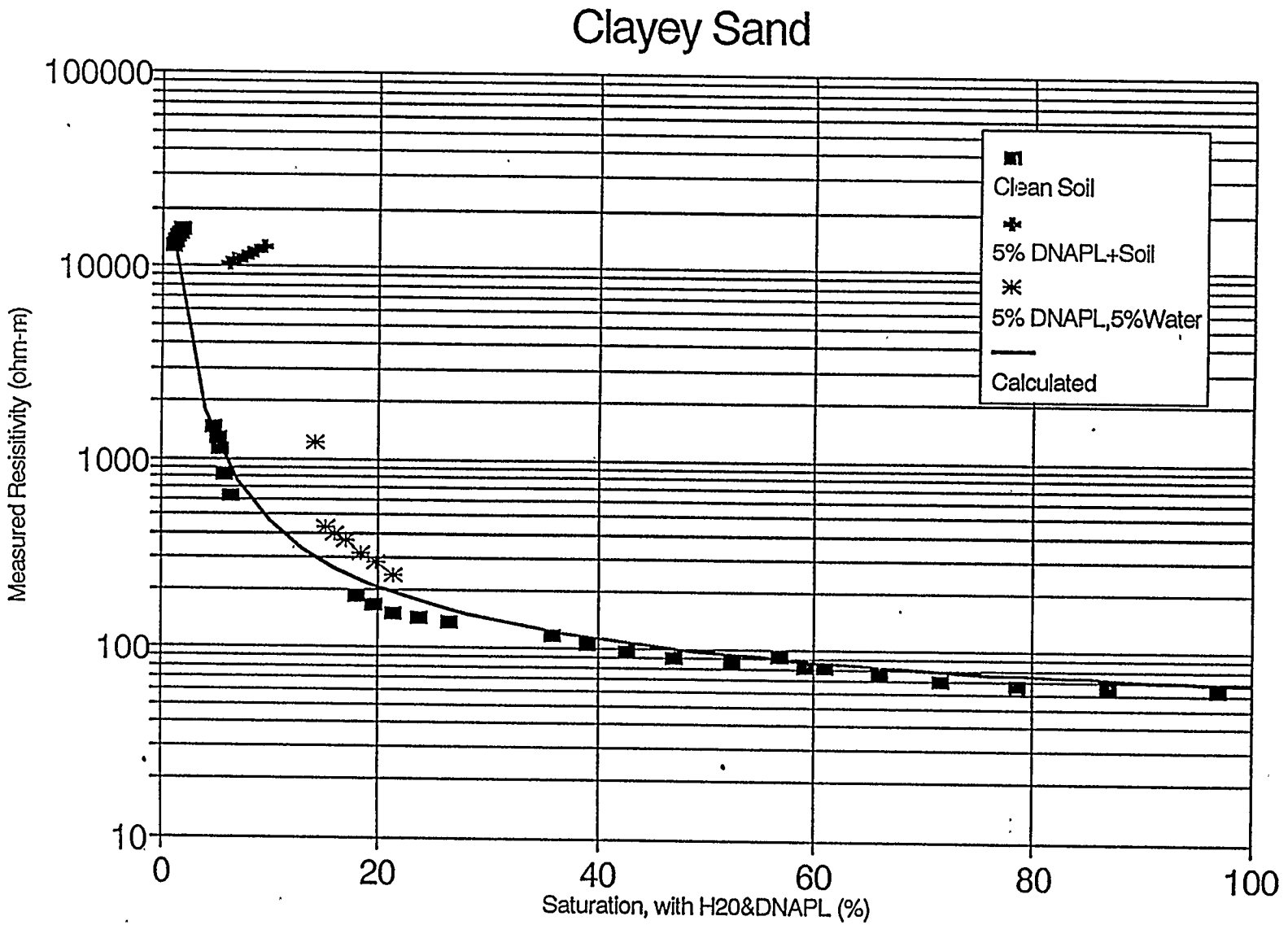


Figure 6.11. Plot of 5% DNAPL test with saturation calculated based on water and DNAPL volume.

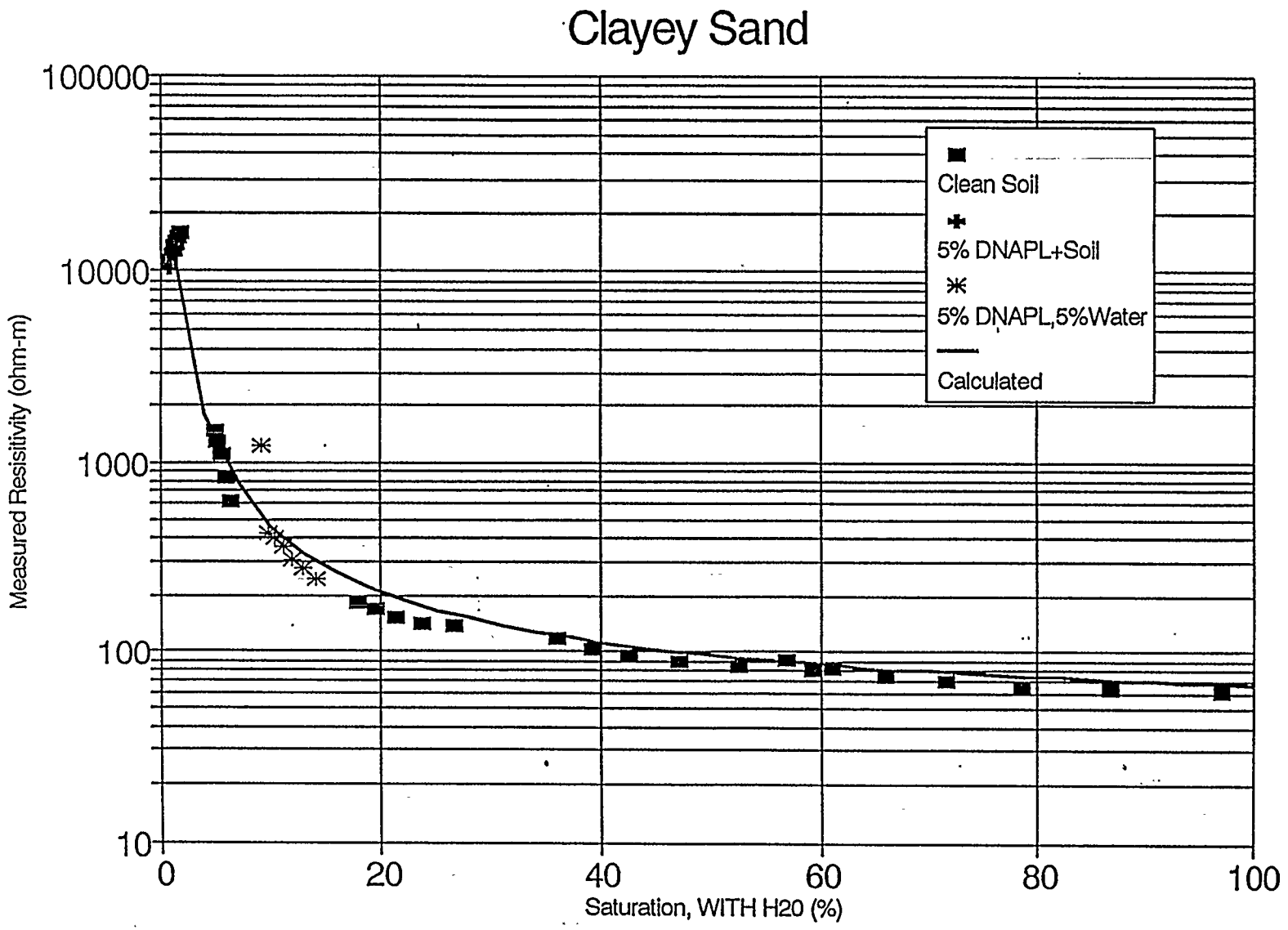


Figure 6.12. Plot of 5% DNAPL test with saturation calculated based on water volume. Conductive pore space reduced by DNAPL volume.

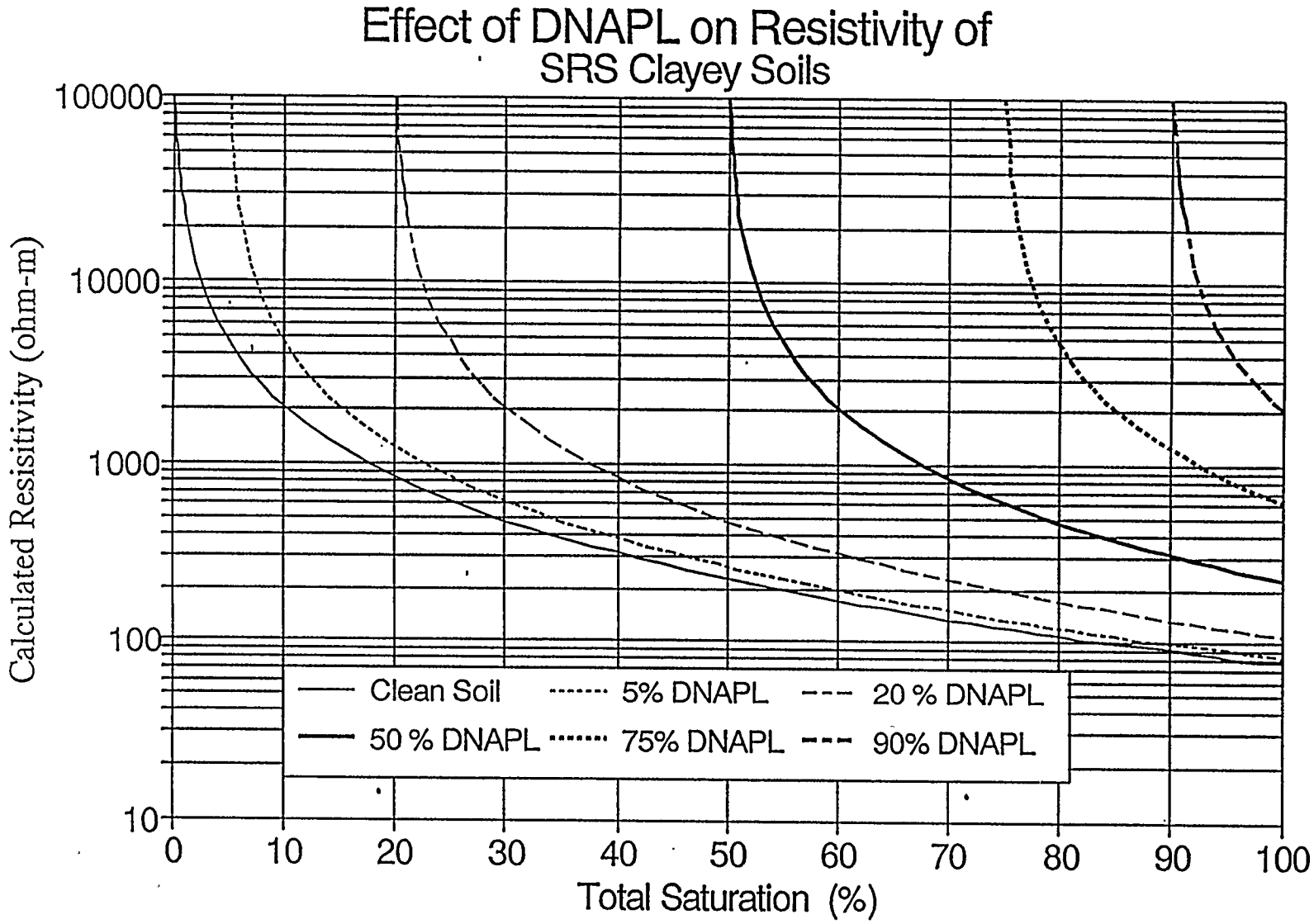


Figure 6.13. Calculation results showing the influence of DNAPL concentration on soil resistivity for SRS clayey soils

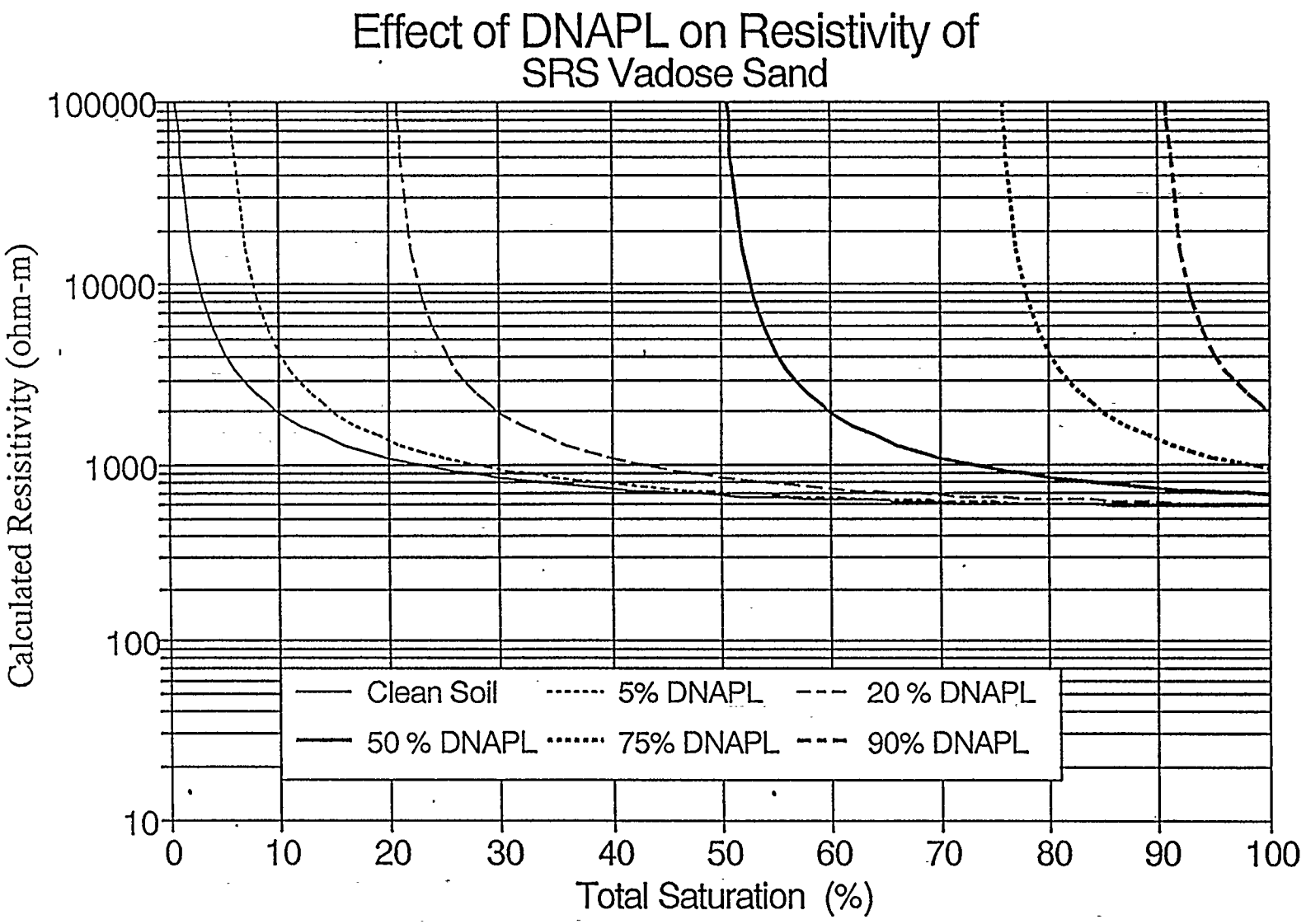


Figure 6.14. Calculation results showing the influence of DNAPL concentration on soil resistivity for the SRS vadose sand

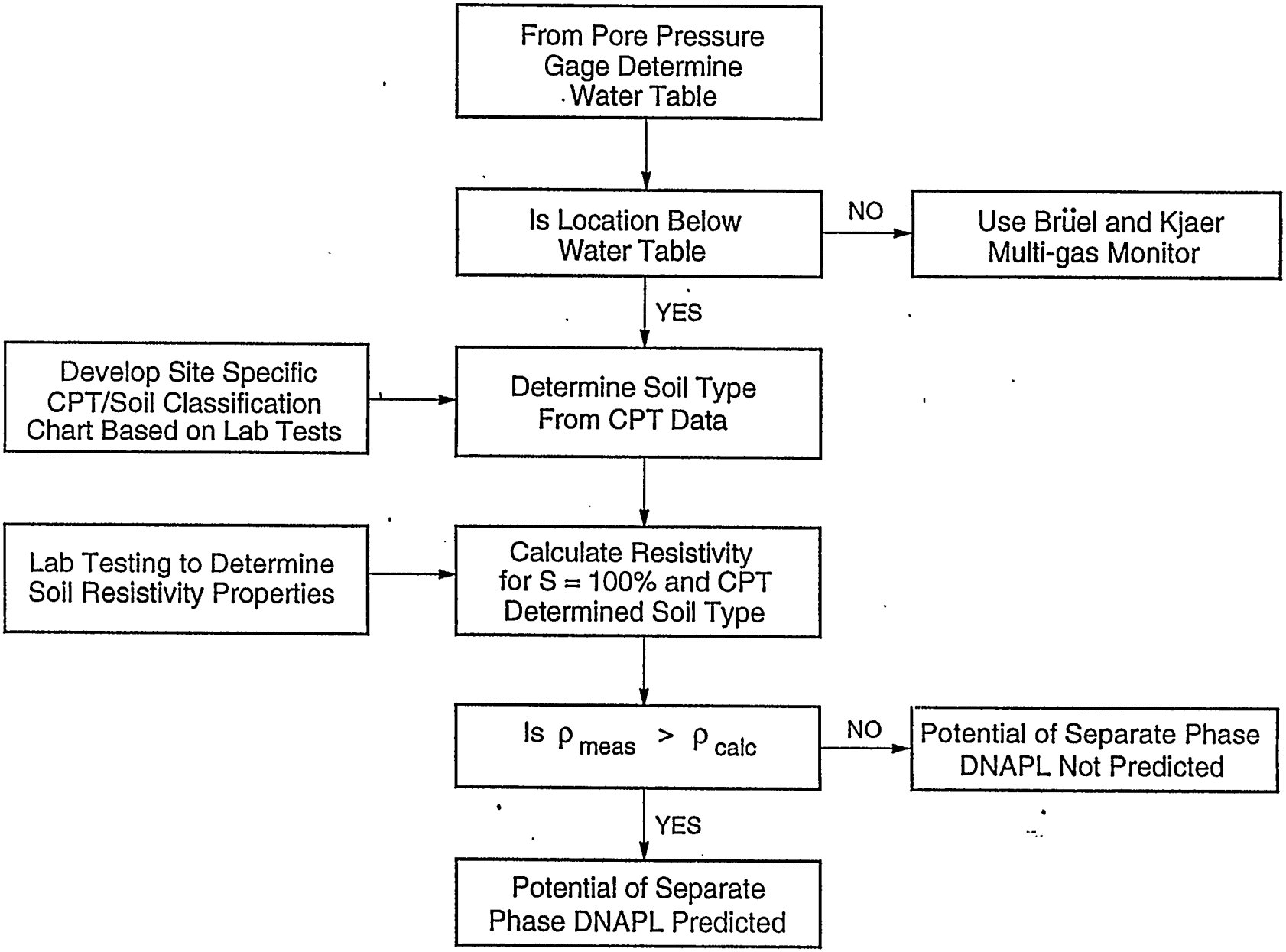


Figure 6.15. Framework for evaluating DNAPL concentration from CPT technique.

CPT-017 APPLIED RESEARCH ASSOCIATES, INC. 07/21/92
North 101955.15 East 50104.06 Elevation 344.3

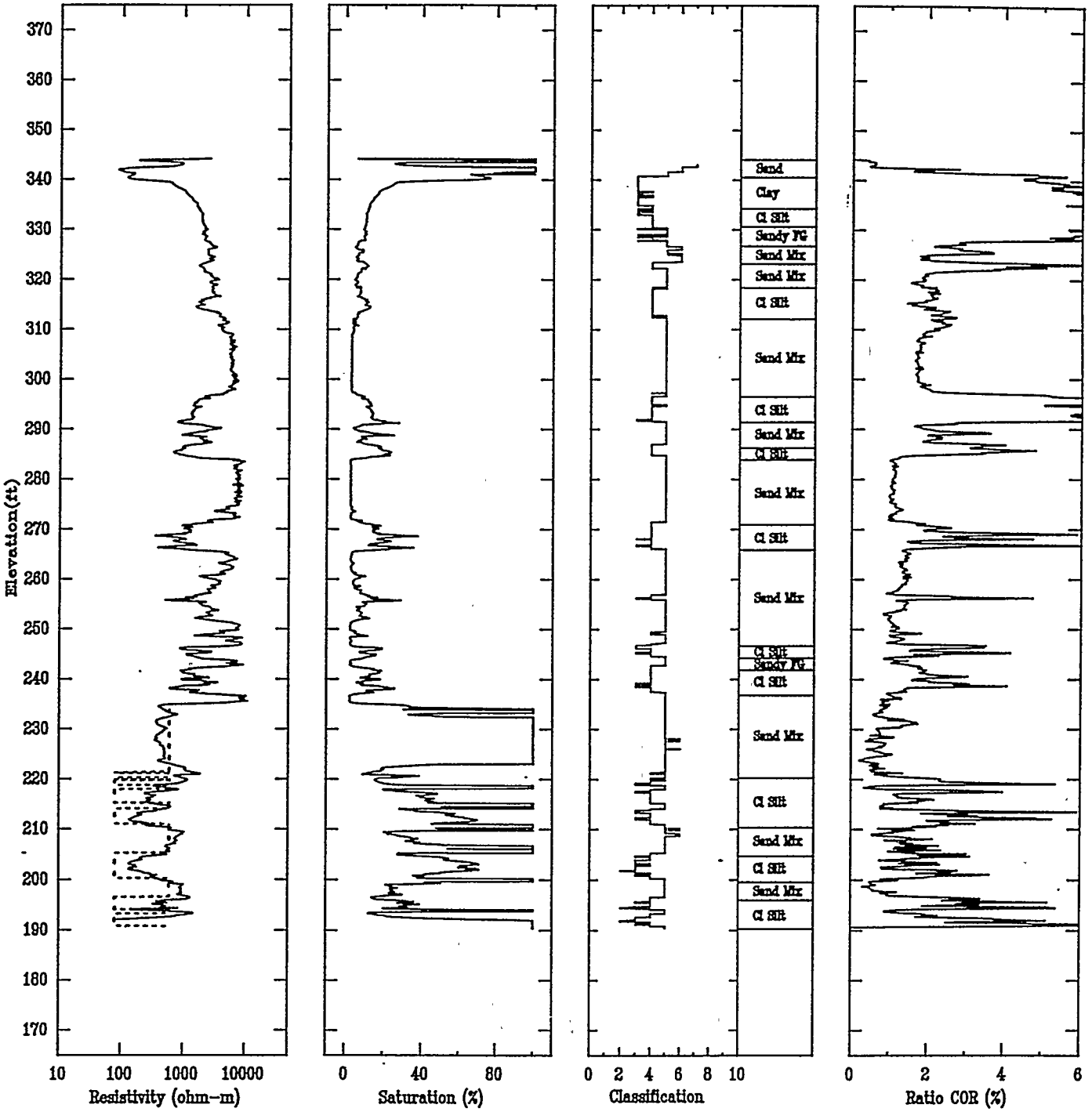


Figure 6.16. Comparison of predicted and measured resistivities below the ground water table and of predicted degrees of saturation for sounding CPT-017.

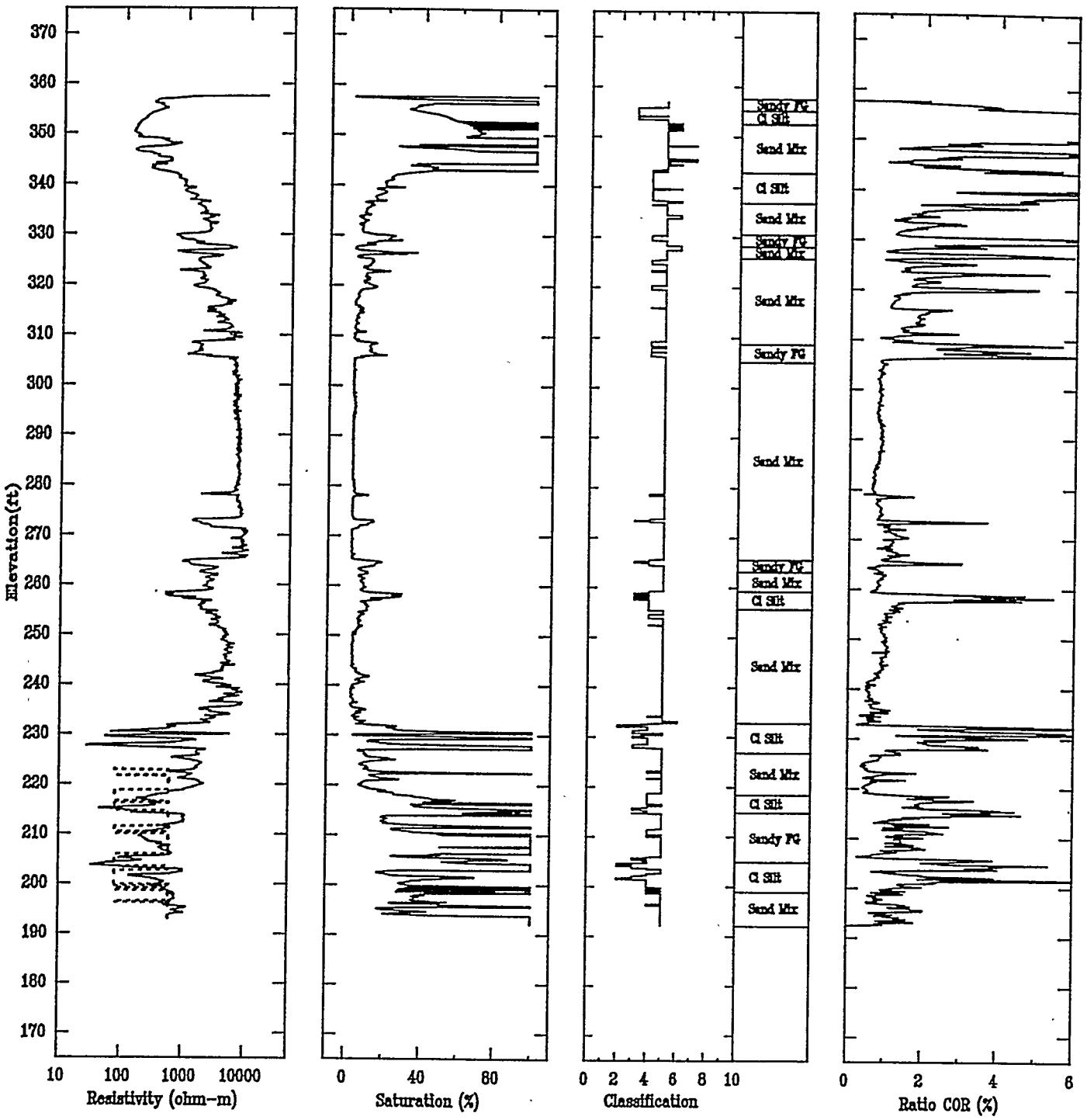


Figure 6.17. Comparison of predicted and measured resistivities below the ground water table and of predicted degrees of saturation for sounding CPT-004.

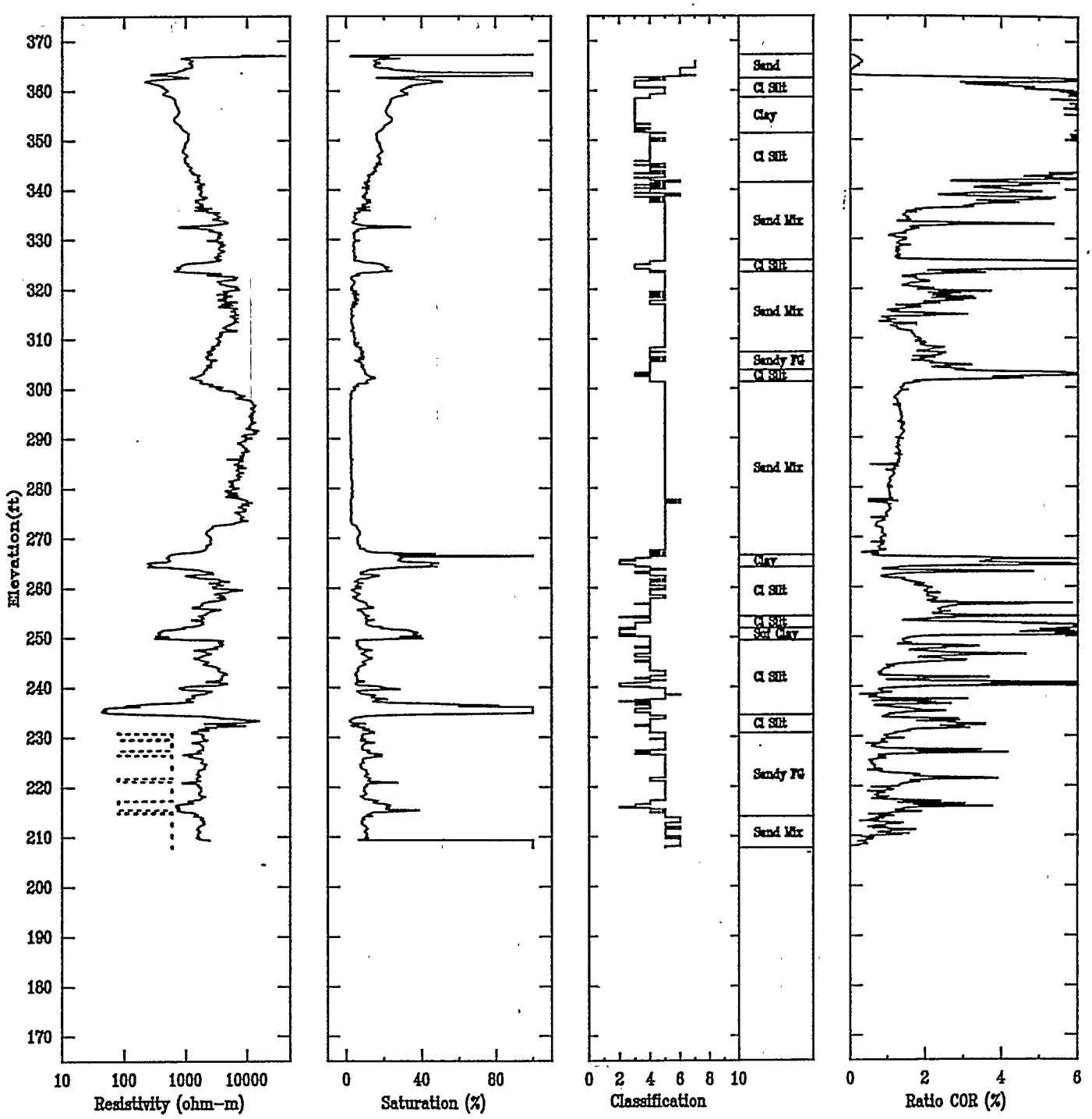


Figure 6.18. Comparison of predicted and measured resistivities below the ground water table and of predicted degrees of saturation for sounding CPT-015A.

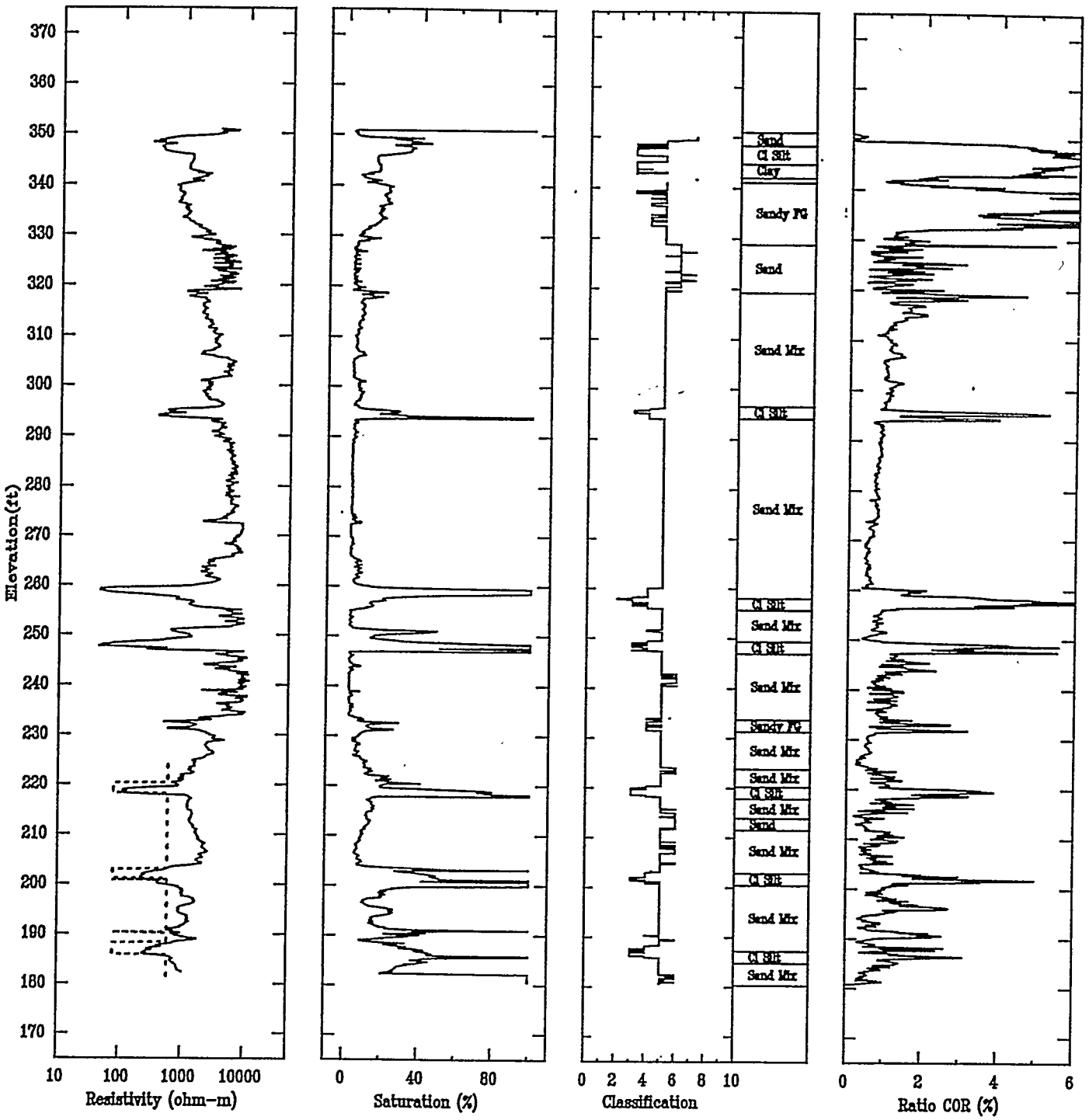


Figure 6.19. Comparison of predicted and measured resistivities below the ground water table and of predicted degrees of saturation for sounding CPT-003.

# SECTION 7
# SUMMARY, CONCLUSIONS AND RECOMMENDATIONS

## SUMMARY

A combined field and laboratory investigation was conducted to evaluate soil resistivity as a method of locating DNAPL contamination at the SRS site. Field efforts consisted of conducting 25 Piezo/Resistivity-Cone Penetration Tests (P/R-CPT) to an average depth of 151 ft. At two locations groundwater and soil gas samples were also obtained. The soil gas samples were analyzed on site with a Bruel & Kjaer multi-gas monitor, which is capable of delineating between 5 gases to the ppm level and for some gases to the ppb level. Laboratory testing was conducted on 5 soil samples obtained from well MSB-3B. Tests conducted on the samples included grain size distribution and evaluation of the soil resistivity as a function of degree of saturation, porosity, density, soil type and DNAPL content. Archie's Model and a saturation based model were evaluated for determining DNAPL concentration from resistivity data. Parametric calculations were conducted for both surface and down hole resistivity surveys to estimate there detection limits. Specific objectives accomplished as apart of this program are listed below and are further discussed in the conclusion section:

- Site characterization using the P/R-ECPT
- Obtaining resistivity data
- Determine the location of DNAPL, using P/R-CPT probe
- Grouting on retraction and tremie grouting of the CPT sounding
- Soil gas and groundwater sampling
- Field analysis of soil gas samples using a multi-gas monitor
- Evaluation of a CPT-based soil classification system
- Preliminary predictions of hydraulic conductivities and soil resistivity below the water table, and vadose zone degree of saturation.

## CONCLUSIONS

### Site Characterization using the P/R-CPT

Once the initial operational problems were worked out, the CPT proved to be a rapid method for characterizing the site. Typically a 180 ft penetration test was completed and tremie grouted each day. Initial operation problems centered around developing sufficient push capacity to penetrate a hard layer located at a depth of about 110 ft. The CPT truck initially used on the project had a push capacity of 22 tons, which was insufficient to penetrate the 110 ft depth layer. A 27 ton rig was mobilized and this rig could penetrate the layer at some locations, however at other locations refusal was encountered. Since this effort, ARA has used a 33 ton truck at SRS which increases the percentage of locations which can be successfully penetrated; however, refusal is still encountered at a high percentage of the sites. It is concluded that a standard 20 ton CPT truck will not successfully penetrate the hard layers at SRS and that only the heaviest CPT trucks (potentially up to 40 tons) can reach the required depths. Even with heavy CPT trucks layers will be encountered which can not be penetrated and penetration aids are required which could consist of on-board CPT drill systems or an adaption of the sonic drill system. Conventional drill systems have been adapted to the CPT (mostly in Europe). A limitation of this procedure is that production rate is decreased and drill spoils are generated. Adaptation of sonic drill systems to the CPT would used high frequency vibration to advance the probe through the hard layer and would not generate additional waste and result in only a modest decrease in the production rate.

### Resistivity Data

A robust CPT resistivity probe was demonstrated which exhibited minimal wear and good survivability of the insulator (which has been a significant problem at stiff sites such as SRS). The data proved to be of high resolution, reproducible and of great value in confirming the location of clay layers identified from the P/R-ECPT tip friction ratio and pore pressure data.

## Grouting on Retraction and Tremie Grouting of the CPT Sounding

A retraction grouting method was demonstrated at the first CPT location and successfully grouted the 140 ft deep sounding with a neat cement grout. This system required a 1.75 in OD push tube to pass the instrumentation and grouting cables. To meet the depth requirements, subsequent soundings were conducted with 1.405 in OD push tubes which can not be used with the retraction grouting system. Tremie grouting was used after the first sounding and was successful. Using tremie grouting, the CPT testing rate was significantly reduced from a typical rate of 300 ft per day to about 180 ft per day. The reduction was due to having to reenter the hole to tremie grout. It is highly desirable to use the 1.75 in push tubes as production rates are increased and the sounding is sure to be grouted. Use of 1.75 in push tubes at this site will require trucks heavier than the 27 ton truck used on this project.

## Soil Gas and Groundwater Sampling

Soil gas and ground water samples were obtained with the 1.405 in push tubes. The soil gas samples were obtained through a teflon tube strung through the push tubes and analyzed by a multi-gas monitor. Water samples were obtained in the same hole using a especially designed bailer which could fit inside the 5/8 in ID of the push tubes. Water was not obtained at all locations and the results of tests on the water samples were not available for this report.

## Field Analysis of Soil Gas Samples Using a Multi-Gas Monitor

Tests results from the gas monitor were very encouraging in that: the monitor appears to be robust and reliable; provides real time estimates of the contaminate type to the ppm level; was relatively simple to use and required only a limited amount of training. In addition, the monitor was easily adapted to the CPT system. This technique used allowed very detailed profiles of contaminates in the vadose zone to be obtained in a rapid and economical manner. To the writers knowledge no other gas monitor provides the range of capabilities or ease of use of the Bruel & Kjaer gas monitor.

### Evaluation of a CPT-Based Soil Classification System

The CPT soil classification system used on this project appear to provide reasonable estimates of soil type. Limited comparisons were made with the available bore log data, however the well log data was not sufficient to fully evaluate the CPT classification chart. A need exist to obtain a data base of soils classifications using the ASTM soil classification system, rather than visual well log classifications. The percentage of sands, silts and clays in the samples is critical to determining soils data and especially of the resistivity data.

### Predictions Using Resistivity Data

Predictions of DNAPL locations and degree of saturation in the vadose zone were made and are encouraging. These predictions were based on a very limited laboratory data base and sufficient data was not available to fully evaluate the predictions. At the beginning of this project it had not been envisioned that the resistivity data could be used to predict degree of saturation in the vadose zone, which is an important parameter in evaluating remediation techniques. Wright (1988?) has conducted research on soils from the Hanford site which shows that soil degree of saturation is related to the diffusion coefficient and hydraulic conductivity (see Figure 7.1). Wright's laboratory work used resistivity to determine soil water contents. With additional laboratory work it may be possible to estimate the diffusion coefficient and hydraulic conductivity, using Wright's laboratory studies as a framework, from resistivity data. This has important implications regarding transport calculations.

## RECOMMENDATIONS

Specific recommendations are as follows:

- The P/R-ECPT should be used to determine soil stratigraphy and type, as well as estimating ground water depths and

gradients. On future programs, dissipations tests should be conducted to determine the water table.

- The B&K gas monitor and CPT soil gas probe should be used in the vadose zone to determine the distribution, type and concentration of DNAPLs.

- Below the water table soil resistivity can theoretically provide estimates of DNAPLs at nearly saturated levels, however, at lower levels of saturation which are of significant interest additional soil characterization work is required.

- For deep soundings at SRS, only high push capacity CPT trucks should be specified. With the current state of CPT development, drilling will be required to penetrate the very stiff layers at depth.

This demonstration project has shown that P/R-ECPT soundings can provide detailed soil profiles and properties in a rapid and cost effective manner. However, several areas were identified that require additional work. These areas include validation of a SRS specific ECPT soil classification chart and laboratory testing of a wider range of soils. The testing should include determination of soil type using ASTM methods, resistivity testing to evaluate the variability of resistivity properties as a function of soil type, degree of saturation and to correlate diffusion coefficients and hydraulic conductivity with resistivity. Measurement of the soil dielectric constant with the CPT should also be investigated as work by Look and Reeves (1992) indicates that the soil degree of saturation can directly estimated from the dielectric constants, independent of soil type. Preliminary indications are that with only minor modifications that the CPT resistivity probe can measure the soil dielectric constant. In addition, development of techniques to penetrate those layers in which the CPT encountered refusal should receive a high priority.

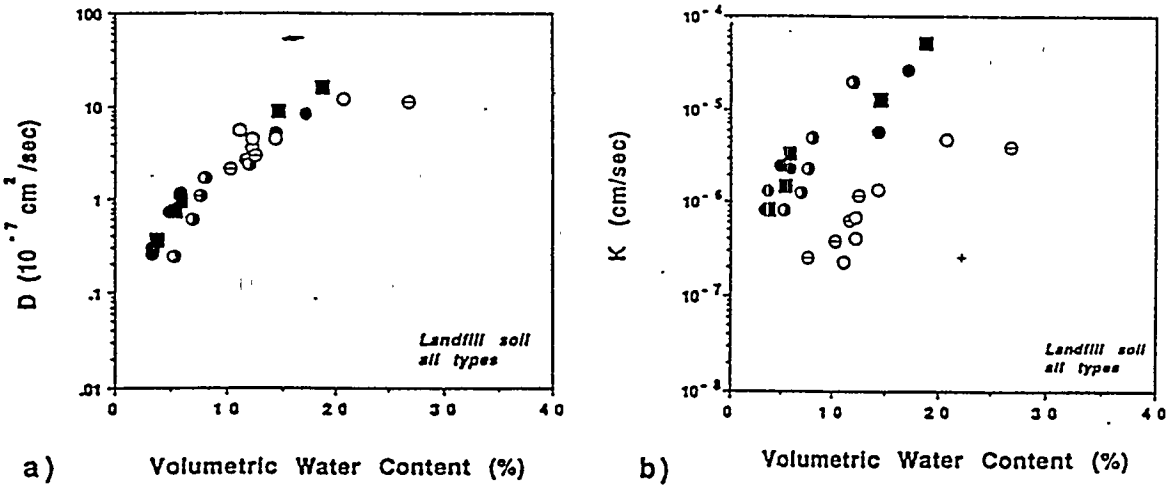


Figure 7.1. a) Diffusion coefficients for Hanford soils under the Landfill site showing strong dependence on water content and weak dependence on soil type. Open circles are loess 2, slashed circles are loess 1, closed circles are lower coarse sand, half-closed circles are upper coarse sand, closed squares are gravel. b) Hydraulic conductivity results for the same soils showing dependence on both soil type and water content (Wright).

## LIST OF REFERENCES


American Society for Testing and Materials, "Standard Method for Deep Quasi-Static, Cone and Friction-Cone Penetration Tests of Soil," ASTM Designation: D3441, 1986.

Annan, A.P., P. Bauman, J.P. Greenhouse, and J.D. Redman, " Geophysics and DNAPLS," *Ground Water Management*, No. 5., Proceedings of the Outdoor Action Conference on Aquifer Restoration, Ground Water Monitoring, and Geophysical Methods, Las Vegas, NV, May 1991.

Chiang, C.Y., K.R. Loos, and R.A. Klopp, "Field Determination of Geological/Chemical Properties of Aquifer by Cone Penetrometry and Headspace Analysis," Groundwater, Vol. 30, No. 3, May-June 1992.

Culley, R.W., F.L. Jagodits, and R.S. Middleton, "E-Phase System Innovations in Subsurface Exploration," 54th Annual Meeting of Transportation Research Board, 1975.

Eddy, C.A., B.B. Looney, J.M. Dougherty, T.C. Hazen, and D.S. Kaback, "Characterization of the Geology, Geochemistry, Hydrology and Microbiology of the In-Situ Air Stripping Demonstration Site at the Savannah River Site," (U), WSRC-RD-91-21, Report prepared for Department of Energy, May 1991.

Eslinger, E., and D. Pevear, *Clay Minerals for Petroleum Geologists and Engineers*, SEPM Short Course Notes No. 22, Society of Economic Paleontologists and Mineralogists, Tulsa, OK, 1988.

Jamiolkowski, M., V.N. Ghionna, R. Lancellota and Pasqualini, "New Correlations of Penetration Test for Design Practice," Invited Lecture, ISOPT-1, March, Balkema Publ., pp 264-296, 1988.

Keys, S.W., and L.M. MacCary, *Techniques of Water-Resources Investigations of the United States Geological Survey*, Ch. E1, "Application of Borehole Geophysics to Water-Resources Investigations," U.S. Geological Survey, Denver, CO, 1971.

Look, B.G., and I.N. Reeves, "The Application of Time Domain Reflectrometry in Geotechnical Instrumentation," *Geotechnical Testing Journal*, GTJODJ, Vol. 15, No. 3, pp. 277-283, September 1992.

Lutenegger, A.J., and M.G. Kabir, "Interpretation of Piezocone Results in Overconsolidated Clays, Penetration Testing in the U.K.," pp. 147-150, 1988.

Mayne, P.W., and R.D. Holtz, "Profiling Stress History from Piezocone Soundings," Japanese Society of Soil Mechanics and Foundation Engineering, Vol. 28, No. 1, pp. 1-13, March 1988.

## LIST OF REFERENCES (CONTINUED)


Mayne, P.W., and J.N. Kay, "Observations on the Development of Pore Water Stresses During Piezo Cone Penetration in Clays," Canadian Geotechnical Journal, Vol. 27, pp 418-428, 1990.

Pfannkuch, H.O., "On the Correlation of Electrical Conductivity Properties of Porous Systems with Viscous Flow Transport Coefficients," Proceedings of the IAHR First International Symposium, Fundamentals of Transport Phenomena in Porous Media, Haifa, pp. 42-54, 1969.

Robertson, P.K., and R.G. Campanella, "Guidelines for Using the CPT, CPTU, and Marchetti DMT for Geotechnical Design: Volume II - Using CPT and CPTU Data," Civil Engineering Dept., University of British Columbia, March 1988.

Saksa, P. and J. Korkealaakso, "Application of Geophysical Methods in Environmental and Municipal Engineering Theoretical Study," Espco Technical Research Center of Finland, October 1987.

Seusy, F.E., "Proposal to Provide Site Characterization Services for Creosote Plume in Newark, New Jersey," ARA Proposal No. 6252 Presented to Dames & Moore, Inc., Cranford, NJ, November 1991.

Shinn, J.D., and A.F. Rauch, "Resistivity Surveys with the Electric Cone Penetration Technique," Applied Research Associates, Inc., March 1990.

Telford, W.M., L.P. Geldart, R.E. Sheriff, and D.A. Keys, *Applied Geophysics*, Ch. 5, Cambridge University Press, NY, 1976.

Timian, D.A., W.L. Bratton, B.E. Fisk, "Piezo Electric Cone Penetration Tests in Support of Geotechnical Investigation at Sections 6/7 and 1/9 of Fresh Kills Landfill, Staten Island, New York - Development of Correlations for Soil Classification and In-Situ Properties," Applied Research Associates, Inc., Contract No. 5693, Report to IT Corporation, May 1992.

Looney, B. B., Rossabi, J. Tuck, D. M., "Assessing DNAPL Contamination, A/M-Area, SRS: Phase I Results Environmental Restoration Division under Contract No. DE-AC09-89SR18035

Wheatcraft, S.W., K.C. Taylor, J.G. Haggard, "An Investigation of Electrical Properties of Porous Media," University of Nevada Report to U.S. Environmental Protection Agency, Las Vegas, NV, December 1984.

Wright, J., "Diffusion Coefficients and Hydraulic Conductivity in Unsaturated Hanford Soils and Sediments," *Radioactive Waste Management*, work performed under DOE Contract No. DE-AC06-76RLO 1830.

# APPENDIX A

## CPT DATA AND PROPERTIES DERIVED FROM THE DATA

Send to print
Shop
make 10 copies
Cover paper - blue
two-Sided except Appendix
Plastic comb

CPT-001 APPLIED RESEARCH ASSOCIATES, INC. 07/14/92

North 104527.29 East 48761.45 Elevation 353.7

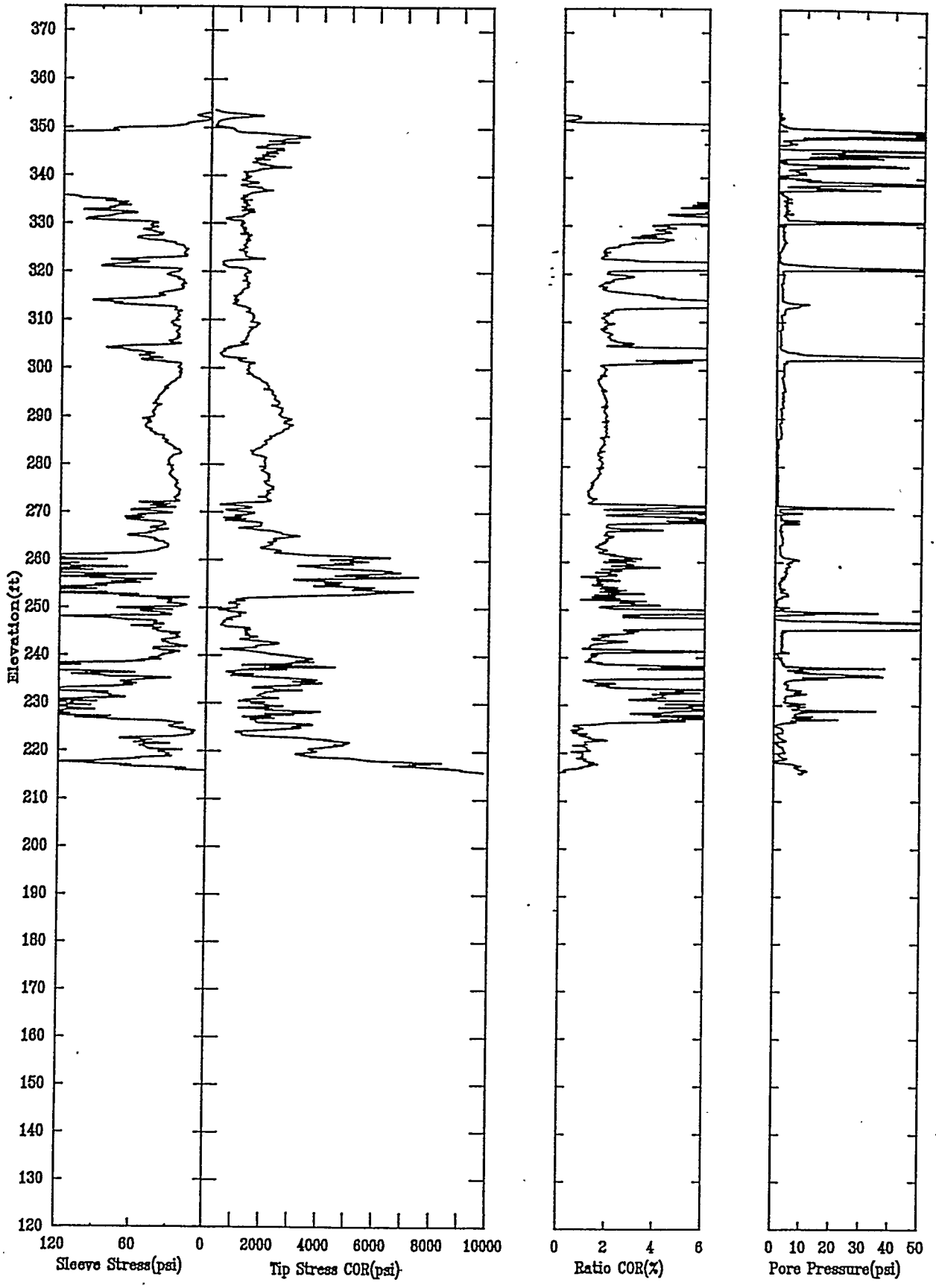

CPT-001 APPLIED RESEARCH ASSOCIATES, INC. 07/14/92

North 104527.29 East 48761.45 Elevation 353.7

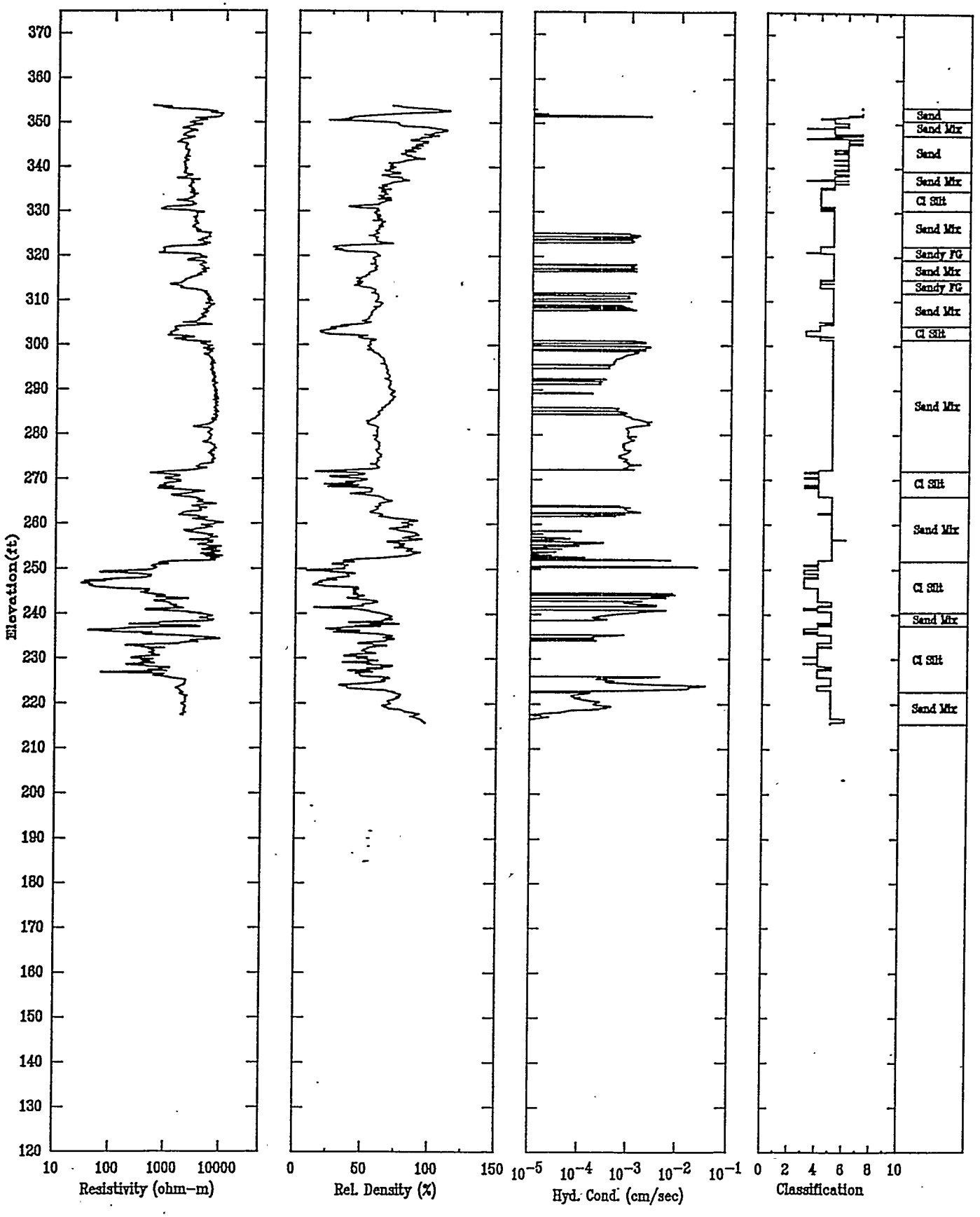

CPT-002 APPLIED RESEARCH ASSOCIATES, INC. 07/16/92

North 104243.57 East 47884.75 Elevation 349.7

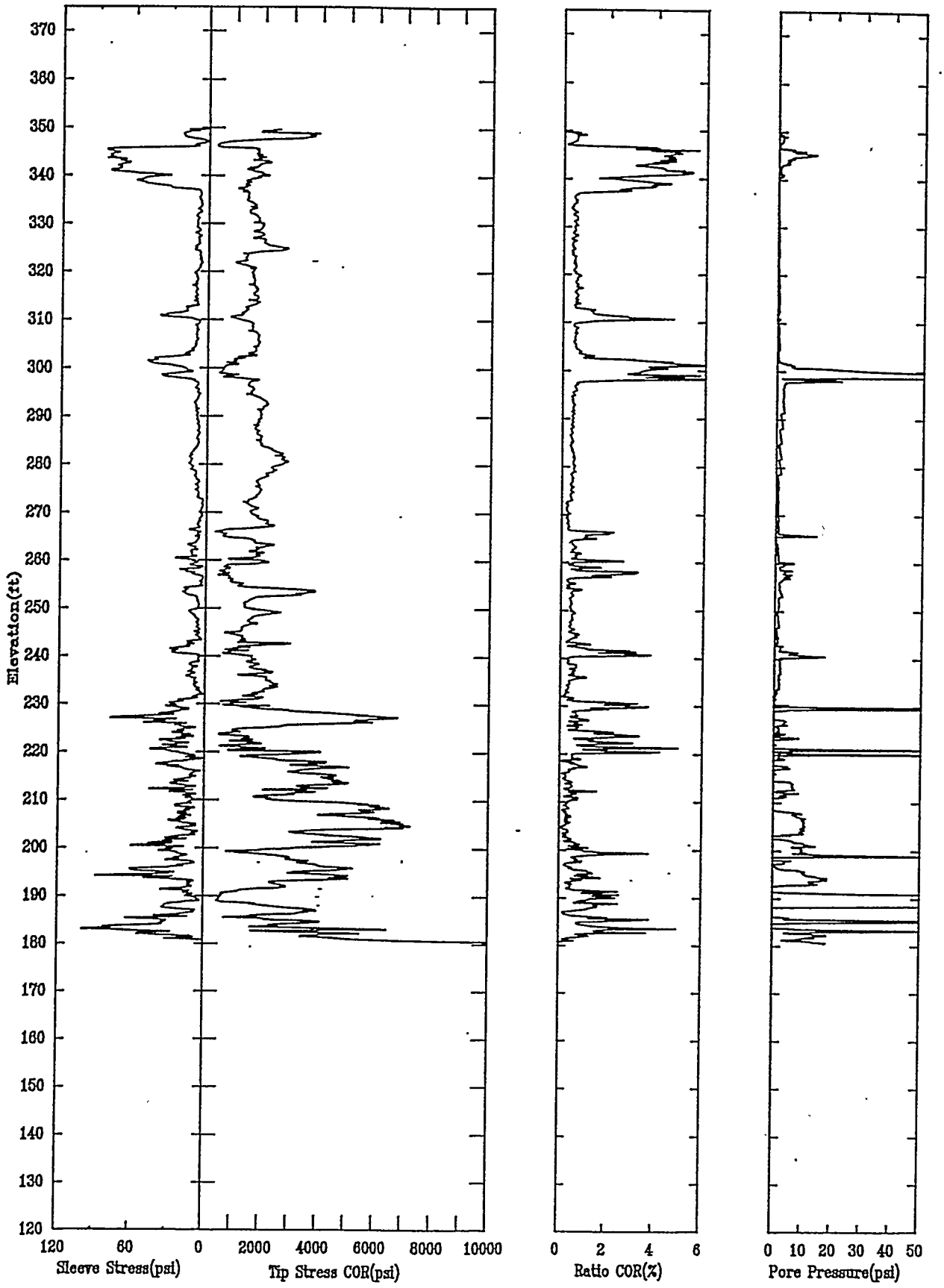

CPT-002 APPLIED RESEARCH ASSOCIATES, INC. 07/16/92

North 104243.57 East 47884.75 Elevation 349.7

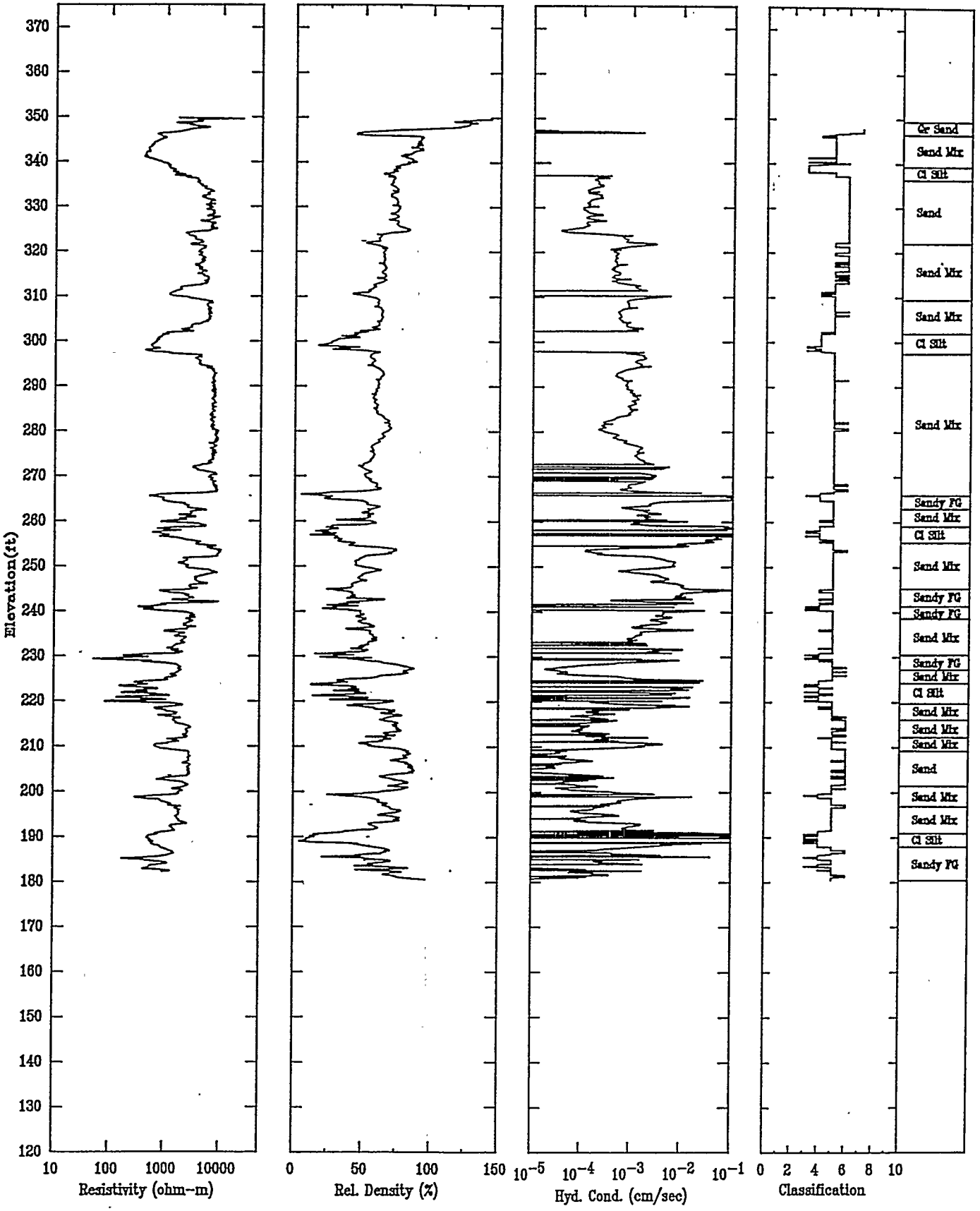

CPT-003 APPLIED RESEARCH ASSOCIATES, INC. 07/20/92

North 103251.70 East 45819.40 Elevation 351.0

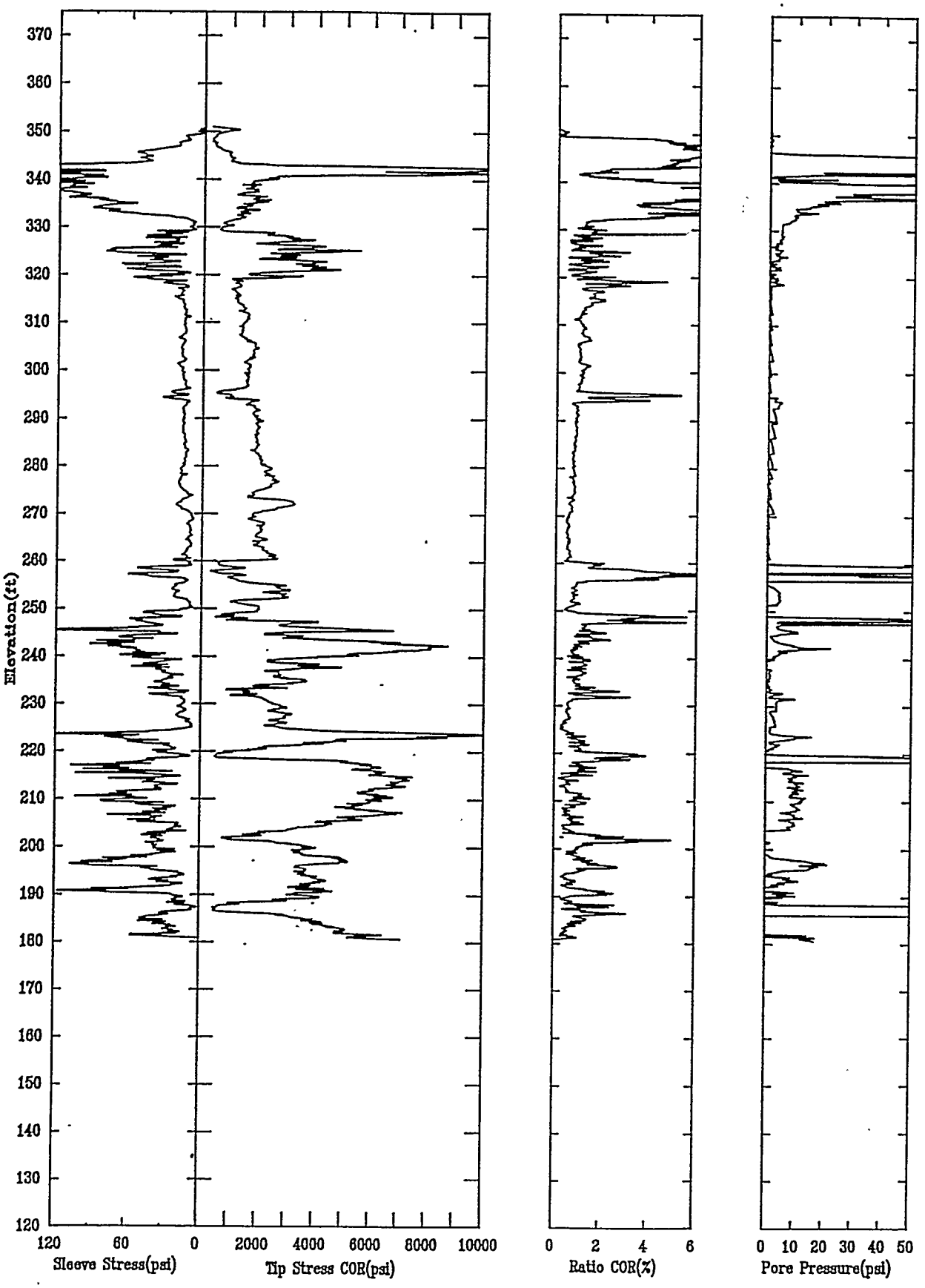

CPT-003 APPLIED RESEARCH ASSOCIATES, INC. 07/20/92

North 103251.70 East 45819.40 Elevation 351.0

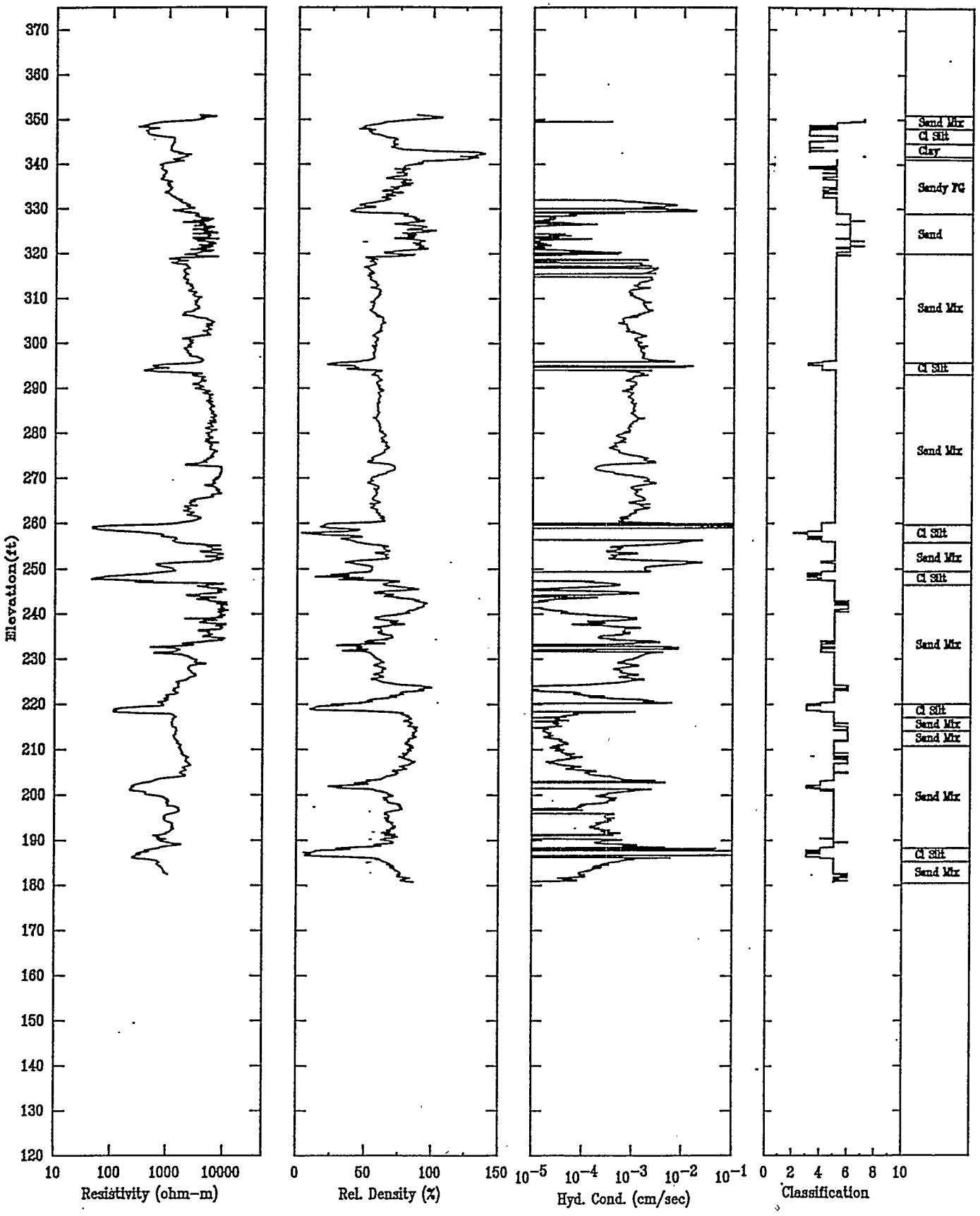

CPT-004 APPLIED RESEARCH ASSOCIATES, INC. 07/18/92

North 104120.50 East 45512.11 Elevation 357.7

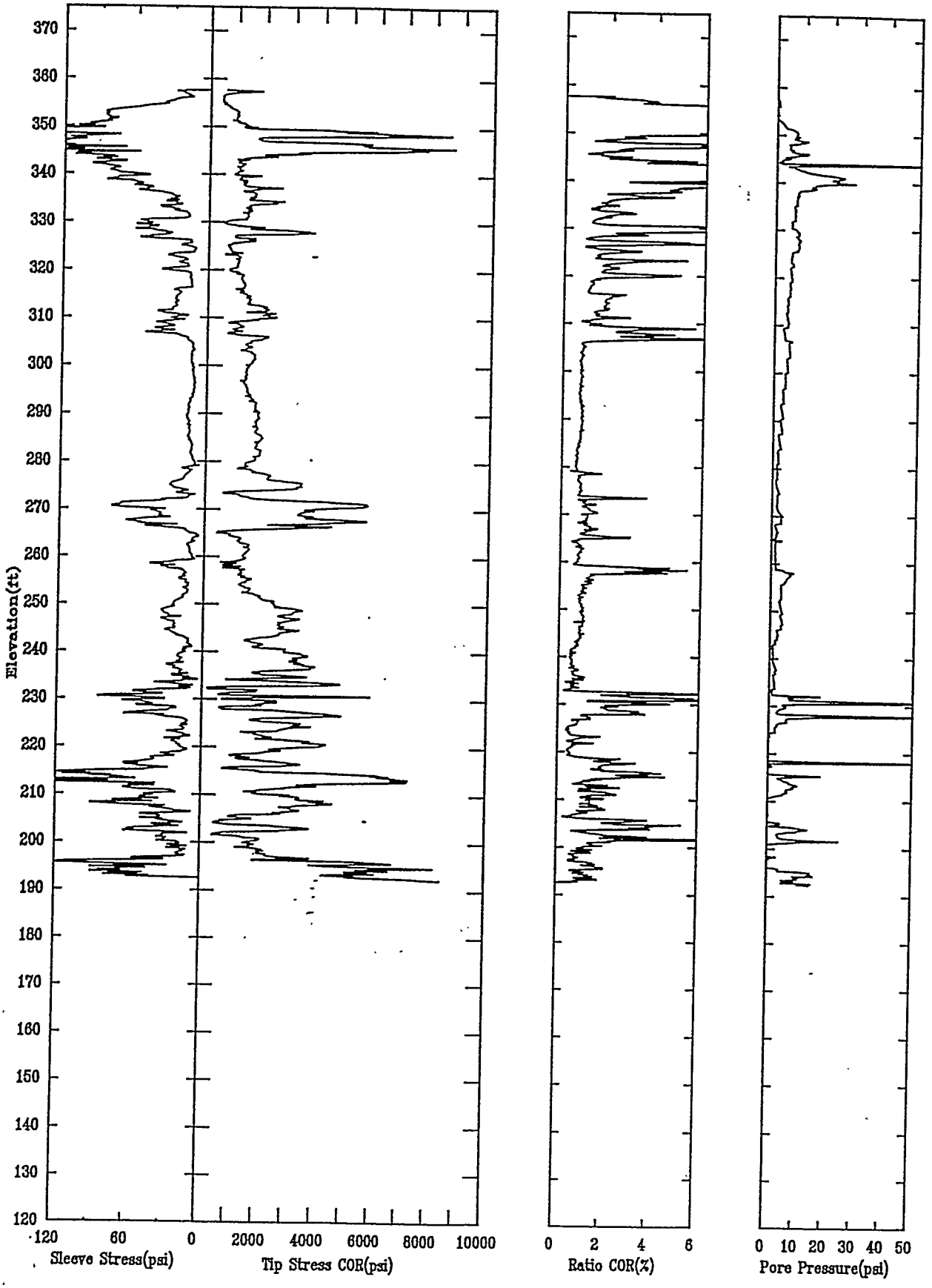

CPT-004 APPLIED RESEARCH ASSOCIATES, INC. 07/18/92

North 104120.50 East 45512.11 Elevation 357.7

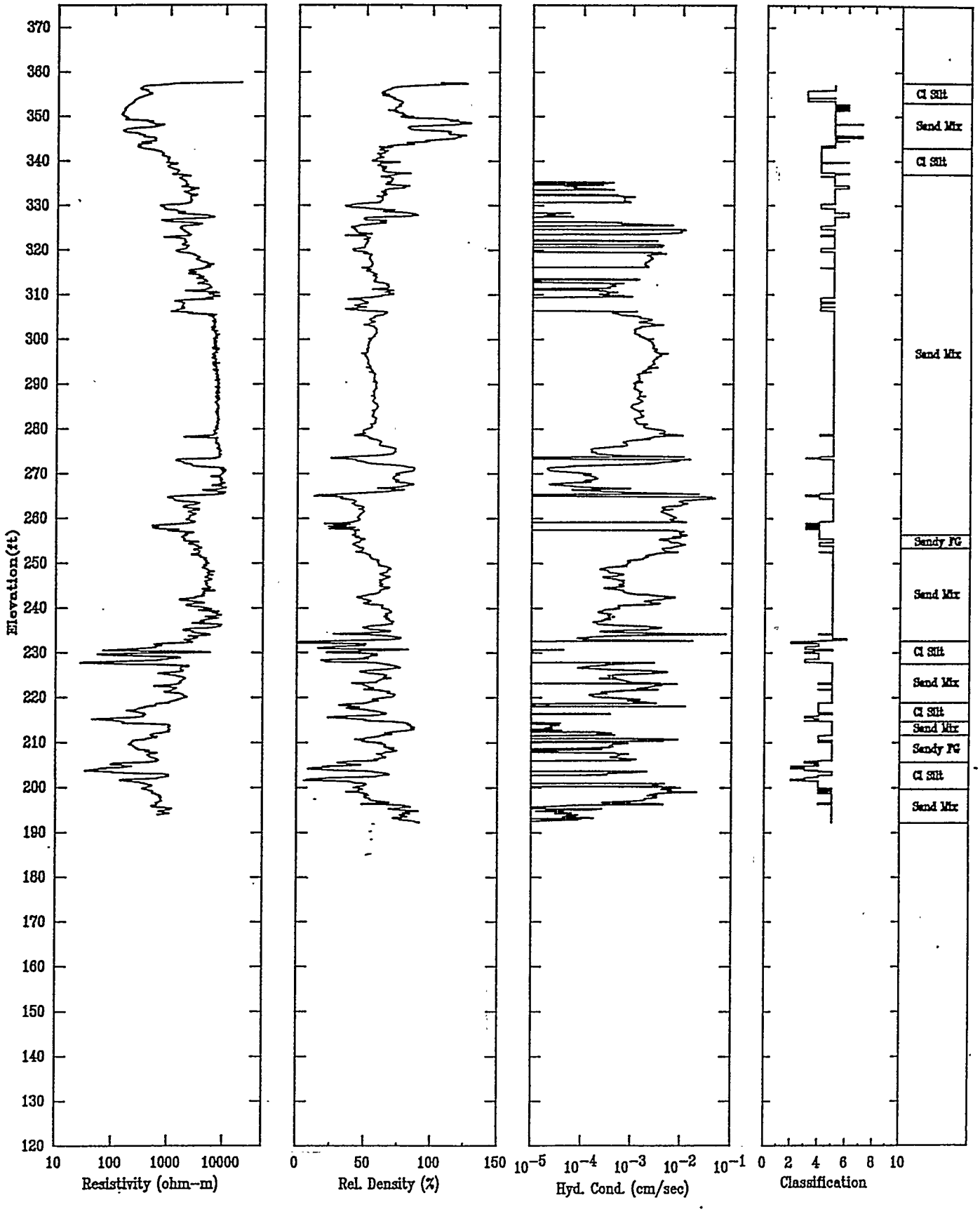

CPT-005 APPLIED RESEARCH ASSOCIATES, INC. 07/11/92

North 103874.72 East 47863.29 Elevation 360.2

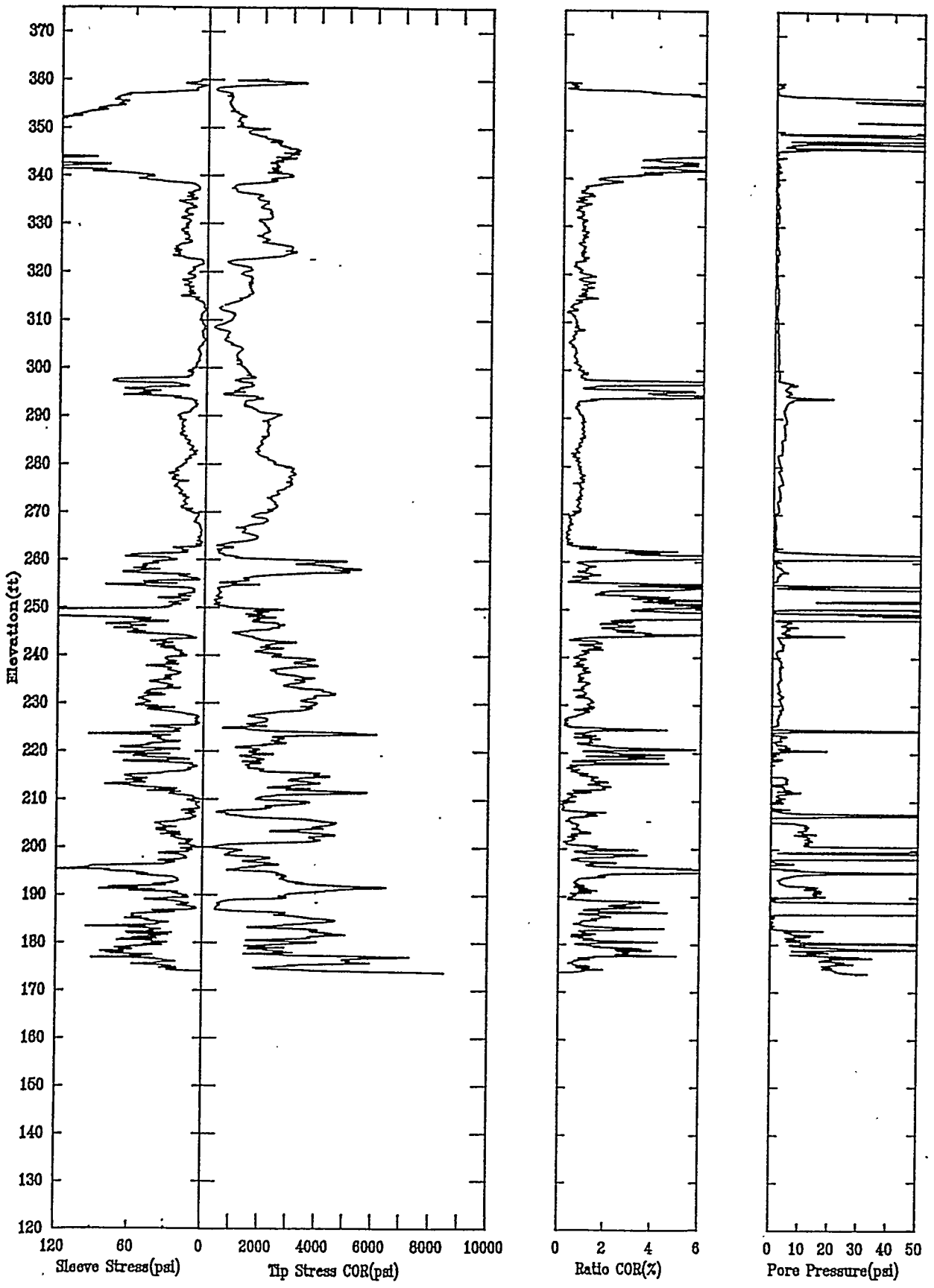

CPT–005 APPLIED RESEARCH ASSOCIATES, INC. 07/11/92

North 103874.72 East 47863.29 Elevation 360.2

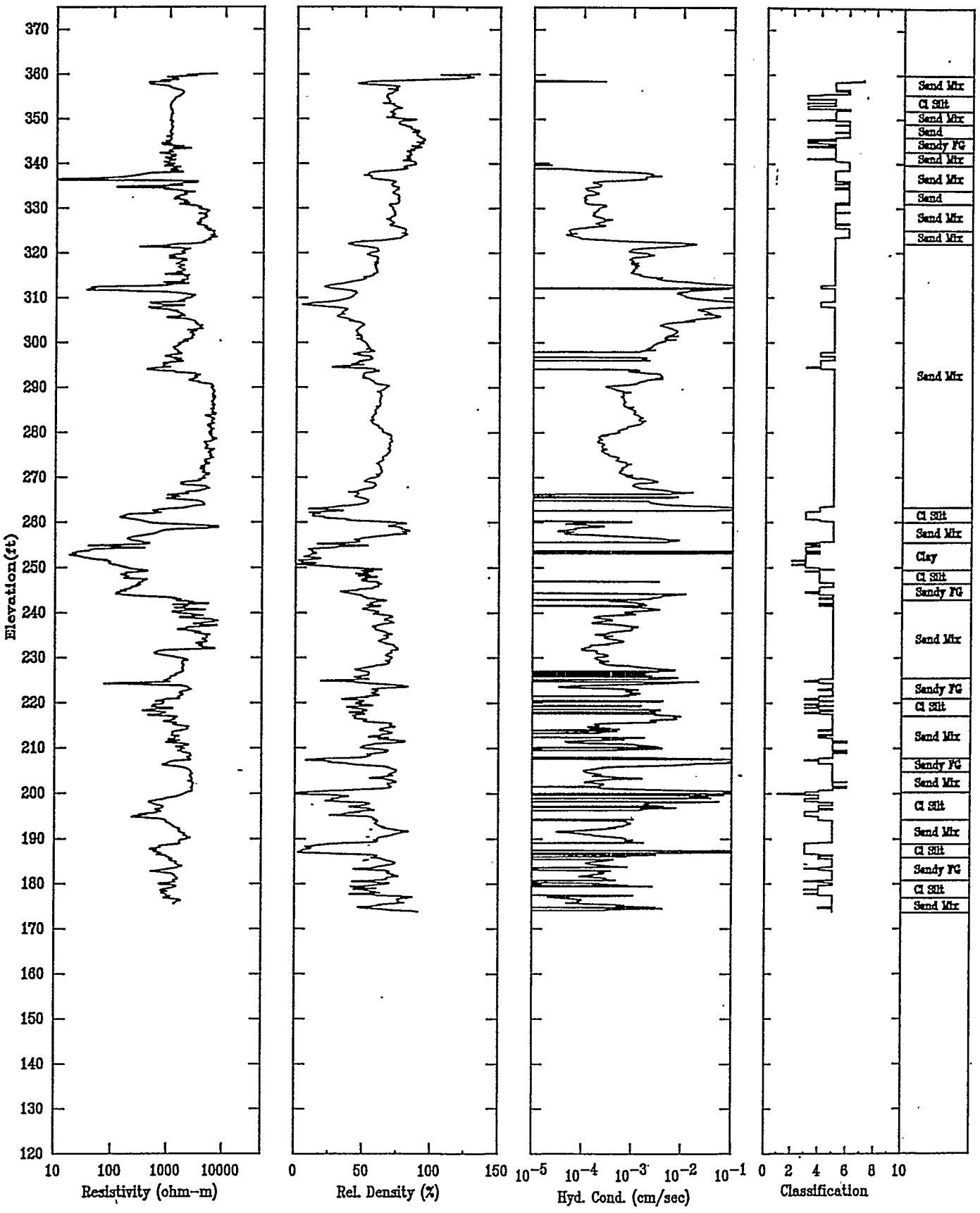

CPT-006 APPLIED RESEARCH ASSOCIATES, INC. 07/13/92

North 103064.78 East 48469.71 Elevation 370.5

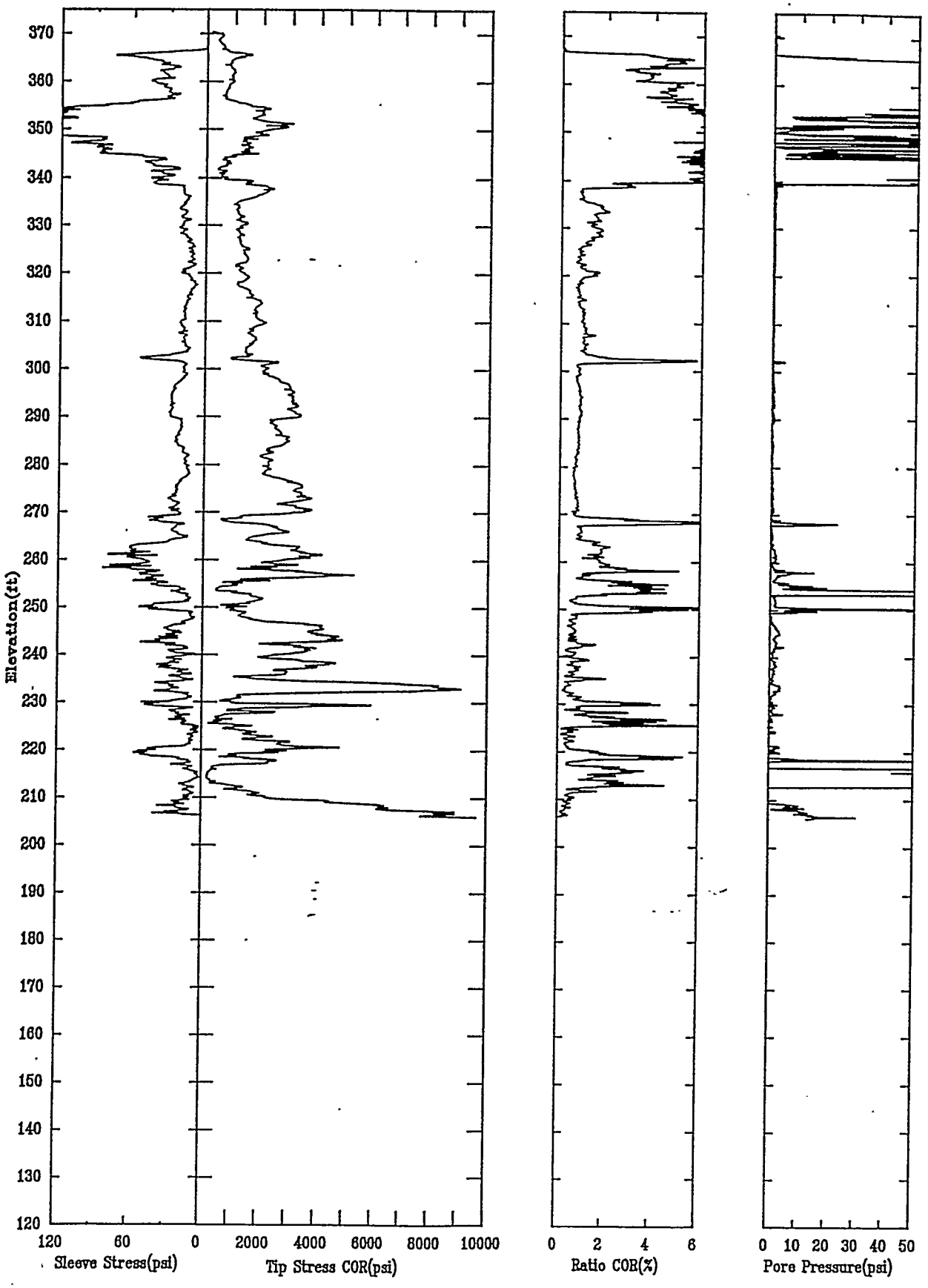

CPT-006 APPLIED RESEARCH ASSOCIATES, INC. 07/13/92

North 103064.78 East 48469.71 Elevation 370.5

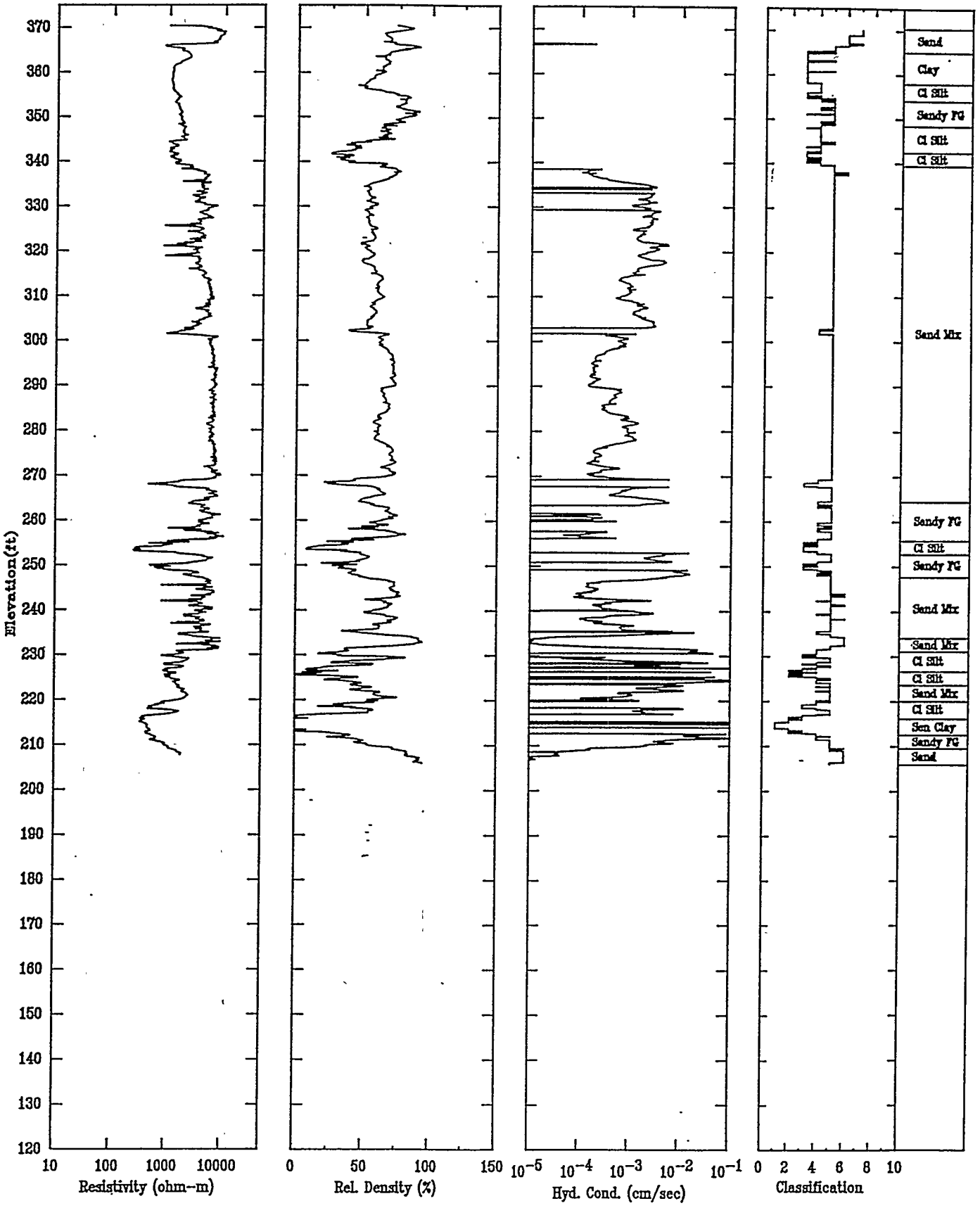

CPT-007 APPLIED RESEARCH ASSOCIATES, INC. 07/24/92

North 102444.36 East 47586.21 Elevation 349.8

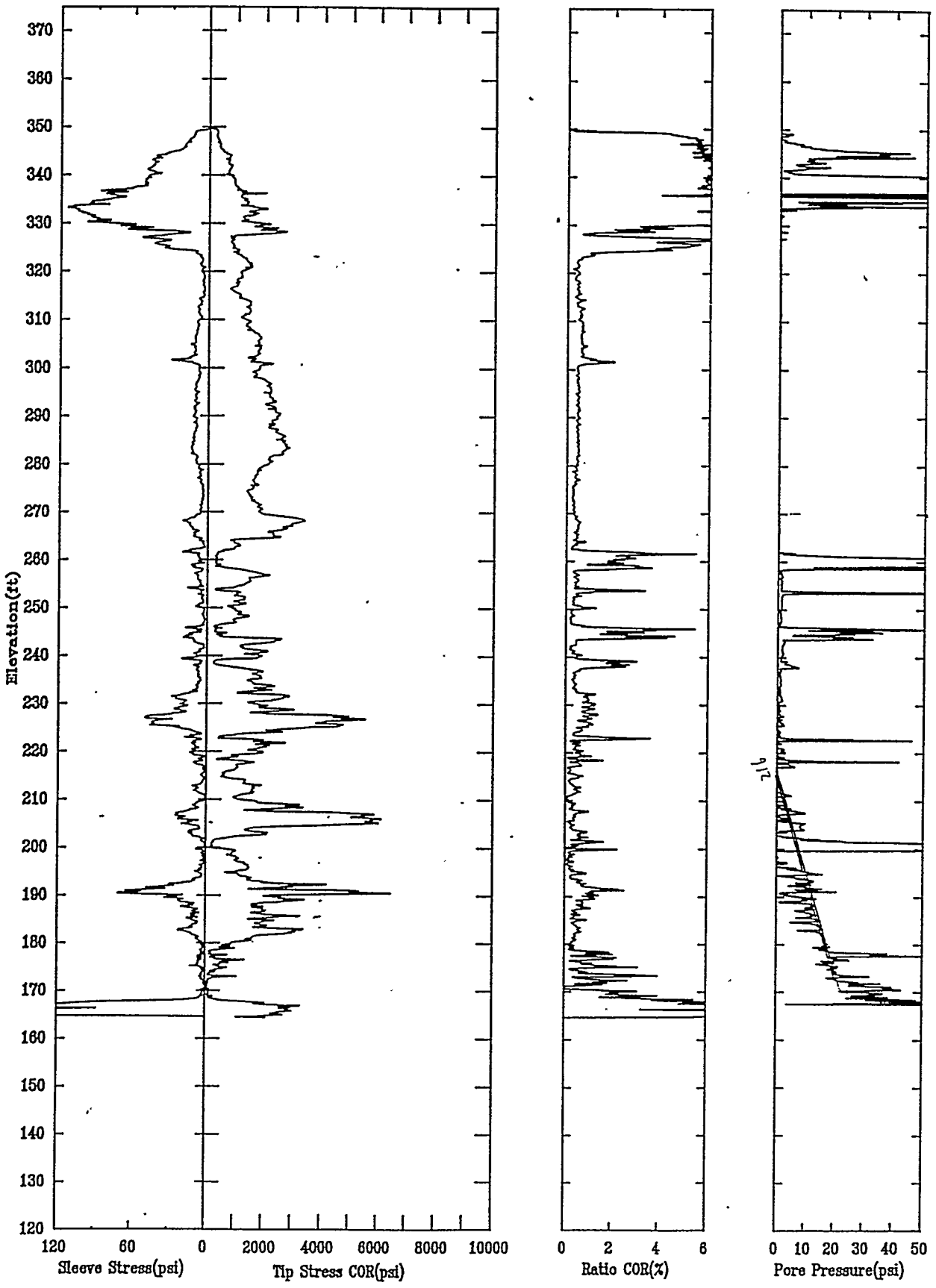

CPT-007 APPLIED RESEARCH ASSOCIATES, INC. 07/24/92

North 102444.36 . East 47586.21 Elevation 349.8

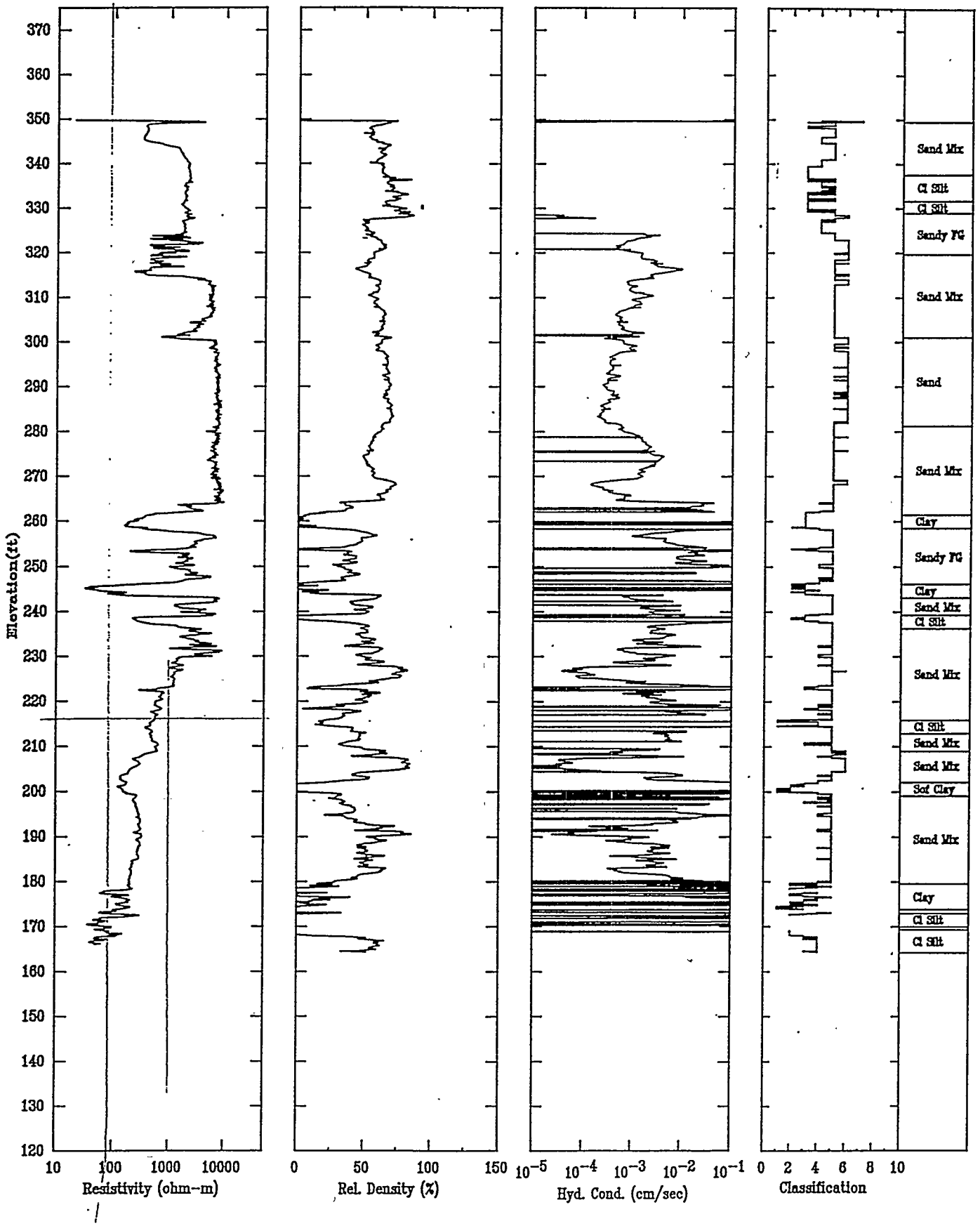

CPT-009 APPLIED RESEARCH ASSOCIATES, INC. 06/24/92

North 100993.00 East 47696.68 Elevation 344.9

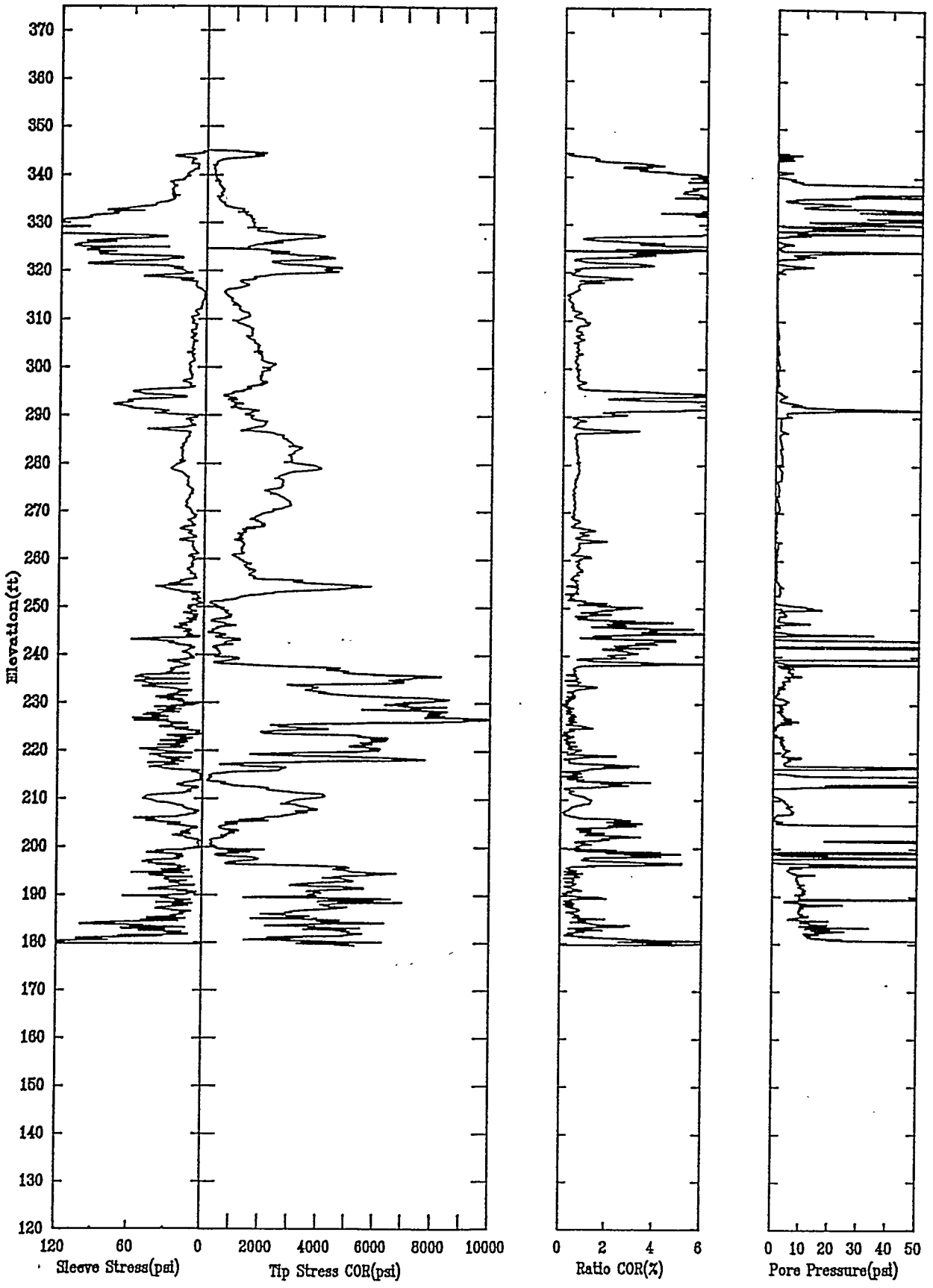

CPT-009 APPLIED RESEARCH ASSOCIATES, INC. 06/24/92

North 100993.00 East 47696.68 Elevation 344.9

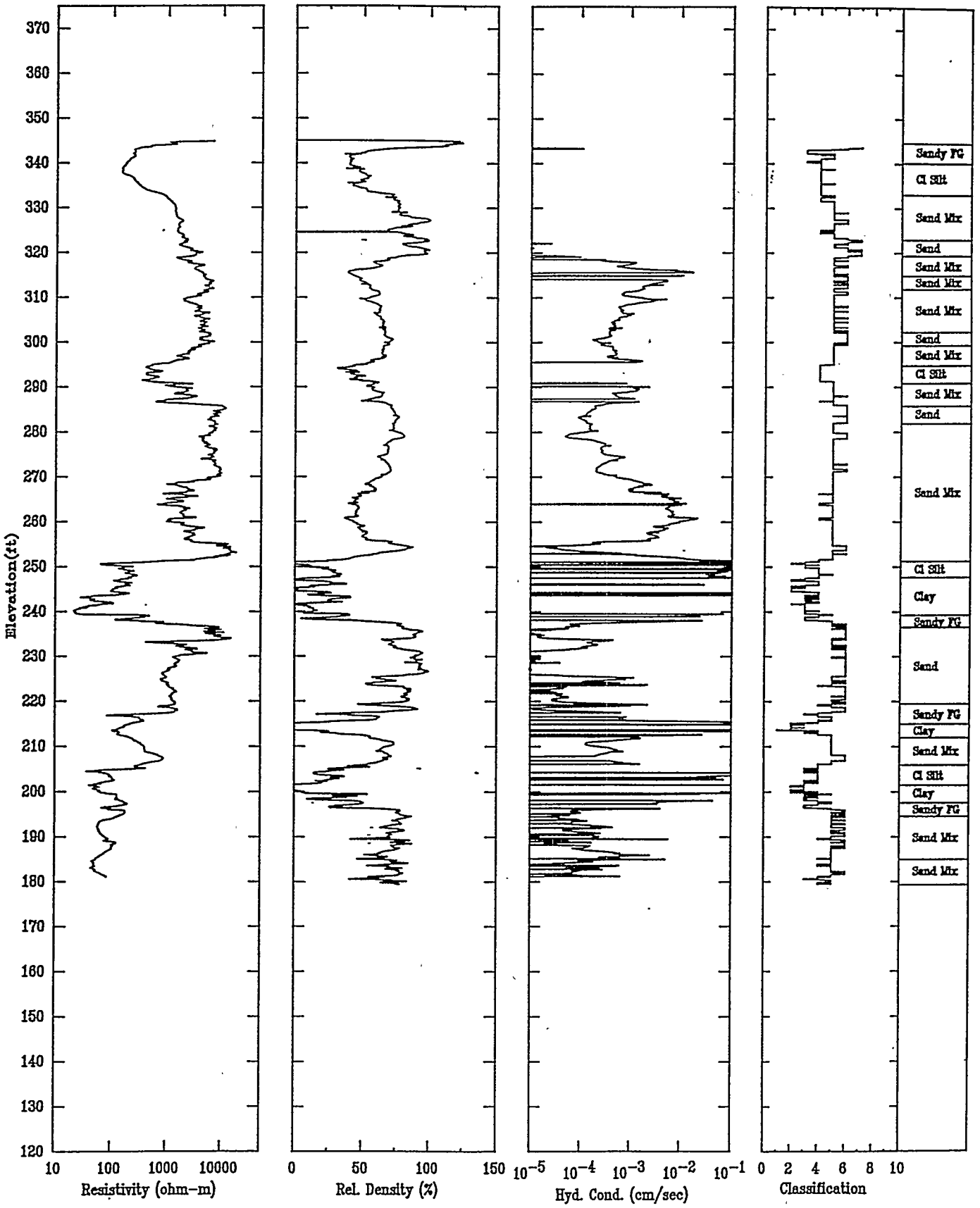

CPT-010 APPLIED RESEARCH ASSOCIATES, INC. 07/22/92

North 100505.84 East 46714.64 Elevation 343.1

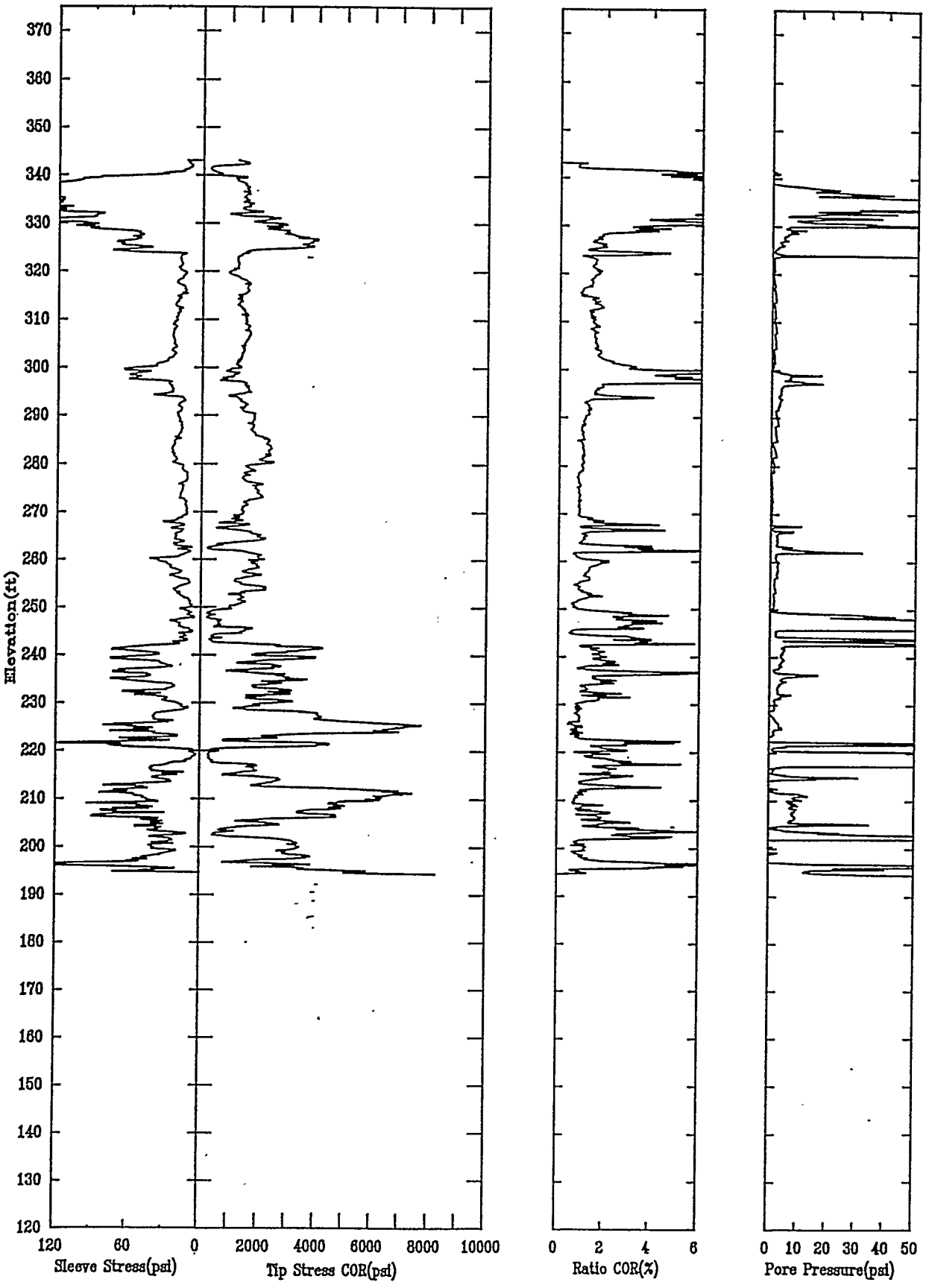

CPT-010 APPLIED RESEARCH ASSOCIATES, INC. 07/22/92

North 100505.84 East 46714.64 Elevation 343.1

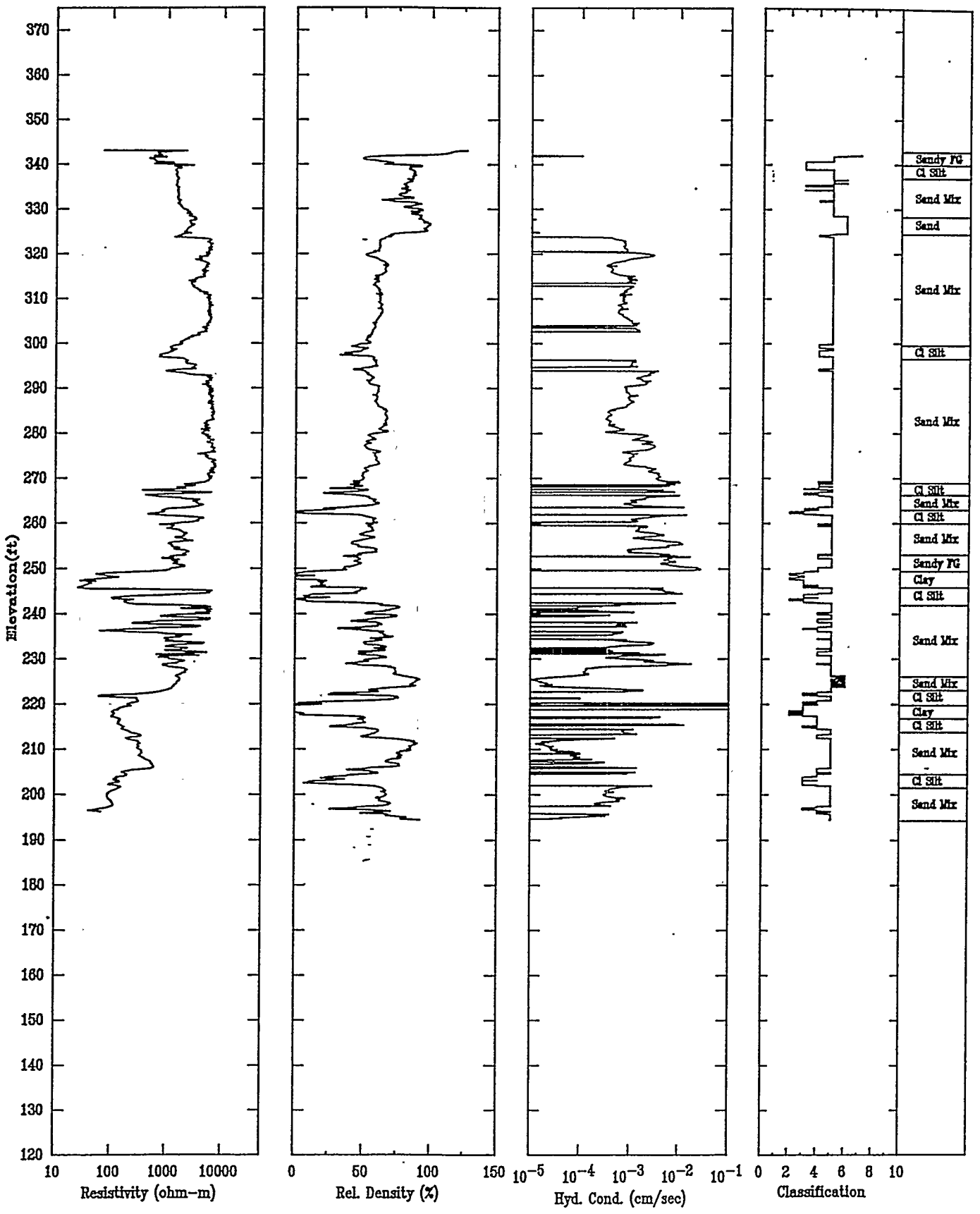

CPT-011 APPLIED RESEARCH ASSOCIATES, INC. 07/22/92

North 101349.24 East 46114.51 Elevation 353.8

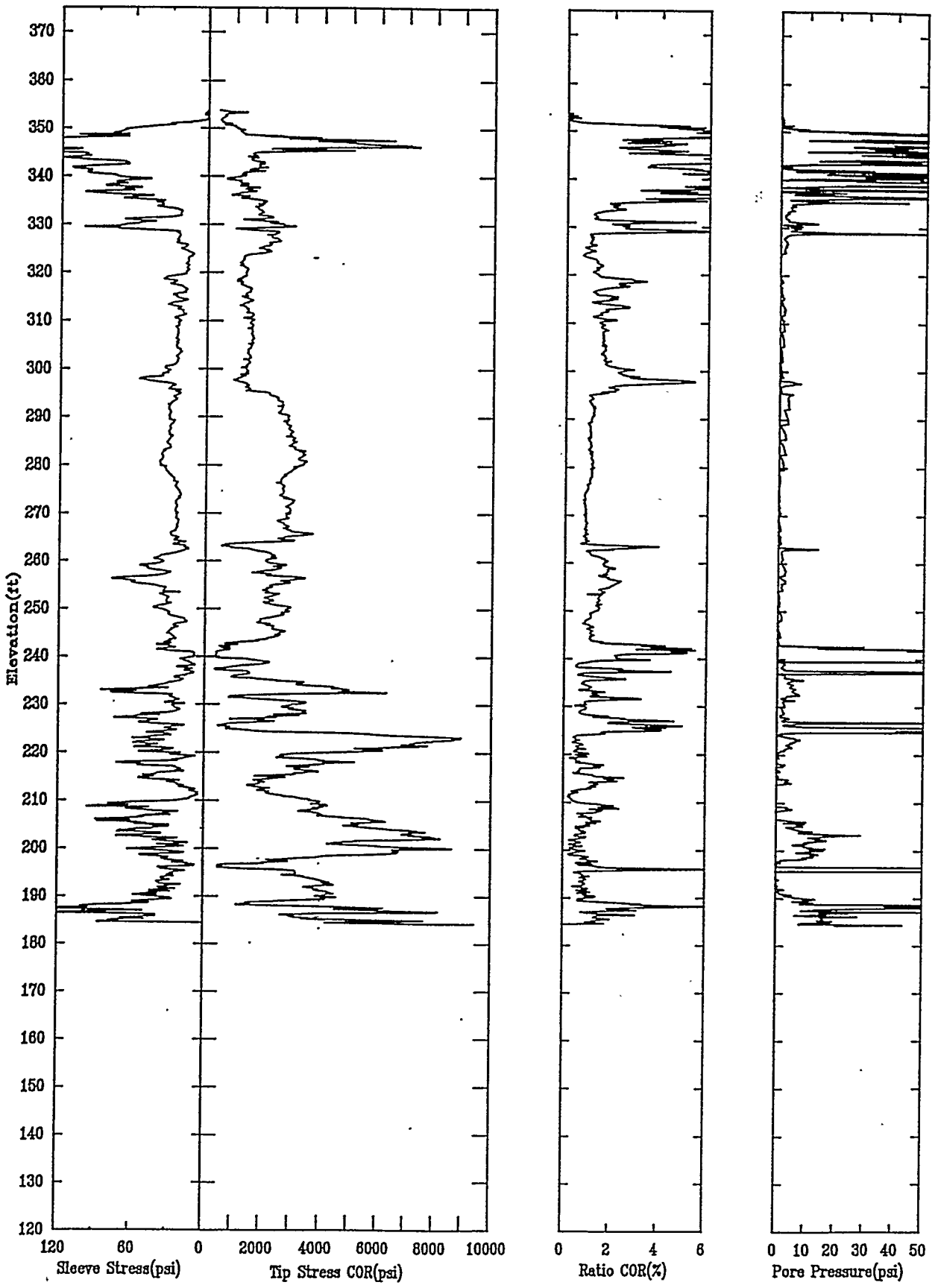

CPT-011 APPLIED RESEARCH ASSOCIATES, INC. 07/22/92

North 101349.24 East 46114.51 Elevation 353.8

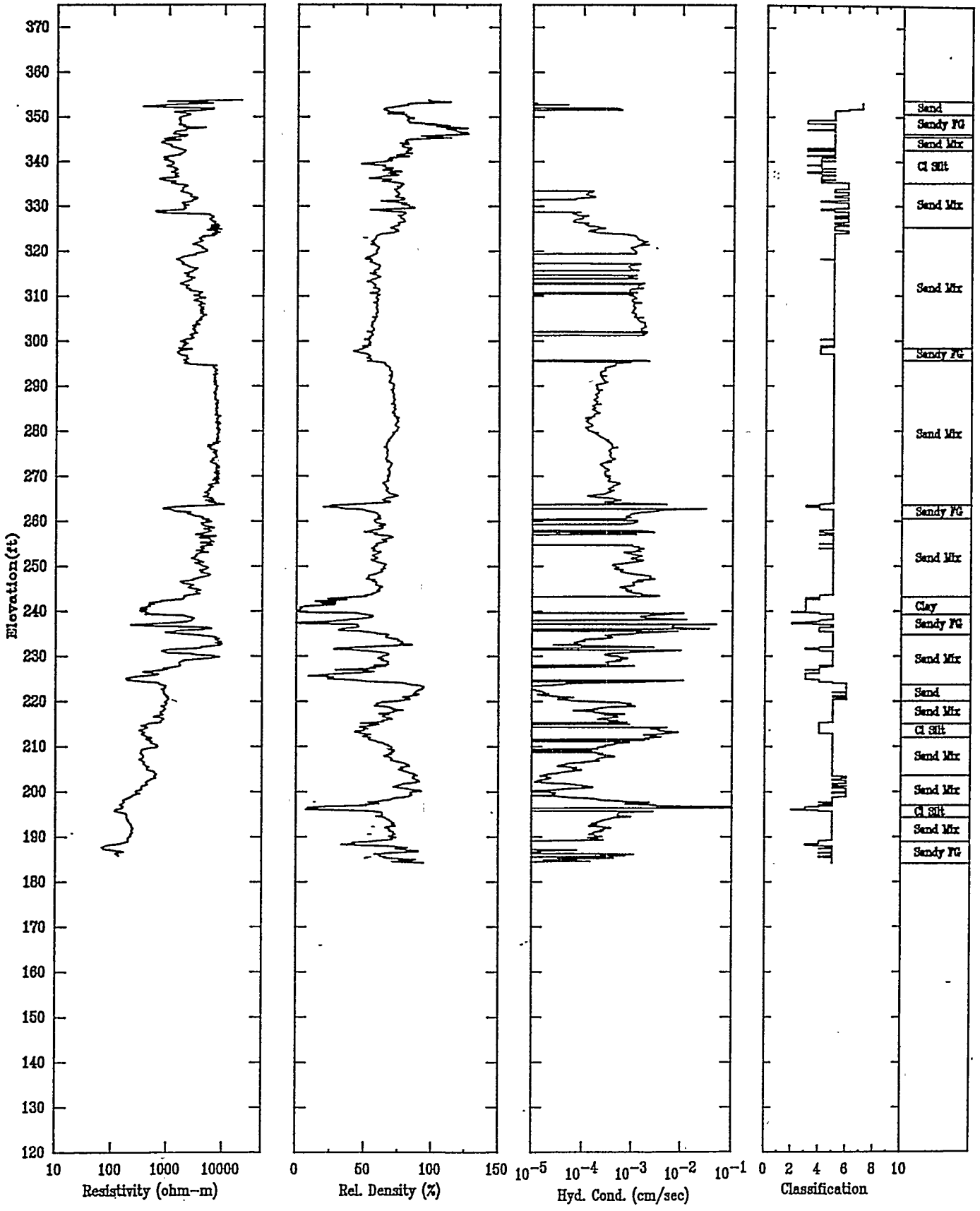

CPT-012 APPLIED RESEARCH ASSOCIATES, INC. 07/17/92

North 103267.58 East 45036.43 Elevation 360.1

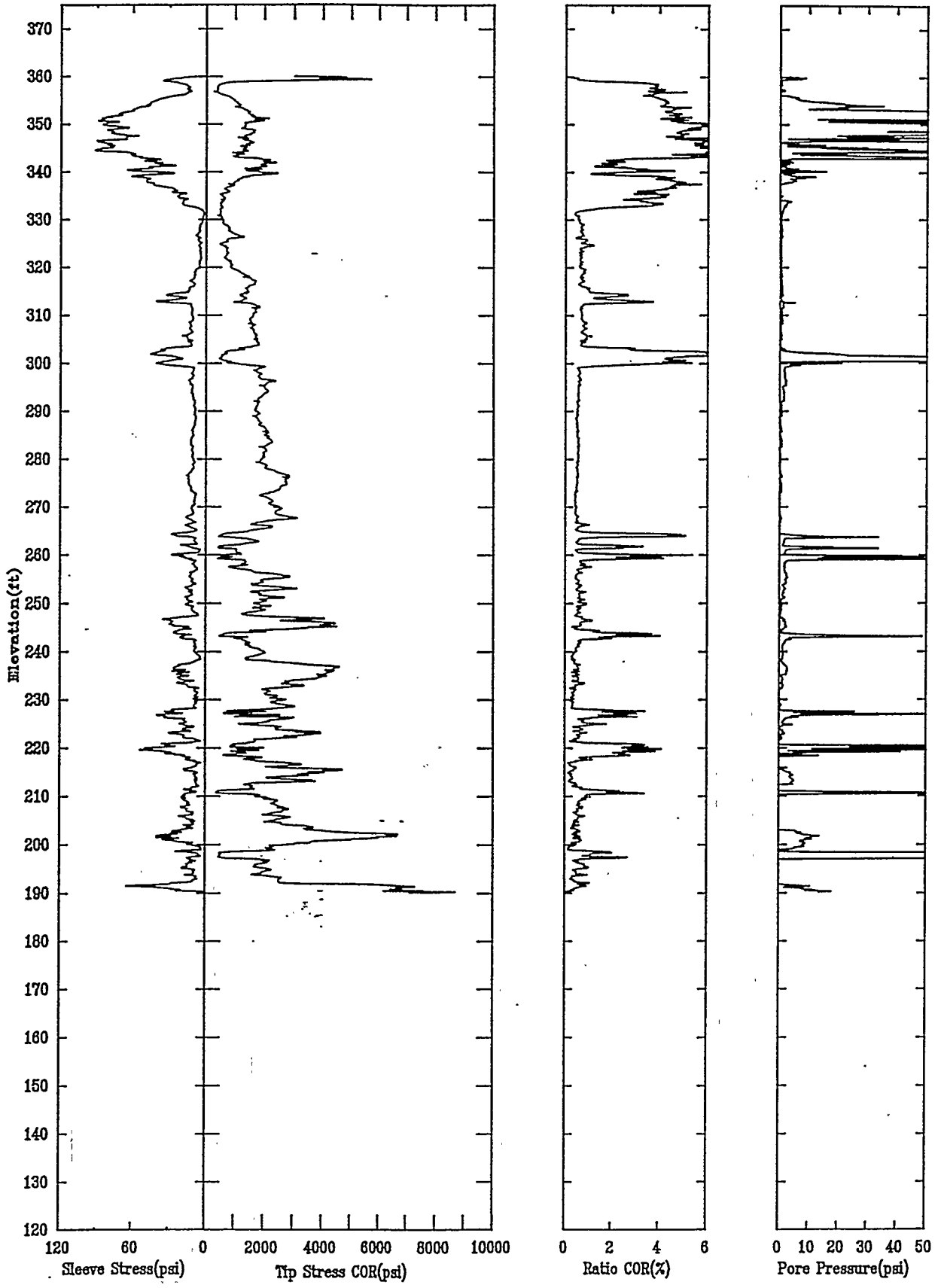

CPT-012 APPLIED RESEARCH ASSOCIATES, INC. 07/17/92

North 103267.58 East 45036.43 Elevation 360.1

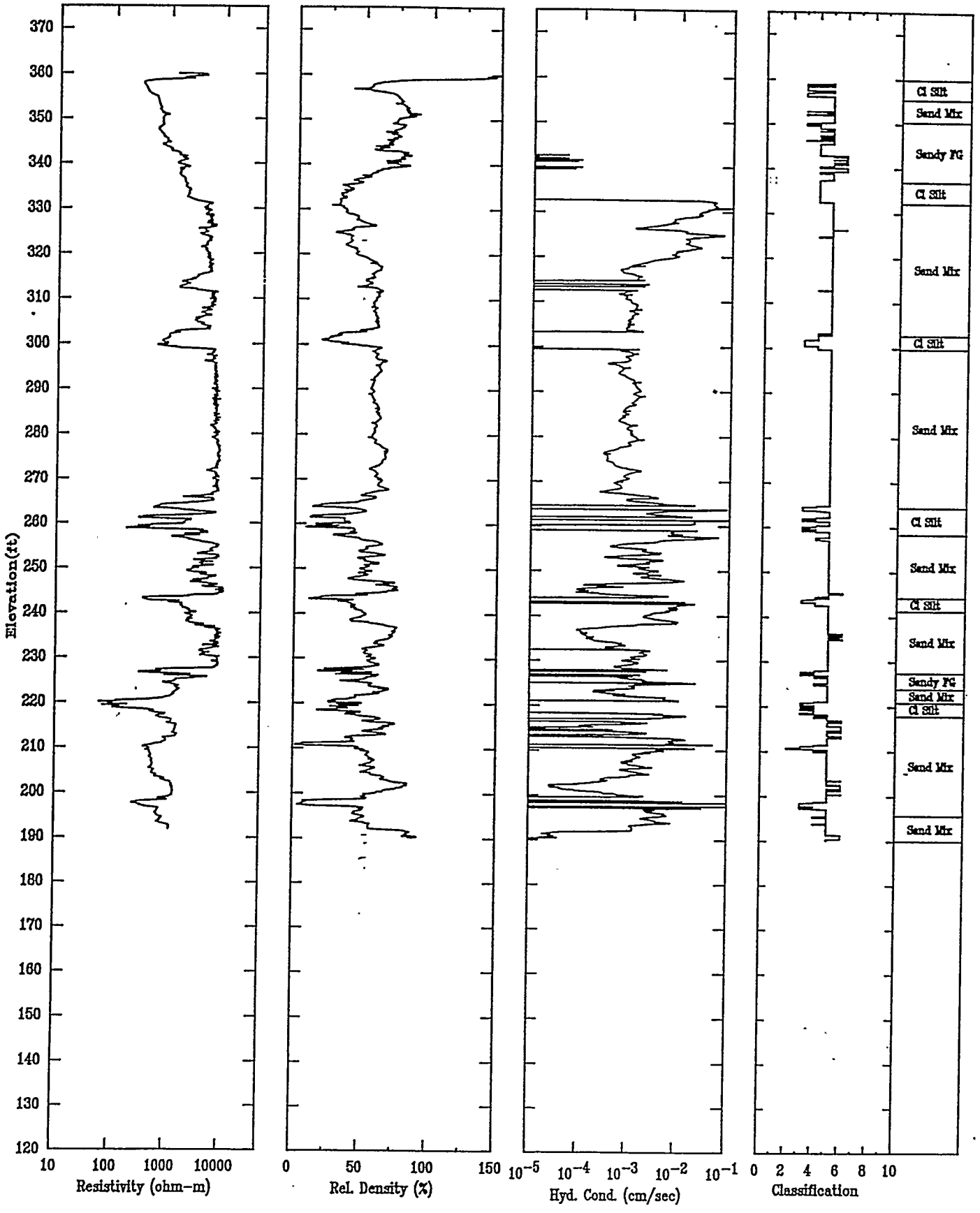

CPT-013A APPLIED RESEARCH ASSOCIATES, INC. 06/19/92

North 103066.76 East 45297.14 Elevation 350.4

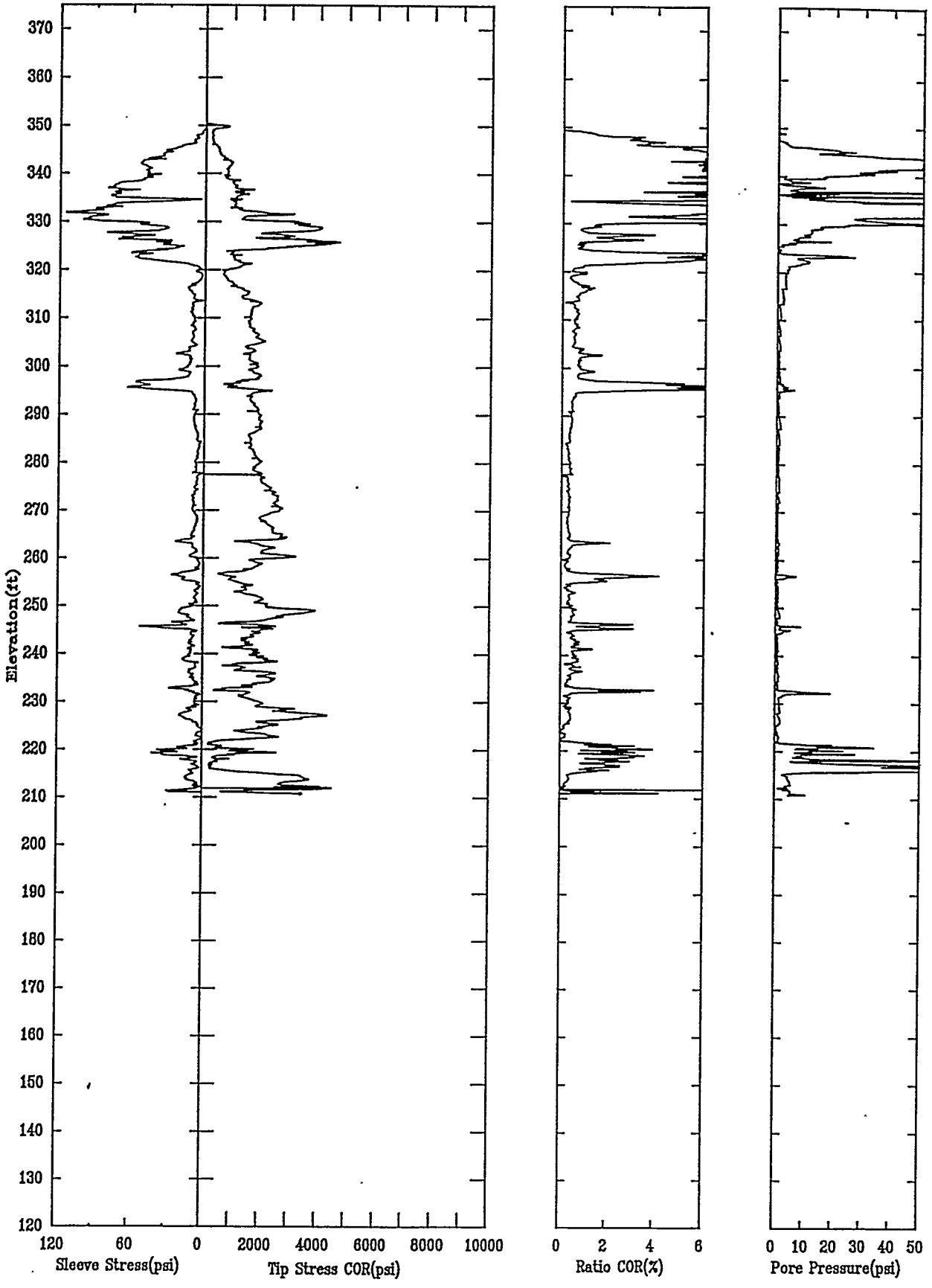

CPT-013A APPLIED RESEARCH ASSOCIATES, INC. 06/19/92

North 103066.76 East 45297.14 Elevation 350.4

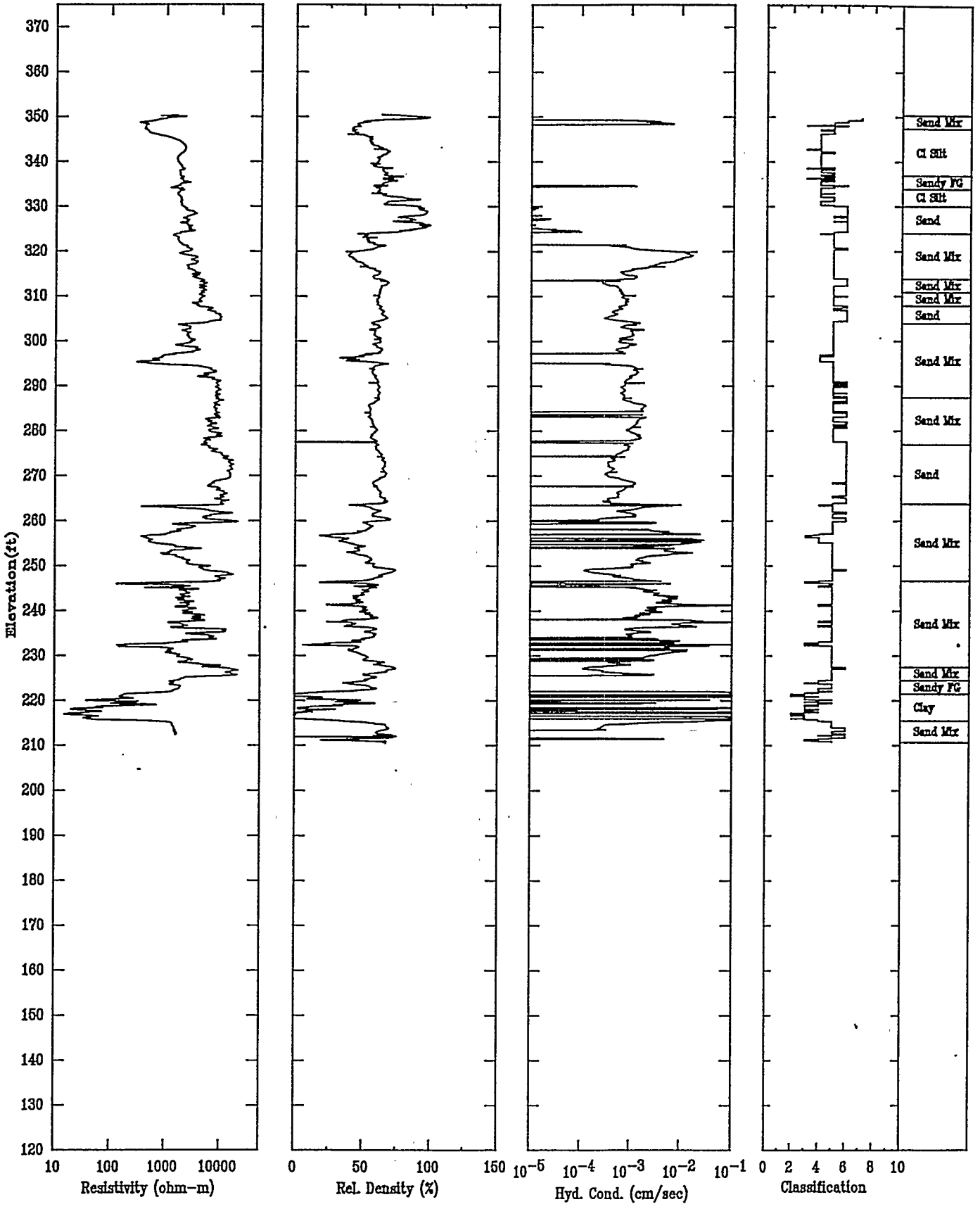

CPT-013B APPLIED RESEARCH ASSOCIATES, INC. 07/25/92

North 103083.19 East 45312.23 Elevation 350.2

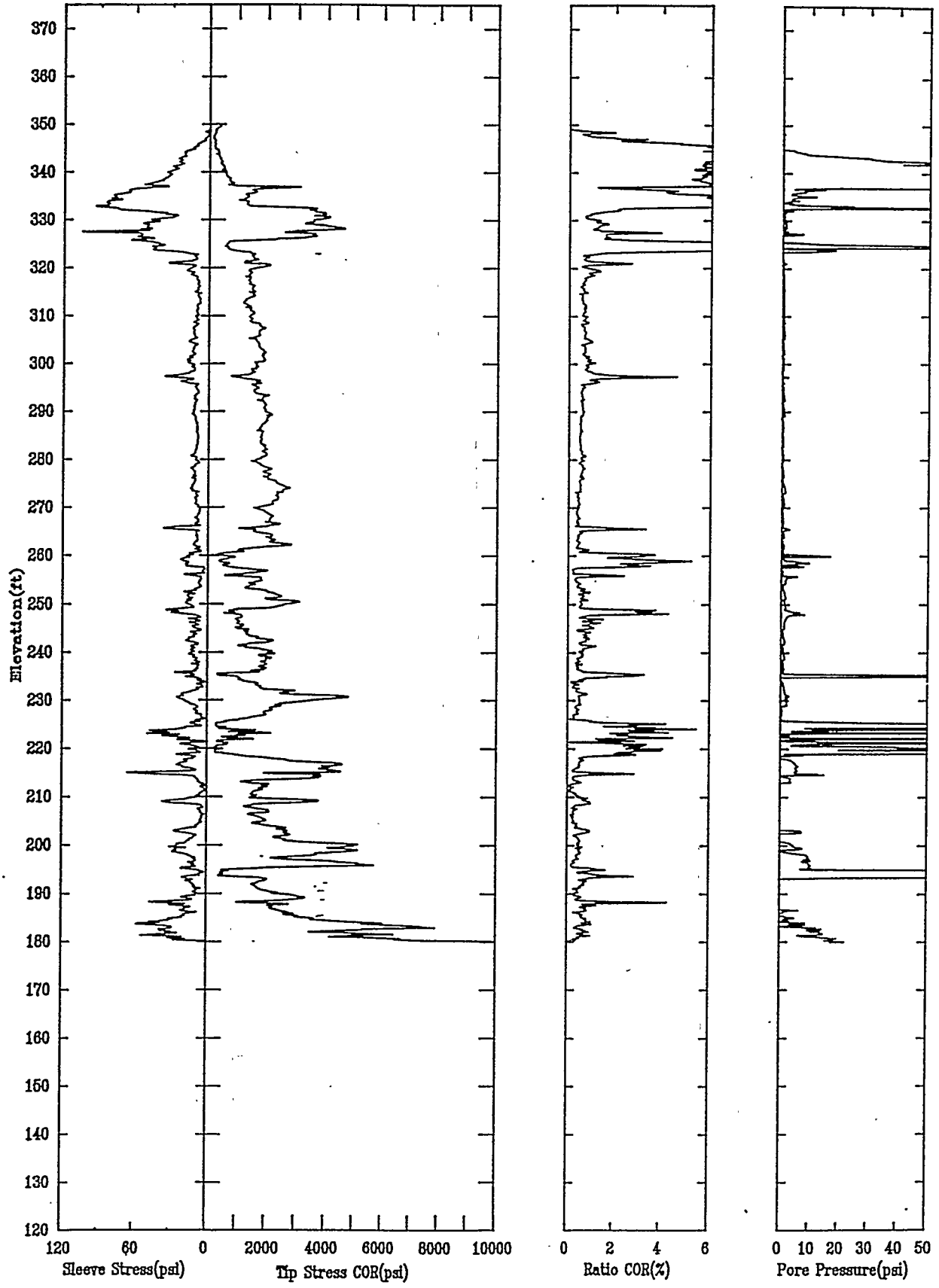

CPT-013B APPLIED RESEARCH ASSOCIATES, INC. 07/25/92

North 103083.19 East 45312.23 Elevation 350.2

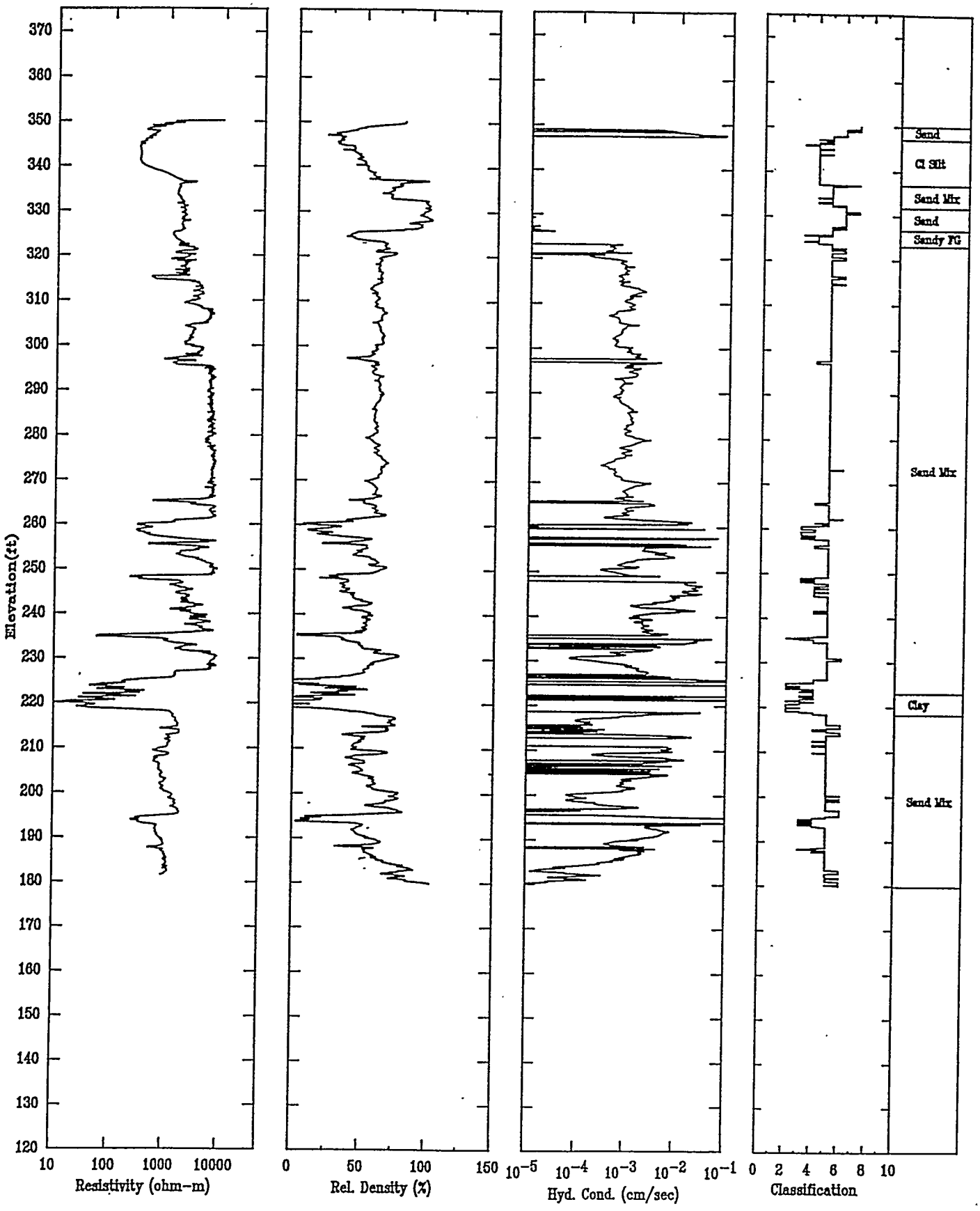

CPT-014 APPLIED RESEARCH ASSOCIATES, INC. 07/01/92

North 102736.28 East 46433.01 Elevation 349.1

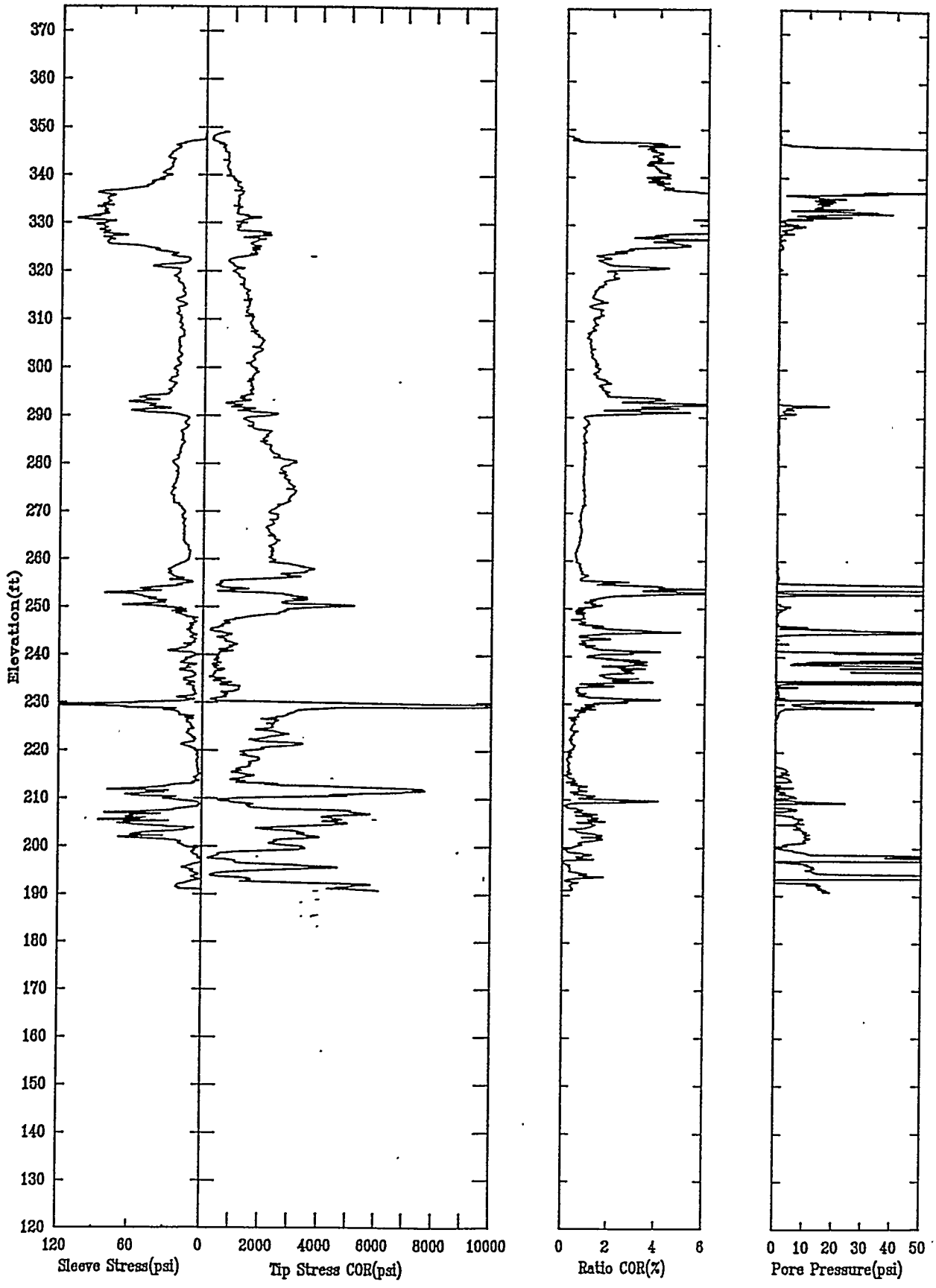

CPT-014 APPLIED RESEARCH ASSOCIATES, INC. 07/01/92

North 102736.28 East 46433.01 Elevation 349.1

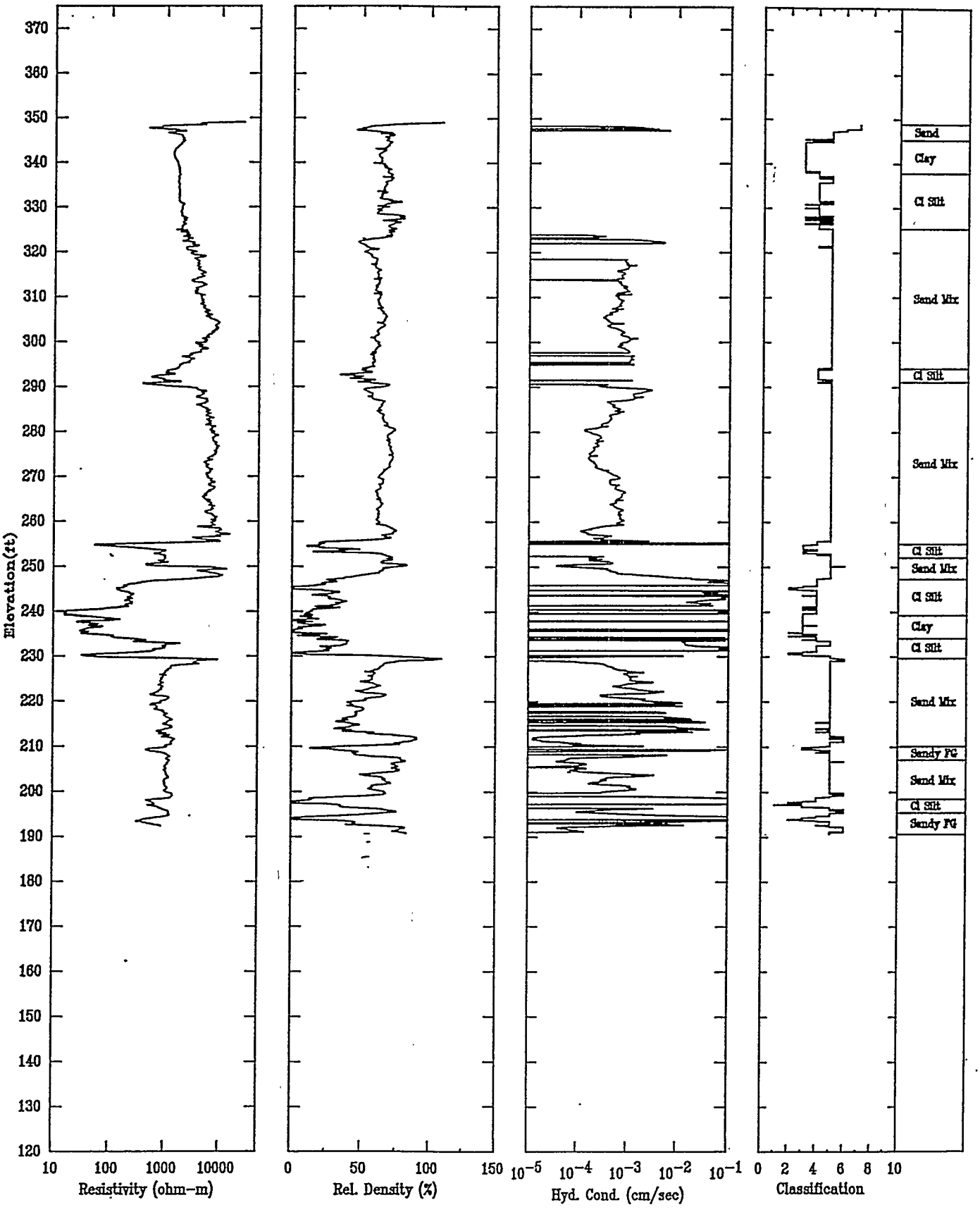

CPT-015A APPLIED RESEARCH ASSOCIATES, INC. 07/06/92

North 102963.77 East 48778.89 Elevation 367.3

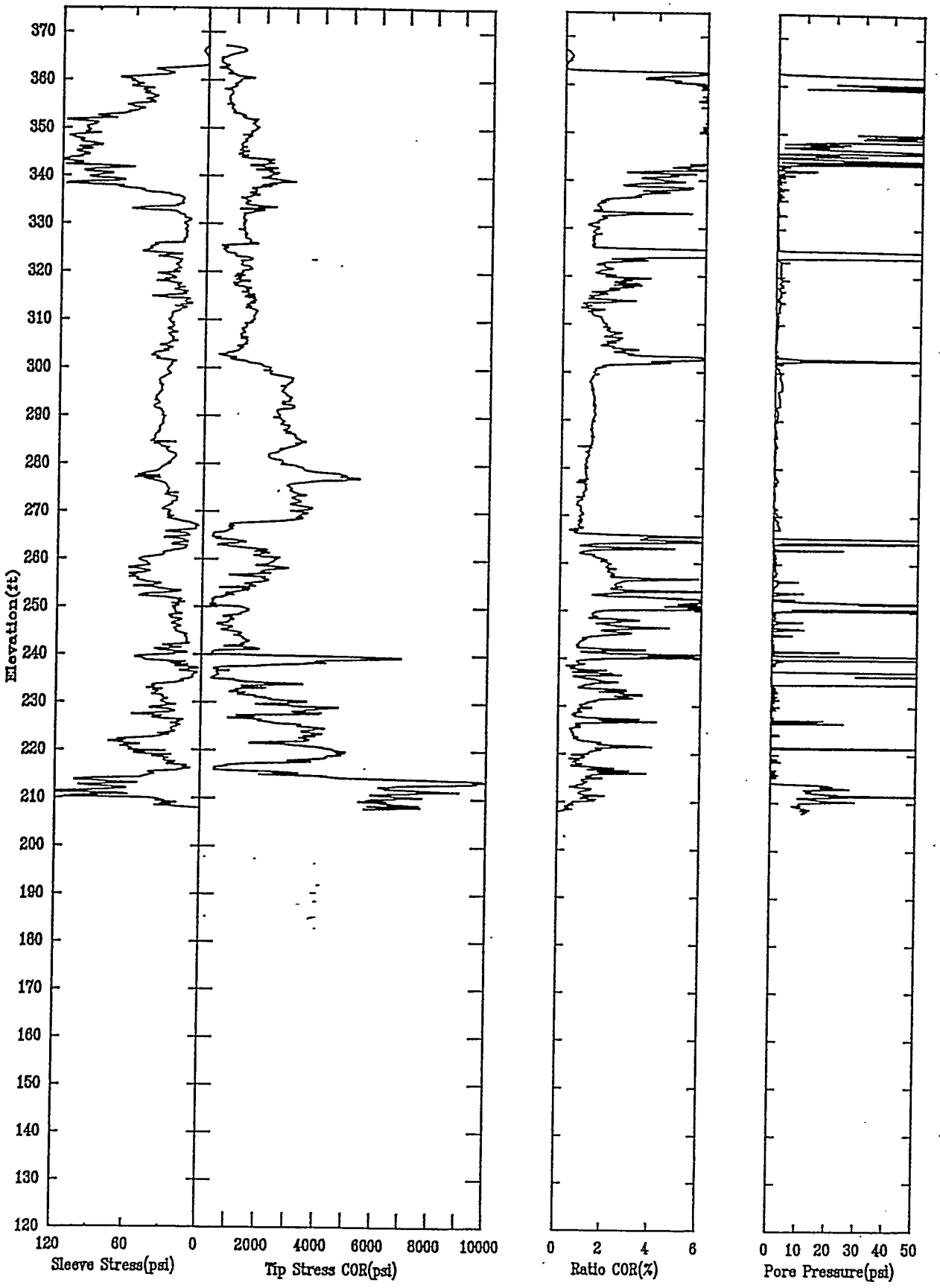

CPT-015A APPLIED RESEARCH ASSOCIATES, INC. 07/06/92

North 102963.77 East 48778.89 Elevation 367.3

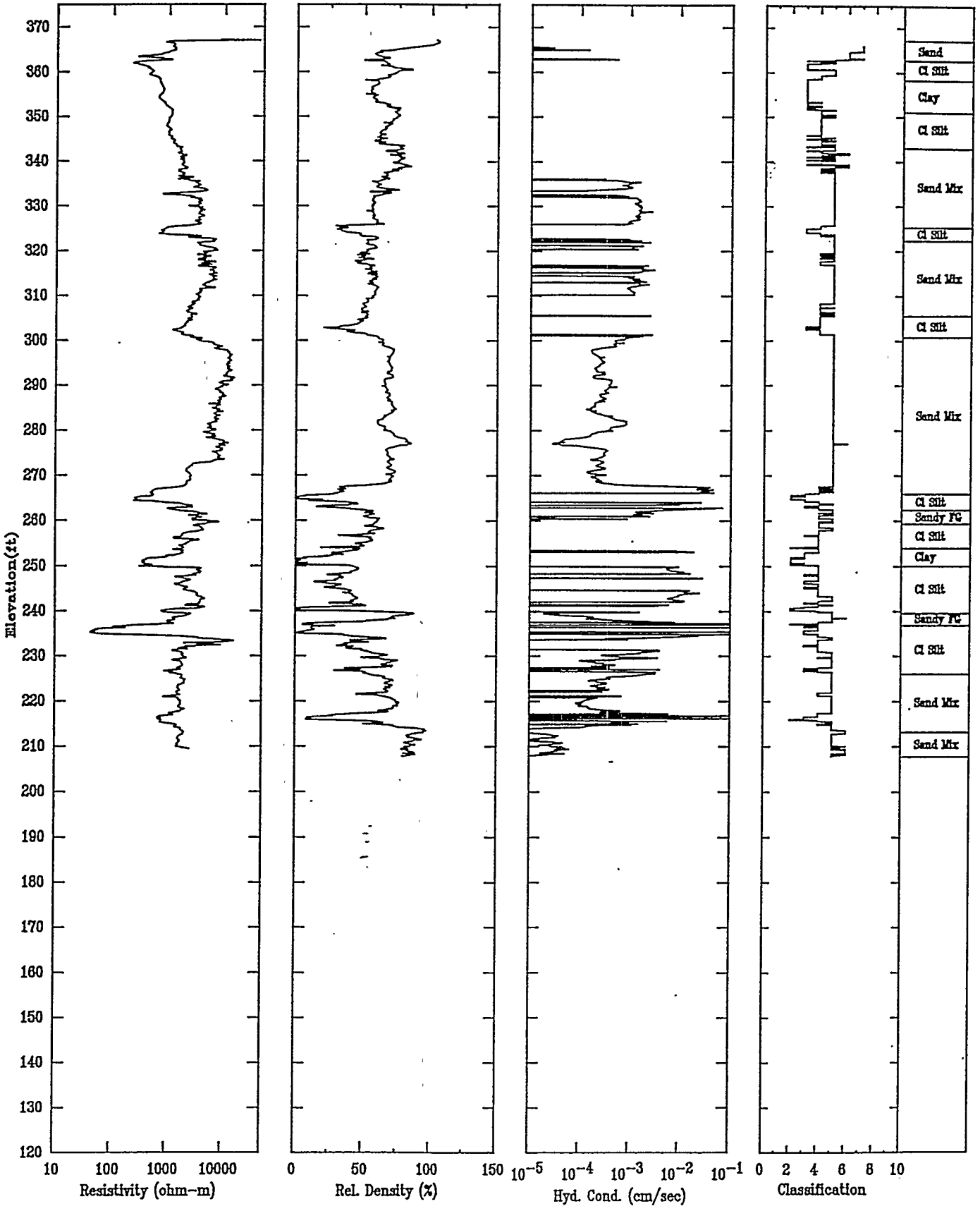

CPT-017 APPLIED RESEARCH ASSOCIATES, INC. 07/21/92

North 101955.15 East 50104.06 Elevation 344.3

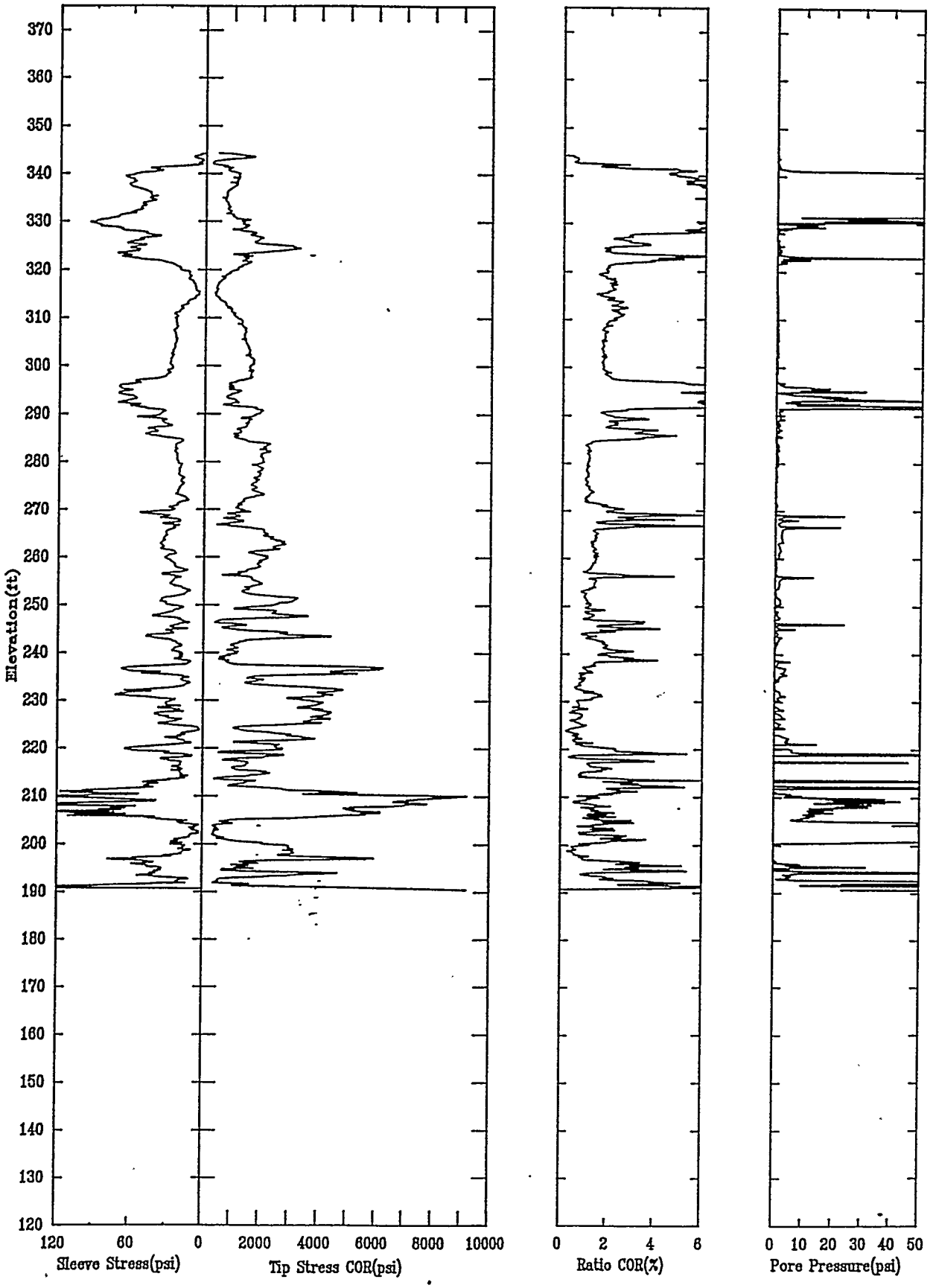

CPT-017 APPLIED RESEARCH ASSOCIATES, INC. 07/21/92

North 101955.15 East 50104.06 Elevation 344.3

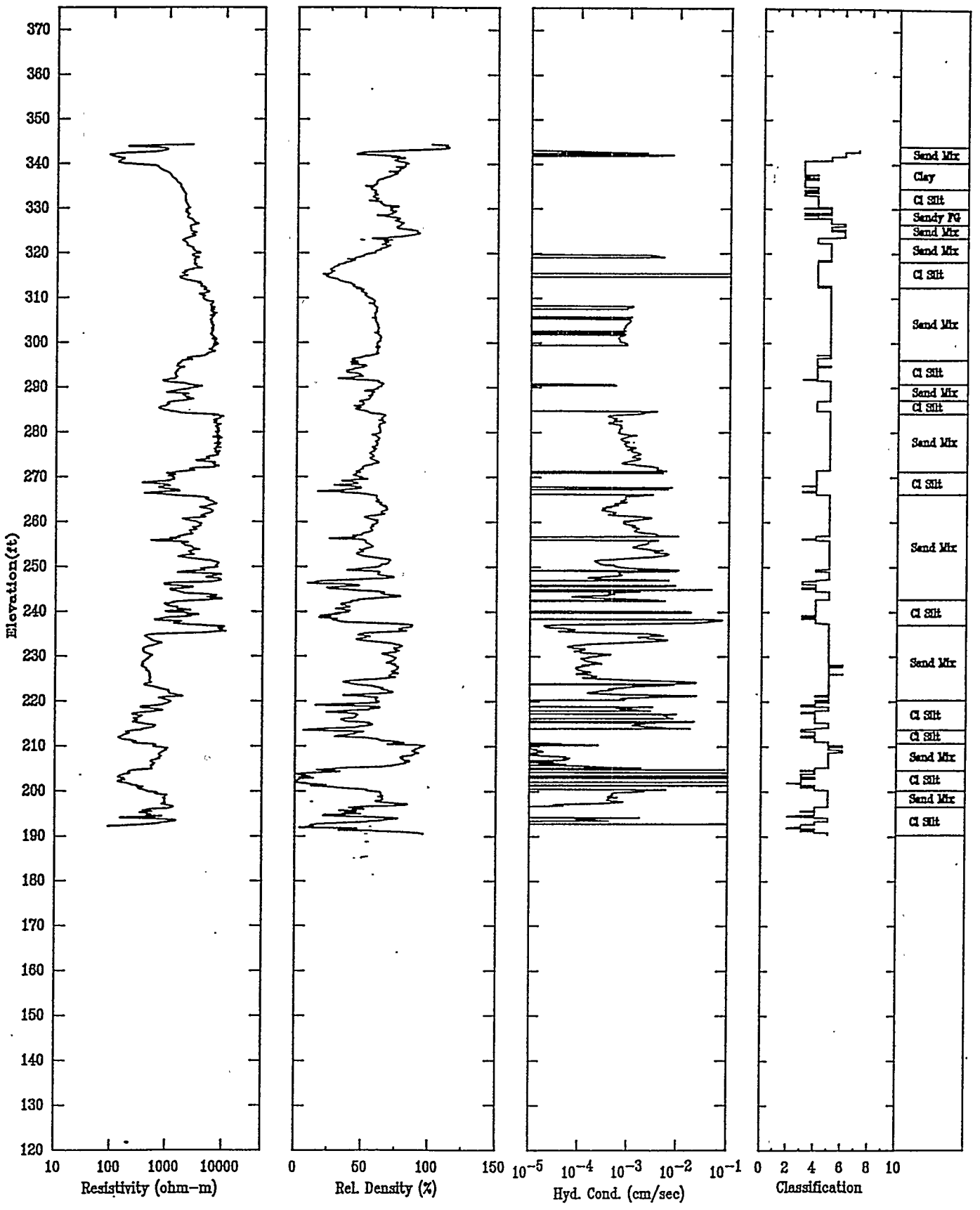

CPT-019A APPLIED RESEARCH ASSOCIATES, INC. 06/23/92

North 102265.49 East 48785.38 Elevation 356.2

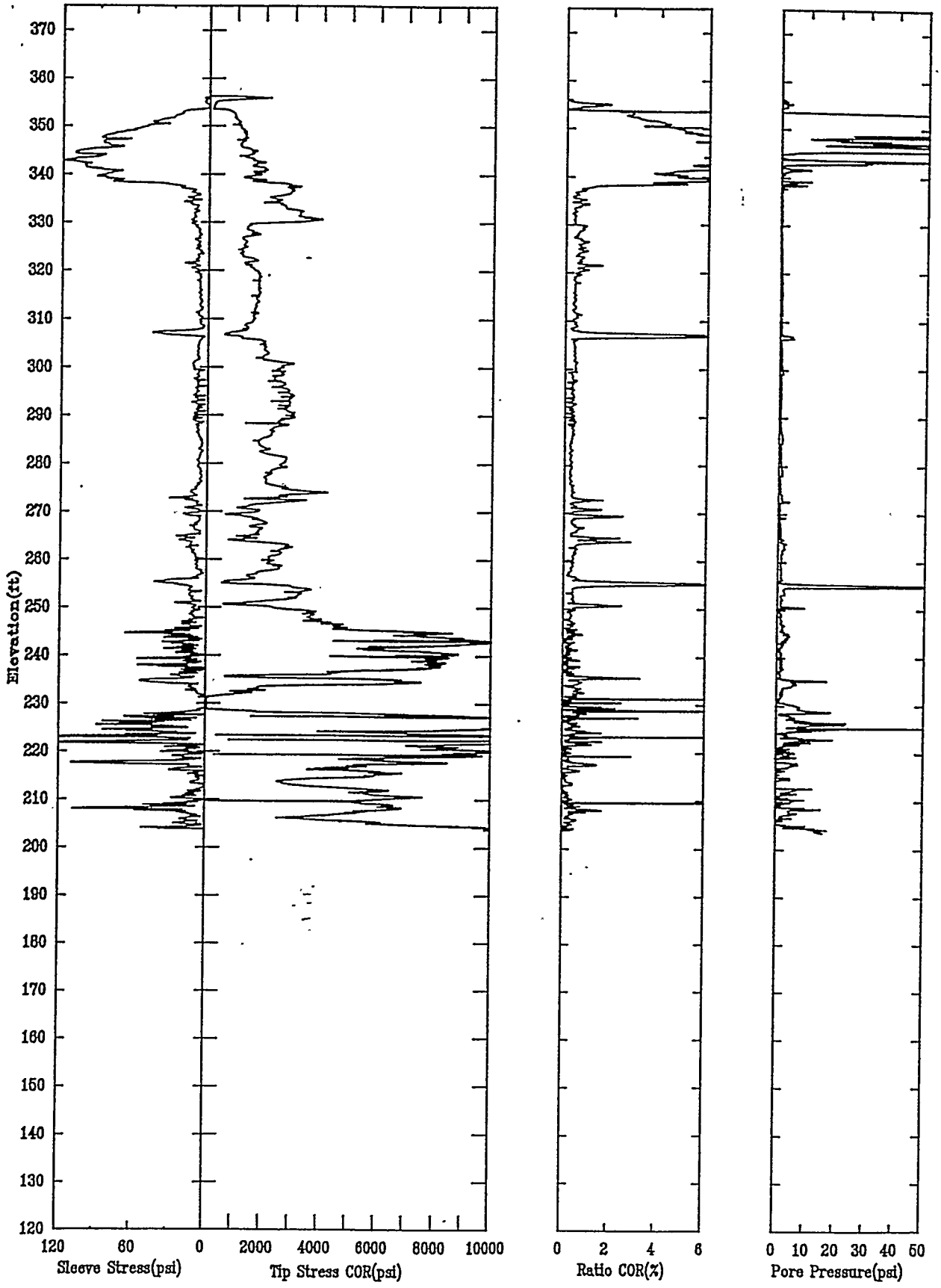

CPT-019A APPLIED RESEARCH ASSOCIATES, INC. 06/23/92

North 102265.49 East 48785.38 Elevation 356.2

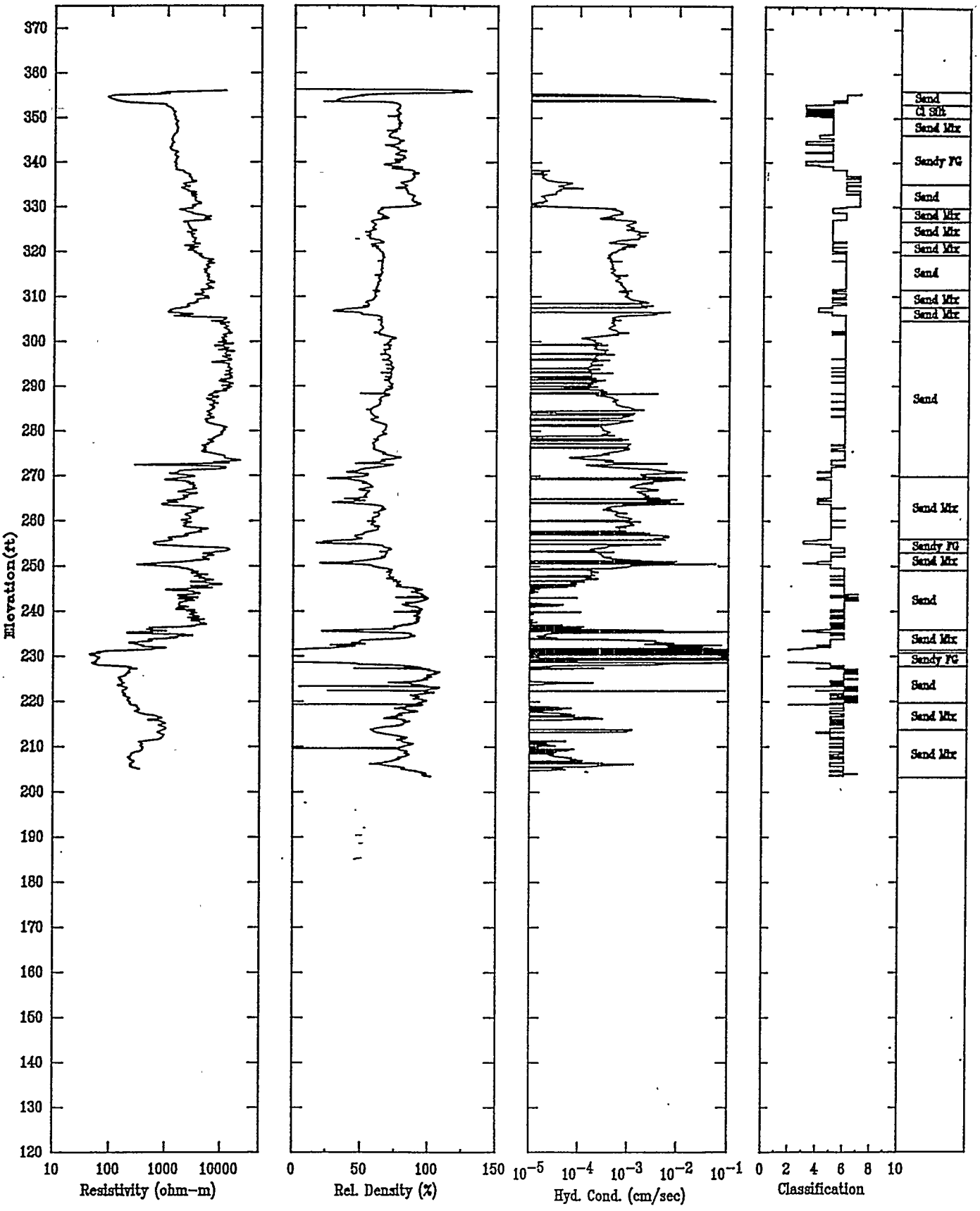

CPT-020A APPLIED RESEARCH ASSOCIATES, INC. 07/07/92

North 102488.19 East 47921.33 Elevation 354.9

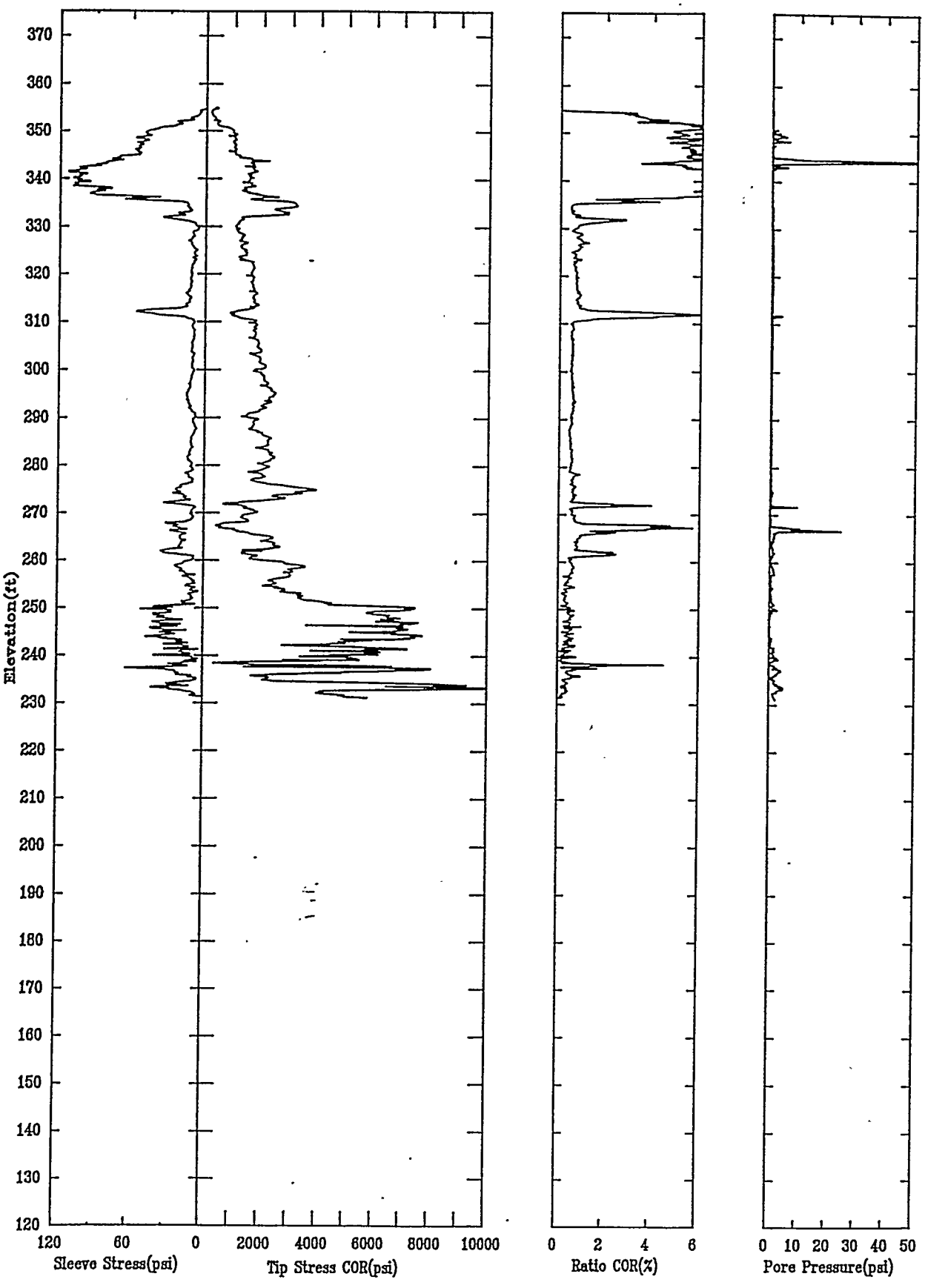

CPT-020A APPLIED RESEARCH ASSOCIATES, INC. 07/07/92

North 102488.19 East 47921.33 Elevation 354.9

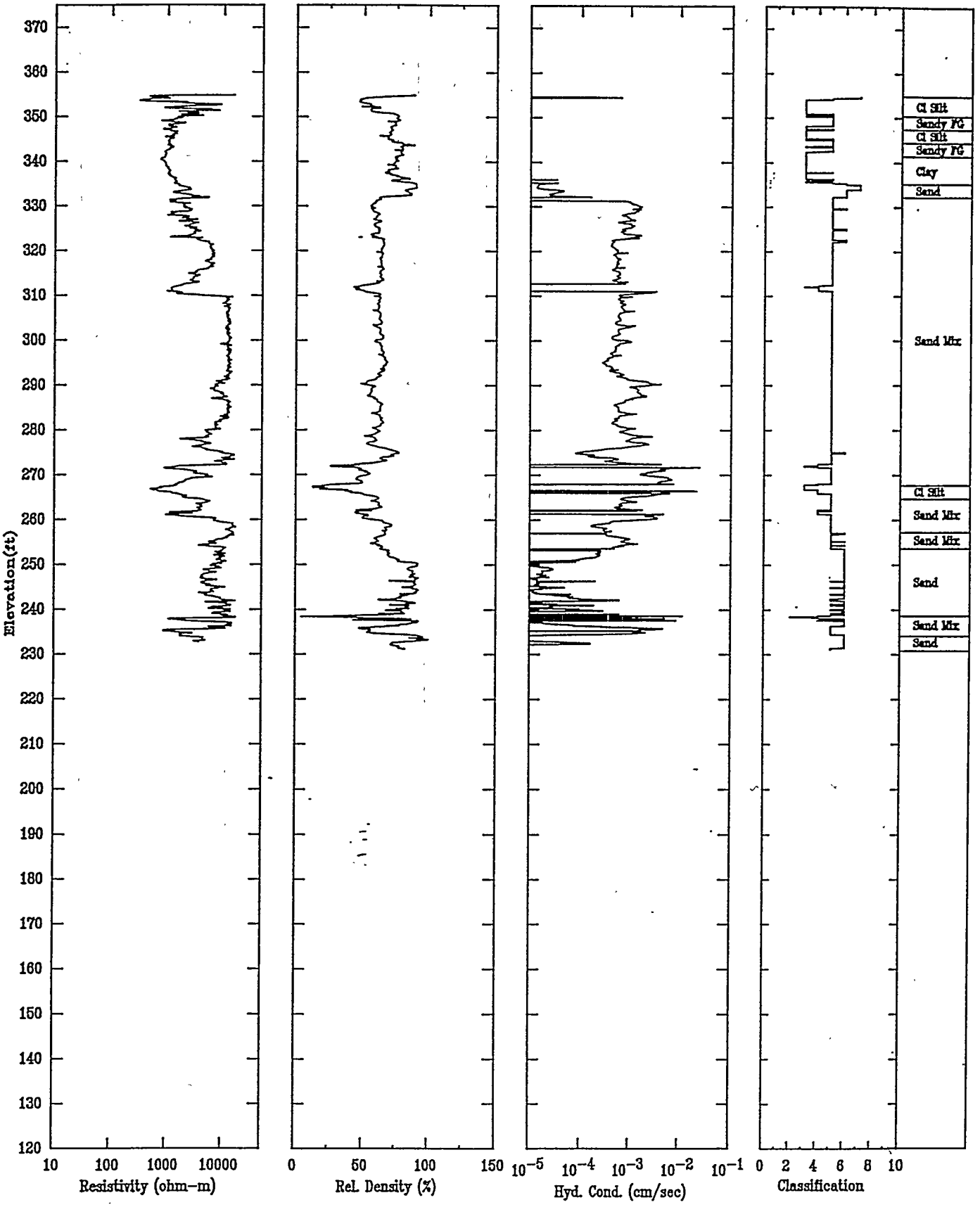

CPT-020B APPLIED RESEARCH ASSOCIATES, INC. 07/10/92

North 102500.20 East 47906.81 Elevation 356.2

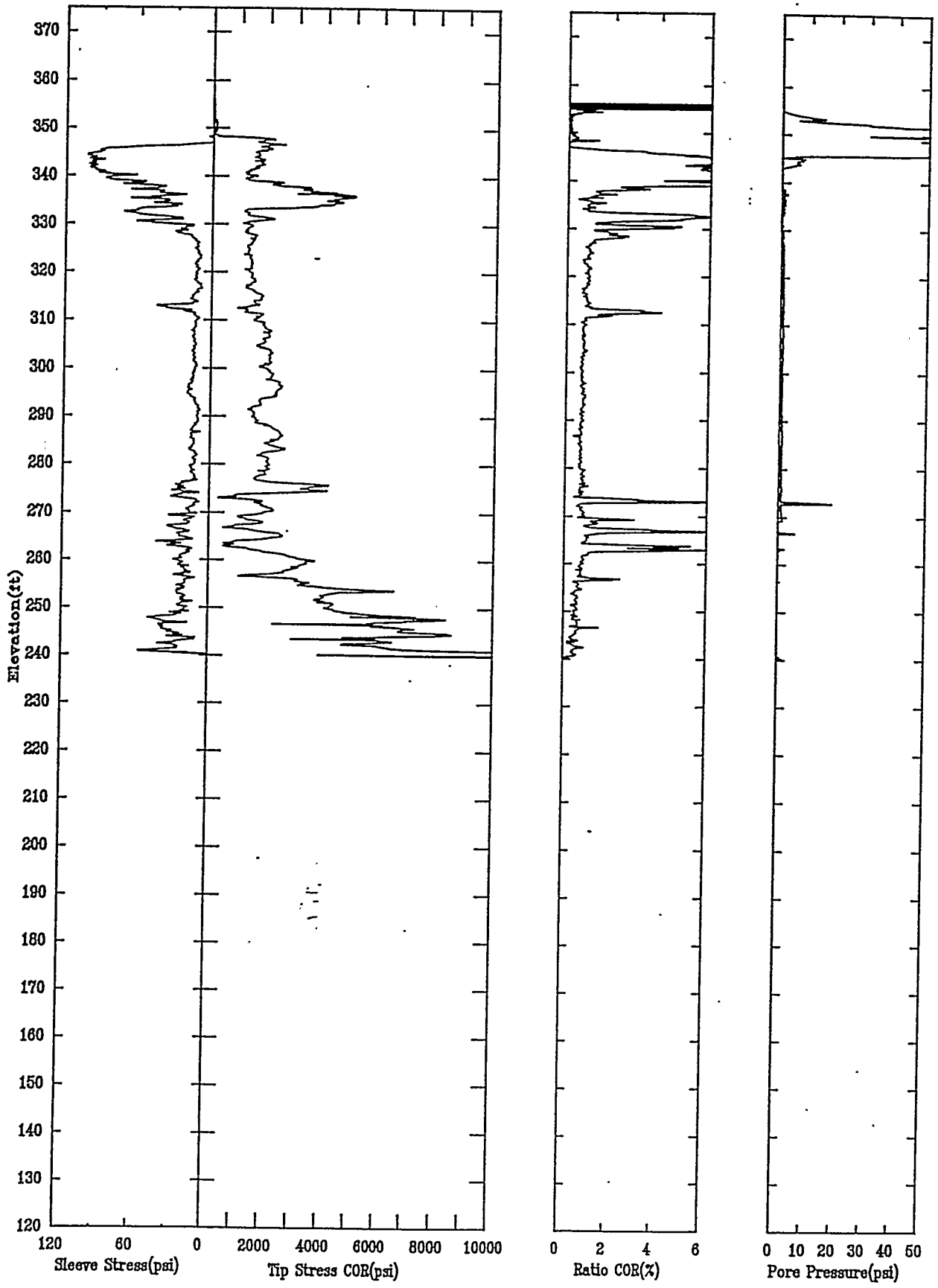

CPT-020B APPLIED RESEARCH ASSOCIATES, INC. 07/10/92

North 102500.20 East 47906.81 Elevation 356.2

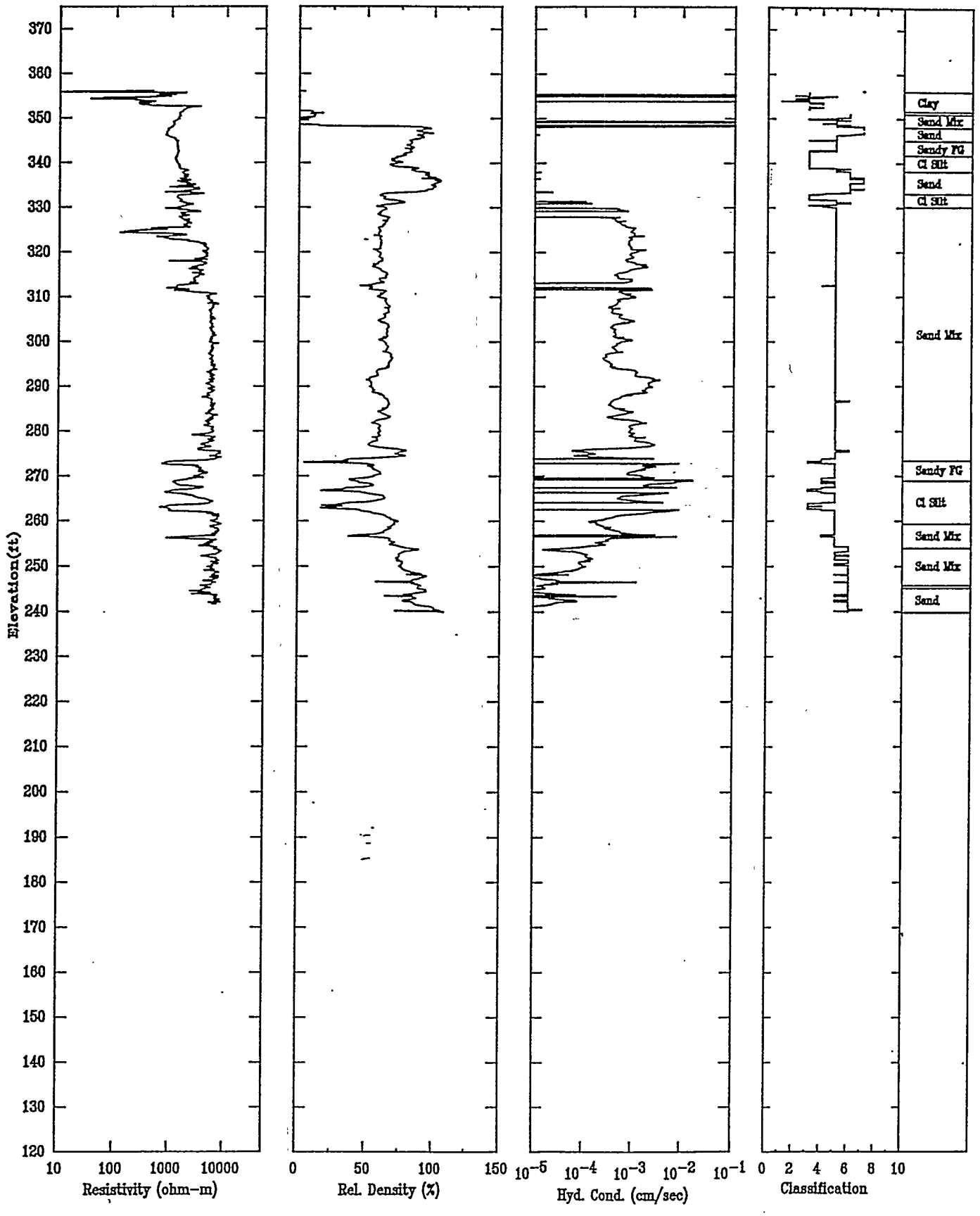

CPT-021 APPLIED RESEARCH ASSOCIATES, INC. 06/30/92

North 101383.04 East 48590.50 Elevation 340.0

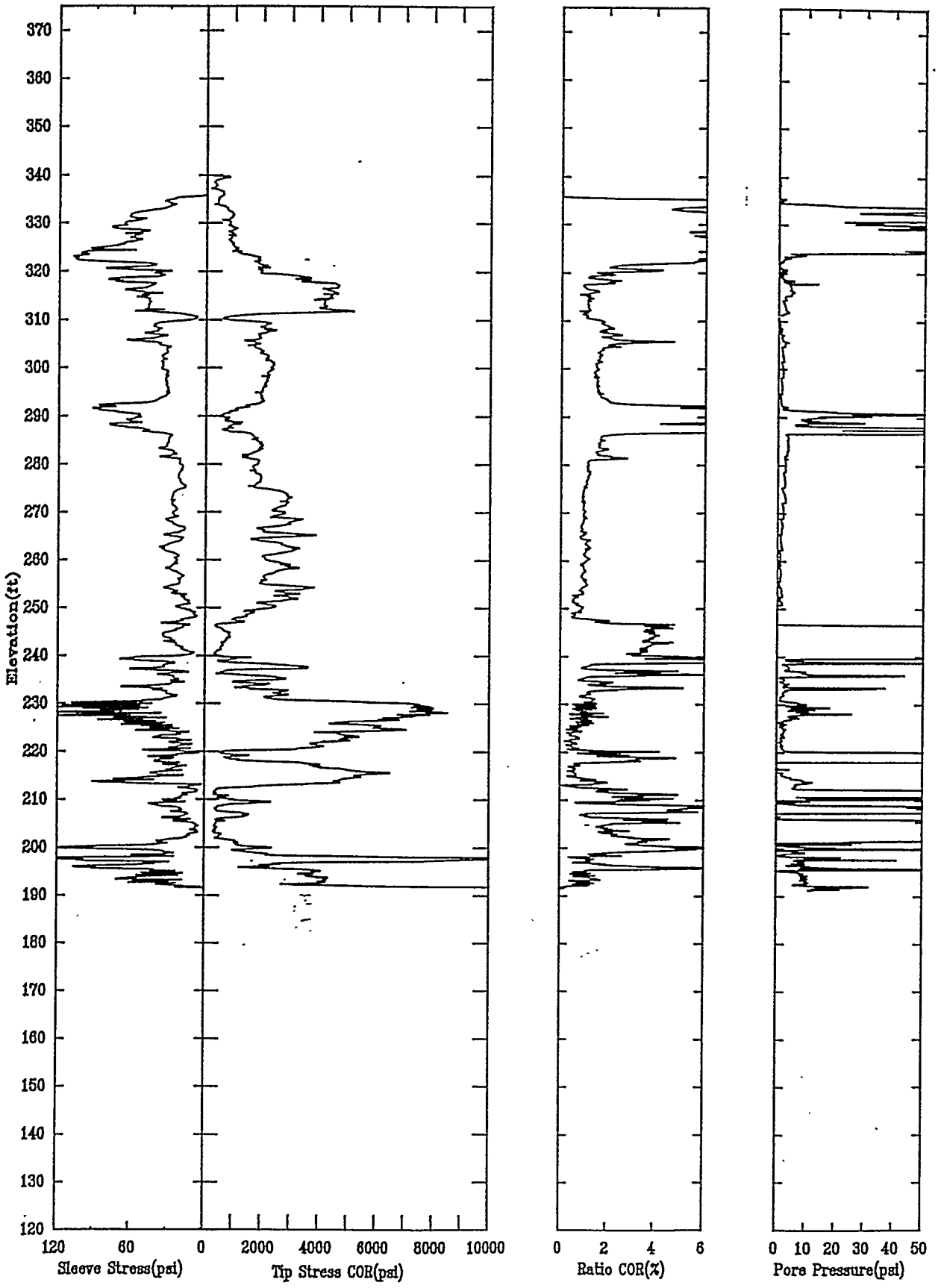

CPT-021 APPLIED RESEARCH ASSOCIATES, INC. 06/30/92

North 101383.04 East 48590.50 Elevation 340.0

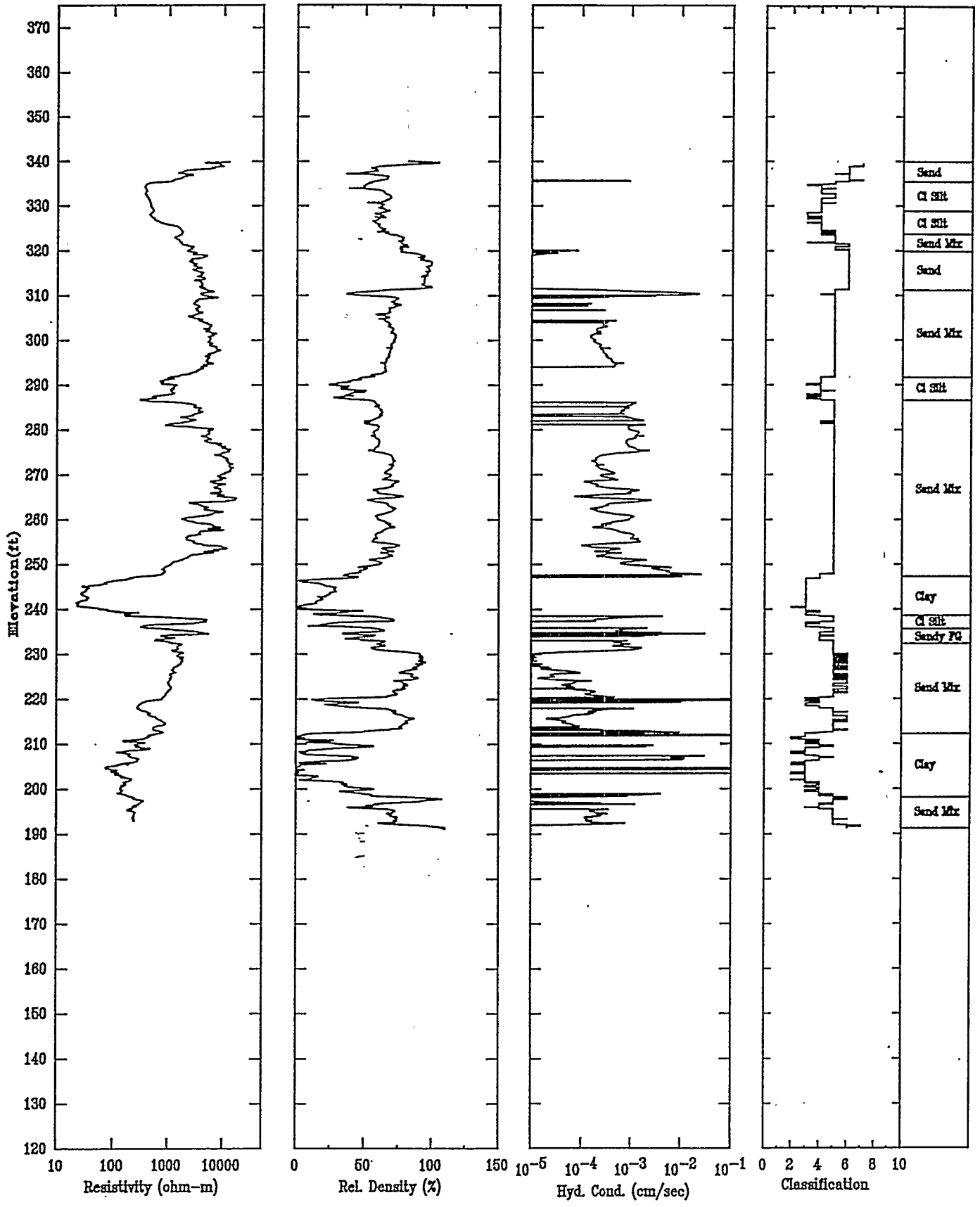

CPT-022 APPLIED RESEARCH ASSOCIATES, INC. 07/24/92

North 102495.85 East 48316.81 Elevation 354.9

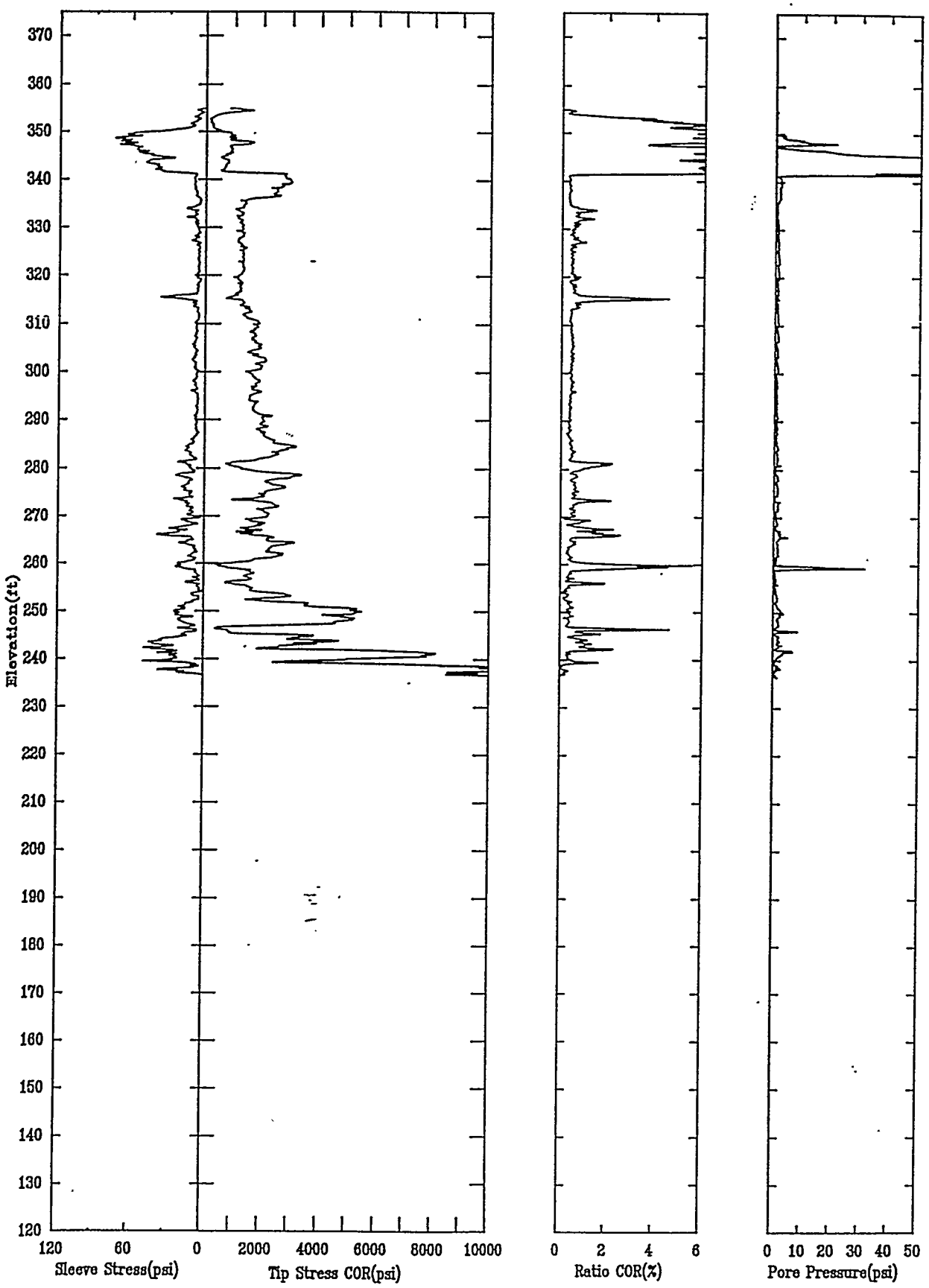

CPT-022 APPLIED RESEARCH ASSOCIATES, INC. 07/24/92

North 102495.85 East 48316.81 Elevation 354.9

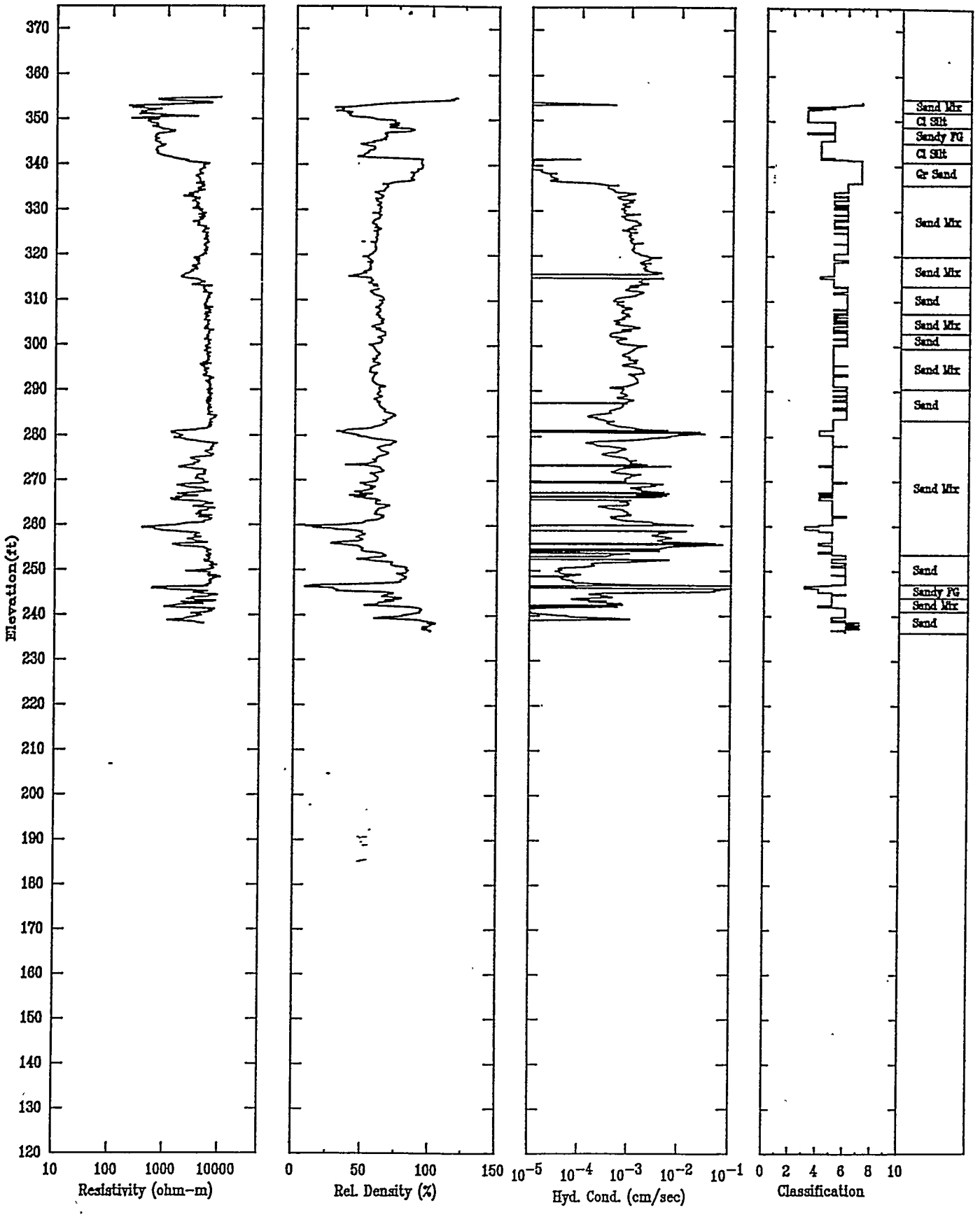

CPT-023A APPLIED RESEARCH ASSOCIATES, INC. 07/27/92

North 103862.03 East 46704.50 Elevation 349.3

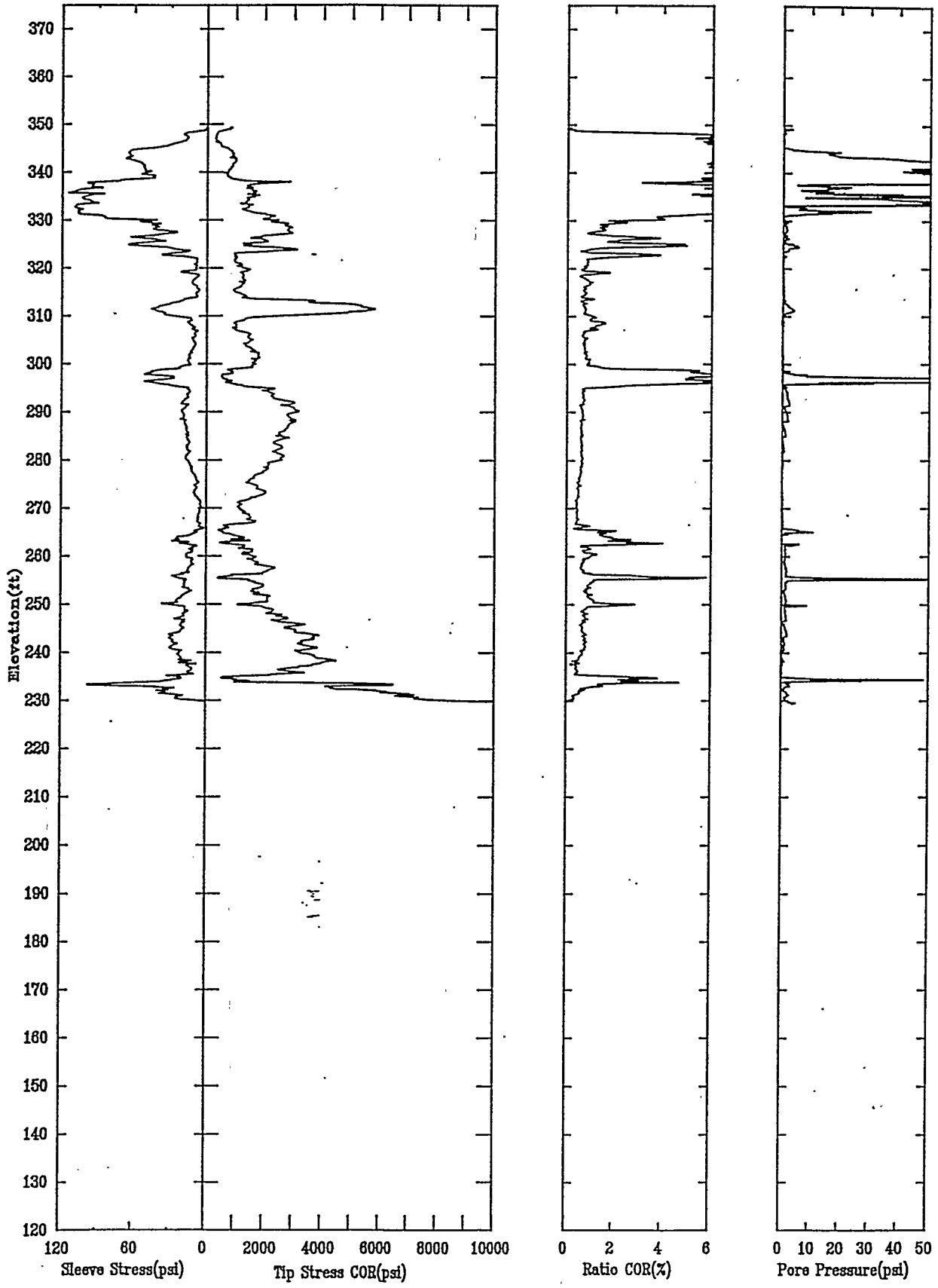

CPT-023A APPLIED RESEARCH ASSOCIATES, INC. 07/27/92

North 103862.03 East 46704.50 Elevation 349.3

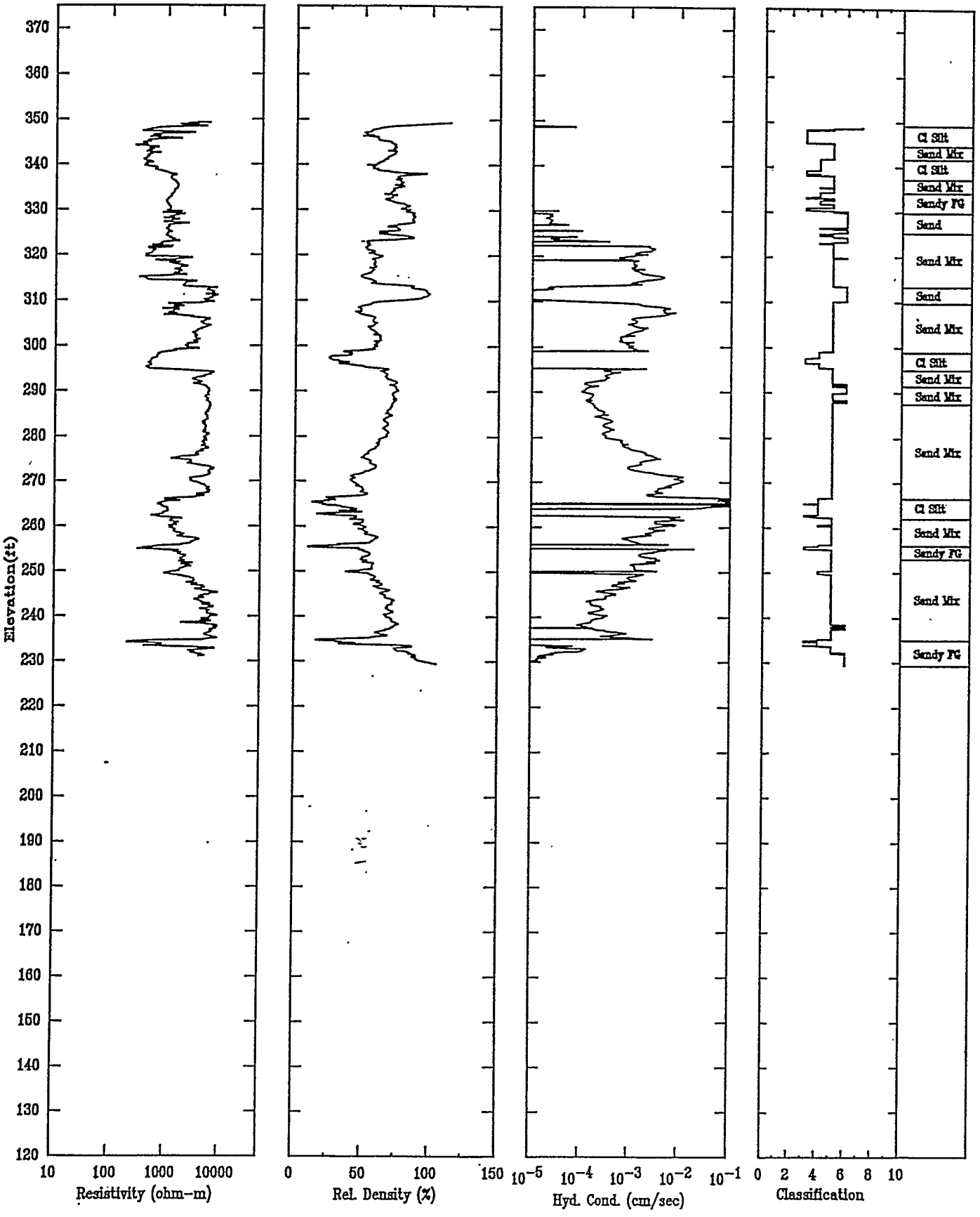

CPT-023B APPLIED RESEARCH ASSOCIATES, INC. 07/28/92

North 103812.47 East 46596.17 Elevation 350.0

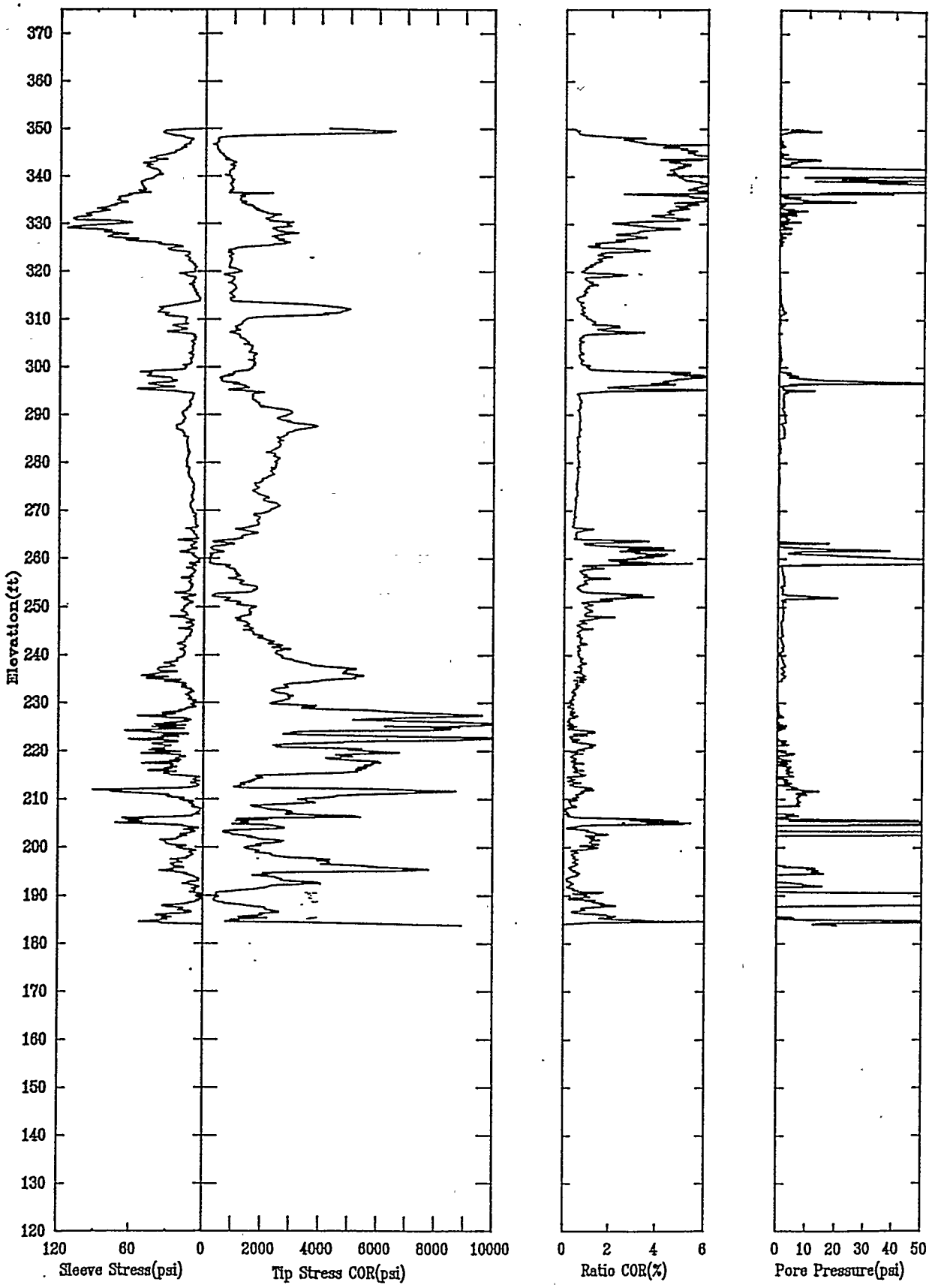

CPT-023B APPLIED RESEARCH ASSOCIATES, INC. 07/28/92

North 103812.47 East 46596.17 Elevation 350.0

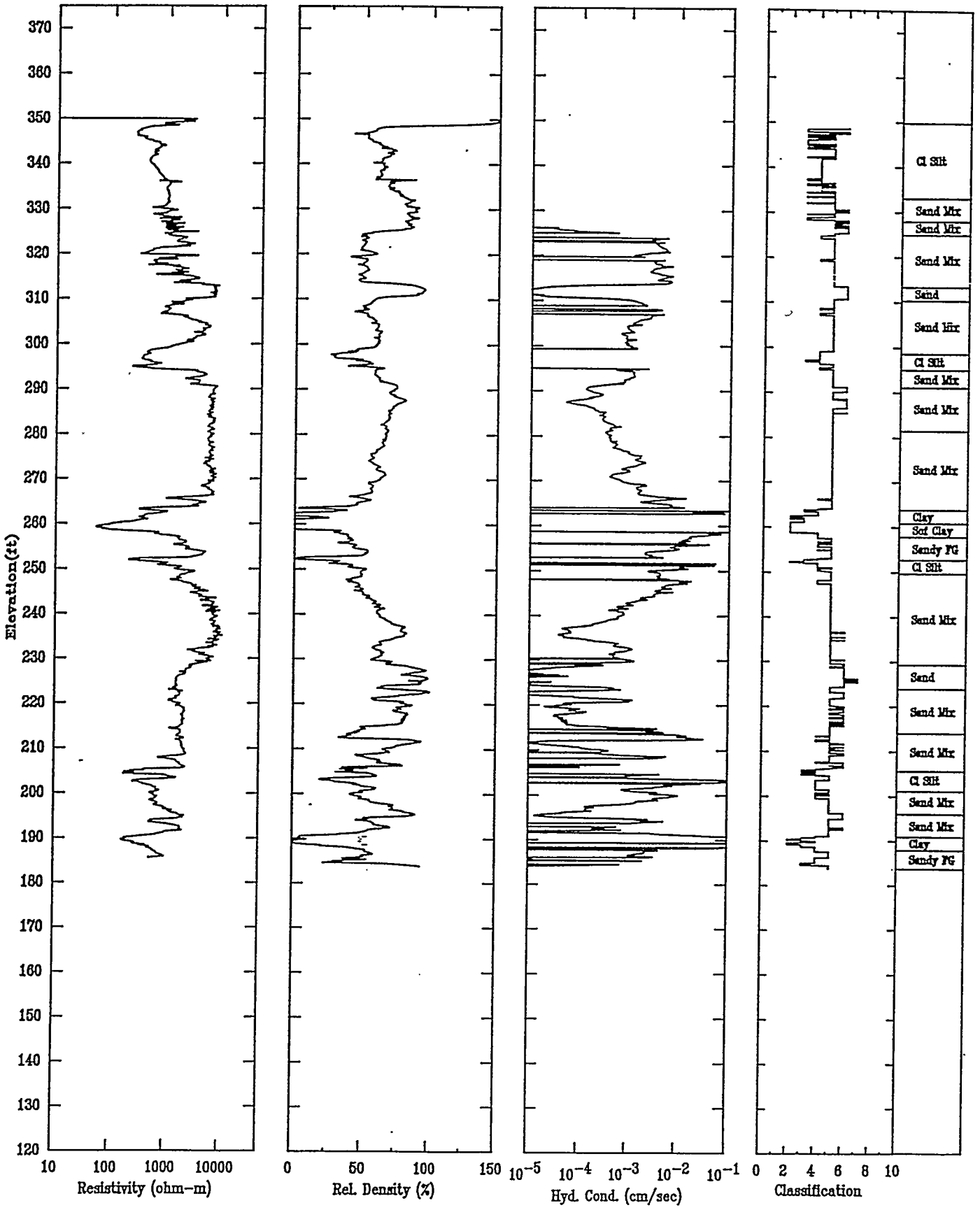

# APPENDIX B

## CPT PREDICTED RESISTIVITY BELOW THE WATER TABLE AND DEGREE OF SATURATION

CPT-001 APPLIED RESEARCH ASSOCIATES, INC. 07/14/92

North 104527.29 East 48761.45 Elevation 353.7

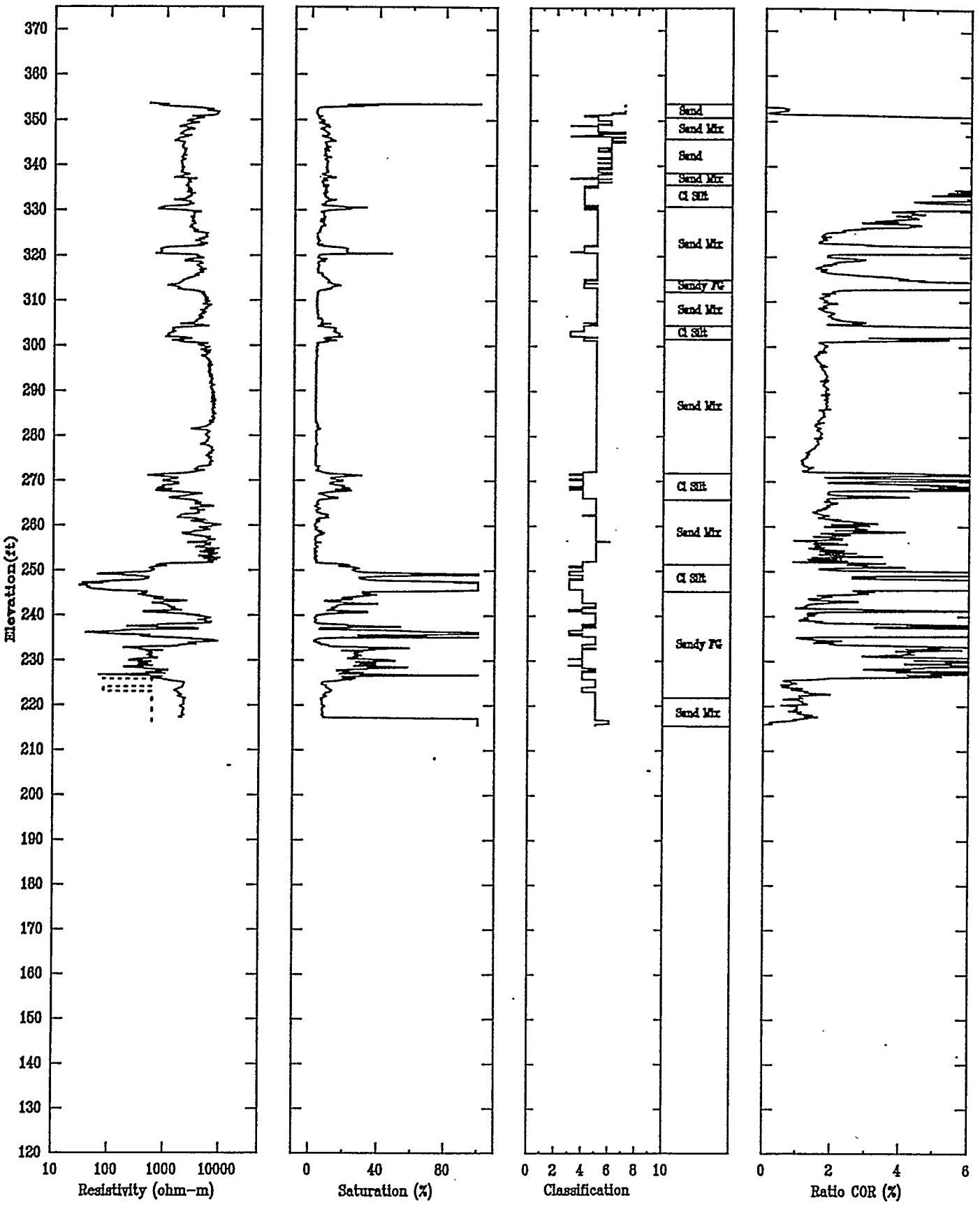

CPT-002 APPLIED RESEARCH ASSOCIATES, INC. 07/16/92

North 104243.57 East 47884.75 Elevation 349.7

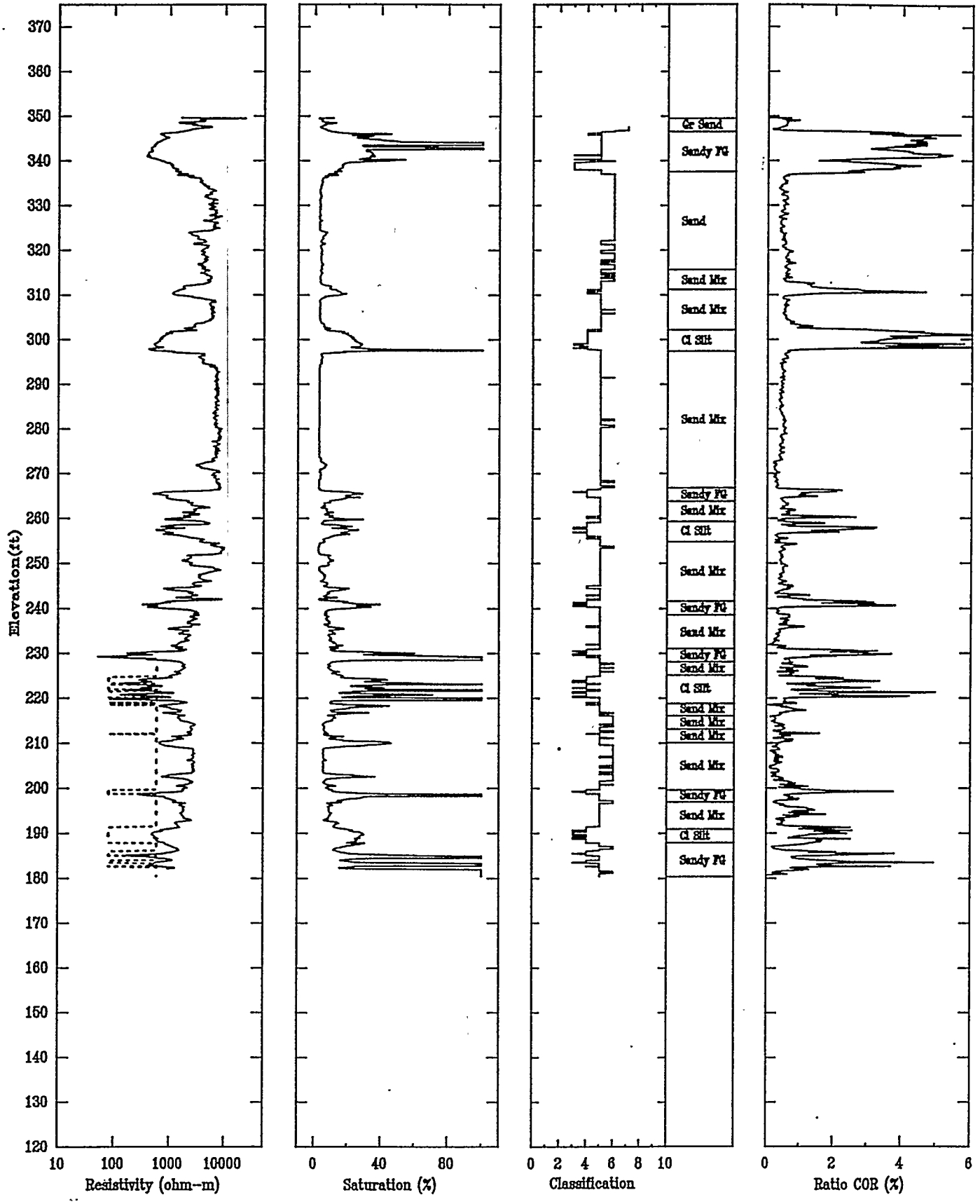

CPT-003 APPLIED RESEARCH ASSOCIATES, INC. 07/20/92

North 103251.70 East 45819.40 Elevation 351.0

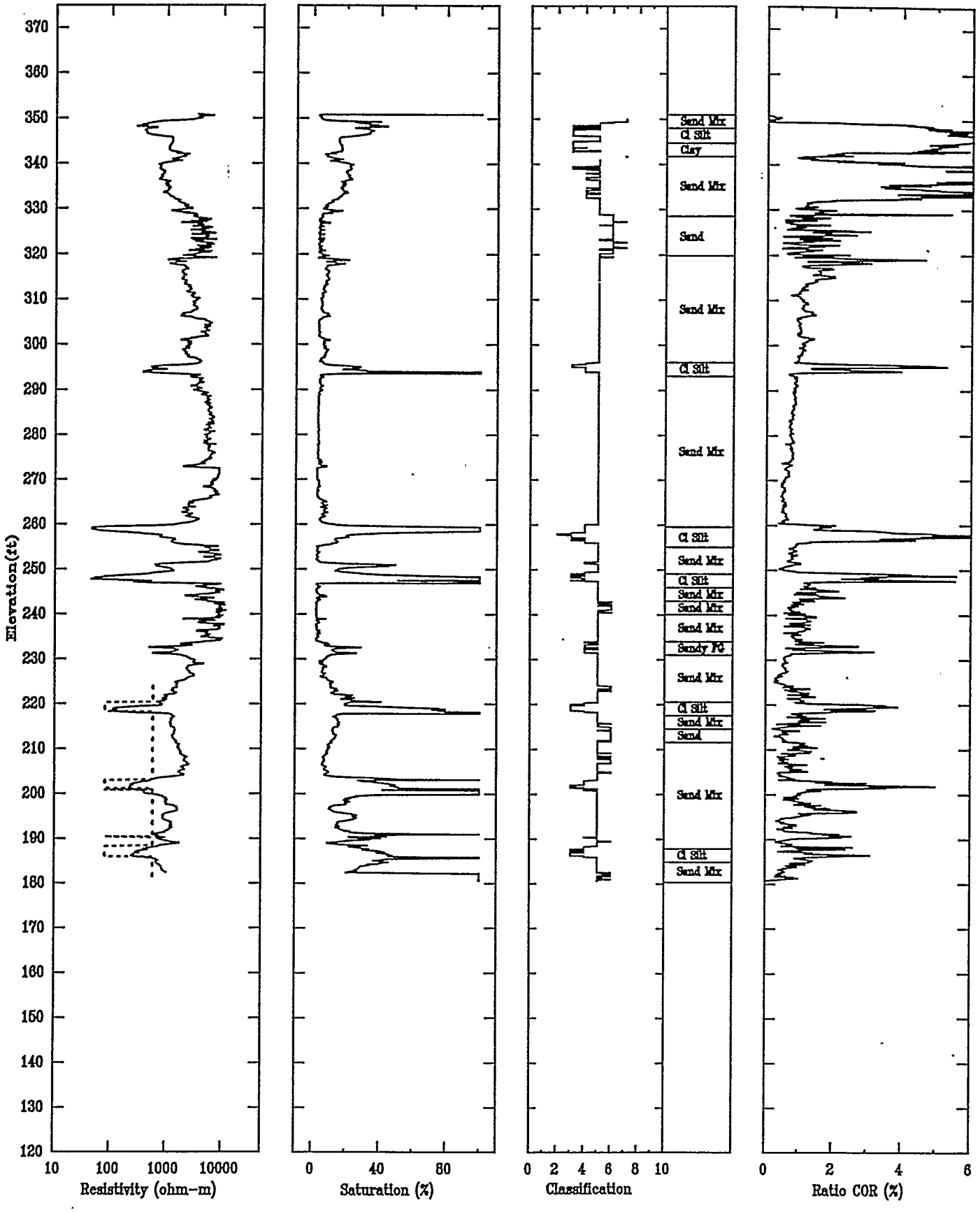

CPT-004 APPLIED RESEARCH ASSOCIATES, INC. 07/18/92

North 104120.50 East 45512.11 Elevation 357.7

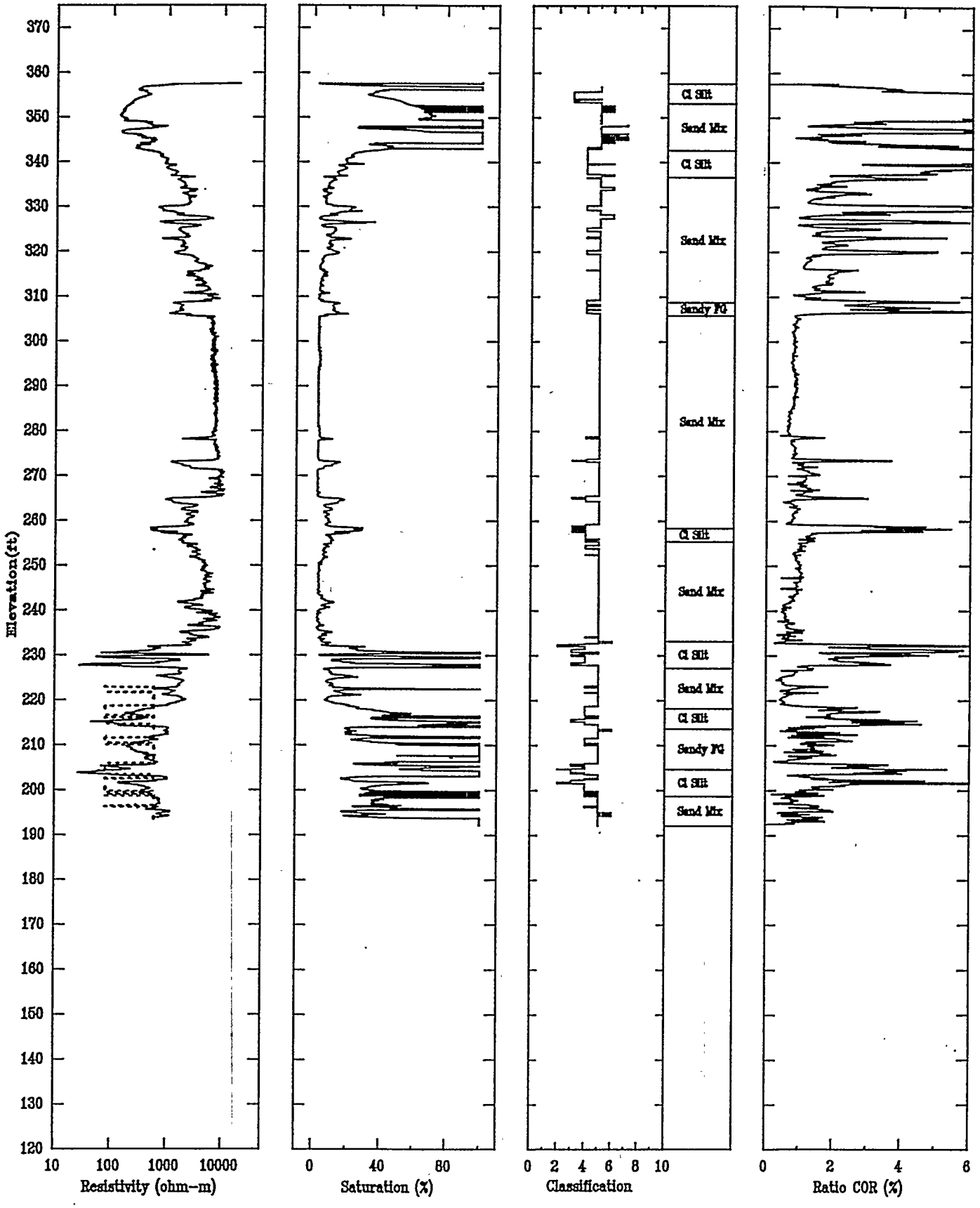

CPT-005 APPLIED RESEARCH ASSOCIATES, INC. 07/11/92

North 103874.72 East 47863.29 Elevation 360.2

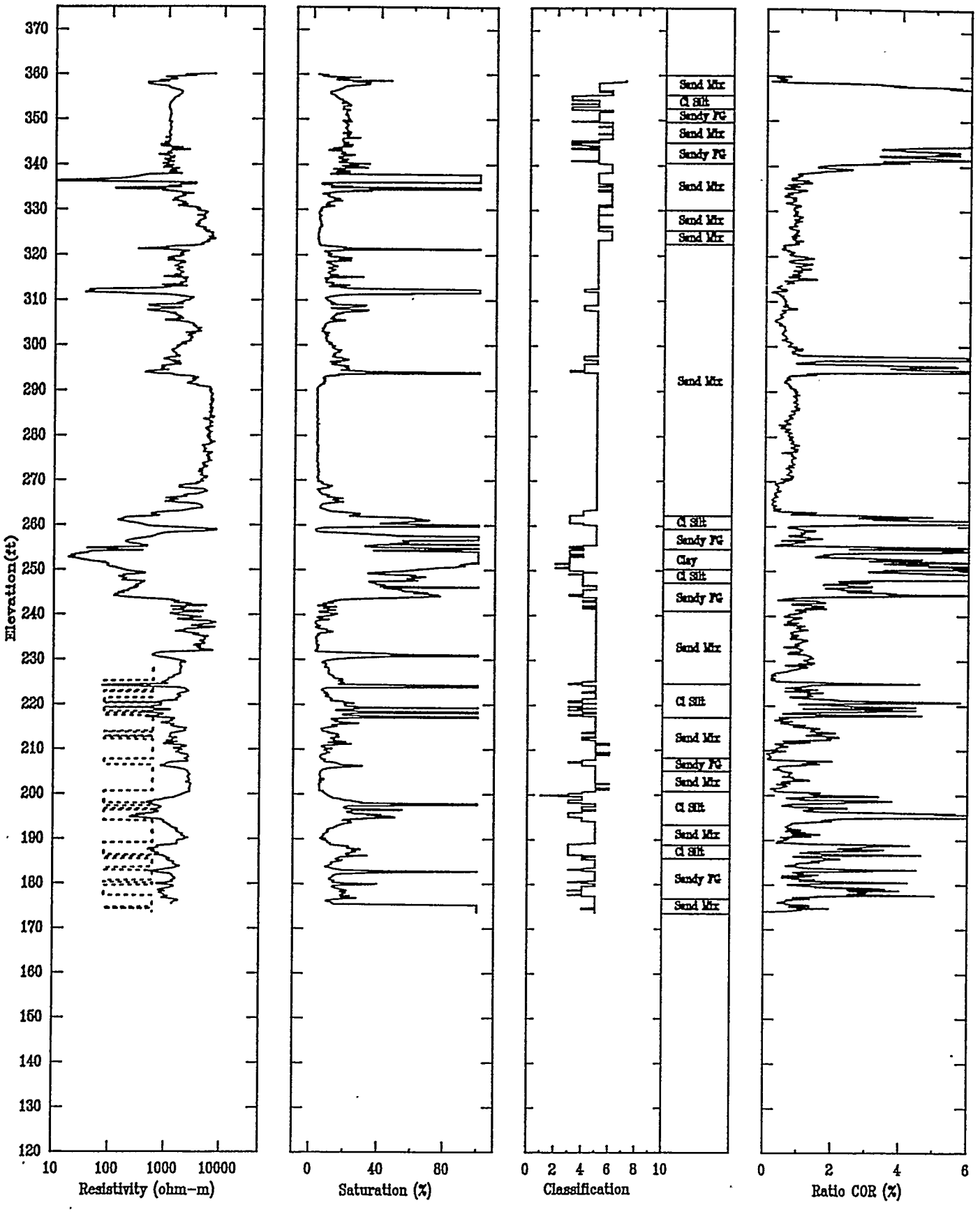

CPT–006 APPLIED RESEARCH ASSOCIATES, INC. 07/13/92

North 103064.78 East 48469.71 Elevation 370.5

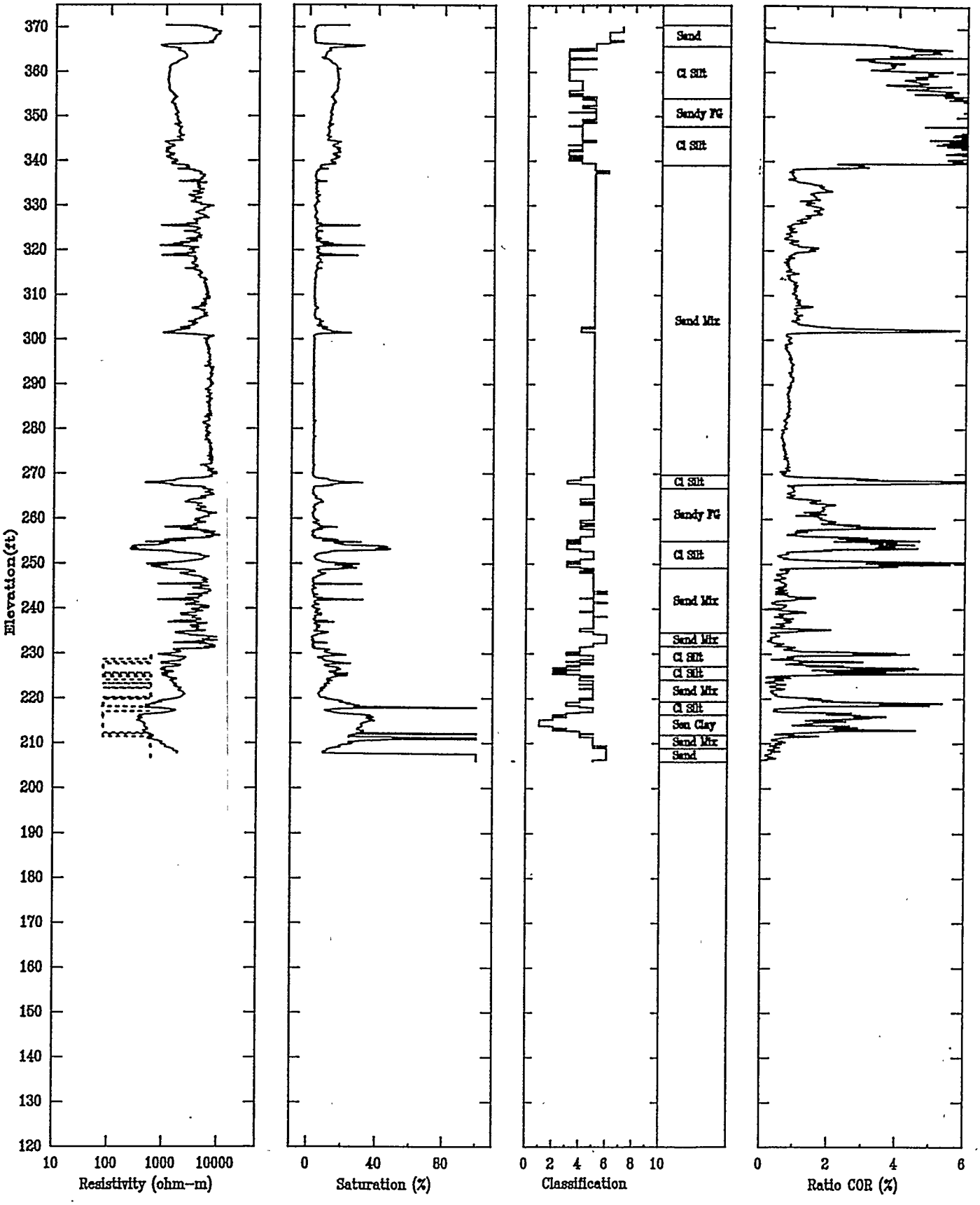

CPT-007 APPLIED RESEARCH ASSOCIATES, INC. 07/24/92

North 102444.36 East 47586.21 Elevation 349.8

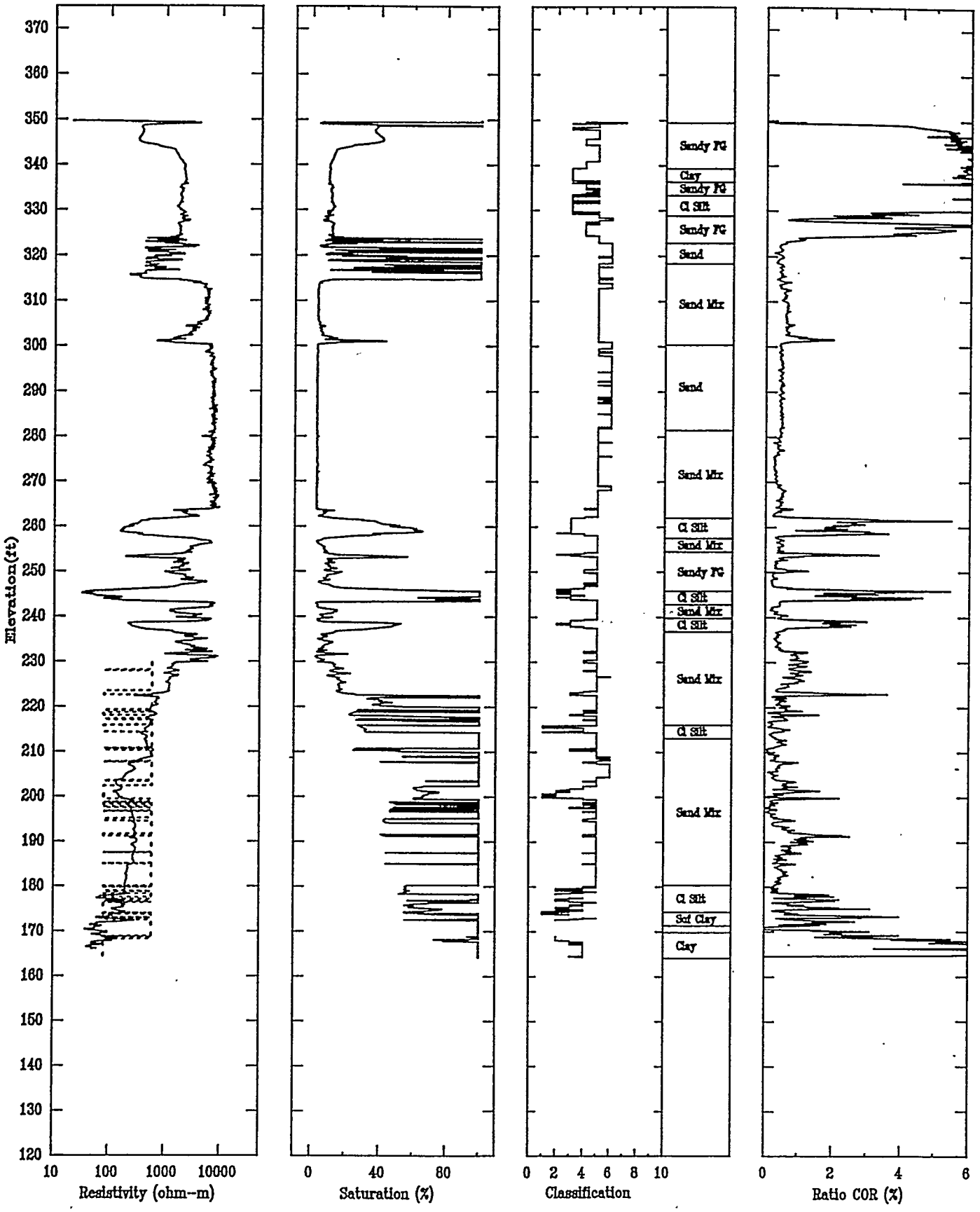

CPT-009 APPLIED RESEARCH ASSOCIATES, INC. 06/24/92

North 100993.00 East 47696.68 Elevation 344.9

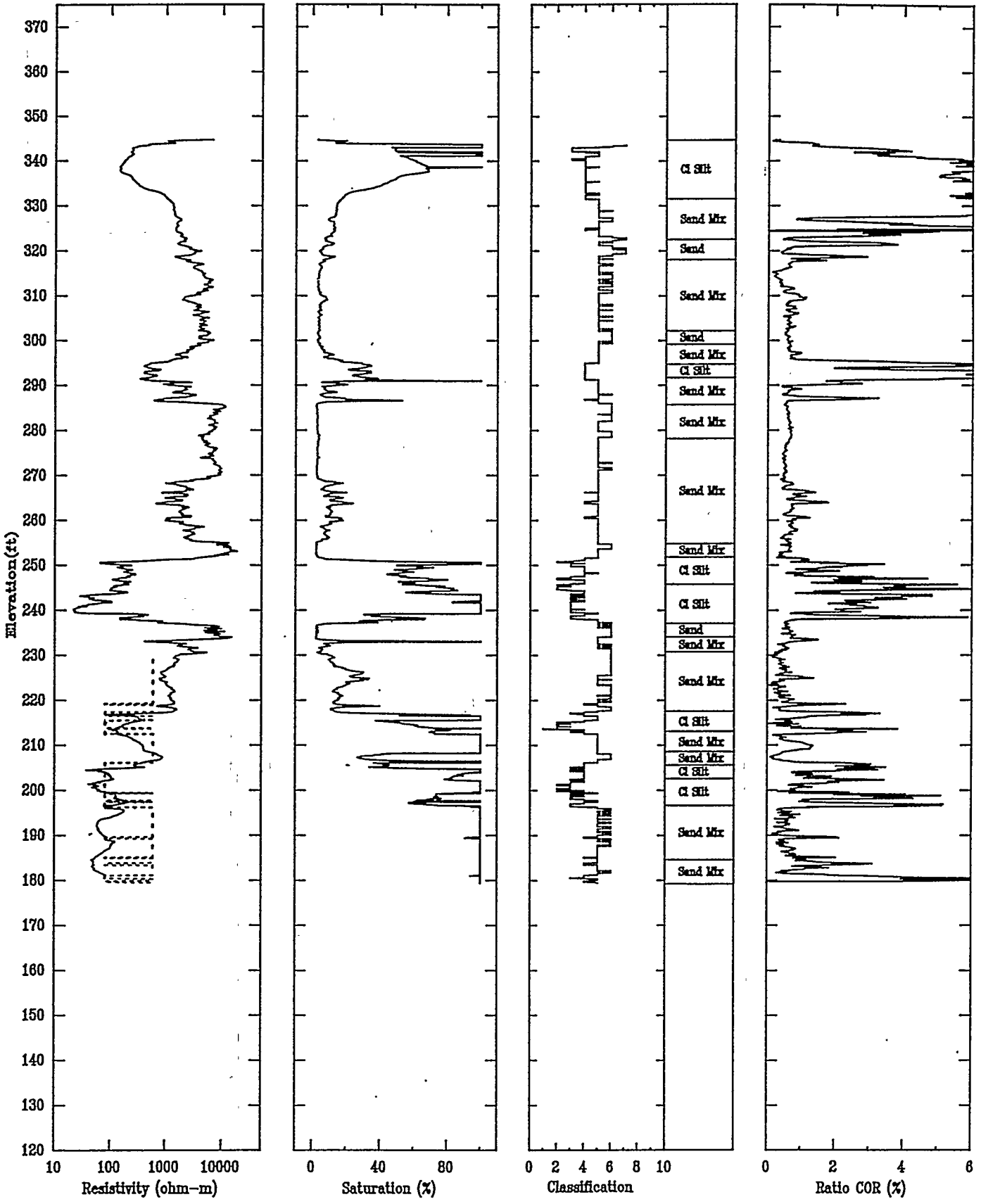

CPT-010 APPLIED RESEARCH ASSOCIATES, INC. 07/22/92

North 100505.84 East 46714.64 Elevation 343.1

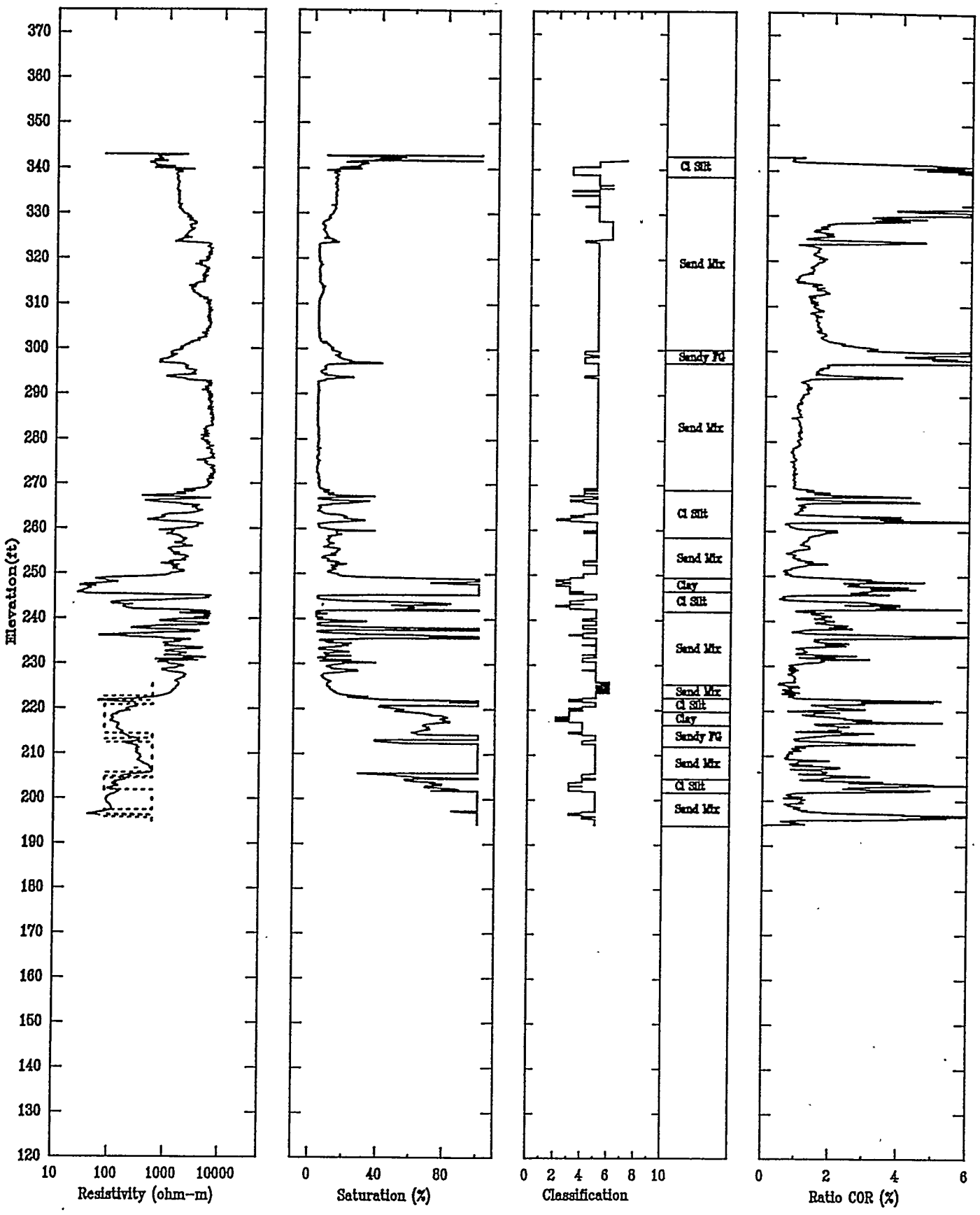

CPT-011 APPLIED RESEARCH ASSOCIATES, INC. 07/22/92

North 101349.24 East 46114.51 Elevation 353.8

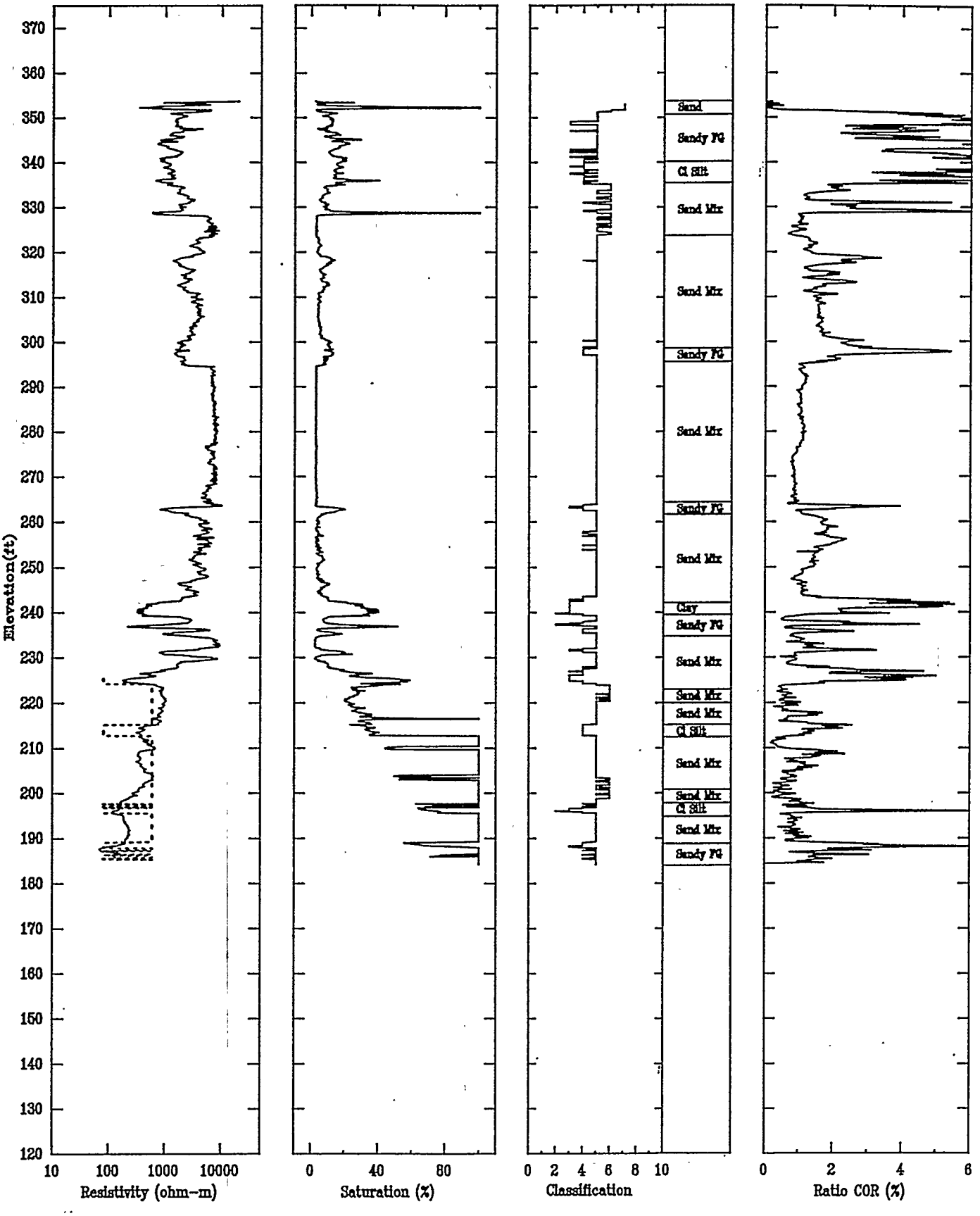

CPT-012 APPLIED RESEARCH ASSOCIATES, INC. 07/17/92

North 103267.58 East 45036.43 Elevation 360.1

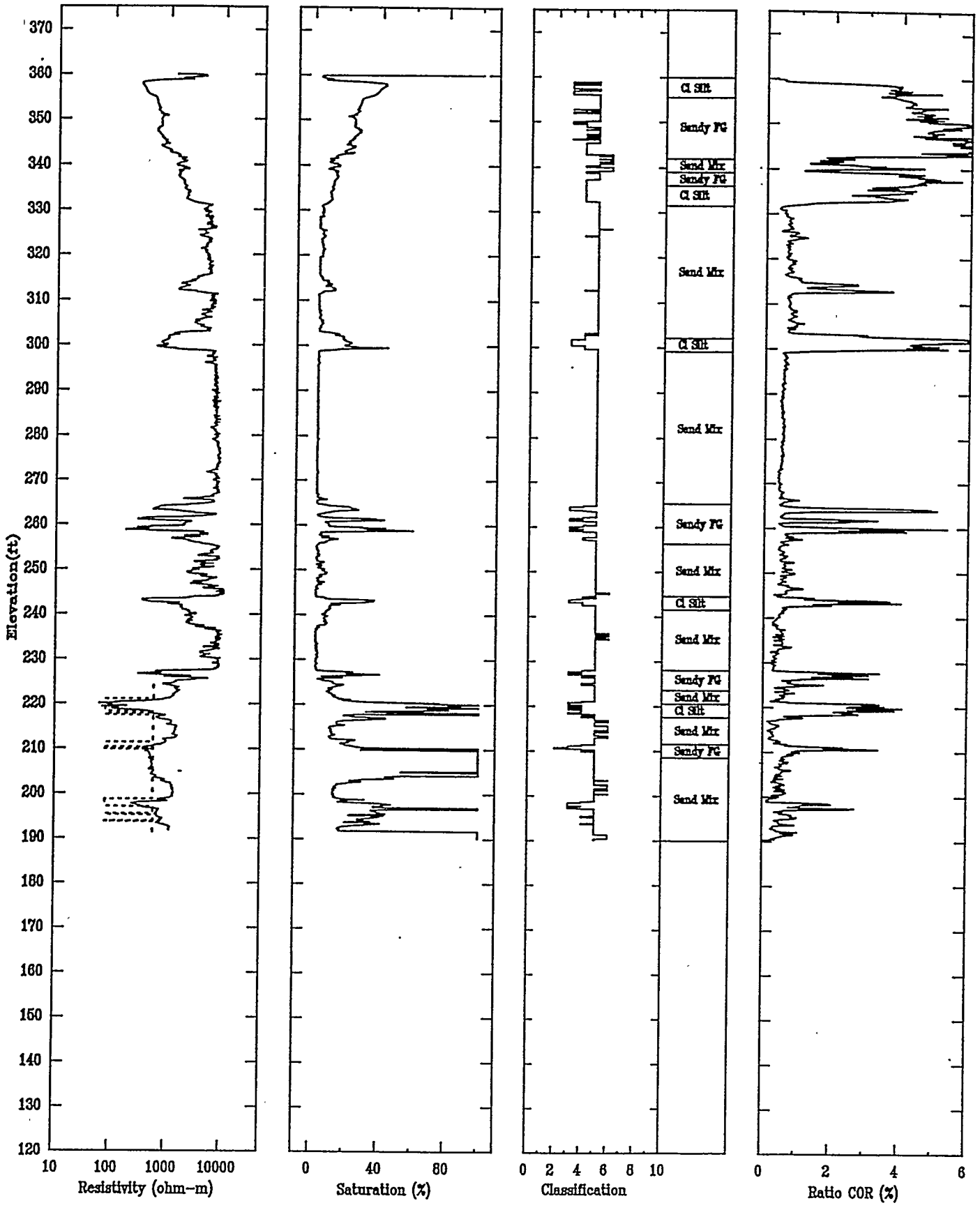

CPT-013A APPLIED RESEARCH ASSOCIATES, INC. 06/19/92

North 103066.76 East 45297.14 Elevation 350.4

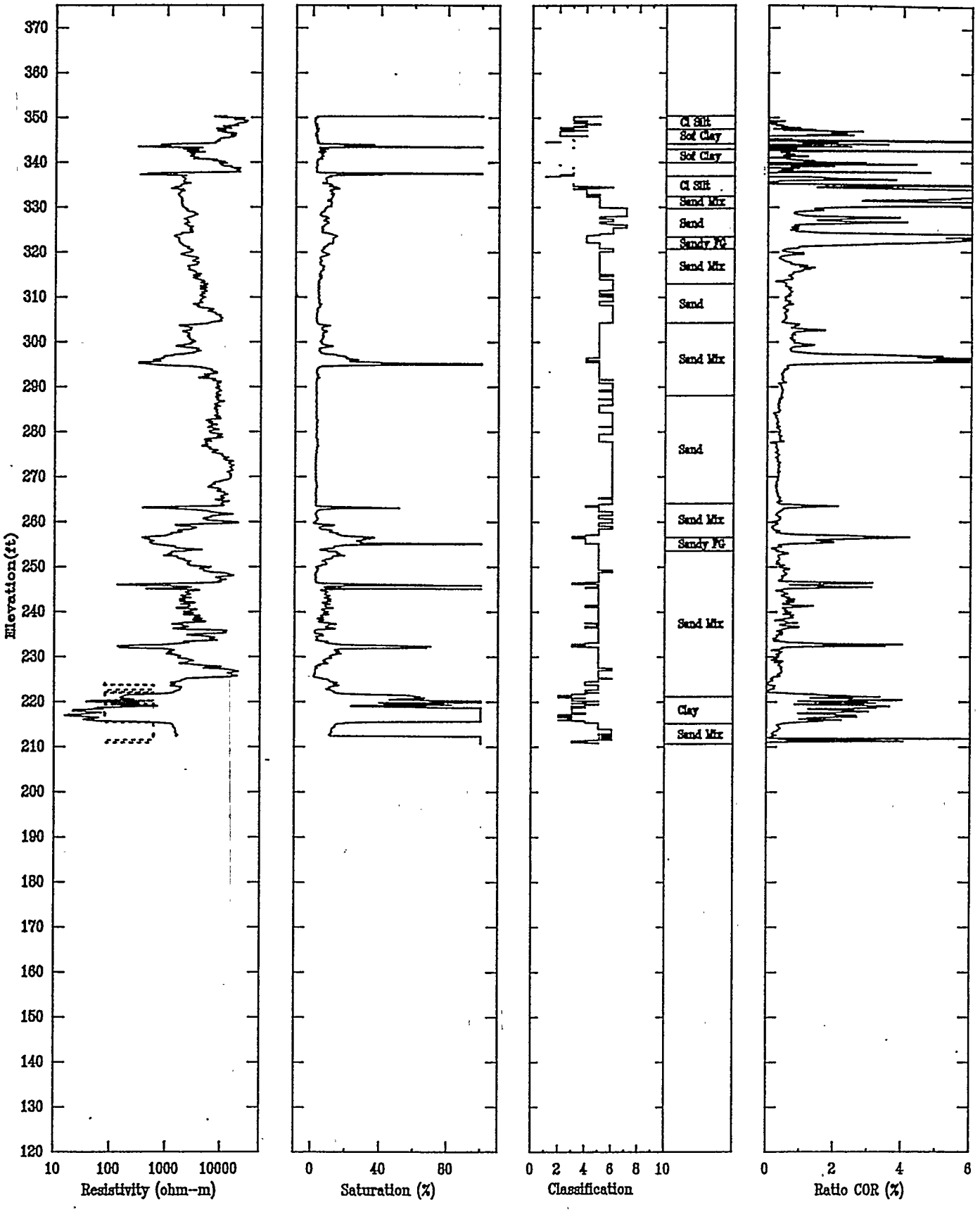

CPT–013B APPLIED RESEARCH ASSOCIATES, INC. 07/25/92

North 103083.19 East 45312.23 Elevation 350.2

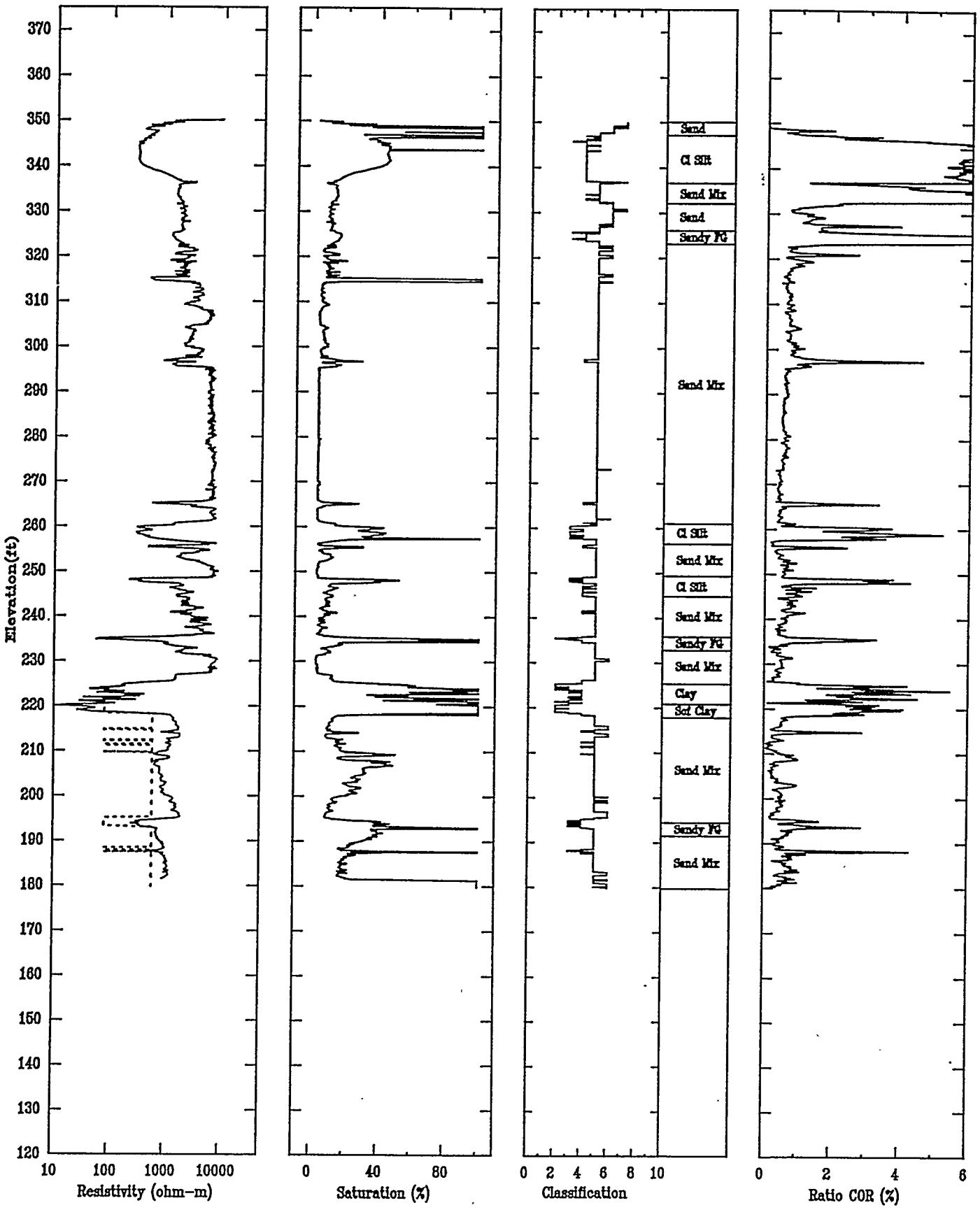

CPT-014 APPLIED RESEARCH ASSOCIATES, INC. 07/01/92

North 102736.28 East 46433.01 Elevation 349.1

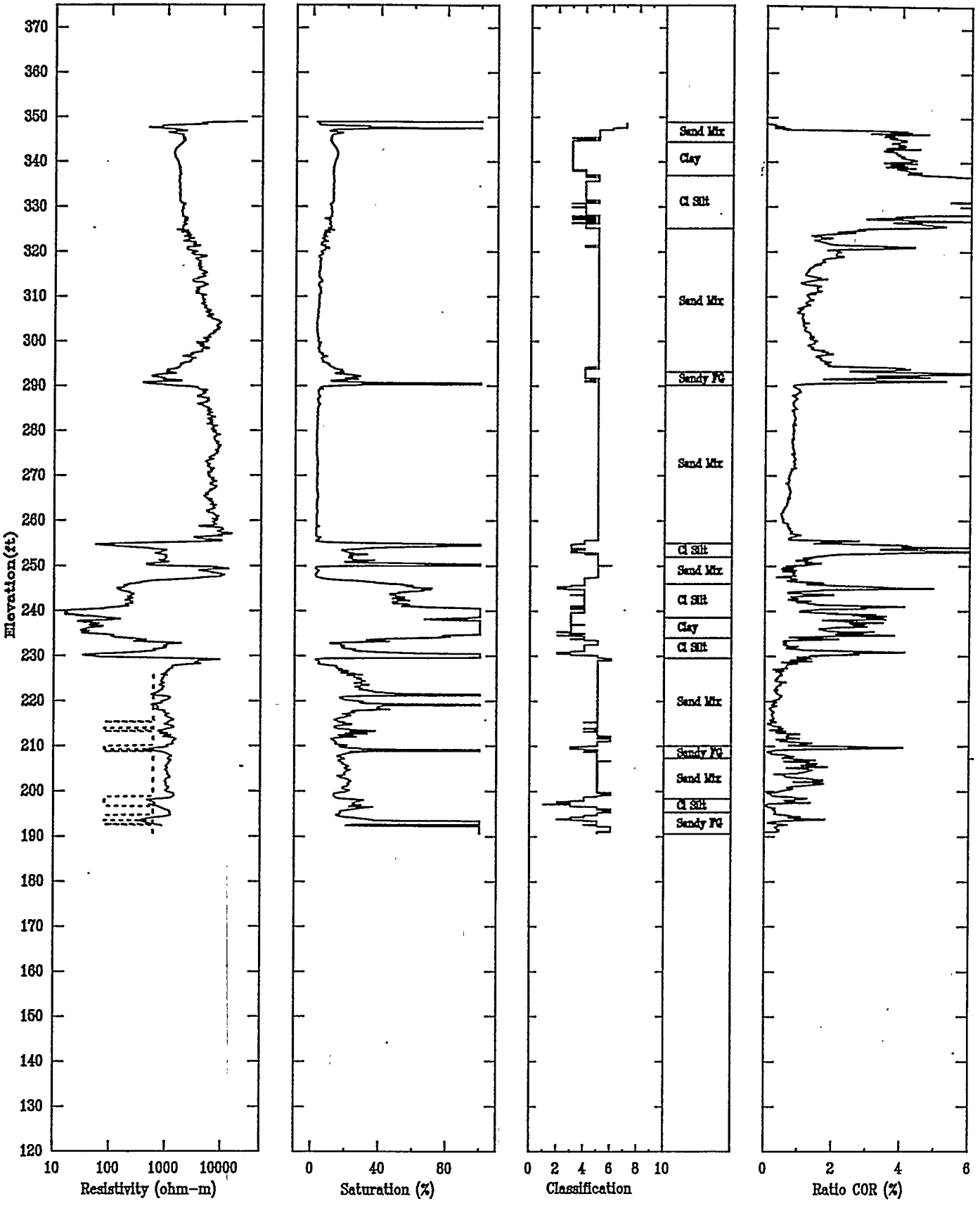

CPT-015A APPLIED RESEARCH ASSOCIATES, INC. 07/06/92

North 102963.77 East 48778.89 Elevation 367.3

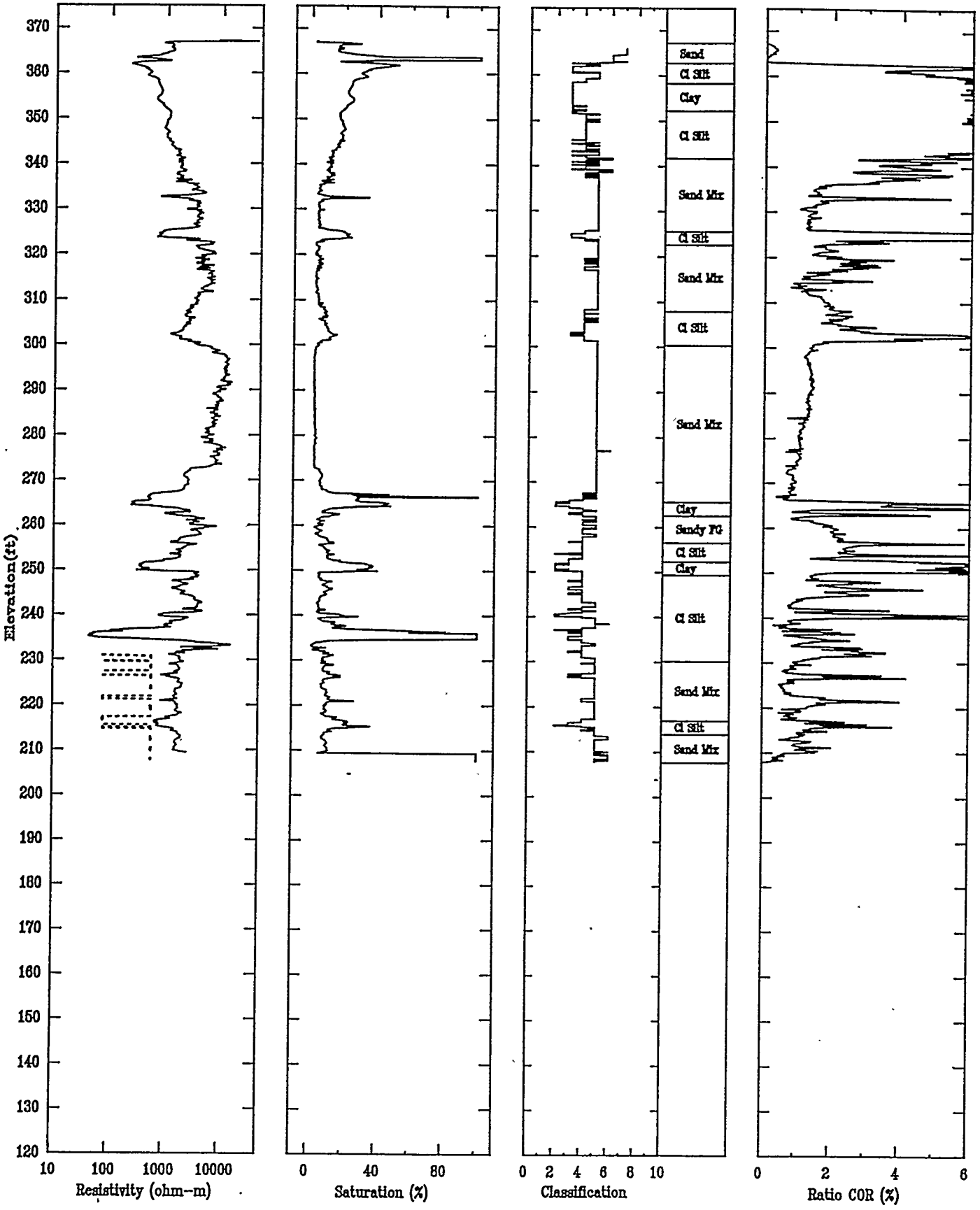

CPT-017 APPLIED RESEARCH ASSOCIATES, INC. 07/21/92

North 101955.15 East 50104.06 Elevation 344.3

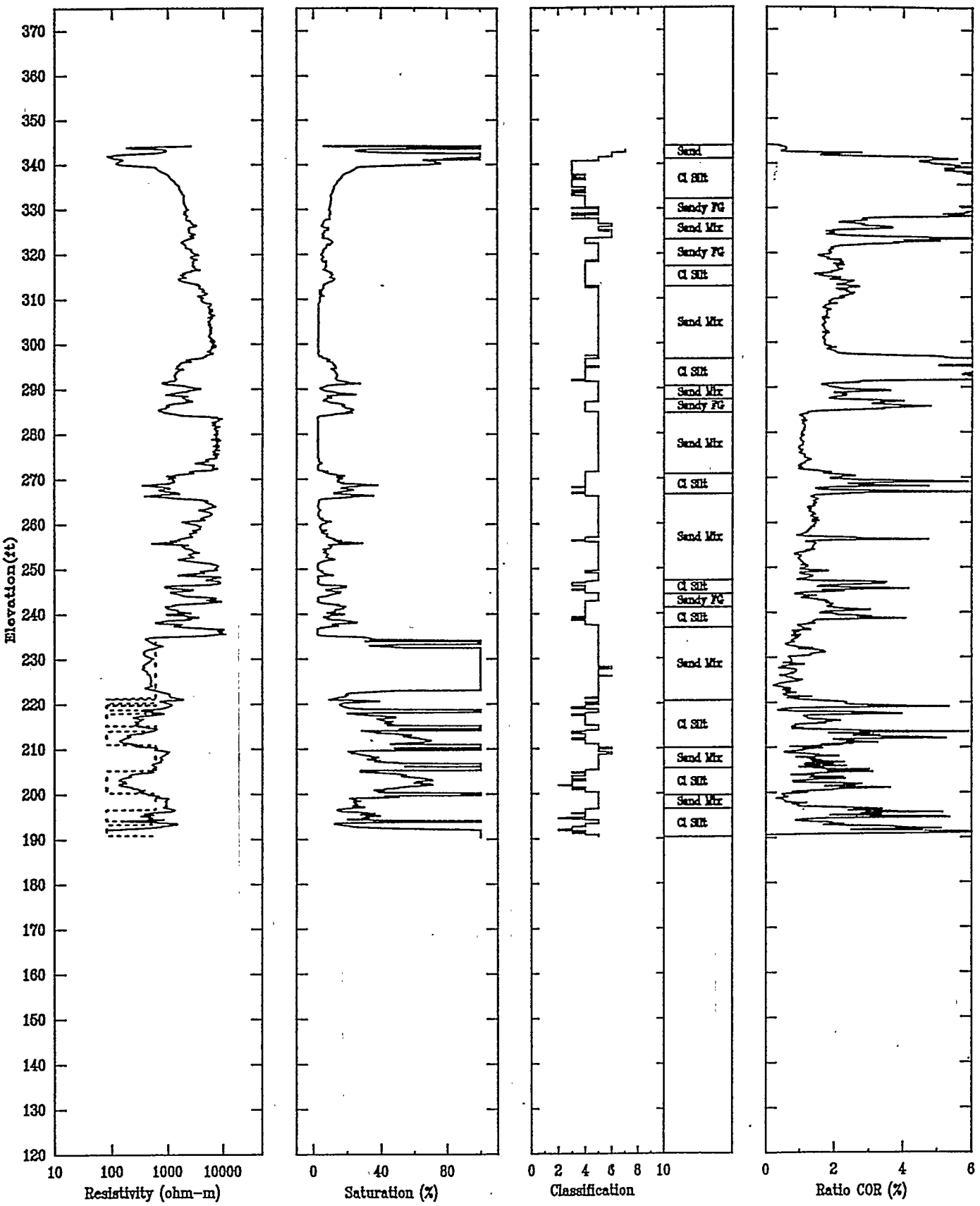

CPT-018A APPLIED RESEARCH ASSOCIATES, INC. 06/22/92

North 102198.82 East 48487.15 Elevation 358.1

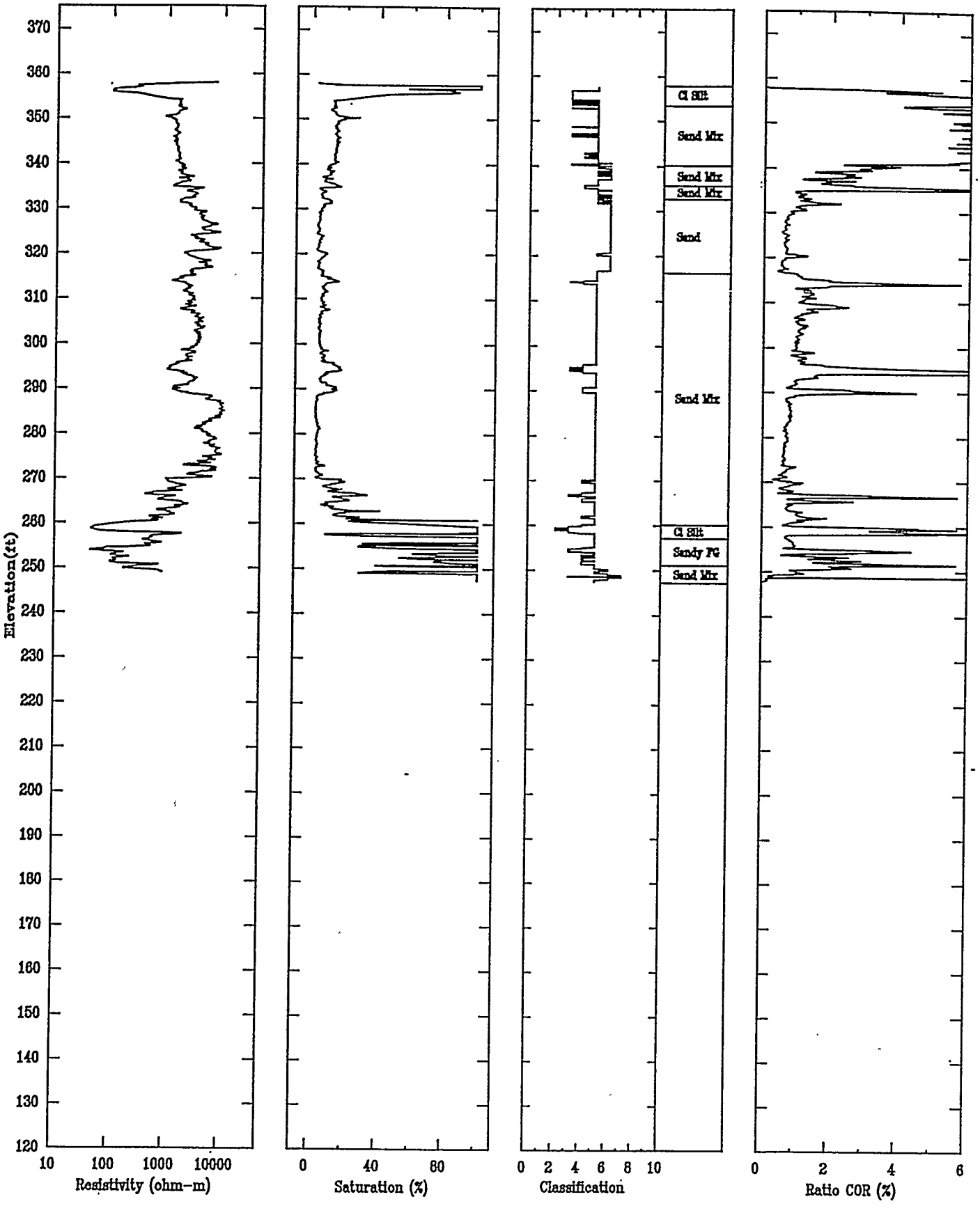

CPT-018B APPLIED RESEARCH ASSOCIATES, INC. 07/23/92

North 102232.17 East 48511.10 Elevation 358.4

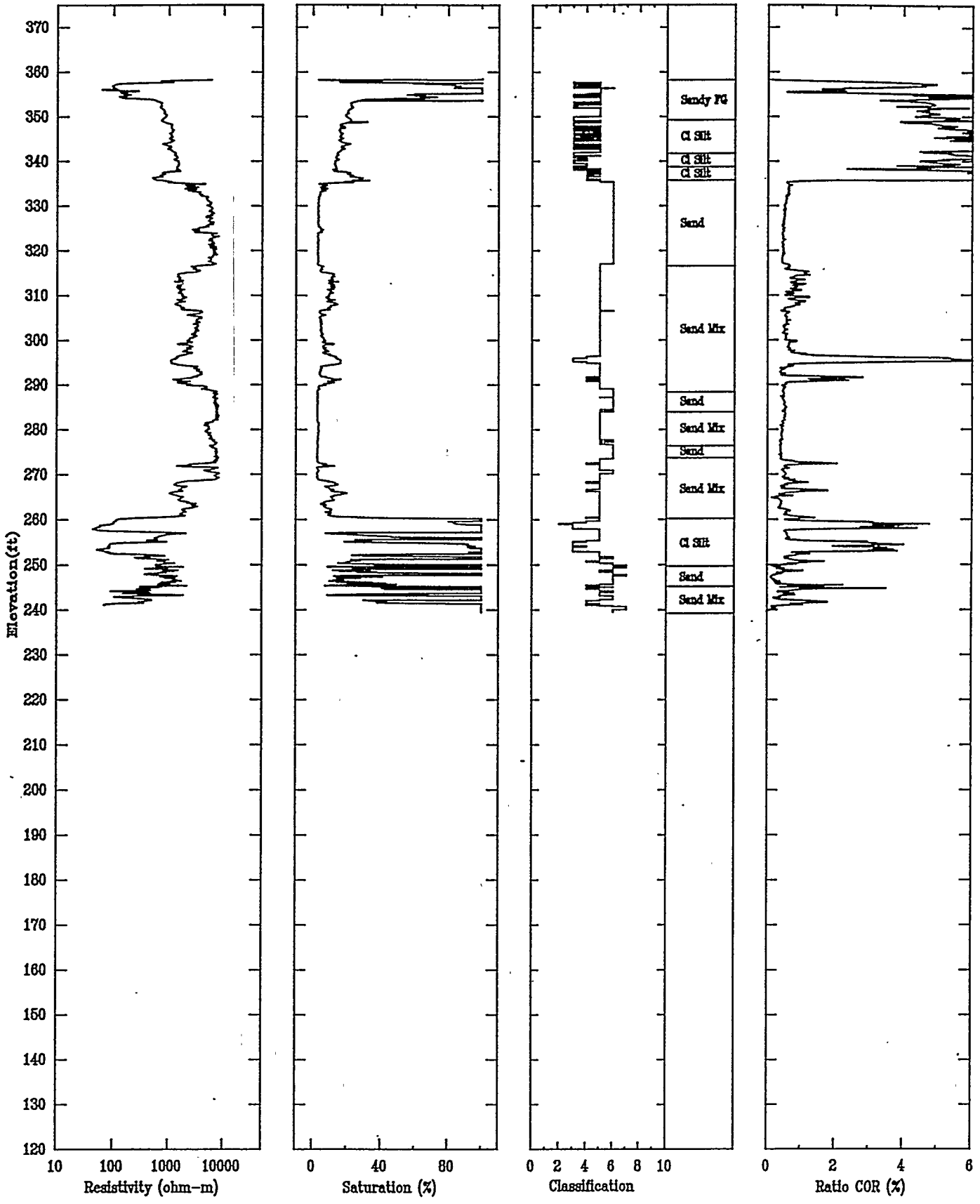

CPT-019A APPLIED RESEARCH ASSOCIATES, INC. 06/23/92

North 102264.49 East 48257.85 Elevation 356.2

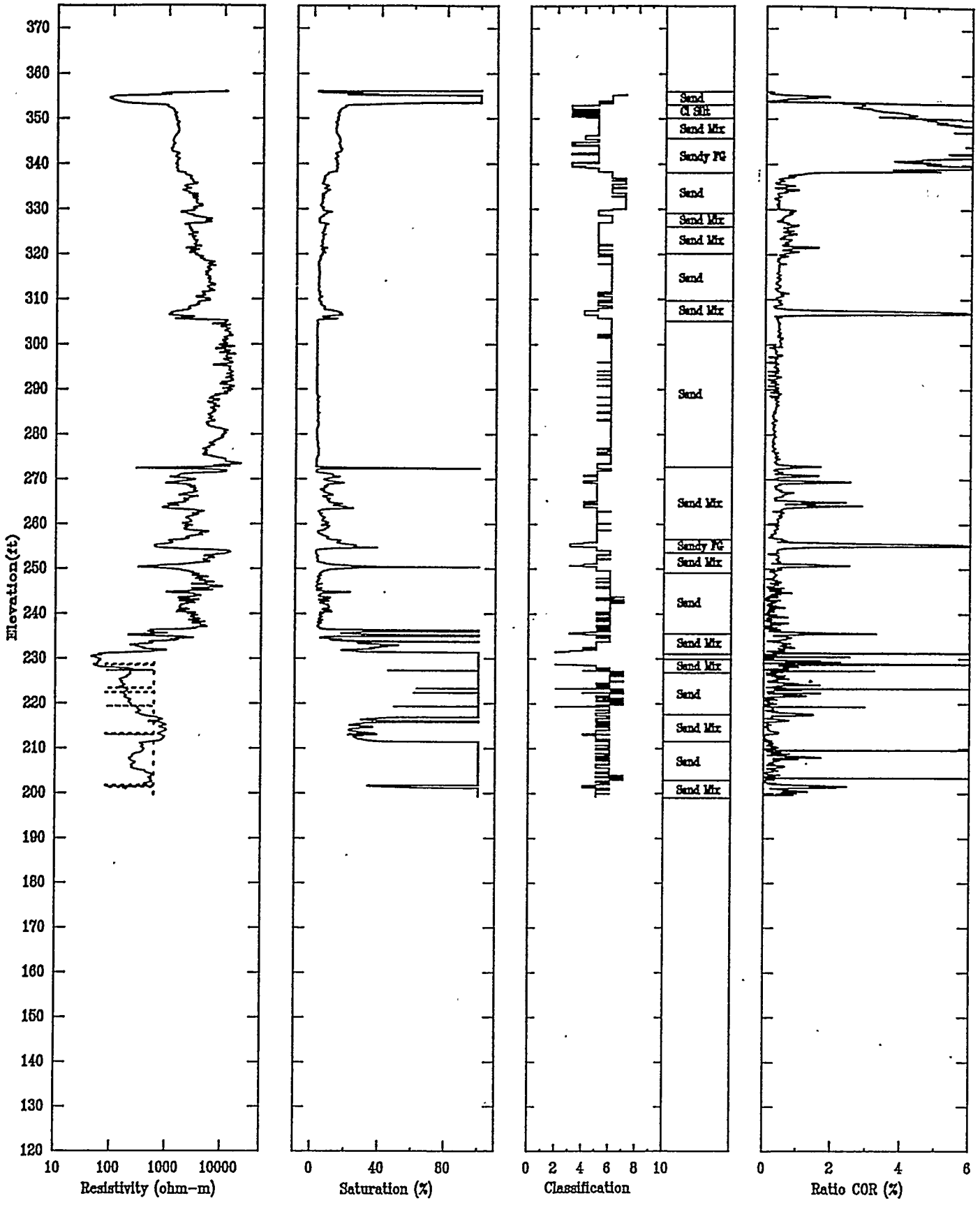

CPT-020A APPLIED RESEARCH ASSOCIATES, INC. 07/07/92

North 102488.19 East 47921.33 Elevation 354.9

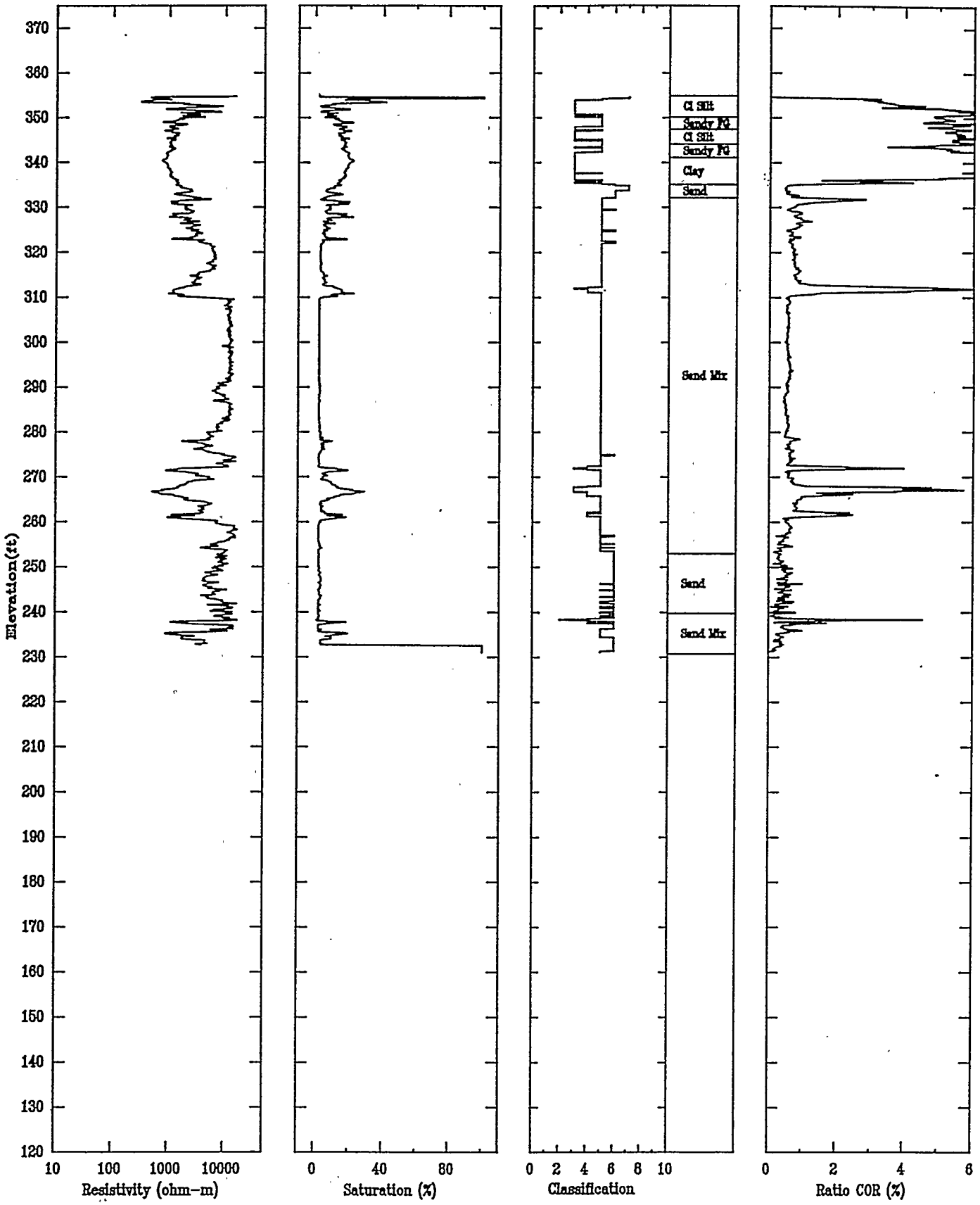

CPT-020B APPLIED RESEARCH ASSOCIATES, INC. 07/10/92

North 102500.20 East 47906.81 Elevation 356.2

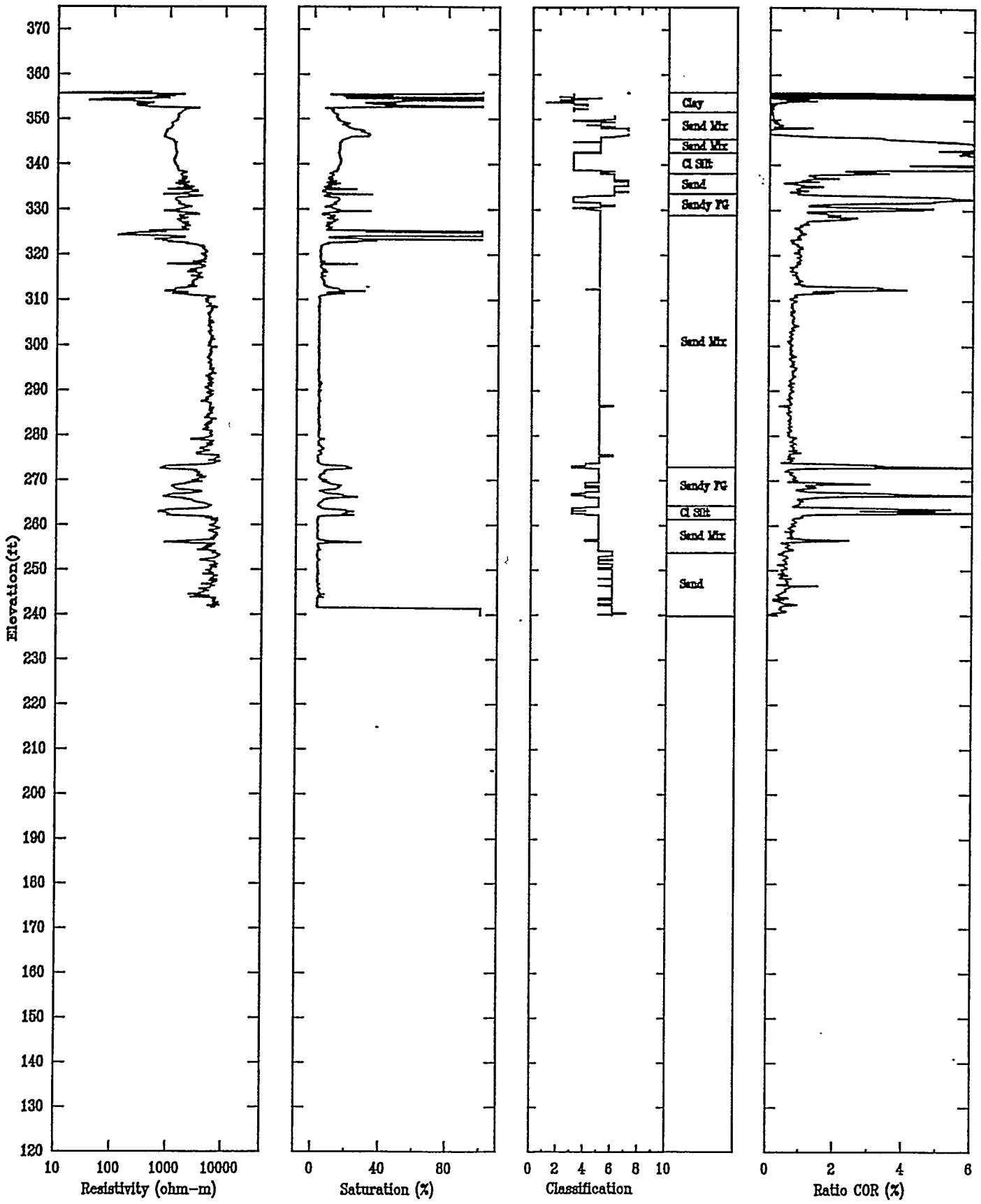

CPT–021 APPLIED RESEARCH ASSOCIATES, INC. 06/30/92

North 101383.04 East 48590.50 Elevation 340.0

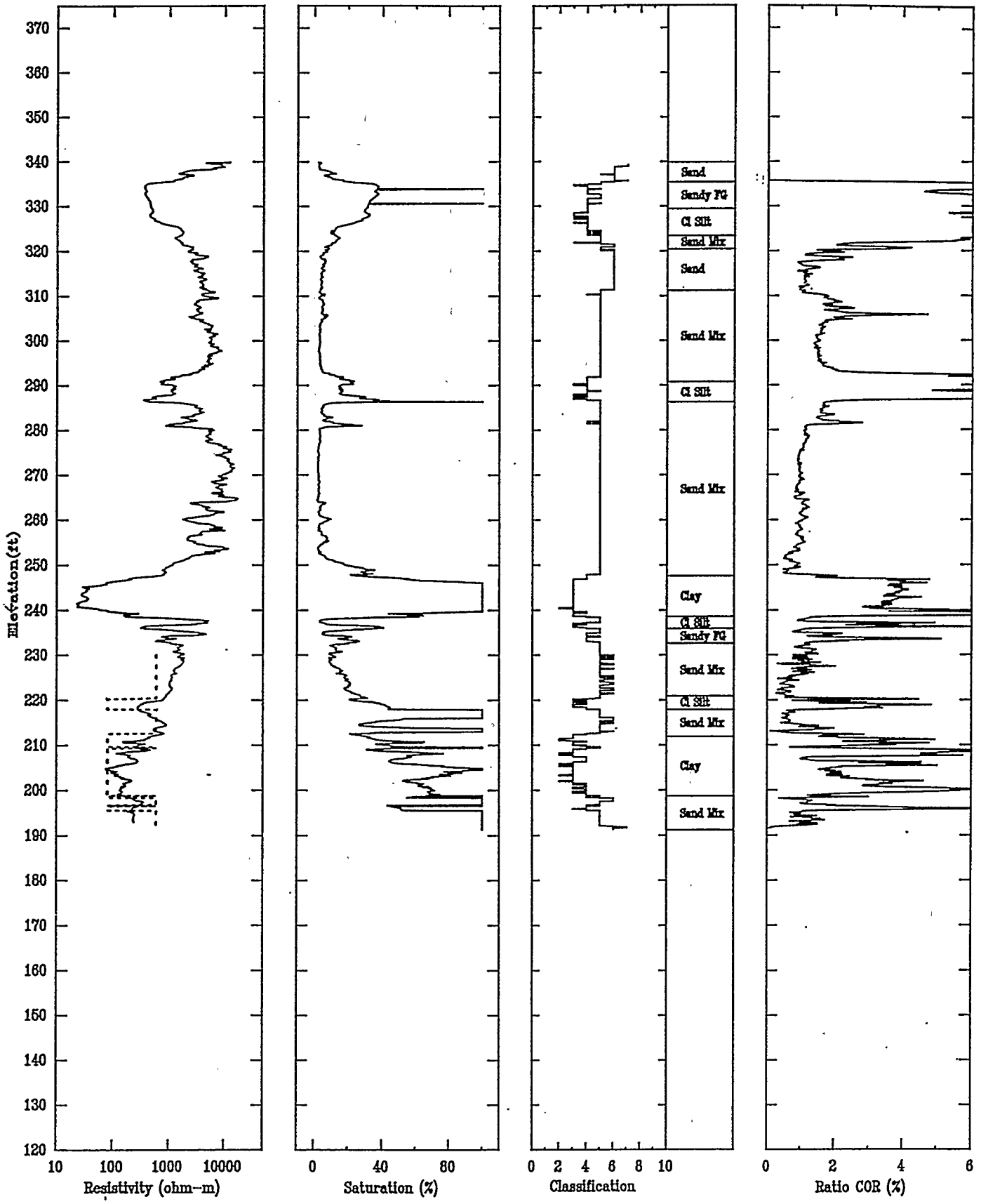

CPT-022 APPLIED RESEARCH ASSOCIATES, INC. 07/24/92

North 102495.85 East 48316.81 Elevation 354.9

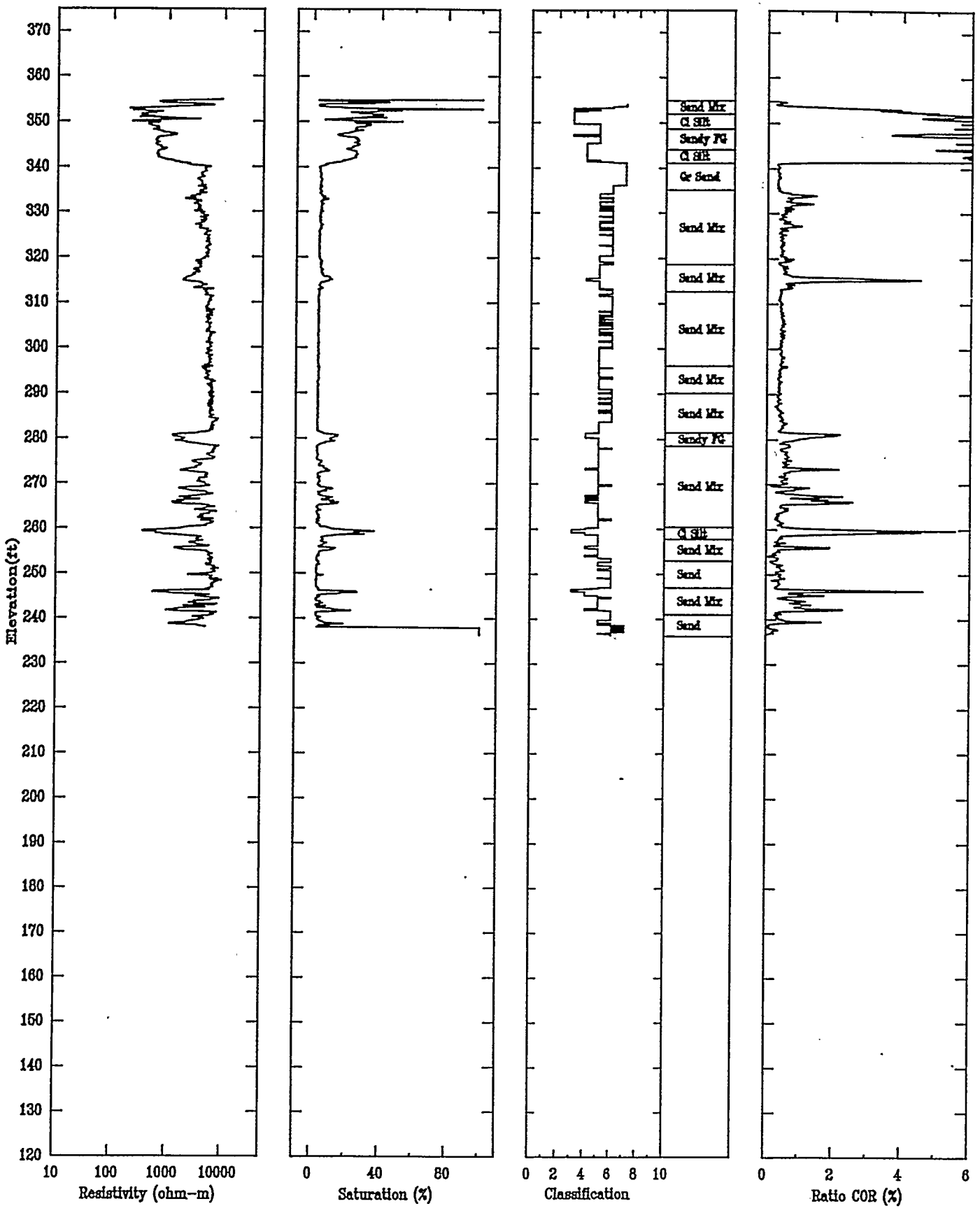

CPT-023A APPLIED RESEARCH ASSOCIATES, INC. 07/27/92

North 103862.03 East 46704.50 Elevation 349.3

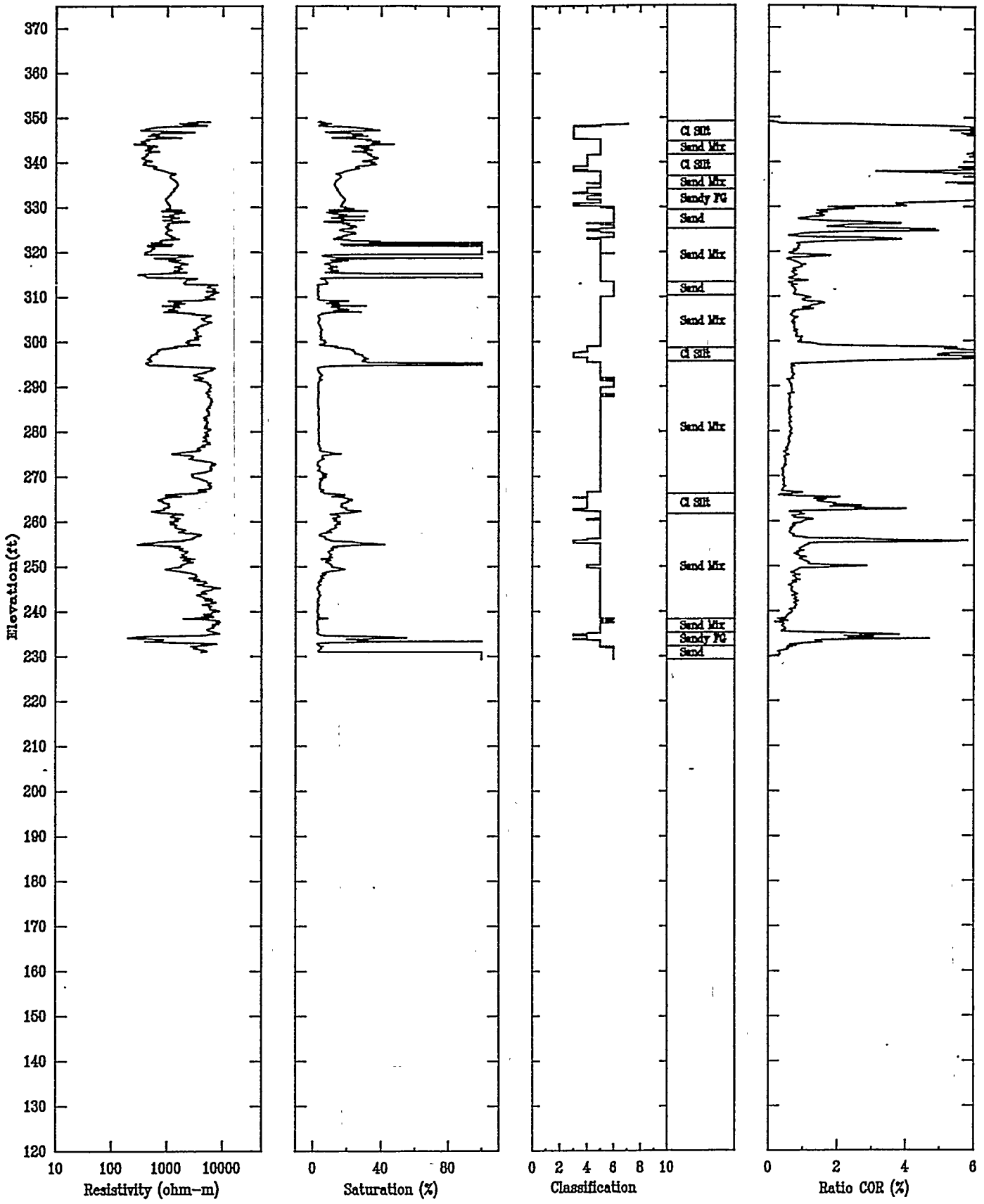

CPT-023B APPLIED RESEARCH ASSOCIATES, INC. 07/28/92

North 103812.47 East 46596.17 Elevation 350.0